

Static Investigation of Two Fluidic Thrust-Vectoring Concepts on a Two-Dimensional Convergent-Divergent Nozzle

*David J. Wing
Langley Research Center • Hampton, Virginia*

This publication is available from the following sources:

NASA Center for AeroSpace Information
800 Elkrige Landing Road
Linthicum Heights, MD 21090-2934
(301) 621-0390

National Technical Information Service (NTIS)
5285 Port Royal Road
Springfield, VA 22161-2171
(703) 487-4650

Summary

A static investigation was conducted in the static test facility of the Langley 16-Foot Transonic Tunnel of two thrust-vectoring concepts which utilize fluidic mechanisms for deflecting the jet of a two-dimensional convergent-divergent nozzle. One concept involved using the Coanda effect to turn a sheet of injected secondary air along a curved sidewall flap and, through entrainment, draw the primary jet in the same direction to produce yaw thrust vectoring. The other concept involved deflecting the primary jet to produce pitch thrust vectoring by injecting secondary air through a transverse slot in the divergent flap, creating an oblique shock in the divergent channel. Geometric variables included nozzle expansion ratio, Coanda sidewall flap angles, and injection slot longitudinal location. Fluidic variables included nozzle pressure ratio from 2 to 10 and secondary weight flow from 0 to 10 percent of the primary weight flow.

Utilizing the Coanda effect to produce yaw thrust vectoring was largely unsuccessful. Small vector angles were produced at low primary nozzle pressure ratios, probably because the momentum of the primary jet was low. The aspect ratio of the nozzle used in the investigation may have hindered the production of significant vector angles.

Significant pitch thrust vector angles were produced by injecting secondary flow through a slot in the divergent flap. Thrust vector angle decreased with increasing nozzle pressure ratio but moderate levels were maintained at the highest nozzle pressure ratio tested. Control of thrust vector angle was achieved by varying the secondary-to-primary weight flow ratio. Linearity of this control was improved by moving the slot location aft. Impingement of the oblique shock on the opposite flap occurred for combinations of low expansion ratio and forward slot injection location, and the effect was to reduce pitch thrust vectoring. Thrust performance generally increased at low nozzle pressure ratios and decreased near the design pressure ratio with the addition of secondary flow.

Introduction

Exhaust nozzles with the capability to redirect the resultant thrust of an engine from the aircraft longitudinal axis will greatly increase the versatility and maneuverability of fighter aircraft (refs. 1 and 2). This improvement in capability is accomplished by providing a means for controlling the aircraft attitude in flight regimes where conventional flight controls are less effective. These regimes include low-speed flight, where dynamic pressure is low, and high-angle-of-attack flight, where flow separation from the wings

disturbs the smooth airflow over conventional tail surfaces, rendering them less effective. With the use of thrust vectoring, attitude control in the form of engine power would be readily available to the pilot through a greater range of airspeeds and attitudes.

The design of high-performance thrust-vectoring exhaust nozzles, however, must consider other constraints as well, including weight, systems complexity, and observability. Many thrust-vectoring concepts work against these design considerations because they usually depend upon the use of variable geometry, or movable hardware. The actuators associated with variable geometry add to the aircraft weight and complexity. These adverse factors and the quest for low observability have led designers to consider fixed-aperture nozzles, those with a fixed exit plane and ideally no externally moving parts.

Fluidic concepts can potentially provide a thrust-vectoring capability to fixed-aperture nozzles. The concept of fluidic thrust vectoring is to deflect the thrust of the jet by using the influence of a second smaller exhaust stream. This secondary flow would typically be injected into or near the primary jet stream and would require few, if any, moving parts. Nozzle weight and complexity could therefore be reduced. The secondary flow may also be used to provide cooling to nozzle surfaces.

An experimental investigation was conducted of two fluidic thrust-vectoring concepts on the dual-flow propulsion simulation system in the static test facility of the Langley 16-Foot Transonic Tunnel. The two concepts were evaluated on a two-dimensional convergent-divergent nozzle. The first concept utilized the Coanda effect in conjunction with a secondary flow stream to turn the jet. The Coanda effect (ref. 3) is the tendency for a fluid to follow the convex curvature of a solid boundary. Secondary flow was injected along the sidewall of the nozzle as a vertical sheet parallel to the primary jet and adjacent to a sidewall flap with convex curvature. As a result of the Coanda effect, it was believed that the injected flow would turn outward with the convex wall and, through entrainment, would deflect the primary jet in the same direction to produce yaw thrust vectoring. Parameters varied for the test of this concept include the nozzle expansion ratio, the Coanda flap (convex sidewall) deflection angle, the Coanda flap length, the secondary flow rate relative to the primary flow rate, and the primary nozzle pressure ratio.

The second concept utilized the injection of a lateral sheet of secondary flow directly into the supersonic primary exhaust through a spanwise slot in the divergent flap. The injection would present an

obstruction to the supersonic flow, causing an oblique shock to form upstream of the slot, which would deflect the primary jet away from the slotted flap. Parameters varied for the test of this concept include nozzle expansion ratio, injection slot axial location, the secondary flow rate relative to the primary flow rate, and the primary nozzle pressure ratio. Either fluidic thrust-vectoring concept could be incorporated individually into a nozzle design to produce single-axis thrust vectoring, or both concepts could be combined to produce multiaxis thrust vectoring. Combined performance will not be discussed here, although some such data were acquired and are tabulated in this report.

The nozzles were tested at static conditions (jet flow only, no external flow). A single nozzle model was built to test both concepts. Primary nozzle pressure ratio was varied from 2 to 10. The percentage of secondary to primary weight flow was varied from 0 to 10 percent. Data acquired included force and moment measurements, internal static pressure measurements, and limited flow visualization including paint flow and schlieren photography.

Symbols

A_t	nozzle throat area, in ²
F_a	thrust measured along nozzle axis, lbf
F_i	total ideal isentropic thrust, lbf, $F_{i,p} + F_{i,c} + F_{i,si}$
$F_{i,c}$	ideal isentropic thrust of left and right Coanda ports, lbf, $w_c \sqrt{\frac{R_j T_{t,c}}{g^2} \frac{2\gamma}{\gamma-1} \left[1 - \left(\frac{p_a}{p_{t,c}} \right)^{(\gamma-1)/\gamma} \right]}$
$F_{i,p}$	ideal isentropic thrust of primary jet, lbf, $w_p \sqrt{\frac{R_j T_{t,j}}{g^2} \frac{2\gamma}{\gamma-1} \left[1 - \left(\frac{p_a}{p_{t,j}} \right)^{(\gamma-1)/\gamma} \right]}$
$F_{i,si}$	ideal isentropic thrust of injection slot, lbf, $w_{si} \sqrt{\frac{R_j T_{t,si}}{g^2} \frac{2\gamma}{\gamma-1} \left[1 - \left(\frac{p_a}{p_{t,si}} \right)^{(\gamma-1)/\gamma} \right]}$
F_n	measured jet normal force, lbf
F_r	gross resultant thrust, lbf, $\sqrt{F_a^2 + F_n^2 + F_s^2}$
F_s	measured jet side force, lbf
g	gravitational constant, 32.174 ft/sec ²

L_f	convergent-divergent flap length measured along nozzle axis from forward end of flap to divergent surface trailing edge (fig. 6(c)), in.
NPR	nozzle pressure ratio, $p_{t,j}/p_a$
$(NPR)_{des}$	design nozzle pressure ratio
p	local internal static pressure, psia
p_a	atmospheric pressure, psia
$p_{t,c}$	average Coanda secondary flow total pressure, psia
$p_{t,j}$	average primary jet total pressure, psia
$P_{t,si}$	slot injection secondary flow total pressure, psia
R	Coanda flap radius, 0.500 in.
R_j	gas constant (for $\gamma = 1.3997$), 1716 ft ² /sec ² -°R
$T_{t,c}$	average Coanda secondary flow total temperature, °R
$T_{t,j}$	average primary jet total temperature, °R
$T_{t,si}$	slot injection secondary flow total temperature, °R
w_c	sum of left and right side measured weight flow rate of Coanda secondary flow, lbf/sec
w_i	ideal primary weight flow rate, choked nozzle, lbf/sec, $A_t p_{t,j} \left(\frac{2}{\gamma+1} \right)^{\frac{\gamma+1}{2(\gamma-1)}} \sqrt{\frac{\gamma g^2}{T_{t,j} R_j}}$
w_p	measured primary weight flow rate, lbf/sec
w_{si}	measured weight flow rate of slot injection secondary flow, lbf/sec
x	axial distance measured aft from forward surface of lower flap (fig. 7), in.
x_c	curvilinear distance along Coanda flap, positive downstream from intersection of curved and planar surfaces (fig. 7), in.
x_s	axial distance from forward end of upper flap to injection slot (fig. 6(c)), in.
x_t	axial distance from forward end of upper or lower flap to nozzle throat (fig. 6(c)), 1.050 in.

y	lateral distance measured inboard from right edge of upper flap (fig. 7), in.
y_t	width of nozzle at throat (fig. 6(c)), 3.983 in.
z_e	vertical distance from outside surface of divergent flap to divergent channel trailing edge at nozzle exit (fig. 6(c)), in.
z_p	vertical distance from top surface of upper flap to center of cylindrical plenum for injection slot (fig. 6(c)), in.
α_s	angle of injection slot measured with respect to vertical, positive inclination toward nozzle exit (fig. 6(c)), deg
β_s	angle of injection-slot plenum supply ducts in upper flap measured with respect to vertical (fig. 6(c)), deg
γ	ratio of specific heats, 1.3997 for air
δ_p	pitch thrust vector angle, deg, $\tan^{-1}(F_n/F_a)$
$\delta_{v,p}$	jet centerline deflection angle as a result of asymmetric upper and lower flaps, positive down, deg, $(\theta_l - \theta_u)/2$
δ_y	yaw thrust vector angle, deg, $\tan^{-1}(F_s/F_a)$
ε	nozzle expansion ratio, $\frac{\text{Exit area}}{\text{Throat area}}$
θ_l	divergence angle of lower flap, positive away from nozzle axis, deg
θ_u	divergence angle of upper flap, positive away from nozzle axis, deg
ϕ_l	left Coanda flap angle measured with respect to nozzle axis, positive away from primary jet, deg
ϕ_r	right Coanda flap angle measured with respect to nozzle axis, positive away from primary jet, deg
ω_c	corrected weight flow ratio of combined left and right Coanda ports, $\frac{w_c \sqrt{T_{t,c}}}{w_p \sqrt{T_{t,j}}}$
ω_{si}	corrected weight flow ratio of slot injection port, $\frac{w_{si} \sqrt{T_{t,si}}}{w_p \sqrt{T_{t,j}}}$

Abbreviations:

2-D two-dimensional

C-D convergent-divergent

M.S. model station, in.

Nozzle Design

Thrust-Vectoring Concepts

Coanda thrust vectoring. Two fluidic thrust-vectoring concepts were studied. One concept employed the Coanda effect to produce yaw thrust vectoring. The Coanda effect is the tendency for a fluid to follow the convex curvature of a solid boundary. The phenomenon occurs because a stream of moving fluid, such as a jet, draws in slower moving, lower energy flow through viscous entrainment, reducing the static pressure in the vicinity of the jet. If a solid wall is placed near the jet, blocking surrounding fluid from filling the void left by the entrainment, the local static pressure drops further between the jet and the wall, drawing the jet in toward the wall.

Research has shown that a thin jet will more likely be affected by the Coanda effect than will a thick jet (refs. 4 to 6). Therefore, for the current investigation, a rectangular nozzle was designed with a thin, vertical, secondary flow injection port located adjacent to the sidewall at the nozzle divergent channel exit plane. A surface with convex curvature (referred to as a Coanda flap) was placed immediately aft (downstream of nozzle exit) and outboard of the injection port. The intent, as shown in figure 1, was for the injected secondary flow to be turned outboard by the Coanda effect and to entrain the primary jet in the same direction, creating thrust vectoring in the yaw direction.

Slot injection thrust vectoring. The second concept was a shock vector control concept and involved deflecting the primary jet in the pitch direction by using an oblique shock wave emanating from one of the divergent flaps. As shown in figure 2, the shock would be created by injecting a sheet of air through a lateral slot in the divergent flap. Although the injected air would quickly be deflected by the primary jet, its emergence from the slot would present a local obstruction to the supersonic exhaust, and an oblique shock would form immediately upstream of the slot. The strength and position of the shock, and therefore the amount of pitch vectoring, would be controlled by varying the secondary injection flow rate. The primary jet would be turned by the oblique shock in the direction away from the slot, and the injected air would fill the void left by the primary jet downstream of the slot near the divergent flap surface.

Models

Nozzle test bed. A single two-dimensional convergent-divergent (2-D C-D) nozzle was used as the test bed for both concepts. The nozzle had a throat area A_t of 3.951 in² and a throat aspect ratio (width to height) of 4.015. Nozzle expansion ratio (exit area divided by throat area) was varied as a geometric parameter for both concepts. The expansion ratios tested were 1.502, 1.944, and 2.405. These values represent a moderate to high range of nozzle expansion ratio, corresponding to aircraft systems which operate on-design at supersonic cruise Mach numbers. The length of the divergent flap was maintained constant as the expansion ratio was varied such that the divergence half-angles were 8.5°, 16°, and 24°. In addition to these symmetric configurations, several pitch-vectorred configurations were tested by combining the 24° half-angle lower flap with the 16° and 8.5° half-angle upper flaps plus an additional -7° upper flap. For these configurations, the flow path centerline was deflected down 4°, 7.75°, and 15.5°, and the expansion ratios based on vertical throat and exit plane areas were 2.172, 1.952, and 1.499. These configurations represent a combined fluidic/mechanical pitch-vectoring system and will not be discussed in this report; the data are, however, presented in tabulated form.

Photographs of the model installed on the test stand are shown in figure 3. In the rear quarter view of figure 3(a), the nozzle can be seen at the center of the photograph with secondary air supply ducts attached to the sides and top. The primary jet exhausts through the dark rectangular region (the nozzle exit) in the center of the model. In-line venturis and motor-controlled valves can be seen in the secondary air supply ducts. Pressure tubing can also be seen leading from the model to a panel on the left side of the test stand. In the side view of figure 3(b), components of the dual-flow test stand can be seen, including plenums for the primary and secondary air and the four S-tubes which supply air to the test stand.

A schematic sketch of the dual-flow propulsion simulation system with the nozzle attached is shown in figure 4. The details of this sketch will be described later in the report. The important features to note at this time are the general flow direction (from left to right) and the delineation between the test stand and the nozzle. The test stand includes all hardware upstream of M.S. 27.080, including the secondary air supply ducts (not shown).

Photographs of the isolated nozzle are shown in figure 5. The front view of the assembled model in

figure 5(a) shows the vertical Coanda injection ports, the horizontal injection slot in the upper flap, and the three secondary air supply duct unions. A partially disassembled view of the model in figure 5(b) shows the major components of the model; they include the upper flap (installed, with injection slot), the lower flap (removed), the main body (which houses plenums for the Coanda secondary air), and the Coanda flaps. Sketches detailing the geometry of the model are shown in figure 6, with internal static pressure orifice locations given in figure 7. A configuration list is presented in table 1, and some critical dimensions are tabulated in table 2.

Main body details. A sketch of the main body with the Coanda flaps installed but with the upper and lower flaps removed is shown in figure 6(a). As shown in view A-A, the nozzle convergence begins in the main body and will be continued by the upper and lower flaps. Secondary air plenums were located in the right and left sides of the main body to supply air to the Coanda ports and in the upper flap to supply air to the pitch injection slot. These plenums were connected to an external air supply by external plumbing. (See fig. 3(a).)

Coanda nozzle details. A detailed sketch of the Coanda plenum and injection port is shown in figure 6(b). The Coanda air was injected as a vertical sheet parallel to the primary jet along the sidewalls of the nozzle. The injected air was accelerated to supersonic speed by a row of 10 convergent-divergent ports (see detail C-C in fig. 6(b)) located in the secondary flow passage just upstream of the sidewall trailing edge (nozzle exit plane).

Flaps were located immediately downstream of the injection ports. The flaps consisted of a rounded upstream surface with a radius of curvature of 0.500 in. and a flat downstream segment, the length of which was varied as a parameter. A short flap and a long flap were tested on selected configurations. (See fig. 6(b).) The ratio of curvature radius to injection stream width was 3.731. Each flap could be pivoted and fixed at an angle relative to the nozzle centerline, thereby providing a convex surface adjacent to the injection port. The Coanda flaps could be set at angles of 0°, 30° outboard, 45° outboard, and 10° inboard. Five combinations were tested including left/right flap angle combinations of 0°/0°, 0°/30°, 0°/45°, -10°/30°, and -10°/45° (a negative angle denotes inboard deflection). Note that although this concept had a fixed aperture, it had movable flaps downstream of the exit plane.

Slot injection nozzle details. A sketch of the upper and lower flaps is presented in figure 6(c). The

flaps formed the larger part of the convergent contour and the entire divergent contour of the nozzle. The injection slot was positioned in the divergent segment of the upper flap and extended symmetrically across 91 percent of the nozzle width. The slot had a width of 0.053 in. and was oriented to inject air perpendicular to the divergent flap surface.

The air supply passage for the injection slot consisted of a rectangular plenum containing a baffle plate and a second cylindrical plenum connected by nine cylindrical supply ducts. The slot was milled along the length of the cylindrical plenum. This arrangement was designed to produce an even distribution of mass flux through the slot along the width of the nozzle. The baffle design is shown in figure 6(d). The effectiveness of the baffle in distributing the mass flux evenly was verified with total pressure measurements along the slot.

The injection slot was tested at two axial stations in the divergent channel, referred to as forward and aft, corresponding to locations approximately 45 percent and 67 percent of the distance from the throat to the exit plane. The flaps were interchangeable, so that variations in slot location and nozzle expansion ratio could be achieved by inserting the appropriate upper and lower flaps. Although this concept was only investigated in the upper flap, an actual nozzle would contain injection slots in both the upper and lower flaps to provide positive and negative pitch-vectoring forces.

Facility Description

The investigation was conducted in the static test facility of the Langley 16-Foot Transonic Tunnel. Testing is conducted in a large room where the jet from a single-engine propulsion simulation system exhausts to atmosphere through an acoustically treated exhaust passage. The static test facility has an air control system that is similar to that of the Langley 16-Foot Transonic Tunnel and is described in reference 7.

Dual Flow Propulsion Simulation System

The test stand, shown in figure 3, is an axisymmetric rig mounted on a six-component cylindrical strain-gauge force balance. Two independently controlled airstreams are supplied to isolated plenum chambers on the test stand through two pairs of S-shaped, stainless steel tubing (S-tubes). The primary air supply is routed through eight radially oriented sonic nozzles to a cylindrical axial duct on the test stand centerline. The primary air in this axial duct then passes through a transition duct (with a

rectangular exit), a choke plate, and an instrumentation section before entering the nozzle and exhausting to atmospheric conditions.

The secondary air supply normally follows a similar path in an annular duct surrounding the primary duct. For the current investigation, however, the sonic nozzles for the secondary flow were plugged, and plumbing for three air lines was installed, routing air from the secondary plenum directly to connections on the nozzle. (See fig. 3(a).) The three air lines included one for each of the two Coanda injection ports and a third line for the pitch injection slot. Each air line contained a remotely operated electric ball valve for flow regulation, a subsonic venturi for measuring weight flow, and sufficient tube length to ensure smooth flow entering the venturi.

The air supplied to the primary jet was delivered by a 15 lb/sec air system containing a pair of parallel critical venturis and an in-line steam heat exchanger to maintain a flow temperature of approximately 540°R. The air supplied to the secondary plenum was delivered by a 3 lb/sec air system containing a single subsonic venturi. No temperature control was available for secondary flow. Secondary flow total temperature in the model varied during the test from approximately 460°R to 530°R, depending on the time of day and the length of each run.

Instrumentation

Forces and moments were measured with a six-component strain-gauge balance located on the jet stand centerline. The metric hardware (supported solely by the force balance) included the test stand plenum chambers, the primary flow ducting to the model, the instrumentation section, the secondary air supply ducting, and the nozzle. Four stainless steel S-shaped tubes, previously described, bridged the metric hardware and the nonmetric support frame to supply air to the jet stand.

Weight flow for the primary flow was measured by a pair of in-line critical-flow venturis located upstream of the S-tubes, each rated to a flow rate of 7.5 lb/sec. Weight flow for each of the three secondary flows was measured with an independent subsonic venturi located in the plumbing between the secondary flow plenum chamber and the nozzle. Total pressure upstream of each venturi was obtained by using a Kiel pitot probe. Static pressure at the venturi throat and total temperature measurements were also obtained. Each venturi was calibrated with the subsonic venturi in the 3 lb/sec air line as a reference. One thermocouple per air line, located immediately upstream of the venturi, was used to measure secondary air temperature.

Static pressure measurements in the model were obtained from individual pressure transducers. The primary jet total pressure was obtained from two rakes containing a total of seven pitot probes in the instrumentation section just upstream of the nozzle entrance station. The pitot probes were connected to individual pressure transducers. Measurements from two thermocouples in the instrumentation section were averaged to provide primary jet total temperature.

Data Reduction

Each data point used in the computations was the average of 50 frames of data, taken at a rate of 10 frames/sec. Five basic performance parameters are used in the presentation of results; they are resultant gross-thrust ratio F_r/F_i , axial thrust ratio F_a/F_i , discharge coefficient w_p/w_i , pitch thrust vector angle δ_p , and yaw thrust vector angle δ_y . With the exception of resultant gross thrust F_r , all balance data in this report are referenced to the model centerline. Reference 8 presents a detailed description of the data reduction procedures used for the current investigation.

A set of corrections was applied to all balance force and moment measurements. Each balance component was initially corrected for model weight tares and isolated-balance interactions. Additional interactions were computed by recalibrating the balance after it was installed in the test stand. The recalibration was necessary because the S-tubes provided a new restraint to the balance. In addition to providing a set of "installed" interactions, this recalibration accounted for the effects of jet operation (pressurization) and nozzle throat area (momentum transfer). The S-tubes were designed to be flexible enough to minimize the static restraint on the force balance, yet retain enough rigidity to withstand the pressurization during jet operation and minimize the effect of pressurization on the static restraints. Residual tares, however, still existed and were a result of the tendency of the S-tubes to deform under pressurization. These residual tares were determined by testing Stratford convergent calibration nozzles with known performance over a range of expected internal pressures and externally applied forces and moments. For the current test, the axial force measurement was calibrated with a precision of within 1 percent of full-scale balance capacity. The remainder of the components were calibrated with a precision of within 0.5 percent of full-scale balance capacity. A general procedure for computing these tares is discussed in more detail in reference 8, although the specific equations for determining the tares have been modified to

correct for the interactions associated with the dual-flow static test stand.

The resultant thrust ratio F_r/F_i is the resultant gross thrust divided by the ideal isentropic thrust. Resultant gross thrust is obtained from the measured axial, normal, and side components of the jet force measured by the force balance. The ideal thrust calculation, accounting for contributions from the primary and all secondary airstreams, was defined as the sum of the thrust contributions resulting from isentropic expansion from stagnation conditions measured for each stream. The definition assumes axial discharge of all jets and can be found in the "Symbols" section.

The axial force ratio F_a/F_i is the ratio of the measured nozzle thrust along the body axis to the total ideal isentropic nozzle thrust. From the definitions of F_a and F_r , one can see that the thrust along the body axis F_a includes geometric losses that result from turning the exhaust vector away from the axial direction, whereas the resultant gross thrust F_r does not.

The nozzle discharge coefficient w_p/w_i is the ratio of measured primary weight flow to ideal primary weight flow and reflects the ability of a nozzle to pass exhaust flow. The discharge coefficient is reduced by any momentum and vena contracta losses (effective throat area less than A_t). The discharge coefficient does not include weight flow contributions of the secondary flows but may show effects on the primary weight flow characteristics caused by the secondary flow injection.

The resultant thrust vector angles δ_p and δ_y are the calculated angles in the pitch and yaw planes. These angles are calculated from the measured normal, side, and axial forces on the model as indicated in the "Symbols" section, and can be increased by either an increase in normal or side forces or a decrease in axial force.

The independent flow parameters for this investigation were the primary jet nozzle pressure ratio and the corrected secondary-to-primary ratio of weight flow for each port. The nozzle pressure ratio (NPR) is the average jet total pressure measured in the instrumentation section divided by atmospheric pressure and was varied in this investigation from 2 to 10. The corrected weight flow ratio is the ratio of measured weight flow rate of the Coanda or slot injection flows to the measured primary weight flow rate, corrected for the difference in temperature between the two streams. (See "Symbols" section.) The weight flow ratio for the Coanda ports is represented by w_c .

This quantity represents the total weight flow ratio through the left and right ports. This ratio was varied from 0 to approximately 0.2 (10 percent of primary weight flow on each side for a total of 20 percent). Coanda flow rate of the two ports was main-

tained approximately equal in this investigation. The corrected weight flow ratio for the injection slot is represented by ω_{sj} , and was varied in this investigation from 0 to approximately 0.1 (10 percent of primary weight flow).

Presentation of Results

A list of configurations tested is presented in table 1. All performance data for the fluidic nozzle are tabulated in tables 3 to 54. Some of these data will not be discussed in this report, including the effects of constraining the Coanda injection with fences (seen in the photographs of fig. 5), physically deflecting the divergent flaps for combined mechanical and fluidic thrust vectoring, and multiaxis fluidic thrust vectoring. The data plots presented in figures 8 to 21 are intended to show typical trends in performance. Static pressure ratio data are also tabulated in this report with selected representative pressure distributions presented in data plots. The data include Coanda flap centerline pressures (tables 55 to 84), injection slot upstream and downstream pressures (tables 85 to 100), and sidewall centerline pressures and lower divergent flap centerline pressures (tables 101 to 116).

Flow visualization photographs for the Coanda vectoring configurations are presented in figures 22 and 23 and discussed in appendix A. Flow visualization photographs for the slot injection vectoring configurations are presented in figures 24 through 27 and discussed in appendix B. The visualization techniques used include focusing schlieren to visualize the external flow field and an oil-based paint flow technique to show internal surface flow patterns. Additionally, limited focusing schlieren was used to visualize the internal flow field associated with injecting secondary air through a slot in a similar 2-D C-D nozzle.

Data for selected nozzle configurations are presented in figures 8 to 21 as follows:

	Figure
Supply pressure requirements for Coanda secondary flow.	8
Supply pressure requirements for slot injection secondary flow.	9
Effect of Coanda flap angles on internal performance. Long Coanda flaps; $\omega_c = 0.10$	10
Effect of Coanda corrected weight flow ratio on internal performance. Long Coanda flaps; $\phi_l = 0^\circ$; $\phi_r = 30^\circ$	11
Effect of Coanda flap length, flap angle, and corrected weight flow ratio on yaw thrust vector angle.	12
Yaw thrust vector angle as a function of Coanda corrected weight flow ratio at different Coanda flap angles and jet nozzle pressure ratios. Long Coanda flaps.	13
Coanda flap static pressure ratio distributions. $\epsilon = 1.502$; long Coanda flaps.	14
Effect of slot injection on internal performance. Forward slot injection; $\phi_l = 0^\circ$; $\phi_r = 0^\circ$; $\omega_c = 0.05$	15
Effect of slot injection on internal performance. Aft slot injection; $\phi_l = 0^\circ$; $\phi_r = 0^\circ$; $\omega_c = 0.05$	16
Effect of slot injection corrected weight flow ratio on pitch thrust vector angle. $\phi_l = 0^\circ$; $\phi_r = 0^\circ$; $\omega_c = 0.05$	17
Lateral static pressure ratio distributions on upstream and downstream sides of injection slot. $\phi_l = 0^\circ$; $\phi_r = 0^\circ$; $\omega_c = 0.05$	18
Upper flap centerline static pressure ratios upstream and downstream of injection slot. $\phi_l = 0^\circ$; $\phi_r = 0^\circ$; $\omega_c = 0.05$	19
Sidewall static pressure ratio distributions between nozzle geometric throat and injection slot. $\phi_l = 0^\circ$; $\phi_r = 0^\circ$; $\omega_c = 0.05$	20
Lower flap static pressure ratio distributions between nozzle geometric throat and injection slot. $\phi_l = 0^\circ$; $\phi_r = 0^\circ$; $\omega_c = 0.05$	21

Discussion of Results

Supply pressure requirements for pumping the secondary flow, expressed as a ratio of secondary total pressure to primary total pressure, are presented in figures 8 and 9. Estimated port areas for the secondary flow are 0.182 in² per side for the Coanda ports and 0.192 in² for the injection slot. Total pressure for the Coanda ports was measured in the plenum immediately upstream of the injection port. However, total pressure for the slot-injected flow immediately upstream of the slot was not available. Therefore, total pressure was obtained at the venturi located in the plumbing leading to the injection slot. Some loss in total pressure likely occurred between the venturi and the slot. However, the loss was probably small enough to provide a realistic estimate of the supply requirements for slot injection.

Secondary total pressure requirements were nearly constant with primary jet NPR, yet were large enough so that a high-pressure supply source such as the engine compressor or some alternate pump would be required for application to flight. The combination of high pressure and high weight flow, if supplied by the engine, might cause a significant penalty on overall system performance. The supply pressure is a function of the injection port area, so that increasing the area would reduce the pressure requirement to provide the same weight flow ratio.

Coanda Thrust Vectoring

Basic performance data for the fluidic nozzle with various Coanda flap angle settings are presented in figure 10. Left and right side Coanda injection port flows were set at equal corrected secondary weight flow ratios of 0.05 (5 percent of primary weight flow per side). Slot injection flow from the divergent flap was shut off for the Coanda thrust-vectoring portion of the investigation, and the slot cavity was not vented to atmosphere.

Nozzle thrust efficiency is typically evaluated by examining the axial and resultant thrust ratios. The thrust ratio curves in figure 10 show typical performance for a C-D nozzle (refs. 9 and 10). Fixed area ratio C-D nozzles reach peak efficiency at the design NPR, $(NPR)_{des}$, which is a function of the exit-to-throat area ratio ϵ and the condition for which the nozzle fully expands the flow to match ambient static pressure at the exit plane with no internal shocks. Large thrust losses are generally incurred at pressure ratios below the design NPR as a result of a pressure mismatch with ambient conditions at the exit plane; the nozzle is overexpanded, resulting in below-ambient pressure, which produces internal drag on

the nozzle divergent flaps. Thrust losses above design NPR are associated with underexpansion of the flow and represent the momentum thrust lost by not fully accelerating the flow through expansion within the nozzle.

The design NPR's based on the expansion ratios of $\epsilon = 1.502$, 1.944, and 2.405 are 6.26, 10.12, and 14.64, respectively. The NPR of the actual peak performance, however, is typically slightly higher in nozzles due to viscous effects. The test NPR range was limited by facility constraints to 2 to 10, which excluded the design condition for the $\epsilon = 2.405$ nozzle.

In the case of the nozzle data presented in figure 10, the nozzles were predominantly overexpanded, with performance improving as design NPR was approached. The reversal in thrust performance of the $\epsilon = 2.405$ nozzle at low NPR corresponds to the internal normal shock progressing through the nozzle and reaching the exit plane. This thrust behavior is predicted by one-dimensional inviscid nozzle theory and does not necessarily indicate internal flow separation from the divergent flaps (ref. 11).

Small variations in thrust ratio occurred with the deflection of the Coanda flaps. At pressure ratios near the design NPR, deflecting the right Coanda flap outward resulted in a 0.5 to 1 percent loss in resultant thrust. Deflecting the left flap inward resulted in an additional 0.5 to 1 percent loss. This deflection of the flap into supersonic flow would result in the formation of an oblique shock which would cause compression on the forward facing flap, resulting in an internal drag force on the nozzle. A longer flap should therefore produce more drag than a shorter flap because of increased projected area.

Discharge coefficient w_p/w_i , as expected, was not affected by variations in Coanda flap angle. The discharge coefficient is a measure of the efficiency at which the nozzle discharges exhaust flow. For a C-D nozzle, this characteristic is fixed once the sonic plane, or throat, is established in the nozzle. The throat is immune to all but the most significant downstream influences, as will be seen in the discussion of slot injection later in the report.

Yaw thrust vector angle is used as a measure of thrust-vectoring ability, and in the case of the Coanda thrust-vectoring configurations in this report, negative δ_y denotes the intended direction of thrust vectoring. As seen in figure 10, yaw thrust vector angles were generally small, below 3° at NPR > 2. The largest thrust vector angle occurred at NPR = 2, where approximately 4° of vectoring was achieved by

the $\varepsilon = 1.944$ nozzle without deflecting the left flap inward. At this condition, the primary jet momentum near the Coanda flaps is relatively small and therefore more susceptible to influence by the pressure gradient from the Coanda effect between the secondary jet and the sidewall. Achieving significant thrust vector angles even at $\text{NPR} = 2$ was probably hindered by the large aspect ratio of the nozzle (throat width-to-height ratio of 4.015).

Deflecting the left flap 10° inboard generally increased the vector angle by 1° to 2° , but this additional turning was more likely attributable to the oblique shock discussed earlier rather than improved Coanda turning. No significant improvements in overall performance were noted.

Significant nonzero pitch thrust vector angles δ_p occurred at $\text{NPR} = 2$, particularly for the $\varepsilon = 1.944$ nozzle (fig. 10(b)). This pitch vectoring was most likely a result of the open injection slot cavity influencing the boundary layer of the primary jet. Boundary-layer separation generally occurs in highly overexpanded nozzles and is usually unstable and sensitive to external influence. Asymmetric separation on the upper and lower divergent flaps, potentially caused in this case by the injection slot cavity, could result in significant pitch thrust vector angles, as may have been the case for the $\varepsilon = 1.944$ nozzle, for which the effect was extreme.

Basic performance data for the nozzle with left and right flaps fixed at 0° and 30° , respectively, are presented in figure 11 with total corrected secondary flow ratio varied from 0 to approximately 0.2. Increasing secondary flow ratio over this range resulted in approximately a 3-percent reduction in axial thrust ratio. Schlieren photography, shown in figure 22(c), reveals the formation of complex oblique shock patterns emanating from the regions of primary and secondary jet interaction, which may have contributed to the loss in thrust efficiency. Another contributor may be that the secondary jets were not operating at their design condition. Examination of the tabulated data shows that the secondary jets were operating below the design pressure ratio of approximately 8.25, calculated from the port expansion ratio, resulting in less than ideal secondary thrust. Once again, discharge coefficient was not affected by injecting secondary flow downstream of the nozzle throat.

Increasing the secondary flow ratio increased yaw thrust vector angle at $\text{NPR} < 6.0$. However, even at low NPR, the largest thrust vector angle produced was no greater than 6° . Furthermore, thrust-vectoring effectiveness rapidly diminished as NPR

was increased. Thrust vector angles of the magnitude attained at low NPR, if sustained, might be sufficient for aircraft trim but are probably not large enough for maneuvering an aircraft.

A comparison of yaw thrust vector angle between similar configurations with short and long Coanda flaps is presented in figure 12. Increasing the flap length offered no substantial improvement in thrust vectoring. For the $\varepsilon = 1.502$ nozzle with $\phi_r = 30^\circ$, small increases in thrust vectoring (less than 2°) were achieved by lengthening the flaps. More significant effects on the thrust vector angles of the $\varepsilon = 2.405$ nozzle were noted, including some reversal in vectoring direction ($\delta_y > 0^\circ$), although no overall improvement was achieved.

The effect of varying corrected secondary weight flow ratio on the yaw thrust vector angle is presented in figure 13. At $\text{NPR} = 2$, the only condition where marginally effective thrust vectoring was observed, thrust vector angle increased with increasing secondary flow ratio. The $\varepsilon = 1.944$ nozzle, at $\text{NPR} = 2$, achieved larger yaw vector angles throughout the range of secondary flow ratios, including the condition of no secondary flow, which suggests that the Coanda effect was acting directly on the primary jet at $\text{NPR} = 2$. This behavior does not occur at $\text{NPR} = 4$. The reason the $\varepsilon = 1.944$ nozzle was affected in this way and not the $\varepsilon = 1.502$ or $\varepsilon = 2.405$ nozzles is not understood, but probably is related to the location of the injection slot in the divergent flap and its effect on internal flow separation.

Static pressure distributions along the left and right Coanda flaps are presented in figure 14 for the $\varepsilon = 1.502$ nozzle. The distributions for the $\varepsilon = 1.944$ and $\varepsilon = 2.405$ nozzles were similar and are therefore not presented. At $\text{NPR} = 2$ (fig. 14(a)), the pressure distributions for the nozzle with the $0^\circ/0^\circ$ flap combination were essentially level at ambient conditions and serve as a baseline for observing the effect of flap deflections. As the right Coanda flap was turned outboard to 30° or 45° , a low-pressure region was formed along the right flap surface when the secondary injection flow was on. This low-pressure region draws the injected flow toward the flap and, in fact, is the mechanism for the Coanda effect. As flow rate was increased, the pressure in this region decreased, thereby increasing the strength of the Coanda effect and the magnitude (although small) of the thrust vector angle.

The pressure distribution on the left flap remained unchanged until the flap was deflected inboard. In this case, a high-pressure region, associated with the compression from an oblique shock, was

formed and provided mechanical thrust vectoring as well as nozzle internal drag.

As NPR was increased to 4 and then to 6 (figs. 14(b) and 14(c)), the pressure deficit on the right flap disappeared, indicating that the Coanda effect was no longer occurring. The local compression regions on the right and left flaps were probably the result of flow interactions between the primary jet and the secondary injected flow.

Slot Injection Thrust Vectoring

Basic performance data are presented in figures 15 and 16 for the forward and aft slot injection configurations. The Coanda flaps were fixed at 0° (no yaw vectoring) and sidewall secondary flow was maintained at $\omega_c = 0.05$ to prevent recirculation into the Coanda injection ports.

As corrected injection flow ratio ω_{si} was increased, overall thrust performance, as indicated by F_r/F_i , was improved at low NPR but was reduced at NPR greater than approximately half of the design NPR. The improvement at low NPR was a result of reduced nozzle overexpansion losses. As discussed earlier, resultant thrust ratio for CD nozzles operating below the design NPR is reduced because the low pressure at the exit plane caused by overexpansion of flow in the divergent channel reduces the thrust of the nozzle. Injecting flow into the divergent channel reduces the nozzle internal volume available for primary flow expansion. As a result, as more flow is injected, the overexpansion of the primary flow is reduced, and the losses associated with overexpansion diminish.

The reduction in resultant thrust ratio at higher NPR's with increasing ω_{si} is probably a result of losses through an oblique shock which forms as a result of the slot-injected flow. Losses associated with the nonaxial direction of the slot injection are minimal, as can be seen by comparing the axial and resultant thrust ratios. The flow physics resulting from the injection of sonic flow perpendicularly into a supersonic stream has been extensively studied and well documented (refs. 12 to 17). The injected flow has been compared to a forward-facing step situated in the supersonic stream in that it produces a similar flow field ahead of the obstruction (ref. 13). The obstruction in either case causes the boundary layer upstream of the obstruction to separate with an oblique separation shock forming at the separation point and extending into the free stream. In the current investigation, this oblique shock was intended to turn the primary jet and create pitch thrust vectoring. The oblique shock, however, also slows the primary

flow, reducing the exit momentum and therefore the thrust. As secondary injection is increased, the shock angle (between the shock and the divergent wall) and momentum losses increase, resulting in lower resultant thrust ratios near the design NPR, as seen in figures 15 and 16. The increase in shock angle can be seen in the oil flow photographs in figure 25. As secondary injection is increased, the separation line upstream of the slot moves forward, shifting the shock upstream into jet flow of lower Mach number. This reduction in Mach number, as well as the increased secondary flow obstruction, would result in an increase in shock angle (shock becomes more normal to flow).

The discharge coefficient w_p/w_i was generally constant with NPR and was not affected by varying the injection flow rate except at NPR = 2. At this condition, high secondary flow ratios resulted in a reduction of as much as 6 percent in weight flow. As will be shown with plots of internal static pressure measurements, the slot injection changed the internal flow field at NPR = 2 to such an extent that the location of the sonic plane, normally near the geometric throat, was altered. The adverse effect on discharge coefficient was reduced as expansion ratio was increased or injection location was moved aft.

As seen in figures 15 and 16, significant levels of pitch thrust vectoring were achieved by the slot injection method. The largest angles measured were approximately 19° at NPR = 2 (fig. 15(c), $\epsilon = 2.405$, forward injection) and approximately 9° at NPR = 10 (fig. 16(b), $\epsilon = 1.944$, aft injection). The largest angles tended to occur at lower NPR's. Generally, larger thrust vector angles are required at low NPR than at high NPR, which corresponds to low-Mach-number flight and high-Mach-number flight, respectively; most high-angle-of-attack maneuvering occurs at low Mach numbers. However, because of overexpansion losses for a fixed aperture nozzle at low NPR, large thrust losses also occur at low NPR. These losses may be too large for consideration of a fluidic thrust-vectoring, fixed-aperture nozzle flight application. It may be possible, however, to control overexpansion losses by symmetric injection from both flaps.

For a given corrected injection flow ratio, as NPR was increased, pitch thrust vector angle tended to decrease to a plateau level and then remain constant. This plateau was not reached for the aft injection location at the higher injection flow ratios for the NPR range tested. The pitch thrust vector angles for these flow ratios, however, are expected to also level off at higher NPR's.

In several of the configurations, a nonzero pitch thrust vector angle was measured for the case of no injected secondary flow. It is possible that the slot itself altered the flow field either by providing a cavity for pressure relief or by causing boundary-layer separation to occur at the slot, as discussed earlier. Both positive and negative pitch thrust vector angles were measured at this condition, so the effect does not appear to be consistent.

The effect of varying corrected injection flow ratio on pitch thrust vector angle is shown in figure 17 at NPR = 4 and NPR = 8. The $\varepsilon = 1.502$ configuration experienced a reversal of pitch vectoring as injection flow ratio was increased, resulting in negative thrust vector angles being produced at the higher corrected injection flow ratios. Surface flow visualization through the use of an oil-based paint flow technique, as shown in figure 25, revealed impingement of the oblique shock on the lower (unslotted) divergent flap. The shock impingement resulted in a “reflected” shock which turned the primary jet back towards the upper (slotted) divergent flap, reversing the direction of thrust vectoring. The $\varepsilon = 1.944$ nozzle with forward injection also appeared to experience a reversal at the highest injection flow ratios. The $\varepsilon = 2.405$ nozzle had no tendency to reverse its vectoring direction, indicating that shock impingement did not occur on the lower flap for the range of parameters tested.

Shifting the injection slot aft resulted in more linear control of pitch thrust vector angle by varying corrected injection flow ratio without reducing the attainable range of vector angles (except for the $\varepsilon = 1.502$ nozzle). Shock impingement on the lower flap (i.e., thrust vectoring reversal) appeared to be delayed to higher secondary flow ratios as indicated by the $\varepsilon = 1.502$ nozzle data in figure 17(b). This result was expected because shifting the injection slot downstream would shift the oblique shock flow field downstream such that shock impingement on the unslotted flap would be less likely to occur. Fortunately, no degradation in thrust vectoring accompanies this shift.

Lateral static pressure ratio distributions immediately upstream and downstream of the injection slot are presented in figure 18. The profiles show predominantly two-dimensional flow with the exception of the lowest nonzero injection flow ratio ($\omega_{si} \approx 0.024$) where some pressure relief around the edge of the slot is evident.

A summary of the upper flap centerline pressure measurements upstream and downstream of the slot is presented in figure 19. As secondary injection was

initiated, a high-pressure region formed upstream of the slot, which in all cases (with flow injection on) was higher than the pressure downstream of the slot. This behavior is in agreement with data from earlier studies of flow injection into a supersonic stream (refs. 12 to 15). According to those studies, the region of lower pressure downstream of the injection slot causes the secondary flow to attach to the aft portion of the flap, and a rapid pressure recovery is achieved to levels slightly higher than the pressure levels that would occur in the absence of secondary injection.

In the present investigation, subambient pressure levels ($p/p_{t,j}$ less than inverse of NPR: 0.25 for NPR = 4 and 0.125 for NPR = 8) were observed downstream of the slot (see fig. 19) for all configurations at various conditions. Previous studies on secondary injection into supersonic streams show that this low-pressure region is followed by a recovery to pressure levels greater than ambient (refs. 12 to 15). However, ambient static pressure ratios ($p/p_{t,j}$ equal to inverse of NPR: 0.25 for NPR = 4 and 0.125 for NPR = 8) were observed for most configurations at the higher injection flow ratios, indicating possibly separated flow downstream of the slot. The desirable flow condition would be attachment of the injected flow as rapidly as possible, rather than fully separated flow, to gain the most thrust benefit from the pressure overshoot in the recovery.

Additional static pressure distributions are presented in figures 20 and 21. Sidewall longitudinal centerline pressure distributions between the geometric throat and the slot station are presented in figure 20 and show the upstream influence of the injection flow. Recall that variations in discharge coefficient were observed with changes in corrected injection flow ratio at low NPR. (See figs. 15 and 16.) Pressure distributions in figure 20 show that the nozzle choke location (sonic velocity, $p/p_{t,j} = 0.5283$) was shifted for the flow combinations of high corrected injection flow ratio and low primary NPR for the $\varepsilon = 1.502$ nozzle. For these conditions, the effective internal contour of the divergent channel was significantly altered, causing the throat location (and area) to change. The $\varepsilon = 1.944$ and $\varepsilon = 2.405$ nozzles were not affected as significantly, although some secondary flow injection influence in the pressure distributions was still evident. It should also be noted that the location of sonic velocity on the sidewall occurs downstream of the geometric throat location (first pressure orifice) for all configurations and flow conditions tested (except for the low NPR, high ω_{si} conditions of the $\varepsilon = 1.502$ nozzle, where sonic velocity was not reached at any of the pressure taps).

Lower flap longitudinal pressure distributions are presented in figure 21. The pressure orifices on the lower flap are at the same longitudinal positions as the sidewall pressure orifices shown in figure 20. Comparison of the distributions in figures 20 and 21 reveals that the sonic line shape (effective throat) was nonplanar; the sonic velocity location on the lower flap apparently occurs upstream of the geometric throat location for all configurations tested. This behavior has been documented for 2-D C-D nozzles through the use of extensive internal pressure measurements and internal flow visualization (ref. 11).

Adverse influence of injected flow on the flow field upstream of the slot was seen primarily at $NPR = 2$ (fig. 21(a)), where subsonic regions appear downstream of a local supersonic region at the geometric throat. Not enough pressure measurements were made to determine the effect on the nozzle throat, although the discharge coefficient data suggested it was adversely affected. In the case of the $\epsilon = 1.502$ nozzle with forward injection, a compression was measured between the second and third orifices at the highest injection flow ratios for $NPR > 2$. This compression was caused by the impingement of the oblique shock between the taps and confirmed by oil-based paint flow visualization, as shown in figure 25.

Conclusions

An investigation was conducted in the static test facility of the Langley 16-Foot Transonic Tunnel of two thrust-vectoring concepts which utilize fluidic mechanisms for deflecting the jet of a two-dimensional convergent-divergent nozzle. One concept involved using the Coanda effect to turn a sheet of injected secondary flow along a curved sidewall flap and, through entrainment, draw the primary jet in the same direction to produce yaw thrust vectoring. The other concept involved deflecting the primary jet to produce pitch thrust vectoring by injecting secondary air through a transverse slot in the divergent flap and creating an oblique shock extending into the divergent channel. Geometric variables included nozzle expansion ratio, sidewall flap angles, and injection slot location. Fluidic variables included varying nozzle pressure ratio (NPR) from 2 to 10 and

varying secondary weight flow from 0 to 20 percent of the primary weight flow (0 to 10 percent for the divergent flap slot injection). Acquired data included forces and moments produced by the nozzle, internal static pressure measurements, and limited flow visualization. Based on the discussion of results, the following conclusions are made:

1. Using the Coanda effect with secondary flow to produce yaw thrust vectoring was largely unsuccessful. The largest thrust vector angles were produced at low NPR, where the primary jet momentum was minimal near the sidewall flaps. At higher NPR, the pressure gradient on the curved flap which drives the Coanda effect disappeared. The high aspect ratio of the nozzle may have hindered the effectiveness of this fluidic vectoring concept.
2. Significant pitch thrust vector angles (approximately 10° to 20°) were achieved by injecting secondary flow through a transverse slot in the divergent channel. The largest angles were generally produced at low NPR. However, reasonable levels were maintained throughout the range of pressure ratios tested. Secondary flow supply pressure requirements were high.
3. Increasing the corrected secondary-to-primary weight flow ratio of the slot-injected flow produced an increase in thrust vector angle. Moving the slot injection location aft improved the linearity of pitch thrust vector angle with increasing secondary flow and caused no degradation in the maximum thrust vector angle achievable.
4. Impingement of an oblique shock on the opposite divergent flap caused the pitch thrust vector angle to decrease as the secondary flow ratio increased. Impingement occurred in nozzles with low expansion ratio combined with forward injection slot locations. Increasing secondary flow ratio also moved the shock impingement location upstream.

NASA Langley Research Center
Hampton, VA 23681-0001
September 23, 1994

Appendix A

Flow Visualization of Coanda Thrust Vectoring

Flow visualization of Coanda thrust vectoring is presented in the following figures:

	Figure
Focusing schlieren photographs showing top view of nozzle for $\varepsilon = 1.502$ and NPR = 6.4 at	
$\phi_l = 0^\circ; \phi_r = 0^\circ; \omega_c = 0.$	22(a)
$\phi_l = 0^\circ; \phi_r = 0^\circ; \omega_c = 0.20.$	22(b)
$\phi_l = 0^\circ; \phi_r = 30^\circ; \omega_c = 0.20.$	22(c)
$\phi_l = -10^\circ; \phi_r = 30^\circ; \omega_c = 0.20.$	22(d)
Photographs showing surface flow patterns on Coanda flaps for $\varepsilon = 1.502$ and NPR = 6.4 at	
$\phi_l = 0^\circ; \phi_r = 0^\circ; \omega_c = 0.20.$	23(a)
$\phi_l = 0^\circ; \phi_r = 30^\circ; \omega_c = 0.20.$	23(b)
$\phi_l = -10^\circ; \phi_r = 30^\circ; \omega_c = 0.20.$	23(c)
$\phi_l = -10^\circ; \phi_r = 30^\circ; \omega_c = 0.20;$ fences installed.	23(d)

Focusing schlieren photographs of the nozzle with the Coanda thrust-vectoring concept are shown in figure 22. The images shown are top views focused on the nozzle centerline with the flow direction from left to right. A description of the focusing schlieren flow visualization technique can be found in reference 18.

Figure 22(a) shows the $0^\circ/0^\circ$ (left/right) flap angle combination on the $\varepsilon = 1.502$ nozzle operating on-design without secondary flow. A symmetric pair of intersecting shocks can be seen which probably emanated from the impingement of the primary jet on the sidewall just downstream of the injection ports. The same configuration with a secondary flow ratio of 0.10 on each side is shown in figure 22(b).

The shock pattern represents the complex interaction of three flow streams with each other and the nozzle surfaces, and some asymmetry can be noted. In figure 22(c), the right flap has been set at 30° . A slight skewing of the shock profile was produced, but no significant turning of the primary jet is observed. In figure 22(d), the left flap is also deflected 10° inboard. An oblique shock emanating from the root of the left flap is evident as is some deflection of the primary jet.

Photographs of the Coanda flaps with surface flow patterns shown by an oil-based paint are shown in figure 23. The paint was a mixture of tempera, kerosene, linseed oil, and pigment. Paint was applied to the surfaces and allowed to dry with the nozzle operating at specified conditions. The photographs show the flaps of the $\varepsilon = 1.502$ nozzle after operating at an NPR near design with a secondary flow ratio of 0.10 on each side.

The flaps in figure 23(a) were set at $0^\circ/0^\circ$ and represent the baseline configuration for the set of photographs shown. Nozzle flow divergence is evident as well as the individual flow structures from the 10 injection ports on each side. In figure 23(b), the right flap was set at 30° . The flow over almost the entire right flap was separated with the separation line located just downstream of the second pressure orifice. This flow separation is evidence of the ineffectiveness of the Coanda vectoring technique. Figure 23(c) shows the surface flow field of the nozzle with the $-10^\circ/30^\circ$ flap combination. Strong impingement of the flow on the left flap dispersed most of the paint before it was able to dry. Figure 23(d) shows the $-10^\circ/30^\circ$ flap combination with fences installed. The right flap remained separated, although the vortical separated pattern seen in figure 23(b) disappeared.

Appendix B

Flow Visualization of Slot Injection Thrust Vectoring

Flow visualization of slot injection thrust vectoring is presented in the following figures:

	Figure
Focusing schlieren photographs showing side view of nozzle for NPR = 10.4 and forward slot injection at—	
$\varepsilon = 1.944; \omega_{si} = 0.$	24(a)
$\varepsilon = 1.944; \omega_{si} = 0.10.$	24(b)
$\varepsilon = 2.405; \omega_{si} = 0.$	24(c)
$\varepsilon = 2.405; \omega_{si} = 0.10.$	24(d)
Photographs showing internal surface flow patterns of nozzle with slot injection for $\varepsilon = 1.502$ and NPR = 6.4 at	
$\omega_{si} = 0.05$; forward injection.	25(a)
$\omega_{si} = 0.10$; forward injection.	25(b)
$\omega_{si} = 0.05$; aft injection.	25(c)
$\omega_{si} = 0.10$; aft injection.	25(d)
Photograph of nozzle used for internal schlieren flow visualization	26
Focusing schlieren photographs of internal flow field of 2-D C-D nozzle at NPR = 2 with—	
No slot injection.	27(a)
Secondary flow injected through upper flap.	27(b)

Focusing schlieren photographs of the external flow field of the nozzle with the slot injection thrust-vectoring concept are shown in figure 24. The photographs show a side view of the nozzle, focused on the nozzle centerline, with the primary jet flowing from left to right.

The $\varepsilon = 1.944$ nozzle with the aft injection slot is shown in figures 24(a) and 24(b) operating at NPR = 10.4 (near design). In figure 24(a), the injection flow is turned off, and in figure 24(b), the corrected injection flow ratio is 0.10. Similar photographs are shown in figures 24(c) and 24(d) for the $\varepsilon = 2.405$ nozzle with the aft injection slot. Primary jet deflection is clearly seen in both sets of photographs, as well as evidence of the artificially created oblique shock in the flow field.

Surface flow patterns of the $\varepsilon = 1.502$ nozzle employing slot injection and operating on-design are shown in figure 25 with the aid of the oil-based paint technique discussed in appendix A. The upper and lower flaps and one sidewall were painted. Assembled model photographs as well as photographs of the disassembled flaps are presented. Figure 25(a)

shows the forward injection slot configuration with a corrected secondary flow ratio of 0.05. In figure 25(b), the corrected secondary flow ratio is increased to 0.10. Similar photographs of the aft injection slot configuration are shown in figures 25(c) and 25(d).

The photographs of the internal sidewalls show the primary flow path deflecting away from the slot as intended. The oblique shock location can also be seen in some cases on the internal sidewall. The photographs of the upper and lower flaps show the separation line upstream of the slot on the upper flap and the shock impingement line on the lower flap. The exception is the aft injection configuration at a corrected secondary flow ratio of 0.05 shown in figure 25(c), where no shock impingement occurred. In figures 25(a) and 25(b), a comparison of separation line and shock impingement locations shows that increasing secondary flow rate not only shifts the shock forward but increases the angle (more normal) as well (impingement line shifted more than separation line). This angle increase is likely the result of a larger effective obstruction and a shift in the shock location upstream to nozzle flow of lower Mach number (closer to the geometric throat), which according to basic shock theory results in a larger shock angle (more normal to the primary flow).

To view the internal flow features of injecting flow into the divergent channel of a 2-D C-D nozzle, a divergent flap outfitted for secondary slot injection was installed on a similar nozzle having transparent sidewalls, shown in figure 26. This nozzle was not part of the current test matrix. Focusing schlieren photographs of the internal flow field of the nozzle operating at NPR = 2 are shown in figure 27. Although the determination of secondary-to-primary flow ratio was not possible at the time of the investigation, the combination of NPR = 2 and the available fixed flow rate of the injection flow appeared to provide a suitable ratio for observing the type of interaction likely present in the flow field of the current investigation.

In figure 27(a), secondary injection is turned off. In figure 27(b), secondary flow is injected through a slot in the upper divergent flap. Injecting secondary flow caused two shocks to form, a separation shock well upstream of the slot and a bow shock immediately upstream of the slot. These two shocks merged to form an oblique shock which impinged on the lower surface. A reflection shock is also evident and appears to terminate at the shear region between the primary jet (now deflected downward) and the injected flow near the top surface. This photograph verifies the flow field described in references 12 to 17 of flow injected laterally into a supersonic stream.

References

1. Bitten, R.; and Selmon, J.: Operational Benefits of Thrust Vector Control (TVC). *High-Angle-of-Attack Technology, Volume I*, Joseph R. Chambers, William P. Gilbert, and Luat T. Nguyen, eds., NASA CP-3149, Part 2, 1992, pp. 587-601.
2. Herbst, W. B.: Future Fighter Technologies. *J. Aircr.*, vol. 17, no. 8, Aug. 1980, pp. 561-566.
3. Coanda, H.: Procédé Propulsion Dans Un Fluide. Brevet Invent. Gr. Cl. 2, no. 762688 République Fran 1932.
4. Panitz, T.; and Wasan, D. T.: Flow Attachment to Solid Surfaces: The Coanda Effect. *AIChE J.*, vol. 18, no. 1, Jan. 1972, pp. 51-57.
5. Bevilaqua, Paul M.; and Lee, John D.: Design of a Supersonic Coanda Jet Nozzle. AIAA-84-0333, Jan. 1984.
6. Ahuja, K. K.: Controlling Plume Deflection by Acoustic Excitation—An Experimental Demonstration. AIAA-90-4006, Oct. 1990.
7. *A User's Guide to the Langley 16-Foot Transonic Tunnel Complex, Revision 1*. NASA TM-102750, 1990. (Supersedes NASA TM-83186.)
8. Mercer, Charles E.; Berrier, Bobby L.; Capone, Francis J.; and Grayston, Alan M.: *Data Reduction Formulas for the 16-Foot Transonic Tunnel NASA Langley Research Center, Revision 2*. NASA TM-107646, 1992.
9. Re, Richard J.; and Leavitt, Laurence D.: *Static Internal Performance Including Thrust Vectoring and Reversing of Two-Dimensional Convergent-Divergent Nozzles*. NASA TP-2253, 1984.
10. Berrier, Bobby L.; and Re, Richard J.: *Effect of Several Geometric Parameters on the Static Internal Performance of Three Nonaxisymmetric Nozzle Concepts*. NASA TP-1468, 1979.
11. Hunter, Craig Allen: An Experimental Analysis of Passive Shock-Boundary Layer Interaction Control for Improving the Off-Design Performance of Jet Exhaust Nozzles. M.S. Thesis, The George Washington Univ., 1993.
12. Spaid, F. W.; and Zukoski, E. E.: A Study of the Interaction of Gaseous Jets From Transverse Slots With Supersonic External Flows. *AIAA J.*, vol. 6, no. 2, Feb. 1968, pp. 205-212.
13. Werle, M. J.; Driftmyer, R. T.; and Shaffer, D. G.: Jet-Interaction-Induced Separation of Supersonic Turbulent Boundary Layers—The Two-Dimensional Problem. AIAA-70-765, June-July 1970.
14. Guhse, R. D.; and Thompson, H. Doyle: Some Aspects of Gaseous Secondary Injection With Application to Thrust Vector Control. AIAA-71-750, June 1971.
15. Aso, Shigeru; Okuyama, Satoshi; and Ando, Yasunori: Experimental Study on Interacting Flow Fields Induced by Normally Injected Secondary Flow Through a Slot Nozzle Into Supersonic Flow. *Memoirs Faculty Eng.*, Kyushu Univ., vol. 51, no. 1, Mar. 1991, pp. 53-62.
16. Fitzgerald, R. E.; and Kampe, R. F.: Boundary Layer TVC for Missile Applications. AIAA-83-1153, June 1983.
17. Azevedo, David: Measured Thrust Losses Associated With Secondary Air Injection Through Nozzle Walls. AIAA-91-2244, June 1991.
18. Weinstein, Leonard M.: An Improved Large-Field Focusing Schlieren System. AIAA-91-0567, Jan. 1991.

Table 1. List of Fluidic Nozzle Configurations
(a) Yaw thrust vectoring; Coanda thrust vectoring

Configuration	Slot location	Expansion ratio, ϵ	Slot injection flow ratio, ω_{si}	Coanda flap length	Coanda flap angles, ϕ_l/ϕ_r , deg	Coanda flow ratio, ω_c
1	Forward	1.502	0	Short	0/0	*0 to 0.2
2	↓	↓	↓	↓	0/30	↓
3	↓	↓	↓	↓	0/45	↓
4	↓	↓	↓	↓	-10/30	↓
5	↓	↓	↓	↓	-10/45	↓
6	↓	↓	↓	Long	0/0	↓
7	↓	↓	↓	↓	0/30	↓
8	↓	↓	↓	↓	0/45	↓
9	↓	↓	↓	↓	-10/30	↓
10	↓	↓	↓	↓	-10/45	↓
11	↓	1.944	↓	Short	0/0	↓
12	↓	↓	↓	↓	0/30	↓
13	↓	↓	↓	↓	0/45	↓
14	↓	↓	↓	↓	-10/30	↓
15	↓	↓	↓	↓	-10/45	↓
16	↓	2.405	↓	↓	0/0	↓
17	↓	↓	↓	↓	0/30	↓
18	↓	↓	↓	↓	0/45	↓
19	↓	↓	↓	↓	-10/30	↓
20	↓	↓	↓	↓	-10/45	↓
21	↓	↓	↓	Long	0/0	↓
22	↓	↓	↓	↓	0/30	↓
23	↓	↓	↓	↓	0/45	↓
24	↓	↓	↓	↓	-10/30	↓
25	↓	↓	↓	↓	-10/45	↓
26	↓	↓	↓	Long/fenced	0/0	↓
27	↓	↓	↓	↓	0/30	↓
28	↓	↓	↓	↓	0/45	↓
29	↓	↓	↓	↓	-10/30	↓
30	↓	↓	↓	↓	-10/45	↓

*Increased from 0 to 0.2 in increments of 0.05.

Table 1. Concluded

(b) Pitch and multiaxis thrust vectoring

Configuration	Slot location	Expansion ratio, ε	Geometric vector angle, $\delta_{v,p}$, deg	Slot injection flow ratio, ω_{si}	Coanda flap length	Coanda flap angles, ϕ_l/ϕ_r , deg	Coanda flow ratio, ω_c
Slot injection							
31	Forward	1.502	0	*0 to 0.1	Long	0/0	0
32	Forward	1.502	↓	↓	↓	↓	0.05, 0.1
33	Aft	1.502	↓	↓	↓	↓	0.05, 0.1
34	Forward	1.944	↓	↓	↓	↓	0
35	Forward	1.944	↓	↓	↓	↓	0.05, 0.1
36	Aft	1.944	↓	↓	↓	↓	0.05, 0.1
37	Forward	2.405	↓	↓	↓	↓	0
38	Forward	↓	↓	↓	↓	↓	0.05, 0.1
39	Aft	↓	↓	↓	↓	↓	0.05, 0.1
40	Forward	↓	↓	↓	Long/fenced	↓	0.05, 0.1
Combined slot injection and divergent flap deflection							
41	Forward	1.499	15.5	*0 to 0.1	Long	0/0	0.05, 0.1
42	Aft	1.499	15.5	↓	↓	↓	↓
43	Forward	1.952	7.75	↓	↓	↓	↓
44	Aft	1.952	7.75	↓	↓	↓	↓
45	Forward	2.172	4	↓	↓	↓	↓
46	Aft	2.172	4	↓	↓	↓	↓
Multiaxis thrust vectoring							
47	Aft	1.944	0	*0 to 0.1	Long	0/45	**0 to 0.2
48	↓	1.944	0	↓	↓	-10/45	↓
49	↓	1.944	0	↓	↓	-10/30	↓
50	↓	1.499	15.5	↓	↓	0/45	↓
51	↓	1.499	15.5	↓	↓	-10/45	↓
52	↓	1.499	15.5	↓	↓	-10/30	↓

*Increased from 0 to 0.1 in increments of 0.025.

**Increased from 0 to 0.2 in increments of 0.05.

Table 2. Dimensions of Fluidic Vectoring Nozzle Model

Configurations	ϵ	$\delta_{v,p}$, deg	θ_u , deg	θ_l , deg
1-10, 31-33	1.502	0	8.5	8.5
11-15, 34-36, 47-49	1.944	0	16	16
16-30, 37-40	2.405	0	24	24
45, 46	2.172	4	16	24
43, 44	1.952	7.75	8.5	24
41, 42, 50, 51, 52	1.499	15.5	-7	24

θ_u and θ_l , deg	Slot location	z_e , in.	L_f , in.	x_s , in.	z_p , in.	α_s , deg	β_s , deg
8.5	Forward	1.515	2.730	1.778	1.361	8.5	10.36
8.5	Aft	1.515	2.730	2.165	1.298	8.5	26.08
16	Forward	1.296	2.716	1.790	1.273	16	9.92
16	Aft	1.296	2.716	2.166	1.165	16	27.27
24	Forward	1.067	2.669	1.790	1.184	24	8.81
24	Aft	1.067	↓	2.147	1.024	24	27.83
-7	Forward	1.964	↓	1.778	1.549	-7	9.70
-7	Aft	1.964	↓	2.101	1.592	-7	22.34

Table 3. Internal Static Performance of Configuration 1

[$\epsilon = 1.502$; forward slot injection; short Coanda flaps; $\phi_l = 0^\circ$; $\phi_r = 0^\circ$]

NPR	ω_{si}	ω_c	$p_{t,si}/p_{t,j}$	$p_{t,c}/p_{t,j}$	F_r/F_i	F_a/F_i	δ_p	δ_y	w_p/w_i
2.002	0.000	0.000	0.308	0.496	0.8807	0.8803	1.73	0.37	0.9816
2.009	0.000	0.049	0.306	0.574	0.8738	0.8734	1.66	0.34	0.9806
2.010	0.000	0.097	0.306	1.040	0.8665	0.8661	1.67	0.28	0.9805
2.013	0.000	0.142	0.305	1.522	0.8667	0.8666	0.88	0.40	0.9805
2.009	0.000	0.188	0.306	2.015	0.8741	0.8740	0.96	0.57	0.9799
3.022	0.000	0.000	0.294	0.327	0.9302	0.9302	0.08	0.16	0.9796
3.036	0.000	0.049	0.294	0.526	0.9220	0.9220	0.16	0.22	0.9799
3.023	0.000	0.096	0.295	1.033	0.9187	0.9187	-0.15	0.37	0.9788
3.019	0.000	0.141	0.294	1.510	0.9196	0.9196	-0.36	0.42	0.9789
3.043	0.000	0.186	0.294	1.994	0.9226	0.9225	-0.37	0.38	0.9783
3.994	0.000	0.000	0.295	0.240	0.9498	0.9498	0.24	0.18	0.9781
3.990	0.000	0.049	0.294	0.522	0.9411	0.9411	0.18	0.15	0.9786
3.987	0.000	0.096	0.294	1.028	0.9406	0.9406	0.01	0.10	0.9777
4.017	0.000	0.138	0.293	1.480	0.9412	0.9412	-0.13	0.24	0.9791
3.999	0.000	0.000	0.295	0.240	0.9505	0.9505	0.11	0.21	0.9778
5.009	0.000	0.000	0.295	0.191	0.9661	0.9661	0.31	0.09	0.9783
5.000	0.000	0.049	0.294	0.524	0.9578	0.9578	0.18	0.05	0.9788
5.018	0.000	0.095	0.294	1.017	0.9592	0.9592	0.01	0.21	0.9783
5.024	0.000	0.139	0.294	1.486	0.9567	0.9567	-0.01	0.22	0.9781
5.006	0.000	0.184	0.294	1.965	0.9538	0.9538	0.04	0.17	0.9775
6.045	0.000	0.000	0.294	0.157	0.9744	0.9743	0.20	0.08	0.9786
6.052	0.000	0.048	0.294	0.511	0.9675	0.9675	0.16	0.05	0.9777
6.051	0.000	0.093	0.294	0.996	0.9662	0.9662	0.00	0.19	0.9775
6.054	0.000	0.138	0.294	1.478	0.9638	0.9638	-0.03	0.15	0.9772
6.044	0.000	0.183	0.294	1.954	0.9604	0.9604	-0.08	0.29	0.9772
6.986	0.000	0.000	0.294	0.136	0.9753	0.9753	0.20	0.07	0.9779
7.038	0.000	0.047	0.295	0.506	0.9707	0.9707	0.11	0.09	0.9777
7.013	0.000	0.094	0.295	1.000	0.9690	0.9690	-0.05	0.19	0.9772
6.980	0.000	0.140	0.294	1.495	0.9656	0.9656	-0.08	0.19	0.9772
7.003	0.000	0.183	0.294	1.944	0.9615	0.9615	0.03	0.35	0.9771
7.999	0.000	0.000	0.295	0.118	0.9756	0.9756	0.15	0.07	0.9772
8.044	0.000	0.046	0.294	0.489	0.9718	0.9718	0.06	0.12	0.9778
8.001	0.000	0.094	0.295	1.003	0.9699	0.9699	-0.06	0.19	0.9771
7.999	0.000	0.137	0.294	1.464	0.9658	0.9658	-0.07	0.23	0.9769
8.016	0.000	0.171	0.294	1.816	0.9627	0.9627	-0.03	0.30	0.9765
9.044	0.000	0.000	0.294	0.104	0.9751	0.9751	0.06	0.06	0.9769
9.042	0.000	0.048	0.294	0.514	0.9725	0.9725	0.03	0.14	0.9760
9.045	0.000	0.093	0.294	0.993	0.9702	0.9702	-0.10	0.19	0.9758
9.047	0.000	0.139	0.294	1.477	0.9650	0.9650	-0.06	0.27	0.9759
10.055	0.000	0.000	0.294	0.092	0.9728	0.9728	0.04	0.04	0.9773
10.040	0.000	0.047	0.294	0.505	0.9694	0.9694	-0.03	0.17	0.9769
10.046	0.000	0.092	0.294	0.983	0.9672	0.9672	-0.08	0.19	0.9764
10.048	0.000	0.135	0.294	1.435	0.9633	0.9633	-0.09	0.29	0.9761

Table 4. Internal Static Performance of Configuration 2

[$\epsilon = 1.502$; forward slot injection; short Coanda flaps; $\phi_i = 0^\circ$; $\phi_r = 30^\circ$]

NPR	ω_{si}	ω_c	$p_{t,si}/p_{t,j}$	$p_{t,c}/p_{t,j}$	F_r/F_i	F_d/F_i	δ_p	δ_y	w_p/w_i
2.023	0.000	0.000	0.301	0.490	0.8799	0.8798	0.83	0.07	0.9810
1.993	0.000	0.051	0.331	0.578	0.8774	0.8766	2.40	-0.31	0.9818
2.041	0.000	0.096	0.297	1.024	0.8641	0.8637	0.75	-1.44	0.9817
2.046	0.000	0.144	0.296	1.531	0.8632	0.8625	0.50	-2.22	0.9815
2.047	0.000	0.191	0.296	2.036	0.8601	0.8589	0.46	-2.93	0.9816
3.028	0.000	0.000	0.293	0.326	0.9304	0.9304	-0.07	0.09	0.9801
3.020	0.000	0.049	0.294	0.530	0.9206	0.9205	0.15	-0.57	0.9799
3.019	0.000	0.097	0.294	1.033	0.9112	0.9110	0.11	-1.37	0.9800
3.019	0.000	0.144	0.294	1.538	0.9083	0.9078	0.05	-1.90	0.9799
3.017	0.000	0.190	0.294	2.029	0.9096	0.9092	-0.20	-1.56	0.9797
4.012	0.000	0.000	0.294	0.243	0.9509	0.9509	0.26	0.10	0.9793
4.057	0.000	0.049	0.293	0.520	0.9388	0.9388	0.27	-0.38	0.9797
4.057	0.000	0.096	0.293	1.028	0.9344	0.9343	0.25	-0.66	0.9794
4.059	0.000	0.142	0.293	1.513	0.9345	0.9345	0.13	-0.08	0.9792
3.977	0.000	0.187	0.306	1.991	0.9336	0.9336	0.05	0.32	0.9783
5.009	0.000	0.000	0.293	0.194	0.9676	0.9676	0.33	0.07	0.9789
5.002	0.000	0.048	0.299	0.513	0.9550	0.9550	0.31	-0.38	0.9791
4.998	0.000	0.095	0.300	1.015	0.9514	0.9514	0.28	-0.23	0.9788
5.001	0.000	0.140	0.298	1.500	0.9506	0.9506	0.05	0.22	0.9785
5.003	0.000	0.186	0.295	1.982	0.9483	0.9482	0.04	0.40	0.9783
6.053	0.000	0.000	0.293	0.160	0.9729	0.9729	0.28	0.01	0.9788
6.058	0.000	0.048	0.294	0.509	0.9619	0.9619	0.19	-0.43	0.9786
6.058	0.000	0.094	0.294	1.009	0.9593	0.9593	0.09	-0.20	0.9784
6.060	0.000	0.140	0.294	1.495	0.9589	0.9589	0.03	0.21	0.9782
6.061	0.000	0.186	0.293	1.981	0.9562	0.9562	-0.02	0.31	0.9780
7.045	0.000	0.000	0.293	0.137	0.9761	0.9761	0.15	0.04	0.9782
7.044	0.000	0.047	0.293	0.504	0.9664	0.9663	0.19	-0.59	0.9781
7.047	0.000	0.093	0.293	0.997	0.9650	0.9650	0.00	-0.10	0.9779
7.049	0.000	0.139	0.293	1.487	0.9628	0.9628	-0.03	0.15	0.9777
7.053	0.000	0.185	0.293	1.966	0.9587	0.9587	0.01	0.19	0.9775
8.017	0.000	0.000	0.294	0.120	0.9760	0.9760	0.15	0.02	0.9779
8.037	0.000	0.048	0.294	0.518	0.9673	0.9672	0.04	-0.53	0.9778
8.043	0.000	0.092	0.294	0.988	0.9674	0.9674	0.03	-0.11	0.9776
8.041	0.000	0.139	0.294	1.482	0.9634	0.9634	-0.04	0.07	0.9773
8.046	0.000	0.170	0.294	1.812	0.9604	0.9604	-0.02	0.10	0.9770
9.030	0.000	0.000	0.294	0.106	0.9759	0.9759	0.11	0.02	0.9768
9.028	0.000	0.048	0.294	0.510	0.9684	0.9683	0.05	-0.52	0.9767
9.033	0.000	0.093	0.294	0.989	0.9674	0.9674	-0.04	-0.13	0.9762
9.036	0.000	0.139	0.294	1.481	0.9630	0.9630	-0.05	0.00	0.9759
10.032	0.000	0.000	0.294	0.095	0.9744	0.9744	0.04	0.02	0.9767
10.048	0.000	0.047	0.294	0.506	0.9676	0.9676	0.02	-0.53	0.9765
10.050	0.000	0.093	0.294	0.990	0.9672	0.9672	-0.07	-0.14	0.9761
10.053	0.000	0.137	0.294	1.460	0.9628	0.9628	-0.04	-0.06	0.9755

Table 5. Internal Static Performance of Configuration 3

[$\varepsilon = 1.502$; forward slot injection; short Coanda flaps; $\phi_l = 0^\circ$; $\phi_r = 45^\circ$]

NPR	ω_{st}	ω_c	$P_{t,si}/P_{t,j}$	$P_{t,r}/P_{t,j}$	F_r/F_i	F_a/F_i	δ_p	δ_y	w_p/w_i
2.021	0.000	0.000	0.301	0.491	0.8796	0.8794	1.35	0.44	0.9808
2.019	0.000	0.049	0.301	0.568	0.8788	0.8783	1.84	-0.14	0.9809
2.018	0.000	0.097	0.301	1.041	0.8609	0.8602	2.06	-1.27	0.9809
2.018	0.000	0.143	0.301	1.530	0.8507	0.8495	1.57	-2.60	0.9806
2.018	0.000	0.188	0.302	2.018	0.8452	0.8438	1.16	-3.09	0.9802
3.044	0.000	0.000	0.295	0.325	0.9330	0.9329	0.01	0.29	0.9792
3.043	0.000	0.048	0.294	0.520	0.9209	0.9209	0.26	-0.43	0.9792
3.042	0.000	0.094	0.295	1.009	0.9060	0.9058	-0.29	-1.22	0.9791
3.043	0.000	0.141	0.294	1.515	0.9069	0.9066	-0.30	-1.34	0.9789
3.043	0.000	0.185	0.294	1.983	0.9146	0.9146	-0.34	-0.61	0.9786
4.034	0.000	0.000	0.295	0.242	0.9526	0.9526	0.20	0.23	0.9784
4.034	0.000	0.048	0.294	0.510	0.9366	0.9366	0.09	-0.15	0.9789
4.036	0.000	0.094	0.294	1.008	0.9285	0.9285	-0.14	-0.51	0.9788
4.040	0.000	0.140	0.294	1.500	0.9355	0.9355	-0.19	0.43	0.9787
4.044	0.000	0.186	0.294	1.987	0.9360	0.9359	-0.14	0.62	0.9781
5.010	0.000	0.000	0.294	0.195	0.9699	0.9699	0.29	0.19	0.9787
5.009	0.000	0.048	0.294	0.515	0.9534	0.9534	0.21	-0.21	0.9787
5.010	0.000	0.094	0.294	1.004	0.9538	0.9538	0.01	0.16	0.9787
5.012	0.000	0.140	0.294	1.498	0.9542	0.9542	-0.05	0.47	0.9783
5.011	0.000	0.186	0.294	1.989	0.9530	0.9530	0.06	0.65	0.9780
6.052	0.000	0.000	0.294	0.161	0.9746	0.9746	0.10	0.10	0.9785
6.045	0.000	0.047	0.294	0.508	0.9611	0.9611	0.02	-0.29	0.9786
6.065	0.000	0.094	0.293	1.002	0.9625	0.9625	-0.06	0.18	0.9785
6.044	0.000	0.139	0.293	1.485	0.9634	0.9634	0.04	0.41	0.9778
6.037	0.000	0.185	0.294	1.967	0.9590	0.9589	-0.02	0.55	0.9775
7.047	0.000	0.000	0.294	0.138	0.9768	0.9768	0.06	0.08	0.9776
7.046	0.000	0.047	0.294	0.507	0.9652	0.9652	0.07	-0.44	0.9778
7.048	0.000	0.093	0.294	0.996	0.9671	0.9670	-0.08	0.14	0.9778
7.048	0.000	0.139	0.294	1.481	0.9653	0.9653	-0.11	0.36	0.9776
7.052	0.000	0.183	0.294	1.944	0.9625	0.9625	-0.10	0.42	0.9770
8.025	0.000	0.000	0.294	0.121	0.9768	0.9768	0.08	0.08	0.9775
8.023	0.000	0.048	0.294	0.512	0.9695	0.9695	0.03	-0.18	0.9775
8.023	0.000	0.092	0.294	0.986	0.9691	0.9691	-0.10	0.10	0.9772
8.028	0.000	0.138	0.294	1.470	0.9651	0.9651	-0.13	0.25	0.9769
8.029	0.000	0.171	0.294	1.819	0.9626	0.9625	-0.09	0.28	0.9767
9.044	0.000	0.000	0.294	0.107	0.9765	0.9765	0.05	0.05	0.9767
9.036	0.000	0.047	0.294	0.506	0.9707	0.9707	0.00	-0.23	0.9764
9.040	0.000	0.092	0.294	0.978	0.9687	0.9687	-0.13	0.05	0.9763
9.046	0.000	0.138	0.294	1.473	0.9656	0.9656	-0.10	0.13	0.9757
10.042	0.000	0.000	0.294	0.095	0.9741	0.9741	-0.05	0.05	0.9764
10.050	0.000	0.047	0.294	0.502	0.9691	0.9691	-0.03	-0.28	0.9763
10.053	0.000	0.092	0.294	0.985	0.9685	0.9685	-0.11	-0.02	0.9759
10.055	0.000	0.137	0.294	1.453	0.9647	0.9647	-0.09	0.10	0.9756

Table 6. Internal Static Performance of Configuration 4

[$\epsilon = 1.502$; forward slot injection; short Coanda flaps; $\phi_l = -10^\circ$; $\phi_r = 30^\circ$]

NPR	ω_{si}	ω_c	$p_{t,si}/p_{t,j}$	$p_{t,c}/p_{t,j}$	F_r/F_i	F_a/F_i	δ_p	δ_y	w_p/w_i
2.012	0.000	0.000	0.305	0.494	0.8823	0.8820	1.40	-0.46	0.9812
1.996	0.000	0.050	0.308	0.583	0.8735	0.8728	1.92	-1.10	0.9807
1.993	0.000	0.099	0.309	1.053	0.8603	0.8590	2.01	-2.51	0.9802
2.003	0.000	0.147	0.306	1.572	0.8621	0.8599	1.48	-3.73	0.9807
1.992	0.000	0.196	0.311	2.099	0.8621	0.8588	1.65	-4.80	0.9803
3.009	0.000	0.000	0.295	0.330	0.9330	0.9329	0.18	-0.13	0.9792
3.000	0.000	0.049	0.295	0.526	0.9224	0.9222	0.46	-1.17	0.9796
3.004	0.000	0.099	0.295	1.055	0.9137	0.9128	0.14	-2.47	0.9789
2.990	0.000	0.147	0.295	1.567	0.9113	0.9096	0.07	-3.48	0.9790
2.996	0.000	0.193	0.295	2.063	0.9122	0.9110	0.08	-3.00	0.9787
4.013	0.000	0.000	0.294	0.244	0.9553	0.9552	0.52	0.17	0.9787
4.018	0.000	0.050	0.293	0.532	0.9416	0.9415	0.44	-0.66	0.9789
3.991	0.000	0.099	0.295	1.059	0.9355	0.9351	0.28	-1.59	0.9779
3.988	0.000	0.146	0.294	1.559	0.9357	0.9355	0.23	-1.30	0.9779
3.986	0.000	0.193	0.295	2.059	0.9338	0.9336	0.16	-1.33	0.9780
5.009	0.000	0.000	0.293	0.196	0.9687	0.9687	0.29	0.07	0.9783
4.996	0.000	0.049	0.294	0.525	0.9566	0.9565	0.34	-0.80	0.9783
5.023	0.000	0.096	0.293	1.023	0.9547	0.9545	0.21	-1.21	0.9781
5.030	0.000	0.144	0.293	1.537	0.9525	0.9523	0.28	-1.12	0.9779
5.014	0.000	0.189	0.293	2.019	0.9483	0.9481	0.08	-1.25	0.9776
6.004	0.000	0.000	0.294	0.162	0.9734	0.9734	0.13	0.03	0.9775
5.991	0.000	0.048	0.294	0.518	0.9622	0.9621	0.10	-0.99	0.9775
5.989	0.000	0.097	0.294	1.034	0.9618	0.9616	0.10	-1.14	0.9774
6.005	0.000	0.143	0.294	1.521	0.9587	0.9585	0.08	-1.10	0.9773
5.984	0.000	0.191	0.294	2.029	0.9525	0.9523	0.10	-1.32	0.9770
7.041	0.000	0.000	0.293	0.137	0.9761	0.9761	0.18	-0.01	0.9775
7.015	0.000	0.048	0.294	0.511	0.9653	0.9651	0.17	-1.13	0.9769
7.030	0.000	0.097	0.294	1.035	0.9638	0.9636	0.10	-1.12	0.9771
7.041	0.000	0.141	0.293	1.505	0.9608	0.9606	0.04	-1.22	0.9769
7.031	0.000	0.190	0.293	2.019	0.9554	0.9552	0.03	-1.34	0.9764
8.031	0.000	0.000	0.294	0.120	0.9758	0.9758	0.13	0.02	0.9769
7.984	0.000	0.049	0.295	0.526	0.9669	0.9667	0.07	-1.13	0.9767
7.998	0.000	0.097	0.295	1.033	0.9650	0.9648	0.03	-1.10	0.9763
8.021	0.000	0.142	0.294	1.513	0.9602	0.9599	-0.02	-1.22	0.9763
7.993	0.000	0.174	0.294	1.846	0.9555	0.9552	0.00	-1.34	0.9760
9.042	0.000	0.000	0.294	0.107	0.9758	0.9758	0.09	-0.02	0.9754
9.002	0.000	0.049	0.295	0.526	0.9682	0.9680	0.05	-1.14	0.9754
9.047	0.000	0.095	0.294	1.019	0.9650	0.9648	0.05	-1.16	0.9756
9.037	0.000	0.143	0.294	1.517	0.9593	0.9590	-0.02	-1.26	0.9749
9.045	0.000	0.153	0.294	1.628	0.9573	0.9571	-0.01	-1.30	0.9751
10.024	0.000	0.000	0.295	0.097	0.9734	0.9734	0.03	-0.07	0.9754
10.035	0.000	0.048	0.294	0.520	0.9665	0.9662	0.04	-1.23	0.9758
10.036	0.000	0.095	0.294	1.017	0.9638	0.9636	-0.03	-1.18	0.9755
10.002	0.000	0.138	0.295	1.471	0.9575	0.9573	-0.10	-1.28	0.9750

Table 7. Internal Static Performance of Configuration 5

[$\varepsilon = 1.502$; forward slot injection; short Coanda flaps; $\phi_l = -10^\circ$; $\phi_r = 45^\circ$]

NPR	ω_{vi}	ω_i	$p_{t,sl}/p_{t,lj}$	$p_{t,sl}/p_{t,lj}$	F_r/F_i	F_d/F_i	δ_p	δ_s	κ_p/w_i
1.997	0.000	0.000	0.455	0.497	0.8870	0.8811	6.61	0.00	0.9799
2.002	0.000	0.048	0.307	0.576	0.8747	0.8736	2.64	-1.04	0.9794
2.001	0.000	0.095	0.307	1.019	0.8609	0.8590	2.99	-2.43	0.9795
2.007	0.000	0.142	0.305	1.528	0.8533	0.8504	2.42	-4.03	0.9796
2.003	0.000	0.188	0.307	2.012	0.8494	0.8451	2.35	-5.29	0.9797
3.016	0.000	0.000	0.294	0.329	0.9319	0.9319	0.37	0.04	0.9790
2.999	0.000	0.049	0.295	0.520	0.9214	0.9212	0.64	-1.15	0.9787
3.014	0.000	0.094	0.294	1.005	0.9090	0.9083	0.26	-2.34	0.9785
2.996	0.000	0.143	0.295	1.534	0.9060	0.9046	0.30	-3.26	0.9783
3.017	0.000	0.188	0.293	2.010	0.9188	0.9180	0.19	-2.34	0.9784
4.023	0.000	0.000	0.294	0.243	0.9528	0.9527	0.40	0.14	0.9785
4.035	0.000	0.049	0.294	0.525	0.9424	0.9423	0.46	-0.56	0.9785
3.980	0.000	0.096	0.294	1.032	0.9339	0.9336	0.38	-1.38	0.9781
3.975	0.000	0.146	0.294	1.564	0.9380	0.9378	0.30	-1.03	0.9776
4.036	0.000	0.188	0.293	2.010	0.9373	0.9370	0.32	-1.16	0.9782
5.011	0.000	0.000	0.293	0.195	0.9685	0.9685	0.45	0.06	0.9784
4.966	0.000	0.050	0.294	0.533	0.9546	0.9545	0.39	-0.74	0.9783
4.987	0.000	0.098	0.295	1.053	0.9555	0.9553	0.34	-0.93	0.9782
5.034	0.000	0.143	0.294	1.532	0.9550	0.9549	0.37	-0.94	0.9779
4.976	0.000	0.192	0.294	2.051	0.9510	0.9508	0.24	-1.14	0.9776
6.015	0.000	0.000	0.294	0.162	0.9743	0.9743	0.30	0.00	0.9777
6.024	0.000	0.049	0.293	0.527	0.9632	0.9631	0.19	-0.93	0.9780
6.031	0.000	0.095	0.293	1.018	0.9645	0.9644	0.17	-0.96	0.9780
6.026	0.000	0.142	0.293	1.514	0.9607	0.9606	0.15	-1.07	0.9777
6.020	0.000	0.188	0.293	2.006	0.9560	0.9558	0.06	-1.21	0.9771
7.047	0.000	0.000	0.293	0.138	0.9767	0.9767	0.20	0.03	0.9778
7.004	0.000	0.048	0.294	0.513	0.9652	0.9650	0.13	-1.03	0.9774
7.020	0.000	0.097	0.294	1.037	0.9665	0.9664	0.07	-0.95	0.9770
6.975	0.000	0.144	0.294	1.533	0.9627	0.9625	0.06	-1.09	0.9766
7.019	0.000	0.190	0.294	2.024	0.9565	0.9563	0.00	-1.27	0.9769
8.036	0.000	0.000	0.294	0.121	0.9765	0.9765	0.06	0.03	0.9769
7.981	0.000	0.048	0.294	0.511	0.9693	0.9692	0.05	-0.85	0.9767
8.019	0.000	0.096	0.294	1.028	0.9670	0.9669	0.00	-1.01	0.9768
8.042	0.000	0.141	0.294	1.507	0.9623	0.9621	-0.05	-1.13	0.9764
8.042	0.000	0.169	0.294	1.801	0.9585	0.9582	-0.06	-1.26	0.9761
9.033	0.000	0.000	0.294	0.108	0.9767	0.9767	0.03	0.01	0.9759
9.040	0.000	0.049	0.294	0.522	0.9695	0.9694	-0.01	-0.94	0.9760
9.037	0.000	0.095	0.294	1.016	0.9662	0.9660	-0.05	-1.04	0.9758
9.011	0.000	0.143	0.294	1.517	0.9607	0.9605	-0.08	-1.19	0.9755
9.031	0.000	0.153	0.294	1.625	0.9590	0.9587	-0.07	-1.25	0.9753
10.048	0.000	0.000	0.294	0.097	0.9743	0.9743	-0.03	-0.08	0.9759
10.052	0.000	0.048	0.294	0.517	0.9675	0.9673	-0.02	-1.04	0.9760
10.031	0.000	0.095	0.294	1.014	0.9645	0.9643	-0.09	-1.11	0.9760
10.036	0.000	0.136	0.294	1.448	0.9596	0.9594	-0.12	-1.22	0.9751

Table 8. Internal Static Performance of Configuration 6

[$\varepsilon = 1.502$; forward slot injection; long Coanda flaps; $\phi_t = 0^\circ$; $\phi_b = 0^\circ$]

NPR	ω_{st}	ω_c	$p_{t,s}/p_{t,j}$	$p_{t,c}/p_{t,j}$	F_j/F_i	F_d/F_i	δ_p	δ_y	w_p/w_j
2.003	0.000	0.000	0.305	0.497	0.8806	0.8800	2.02	0.57	0.9801
1.991	0.000	0.048	0.311	0.574	0.8764	0.8754	2.67	0.53	0.9797
1.994	0.000	0.097	0.308	1.033	0.8715	0.8709	2.00	0.48	0.9796
1.998	0.000	0.146	0.307	1.556	0.8718	0.8714	1.53	0.63	0.9797
1.998	0.000	0.193	0.306	2.062	0.8781	0.8778	1.21	0.55	0.9795
4.006	0.000	0.000	0.293	0.238	0.9506	0.9506	0.01	0.19	0.9783
4.001	0.000	0.049	0.293	0.529	0.9441	0.9441	0.11	0.19	0.9785
3.995	0.000	0.098	0.294	1.047	0.9428	0.9428	-0.07	0.25	0.9778
3.992	0.000	0.146	0.294	1.554	0.9440	0.9440	0.04	0.14	0.9776
4.014	0.000	0.190	0.293	2.029	0.9432	0.9432	0.03	0.03	0.9780
5.996	0.000	0.000	0.294	0.154	0.9724	0.9724	0.12	0.06	0.9778
5.995	0.000	0.049	0.294	0.529	0.9688	0.9688	0.03	0.11	0.9778
6.007	0.000	0.097	0.293	1.034	0.9676	0.9676	0.03	0.13	0.9777
6.008	0.000	0.144	0.293	1.541	0.9655	0.9655	0.05	0.13	0.9776
6.000	0.000	0.191	0.294	2.037	0.9611	0.9611	-0.02	0.16	0.9773
7.985	0.000	0.000	0.294	0.115	0.9772	0.9772	0.04	0.03	0.9774
8.011	0.000	0.049	0.294	0.525	0.9743	0.9743	0.03	0.14	0.9771
7.982	0.000	0.097	0.294	1.040	0.9717	0.9717	0.03	0.19	0.9769
8.005	0.000	0.144	0.294	1.532	0.9679	0.9679	0.03	0.23	0.9768
7.993	0.000	0.177	0.294	1.880	0.9642	0.9642	0.01	0.25	0.9766
10.002	0.000	0.000	0.294	0.093	0.9750	0.9750	0.07	0.14	0.9762
10.040	0.000	0.049	0.294	0.529	0.9723	0.9723	0.04	0.22	0.9762
10.008	0.000	0.097	0.294	1.035	0.9694	0.9694	0.00	0.22	0.9758
10.009	0.000	0.141	0.294	1.496	0.9647	0.9647	-0.02	0.25	0.9753

Table 9. Internal Static Performance of Configuration 7

[$\varepsilon = 1.502$; forward slot injection; long Coanda flaps; $\phi_l = 0^\circ$; $\phi_r = 30^\circ$]

NPR	ω_{N1}	ω_c	$p_{t,N1}/p_{t,j}$	$p_{t,d}/p_{t,j}$	F_p/F_t	F_d/F_t	δ_p	δ_y	w_p/w_t
1.996	0.000	0.000	0.308	0.497	0.8813	0.8809	1.62	-0.37	0.9812
1.998	0.000	0.051	0.306	0.579	0.8779	0.8773	2.02	-0.87	0.9807
1.994	0.000	0.100	0.307	1.064	0.8671	0.8661	2.06	-1.74	0.9806
1.986	0.000	0.149	0.322	1.591	0.8651	0.8633	2.52	-2.73	0.9808
1.993	0.000	0.197	0.307	2.109	0.8646	0.8624	1.96	-3.58	0.9803
4.004	0.000	0.000	0.294	0.242	0.9517	0.9517	0.35	0.25	0.9789
3.989	0.000	0.050	0.294	0.530	0.9399	0.9399	0.28	-0.55	0.9788
4.001	0.000	0.100	0.293	1.063	0.9358	0.9355	0.23	-1.24	0.9787
3.988	0.000	0.148	0.294	1.581	0.9305	0.9300	0.21	-1.79	0.9783
3.997	0.000	0.196	0.294	2.083	0.9251	0.9245	0.23	-2.04	0.9781
6.007	0.000	0.000	0.294	0.158	0.9739	0.9739	0.18	0.43	0.9783
6.002	0.000	0.050	0.294	0.531	0.9648	0.9648	0.25	-0.26	0.9779
5.992	0.000	0.099	0.294	1.054	0.9567	0.9566	0.16	-0.86	0.9778
6.001	0.000	0.146	0.294	1.554	0.9526	0.9525	0.12	-0.78	0.9775
6.007	0.000	0.192	0.293	2.049	0.9459	0.9458	0.09	-0.99	0.9775
7.996	0.000	0.000	0.294	0.118	0.9761	0.9761	0.19	0.22	0.9772
8.017	0.000	0.049	0.294	0.530	0.9678	0.9677	0.19	-0.63	0.9771
7.991	0.000	0.098	0.294	1.051	0.9598	0.9597	0.12	-1.03	0.9770
8.014	0.000	0.146	0.294	1.551	0.9552	0.9550	0.11	-1.13	0.9766
7.991	0.000	0.178	0.294	1.886	0.9498	0.9496	0.09	-1.13	0.9766
9.997	0.000	0.000	0.294	0.094	0.9731	0.9731	0.11	0.15	0.9760
10.037	0.000	0.049	0.294	0.523	0.9641	0.9640	0.03	-0.95	0.9759
9.939	0.000	0.098	0.294	1.044	0.9609	0.9607	0.04	-0.98	0.9755
9.984	0.000	0.142	0.294	1.505	0.9546	0.9544	0.01	-1.15	0.9751

Table 10. Internal Static Performance of Configuration 8

[$\epsilon = 1.502$; forward slot injection; long Coanda flaps; $\phi_l = 0^\circ$; $\phi_r = 45^\circ$]

NPR	ω_{si}	ω_c	$p_{t,s}/p_{t,j}$	$p_{t,c}/p_{t,j}$	F_r/F_i	F_d/F_i	δ_p	δ_y	w_p/w_i
2.020	0.000	0.000	0.301	0.492	0.8820	0.8816	1.62	0.00	0.9803
2.019	0.000	0.051	0.301	0.580	0.8767	0.8764	1.62	-0.46	0.9797
2.019	0.000	0.101	0.301	1.073	0.8594	0.8586	1.79	-1.71	0.9799
2.019	0.000	0.148	0.301	1.574	0.8531	0.8518	1.31	-2.84	0.9797
2.022	0.000	0.194	0.301	2.072	0.8462	0.8442	1.18	-3.80	0.9796
3.012	0.000	0.000	0.294	0.329	0.9341	0.9341	-0.02	0.16	0.9787
3.011	0.000	0.051	0.294	0.539	0.9222	0.9221	0.04	-0.72	0.9788
3.013	0.000	0.098	0.294	1.049	0.9111	0.9108	-0.14	-1.53	0.9786
3.014	0.000	0.145	0.294	1.551	0.9040	0.9034	-0.20	-2.20	0.9785
3.017	0.000	0.193	0.294	2.059	0.9135	0.9133	-0.33	-1.16	0.9783
4.000	0.000	0.000	0.293	0.243	0.9519	0.9518	0.16	0.44	0.9782
3.998	0.000	0.050	0.294	0.534	0.9389	0.9389	0.20	-0.38	0.9783
4.005	0.000	0.099	0.294	1.055	0.9308	0.9306	0.03	-1.06	0.9781
4.002	0.000	0.146	0.293	1.553	0.9339	0.9338	-0.04	-0.71	0.9781
4.004	0.000	0.194	0.294	2.067	0.9355	0.9355	-0.05	-0.18	0.9779
5.016	0.000	0.000	0.294	0.192	0.9686	0.9685	0.16	0.52	0.9782
5.019	0.000	0.050	0.294	0.532	0.9553	0.9552	0.22	-0.27	0.9783
5.020	0.000	0.097	0.294	1.042	0.9481	0.9480	0.11	-0.58	0.9783
5.021	0.000	0.146	0.294	1.559	0.9542	0.9542	-0.02	0.34	0.9782
5.024	0.000	0.193	0.294	2.057	0.9523	0.9523	0.06	0.64	0.9779
6.000	0.000	0.000	0.293	0.160	0.9744	0.9744	0.08	0.45	0.9781
5.998	0.000	0.048	0.294	0.516	0.9622	0.9622	0.11	-0.24	0.9781
6.002	0.000	0.098	0.293	1.048	0.9610	0.9610	0.02	-0.01	0.9780
5.999	0.000	0.144	0.294	1.536	0.9612	0.9612	-0.09	0.36	0.9779
6.002	0.000	0.190	0.294	2.024	0.9576	0.9576	-0.13	0.56	0.9777
7.002	0.000	0.000	0.293	0.137	0.9770	0.9770	0.10	0.33	0.9780
7.006	0.000	0.050	0.293	0.535	0.9650	0.9650	0.07	-0.39	0.9778
7.008	0.000	0.097	0.293	1.037	0.9669	0.9669	-0.08	0.09	0.9777
7.009	0.000	0.145	0.294	1.549	0.9645	0.9645	-0.12	0.28	0.9776
7.014	0.000	0.192	0.293	2.038	0.9598	0.9598	-0.14	0.42	0.9774
8.004	0.000	0.000	0.293	0.120	0.9764	0.9764	0.01	0.24	0.9772
7.999	0.000	0.049	0.294	0.524	0.9671	0.9671	0.06	-0.37	0.9775
8.000	0.000	0.097	0.294	1.036	0.9676	0.9676	-0.09	0.03	0.9773
7.995	0.000	0.145	0.294	1.543	0.9645	0.9645	-0.11	0.16	0.9772
7.992	0.000	0.177	0.294	1.879	0.9613	0.9613	-0.06	0.22	0.9769
9.016	0.000	0.000	0.294	0.106	0.9752	0.9752	0.03	0.24	0.9770
9.016	0.000	0.049	0.294	0.525	0.9678	0.9678	-0.03	-0.35	0.9771
9.022	0.000	0.097	0.294	1.039	0.9673	0.9673	-0.08	-0.08	0.9769
9.025	0.000	0.144	0.294	1.528	0.9634	0.9634	-0.12	0.03	0.9766
10.012	0.000	0.000	0.294	0.095	0.9741	0.9741	-0.03	0.15	0.9761
10.007	0.000	0.049	0.294	0.524	0.9673	0.9673	-0.05	-0.44	0.9763
10.002	0.000	0.097	0.294	1.038	0.9670	0.9670	-0.10	-0.20	0.9760
10.020	0.000	0.142	0.294	1.507	0.9622	0.9622	-0.11	-0.14	0.9756

Table 11. Internal Static Performance of Configuration 9

[$\epsilon = 1.502$; forward slot injection; long Coanda flaps; $\phi_l = -10^\circ$; $\phi_r = 30^\circ$]

NPR	ω_{si}	ω_c	$p_{t,si}/p_{t,j}$	$p_{t,c}/p_{t,j}$	F_r/F_i	F_d/F_i	δ_p	δ_s	w_p/w_i
2.006	0.000	0.000	0.305	0.496	0.8785	0.8778	2.23	-0.72	0.9800
1.999	0.000	0.049	0.307	0.577	0.8762	0.8752	2.37	-1.16	0.9807
1.997	0.000	0.097	0.308	1.036	0.8630	0.8615	2.24	-2.55	0.9800
1.996	0.000	0.149	0.308	1.595	0.8601	0.8578	1.58	-3.92	0.9799
1.996	0.000	0.194	0.308	2.077	0.8580	0.8543	1.60	-5.11	0.9800
2.997	0.000	0.000	0.294	0.331	0.9298	0.9297	0.04	-0.80	0.9788
2.997	0.000	0.050	0.294	0.536	0.9230	0.9227	0.16	-1.62	0.9788
2.998	0.000	0.098	0.294	1.046	0.9128	0.9116	-0.01	-2.89	0.9787
3.000	0.000	0.144	0.294	1.541	0.9080	0.9057	-0.17	-4.02	0.9783
3.000	0.000	0.192	0.295	2.048	0.9011	0.8979	-0.28	-4.83	0.9784
4.033	0.000	0.000	0.294	0.243	0.9529	0.9529	0.22	-0.25	0.9780
4.030	0.000	0.050	0.294	0.530	0.9404	0.9401	0.19	-1.37	0.9782
4.030	0.000	0.098	0.294	1.049	0.9346	0.9337	0.18	-2.58	0.9780
4.031	0.000	0.145	0.294	1.548	0.9254	0.9238	-0.04	-3.36	0.9779
4.031	0.000	0.193	0.294	2.064	0.9203	0.9183	-0.17	-3.78	0.9778
5.041	0.000	0.000	0.294	0.193	0.9694	0.9694	0.20	-0.17	0.9781
5.043	0.000	0.049	0.294	0.527	0.9564	0.9561	0.31	-1.33	0.9784
5.040	0.000	0.097	0.294	1.042	0.9489	0.9481	0.22	-2.36	0.9782
5.039	0.000	0.144	0.294	1.542	0.9391	0.9377	0.09	-3.10	0.9780
5.042	0.000	0.192	0.294	2.047	0.9394	0.9384	-0.01	-2.61	0.9779
6.028	0.000	0.000	0.294	0.161	0.9741	0.9741	0.13	-0.26	0.9780
6.024	0.000	0.048	0.294	0.511	0.9623	0.9620	0.10	-1.47	0.9780
6.027	0.000	0.097	0.294	1.037	0.9540	0.9530	0.04	-2.55	0.9780
6.027	0.000	0.145	0.294	1.552	0.9492	0.9483	-0.08	-2.56	0.9778
6.027	0.000	0.191	0.294	2.032	0.9399	0.9385	-0.13	-3.18	0.9774
7.049	0.000	0.000	0.293	0.137	0.9755	0.9754	0.06	-0.51	0.9777
7.050	0.000	0.048	0.294	0.511	0.9653	0.9649	0.10	-1.71	0.9778
7.060	0.000	0.098	0.294	1.042	0.9545	0.9534	-0.02	-2.82	0.9776
7.064	0.000	0.144	0.294	1.537	0.9492	0.9480	-0.05	-2.85	0.9773
7.014	0.000	0.192	0.294	2.039	0.9403	0.9387	-0.06	-3.28	0.9770
8.034	0.000	0.000	0.293	0.120	0.9759	0.9758	0.08	-0.69	0.9773
8.031	0.000	0.049	0.294	0.523	0.9648	0.9642	0.02	-1.99	0.9775
8.034	0.000	0.098	0.294	1.045	0.9561	0.9550	-0.08	-2.77	0.9774
8.029	0.000	0.145	0.294	1.550	0.9485	0.9472	-0.10	-3.09	0.9771
8.033	0.000	0.176	0.294	1.871	0.9433	0.9418	-0.10	-3.21	0.9767
8.989	0.000	0.000	0.294	0.107	0.9735	0.9733	0.05	-0.88	0.9772
8.992	0.000	0.049	0.294	0.530	0.9644	0.9637	-0.01	-2.18	0.9770
9.001	0.000	0.096	0.294	1.020	0.9560	0.9549	-0.06	-2.72	0.9769
8.997	0.000	0.144	0.294	1.534	0.9468	0.9454	-0.11	-3.12	0.9765
9.007	0.000	0.158	0.294	1.676	0.9452	0.9437	-0.06	-3.15	0.9764
10.012	0.000	0.000	0.294	0.096	0.9719	0.9717	-0.01	-1.01	0.9763
10.006	0.000	0.049	0.294	0.523	0.9612	0.9604	-0.04	-2.42	0.9763
10.009	0.000	0.098	0.294	1.045	0.9537	0.9526	-0.10	-2.78	0.9761
10.013	0.000	0.141	0.294	1.501	0.9462	0.9447	-0.06	-3.13	0.9758

Table 12. Internal Static Performance of Configuration 10

[$\varepsilon = 1.502$; forward slot injection; long Coanda flaps; $\phi_l = -10^\circ$; $\phi_r = 45^\circ$]

NPR	ω_{si}	ω_c	$p_{t,s}/p_{t,j}$	$p_{t,c}/p_{t,j}$	F_r/F_i	F_d/F_i	δ_p	δ_y	w_p/w_i
2.008	0.000	0.000	0.303	0.495	0.8765	0.8760	1.72	-0.96	0.9801
2.008	0.000	0.051	0.304	0.582	0.8739	0.8733	1.67	-1.43	0.9804
2.008	0.000	0.100	0.304	1.059	0.8571	0.8554	1.80	-3.11	0.9802
2.009	0.000	0.147	0.303	1.568	0.8490	0.8458	1.59	-4.73	0.9805
2.010	0.000	0.197	0.303	2.103	0.8441	0.8393	1.25	-6.01	0.9800
3.032	0.000	0.000	0.295	0.327	0.9310	0.9309	0.14	-0.77	0.9788
3.035	0.000	0.051	0.295	0.541	0.9214	0.9210	0.31	-1.72	0.9790
3.036	0.000	0.100	0.295	1.066	0.9084	0.9071	-0.01	-3.05	0.9788
3.036	0.000	0.145	0.295	1.546	0.9016	0.8992	-0.06	-4.18	0.9790
3.035	0.000	0.194	0.295	2.070	0.9097	0.9080	-0.21	-3.48	0.9786
4.021	0.000	0.000	0.294	0.244	0.9539	0.9538	0.30	-0.16	0.9785
4.017	0.000	0.050	0.294	0.530	0.9396	0.9394	0.31	-1.27	0.9783
4.018	0.000	0.098	0.294	1.047	0.9281	0.9271	0.12	-2.69	0.9784
4.019	0.000	0.145	0.294	1.553	0.9335	0.9327	-0.01	-2.35	0.9784
4.020	0.000	0.194	0.294	2.071	0.9333	0.9327	-0.03	-2.10	0.9781
4.999	0.000	0.000	0.294	0.195	0.9694	0.9693	0.27	-0.05	0.9784
5.037	0.000	0.048	0.294	0.517	0.9557	0.9555	0.30	-1.20	0.9787
5.035	0.000	0.098	0.294	1.048	0.9483	0.9477	0.23	-2.12	0.9787
5.040	0.000	0.147	0.294	1.568	0.9511	0.9507	0.08	-1.68	0.9781
5.040	0.000	0.191	0.294	2.040	0.9483	0.9479	-0.08	-1.57	0.9780
6.041	0.000	0.000	0.294	0.162	0.9754	0.9754	0.24	-0.20	0.9781
6.038	0.000	0.049	0.294	0.529	0.9610	0.9607	0.20	-1.43	0.9782
6.037	0.000	0.098	0.294	1.044	0.9592	0.9588	0.04	-1.72	0.9780
6.038	0.000	0.142	0.294	1.513	0.9571	0.9567	0.02	-1.68	0.9777
6.038	0.000	0.191	0.294	2.034	0.9532	0.9528	-0.04	-1.62	0.9776
7.010	0.000	0.000	0.294	0.140	0.9760	0.9760	0.17	-0.38	0.9777
7.004	0.000	0.048	0.294	0.514	0.9620	0.9616	0.06	-1.66	0.9778
7.003	0.000	0.098	0.294	1.048	0.9631	0.9627	0.00	-1.71	0.9778
7.006	0.000	0.143	0.294	1.525	0.9593	0.9588	-0.08	-1.71	0.9775
7.011	0.000	0.191	0.294	2.033	0.9526	0.9522	-0.06	-1.81	0.9773
8.032	0.000	0.000	0.294	0.122	0.9758	0.9758	0.12	-0.61	0.9773
8.032	0.000	0.047	0.294	0.501	0.9642	0.9638	0.10	-1.75	0.9774
8.042	0.000	0.097	0.294	1.040	0.9624	0.9619	-0.04	-1.84	0.9773
8.051	0.000	0.144	0.294	1.539	0.9579	0.9574	-0.05	-1.85	0.9769
8.056	0.000	0.166	0.294	1.769	0.9556	0.9551	0.03	-1.88	0.9770
9.020	0.000	0.000	0.294	0.109	0.9746	0.9745	0.13	-0.77	0.9769
9.033	0.000	0.050	0.294	0.537	0.9654	0.9649	0.06	-1.79	0.9768
9.029	0.000	0.096	0.294	1.027	0.9625	0.9620	-0.03	-1.90	0.9766
9.020	0.000	0.143	0.294	1.525	0.9567	0.9562	-0.02	-1.94	0.9763
9.996	0.000	0.000	0.294	0.098	0.9723	0.9722	0.10	-0.94	0.9763
10.010	0.000	0.050	0.295	0.530	0.9632	0.9627	-0.01	-1.88	0.9761
10.018	0.000	0.096	0.294	1.025	0.9605	0.9599	-0.06	-1.97	0.9759
10.031	0.000	0.133	0.294	1.420	0.9559	0.9553	0.00	-2.03	0.9757

Table 13. Internal Static Performance of Configuration 11

[$\varepsilon = 1.944$; forward slot injection; long Coanda flaps; $\phi_l = 0^\circ$; $\phi_r = 0^\circ$]

NPR	ω_{s1}	ω_c	$p_{t,s1}/p_{t,j}$	$p_{t,c}/p_{t,j}$	F_r/F_i	F_a/F_i	δ_p	δ_y	w_p/w_i
2.010	0.000	0.000	0.372	0.485	0.7991	0.7924	-7.39	-0.95	0.9663
2.009	0.000	0.052	0.361	0.579	0.7963	0.7885	-7.99	-0.72	0.9665
2.010	0.000	0.101	0.344	1.062	0.7829	0.7750	-8.16	0.13	0.9664
2.010	0.000	0.150	0.333	1.584	0.7917	0.7838	-8.06	0.54	0.9664
2.011	0.000	0.199	0.331	2.097	0.8027	0.7959	-7.41	0.82	0.9662
3.992	0.000	0.000	0.214	0.221	0.9077	0.9077	-0.06	0.13	0.9730
3.996	0.000	0.000	0.214	0.221	0.9080	0.9080	-0.07	0.05	0.9731
3.999	0.000	0.051	0.215	0.540	0.9036	0.9036	0.02	0.16	0.9731
4.000	0.000	0.099	0.215	1.056	0.9045	0.9045	-0.23	0.24	0.9728
4.001	0.000	0.148	0.215	1.577	0.9054	0.9054	-0.21	0.13	0.9729
4.002	0.000	0.194	0.215	2.062	0.9054	0.9053	-0.39	-0.01	0.9723
6.008	0.000	0.000	0.214	0.140	0.9541	0.9541	0.04	-0.11	0.9754
6.007	0.000	0.050	0.214	0.534	0.9500	0.9500	0.07	-0.17	0.9753
6.009	0.000	0.096	0.214	1.029	0.9501	0.9501	-0.11	0.04	0.9754
6.011	0.000	0.145	0.214	1.549	0.9480	0.9480	-0.16	0.15	0.9751
6.012	0.000	0.190	0.214	2.018	0.9440	0.9440	-0.20	0.54	0.9749
7.990	0.000	0.000	0.214	0.098	0.9722	0.9722	0.03	-0.16	0.9765
7.991	0.000	0.049	0.214	0.528	0.9697	0.9697	-0.04	-0.11	0.9767
7.990	0.000	0.095	0.214	1.012	0.9661	0.9661	-0.11	0.06	0.9765
7.984	0.000	0.143	0.214	1.527	0.9637	0.9637	-0.14	0.05	0.9761
7.981	0.000	0.172	0.214	1.826	0.9602	0.9602	-0.12	0.03	0.9756
9.996	0.000	0.000	0.213	0.076	0.9775	0.9775	-0.05	-0.06	0.9760
10.024	0.000	0.051	0.214	0.546	0.9768	0.9768	-0.10	-0.07	0.9764
9.983	0.000	0.096	0.214	1.026	0.9741	0.9740	-0.16	0.03	0.9761
9.982	0.000	0.137	0.214	1.459	0.9700	0.9700	-0.16	0.02	0.9759

Table 14. Internal Static Performance of Configuration 12

[$\varepsilon = 1.944$; forward slot injection; long Coanda flaps; $\phi_l = 0^\circ$; $\phi_r = 30^\circ$]

NPR	ω_{si}	ω_c	$p_{t,si}/p_{t,j}$	$p_{t,c}/p_{t,j}$	F_r/F_i	F_d/F_i	δ_p	δ_y	w_p/w_i
1.999	0.000	0.000	0.480	0.476	0.8822	0.8366	18.29	-2.94	0.9645
1.995	0.000	0.053	0.482	0.583	0.8796	0.8377	17.50	-3.20	0.9645
1.995	0.000	0.104	0.482	1.088	0.8641	0.8262	16.66	-3.73	0.9643
1.995	0.000	0.153	0.482	1.612	0.8552	0.8222	15.25	-4.96	0.9644
1.996	0.000	0.202	0.481	2.121	0.8526	0.8222	14.34	-5.63	0.9642
4.014	0.000	0.000	0.214	0.226	0.9060	0.9058	0.03	1.18	0.9732
4.018	0.000	0.051	0.215	0.535	0.8998	0.8998	0.11	-0.03	0.9731
4.014	0.000	0.100	0.214	1.061	0.8945	0.8944	-0.04	-0.71	0.9733
4.017	0.000	0.146	0.214	1.547	0.8915	0.8913	-0.11	-1.24	0.9728
4.017	0.000	0.195	0.215	2.069	0.8963	0.8963	-0.33	-0.48	0.9725
6.019	0.000	0.000	0.213	0.152	0.9535	0.9534	0.07	0.76	0.9758
6.022	0.000	0.051	0.214	0.543	0.9423	0.9423	0.02	0.26	0.9758
6.023	0.000	0.097	0.213	1.040	0.9397	0.9397	-0.09	0.50	0.9754
6.023	0.000	0.145	0.213	1.544	0.9366	0.9365	-0.13	0.56	0.9750
6.028	0.000	0.191	0.213	2.027	0.9292	0.9292	-0.11	0.21	0.9748
8.013	0.000	0.000	0.213	0.114	0.9711	0.9710	0.05	0.49	0.9770
8.011	0.000	0.049	0.213	0.523	0.9647	0.9646	-0.01	0.26	0.9769
8.014	0.000	0.095	0.214	1.020	0.9604	0.9604	-0.15	0.43	0.9764
8.022	0.000	0.143	0.213	1.519	0.9559	0.9559	-0.16	0.33	0.9763
8.015	0.000	0.171	0.213	1.815	0.9528	0.9527	-0.10	0.31	0.9762
10.031	0.000	0.000	0.213	0.092	0.9779	0.9779	-0.04	0.37	0.9765
9.981	0.000	0.050	0.213	0.531	0.9699	0.9699	-0.11	0.05	0.9766
9.985	0.000	0.096	0.213	1.025	0.9658	0.9658	-0.18	0.04	0.9761
9.989	0.000	0.137	0.213	1.463	0.9632	0.9632	-0.18	0.16	0.9758

Table 15. Internal Static Performance of Configuration 13

[$\epsilon = 1.944$; forward slot injection; long Coanda flaps; $\phi_l = 0^\circ$; $\phi_r = 45^\circ$]

NPR	$\omega_{s,i}$	ω_c	$p_{t,s,i}/p_{t,j}$	$p_{t,c}/p_{t,j}$	F_r/F_t	F_d/F_i	δ_p	δ_y	w_p/w_i
1.997	0.000	0.000	0.481	0.476	0.8768	0.8290	18.79	-3.11	0.9652
1.996	0.000	0.051	0.482	0.577	0.8837	0.8388	18.19	-2.46	0.9643
1.997	0.000	0.100	0.482	1.054	0.8597	0.8205	16.99	-3.81	0.9644
1.997	0.000	0.150	0.482	1.581	0.8417	0.8048	16.22	-5.48	0.9642
1.997	0.000	0.197	0.482	2.070	0.8371	0.8043	15.05	-5.94	0.9642
3.996	0.000	0.000	0.215	0.232	0.9049	0.9045	0.15	1.74	0.9734
3.995	0.000	0.051	0.215	0.536	0.8979	0.8979	0.13	-0.04	0.9731
3.995	0.000	0.098	0.215	1.043	0.8902	0.8902	-0.22	-0.79	0.9730
3.995	0.000	0.145	0.215	1.547	0.8969	0.8969	-0.32	-0.42	0.9728
3.995	0.000	0.191	0.215	2.033	0.8987	0.8987	-0.32	-0.21	0.9725
5.994	0.000	0.000	0.214	0.154	0.9537	0.9536	-0.02	1.02	0.9756
5.992	0.000	0.049	0.214	0.530	0.9428	0.9428	-0.05	0.66	0.9758
5.998	0.000	0.097	0.213	1.038	0.9420	0.9418	-0.14	1.05	0.9755
6.000	0.000	0.144	0.213	1.538	0.9415	0.9413	-0.22	1.30	0.9755
6.002	0.000	0.189	0.213	2.011	0.9388	0.9385	-0.19	1.33	0.9752
8.007	0.000	0.000	0.213	0.114	0.9714	0.9713	0.00	0.77	0.9765
7.998	0.000	0.049	0.213	0.528	0.9650	0.9649	-0.17	0.71	0.9766
7.984	0.000	0.096	0.213	1.032	0.9623	0.9622	-0.15	0.84	0.9764
7.986	0.000	0.142	0.213	1.513	0.9592	0.9591	-0.15	0.84	0.9761
7.987	0.000	0.174	0.213	1.843	0.9565	0.9563	-0.16	0.88	0.9761
9.993	0.000	0.000	0.213	0.093	0.9774	0.9774	-0.08	0.54	0.9767
10.000	0.000	0.048	0.214	0.518	0.9729	0.9729	-0.15	0.39	0.9765
10.001	0.000	0.096	0.214	1.026	0.9698	0.9698	-0.23	0.51	0.9763
10.004	0.000	0.138	0.213	1.472	0.9656	0.9656	-0.18	0.46	0.9759

Table 16. Internal Static Performance of Configuration 14

[$\epsilon = 1.944$; forward slot injection; long Coanda flaps; $\phi_f = -10^\circ$; $\phi_r = 45^\circ$]

NPR	ω_{si}	ω_c	$p_{t,si}/p_{t,j}$	$p_{t,c}/p_{t,j}$	F_r/F_i	F_d/F_i	δ_p	δ_y	w_p/w_i
1.994	0.000	0.000	0.482	0.480	0.8728	0.8252	18.57	-4.29	0.9647
1.988	0.000	0.052	0.484	0.589	0.8759	0.8326	17.72	-3.79	0.9643
1.990	0.000	0.101	0.483	1.057	0.8577	0.8181	16.76	-5.23	0.9643
1.991	0.000	0.151	0.483	1.581	0.8400	0.8037	15.46	-7.19	0.9643
1.992	0.000	0.200	0.483	2.109	0.8325	0.7982	14.58	-8.10	0.9640
4.030	0.000	0.000	0.214	0.232	0.9063	0.9061	0.04	1.24	0.9736
4.017	0.000	0.051	0.214	0.542	0.8977	0.8975	0.15	-0.99	0.9732
4.018	0.000	0.098	0.214	1.048	0.8893	0.8886	-0.22	-2.33	0.9730
4.021	0.000	0.147	0.214	1.564	0.8919	0.8911	-0.32	-2.51	0.9727
4.023	0.000	0.194	0.214	2.053	0.8961	0.8953	-0.40	-2.34	0.9725
6.013	0.000	0.000	0.213	0.155	0.9554	0.9553	0.01	0.67	0.9755
6.009	0.000	0.049	0.213	0.527	0.9431	0.9431	-0.02	-0.26	0.9757
6.010	0.000	0.098	0.213	1.046	0.9420	0.9419	-0.14	-0.50	0.9757
6.010	0.000	0.146	0.213	1.550	0.9394	0.9393	-0.17	-0.59	0.9752
6.013	0.000	0.191	0.213	2.028	0.9346	0.9345	-0.21	-0.79	0.9750
8.020	0.000	0.000	0.213	0.117	0.9724	0.9724	0.01	0.23	0.9768
8.028	0.000	0.049	0.213	0.528	0.9653	0.9653	-0.05	-0.57	0.9771
8.026	0.000	0.095	0.213	1.013	0.9615	0.9614	-0.22	-0.75	0.9765
8.029	0.000	0.143	0.213	1.526	0.9544	0.9543	-0.24	-1.06	0.9762
8.030	0.000	0.172	0.213	1.825	0.9350	0.9348	-0.23	-1.07	0.9759
9.987	0.000	0.000	0.213	0.096	0.9785	0.9785	-0.06	0.05	0.9766
9.983	0.000	0.050	0.213	0.530	0.9704	0.9702	-0.13	-0.97	0.9765
9.984	0.000	0.096	0.213	1.027	0.9662	0.9660	-0.21	-1.14	0.9764
9.988	0.000	0.138	0.213	1.467	0.9605	0.9602	-0.21	-1.28	0.9758

Table 17. Internal Static Performance of Configuration 15

[$\varepsilon = 1.944$; forward slot injection; long Coanda flaps; $\phi_f = -10^\circ$; $\phi_r = 30^\circ$]

NPR	ω_{si}	ω_i	$p_{t,si}/p_{t,j}$	$p_{t,ci}/p_{t,j}$	F_r/F_i	F_d/F_i	δ_p	δ_v	w_p/w_i
2.012	0.000	0.000	0.252	0.489	0.8484	0.8187	-14.68	-4.16	0.9658
2.003	0.000	0.051	0.248	0.576	0.8475	0.8177	-14.21	-5.75	0.9649
2.002	0.000	0.103	0.256	1.081	0.8309	0.8033	-13.17	-7.01	0.9649
2.002	0.000	0.151	0.256	1.581	0.8342	0.8054	-12.98	-7.96	0.9650
2.003	0.000	0.200	0.255	2.103	0.8370	0.8085	-12.39	-8.71	0.9645
4.002	0.000	0.000	0.215	0.229	0.9093	0.9092	0.22	0.72	0.9731
4.007	0.000	0.051	0.215	0.537	0.8988	0.8987	0.18	-0.98	0.9734
4.009	0.000	0.100	0.215	1.063	0.8928	0.8920	-0.09	-2.47	0.9731
4.011	0.000	0.146	0.215	1.546	0.8880	0.8865	-0.41	-3.34	0.9730
4.012	0.000	0.195	0.215	2.074	0.8886	0.8873	-0.40	-2.99	0.9728
6.010	0.000	0.000	0.213	0.154	0.9556	0.9556	-0.05	0.54	0.9760
6.006	0.000	0.050	0.213	0.534	0.9435	0.9435	-0.08	-0.61	0.9759
6.010	0.000	0.097	0.213	1.037	0.9385	0.9383	-0.18	-1.21	0.9758
6.005	0.000	0.145	0.214	1.542	0.9326	0.9322	-0.29	-1.52	0.9752
6.008	0.000	0.191	0.213	2.027	0.9249	0.9243	-0.26	-1.95	0.9748
8.028	0.000	0.000	0.213	0.114	0.9715	0.9715	-0.08	0.16	0.9770
8.016	0.000	0.049	0.213	0.521	0.9624	0.9623	-0.18	-0.93	0.9769
8.022	0.000	0.095	0.213	1.019	0.9555	0.9552	-0.26	-1.40	0.9767
8.019	0.000	0.143	0.214	1.523	0.9486	0.9482	-0.28	-1.67	0.9765
8.028	0.000	0.173	0.213	1.835	0.9442	0.9437	-0.27	-1.90	0.9759
10.032	0.000	0.000	0.213	0.094	0.9784	0.9784	-0.09	-0.14	0.9769
10.033	0.000	0.049	0.214	0.528	0.9658	0.9655	-0.24	-1.34	0.9766
10.043	0.000	0.094	0.214	1.000	0.9584	0.9578	-0.31	-1.93	0.9760
10.047	0.000	0.138	0.214	1.464	0.9530	0.9525	-0.31	-1.98	0.9758

Table 18. Internal Static Performance of Configuration 16

[$\varepsilon = 2.405$; forward slot injection; short Coanda flaps; $\phi_l = 0^\circ$; $\phi_r = 0^\circ$]

NPR	ω_{si}	ω_c	$p_{t,si}/p_{t,j}$	$p_{t,c}/p_{t,j}$	F_r/F_i	F_a/F_i	δ_p	δ_y	w_p/w_i
2.002	0.000	0.000	0.484	0.488	0.8678	0.8673	1.99	0.53	0.9756
2.007	0.000	0.051	0.488	0.576	0.8967	0.8922	5.73	-0.67	0.9744
2.005	0.000	0.101	0.481	1.071	0.8569	0.8563	2.09	0.48	0.9762
2.008	0.000	0.151	0.488	1.601	0.8905	0.8863	5.50	-0.83	0.9746
2.008	0.000	0.201	0.489	2.137	0.8916	0.8882	4.96	-0.78	0.9742
4.005	0.000	0.000	0.148	0.239	0.8374	0.8374	0.02	0.13	0.9793
4.006	0.000	0.051	0.148	0.547	0.8402	0.8401	0.21	0.34	0.9798
3.998	0.000	0.099	0.148	1.058	0.8457	0.8457	0.00	0.20	0.9789
4.019	0.000	0.146	0.148	1.557	0.8504	0.8504	-0.13	0.32	0.9787
3.987	0.000	0.191	0.148	2.044	0.8535	0.8535	-0.17	0.47	0.9781
5.987	0.000	0.000	0.149	0.161	0.8882	0.8882	0.21	0.16	0.9789
5.983	0.000	0.049	0.149	0.525	0.8826	0.8826	0.15	0.16	0.9788
5.984	0.000	0.097	0.149	1.035	0.8875	0.8875	0.00	0.45	0.9785
5.986	0.000	0.143	0.149	1.531	0.8888	0.8888	-0.04	0.44	0.9783
5.990	0.000	0.189	0.148	2.014	0.8890	0.8890	-0.02	0.60	0.9780
7.996	0.000	0.000	0.149	0.122	0.9244	0.9244	0.04	0.12	0.9786
7.999	0.000	0.049	0.149	0.521	0.9201	0.9201	0.01	-0.05	0.9785
8.003	0.000	0.096	0.149	1.026	0.9223	0.9223	-0.09	0.31	0.9781
8.009	0.000	0.142	0.149	1.511	0.9218	0.9218	-0.04	0.42	0.9778
8.018	0.000	0.169	0.149	1.795	0.9196	0.9196	-0.06	0.43	0.9776
10.003	0.000	0.000	0.149	0.097	0.9422	0.9422	0.00	0.05	0.9783
9.990	0.000	0.049	0.149	0.525	0.9384	0.9384	-0.09	-0.03	0.9789
9.993	0.000	0.095	0.149	1.018	0.9384	0.9384	-0.17	0.34	0.9783
9.990	0.000	0.135	0.149	1.438	0.9354	0.9354	-0.12	0.40	0.9778

Table 19. Internal Static Performance of Configuration 17

[$\varepsilon = 2.405$; forward slot injection; short Coanda flaps; $\phi_l = 0^\circ$; $\phi_r = 30^\circ$]

NPR	ω_{vi}	ω_c	$p_{t,s}/p_{t,j}$	$p_{t,c}/p_{t,j}$	F_r/F_i	F_d/F_i	δ_p	δ_v	w_p/w_i
1.994	0.000	0.000	0.493	0.491	0.9025	0.8988	5.16	-0.63	0.9742
1.997	0.000	0.051	0.492	0.577	0.8978	0.8941	5.10	-1.03	0.9747
1.998	0.000	0.100	0.492	1.062	0.8785	0.8747	4.77	-2.36	0.9750
2.002	0.000	0.149	0.491	1.589	0.8747	0.8712	4.05	-3.13	0.9750
2.002	0.000	0.195	0.490	2.080	0.8746	0.8707	3.89	-3.68	0.9745
4.011	0.000	0.000	0.150	0.243	0.8345	0.8345	-0.57	0.34	0.9804
4.015	0.000	0.050	0.150	0.538	0.8341	0.8341	-0.44	0.49	0.9806
4.017	0.000	0.097	0.150	1.044	0.8345	0.8345	-0.54	-0.10	0.9801
4.018	0.000	0.144	0.151	1.546	0.8410	0.8409	-0.75	0.54	0.9800
4.020	0.000	0.190	0.150	2.033	0.8465	0.8464	-0.70	0.56	0.9797
6.026	0.000	0.000	0.149	0.162	0.8860	0.8860	-0.17	0.20	0.9799
6.023	0.000	0.048	0.149	0.520	0.8805	0.8805	-0.10	0.41	0.9799
6.029	0.000	0.096	0.149	1.034	0.8821	0.8820	-0.23	0.60	0.9796
6.031	0.000	0.141	0.149	1.508	0.8832	0.8832	-0.32	0.36	0.9795
6.017	0.000	0.188	0.149	2.009	0.8826	0.8826	-0.36	0.24	0.9791
8.028	0.000	0.000	0.149	0.122	0.9236	0.9236	-0.08	0.17	0.9794
8.026	0.000	0.048	0.149	0.514	0.9175	0.9175	-0.14	0.26	0.9794
8.020	0.000	0.096	0.149	1.024	0.9173	0.9173	-0.24	0.37	0.9789
8.025	0.000	0.140	0.149	1.498	0.9162	0.9162	-0.29	0.20	0.9785
8.026	0.000	0.169	0.149	1.796	0.9139	0.9139	-0.22	0.06	0.9783
10.021	0.000	0.000	0.149	0.098	0.9411	0.9411	-0.18	0.11	0.9786
10.020	0.000	0.048	0.149	0.521	0.9353	0.9353	-0.26	0.28	0.9787
10.028	0.000	0.095	0.149	1.016	0.9351	0.9350	-0.33	0.34	0.9782
10.035	0.000	0.136	0.149	1.445	0.9320	0.9320	-0.28	0.09	0.9776

Table 20. Internal Static Performance of Configuration 18

[$\epsilon = 2.405$; forward slot injection; short Coanda flaps; $\phi_f = 0^\circ$; $\phi_r = 45^\circ$]

NPR	ω_{s_i}	ω_c	$p_{t,s}/p_{t,j}$	$p_{t,a}/p_{t,j}$	F_r/F_i	F_d/F_i	δ_p	δ_v	w_p/w_i
2.007	0.000	0.000	0.489	0.488	0.8969	0.8932	5.16	-0.58	0.9744
2.007	0.000	0.050	0.489	0.571	0.8931	0.8894	5.12	-0.81	0.9748
2.006	0.000	0.101	0.489	1.067	0.8712	0.8676	4.77	-2.16	0.9757
2.007	0.000	0.150	0.489	1.589	0.8616	0.8576	4.31	-3.43	0.9744
2.008	0.000	0.197	0.488	2.096	0.8595	0.8557	3.94	-3.70	0.9740
4.005	0.000	0.000	0.151	0.244	0.8307	0.8306	-0.53	0.67	0.9800
4.007	0.000	0.050	0.151	0.531	0.8334	0.8333	-0.39	0.92	0.9802
4.009	0.000	0.098	0.151	1.045	0.8355	0.8354	-0.53	0.69	0.9798
4.011	0.000	0.145	0.151	1.547	0.8440	0.8437	-0.69	1.24	0.9795
4.012	0.000	0.191	0.151	2.036	0.8486	0.8483	-0.74	1.17	0.9793
5.986	0.000	0.000	0.150	0.163	0.8824	0.8824	-0.17	0.33	0.9798
5.983	0.000	0.049	0.150	0.528	0.8787	0.8787	-0.23	0.63	0.9797
5.985	0.000	0.097	0.150	1.038	0.8821	0.8820	-0.34	0.93	0.9796
5.989	0.000	0.143	0.150	1.533	0.8840	0.8839	-0.34	0.74	0.9792
5.987	0.000	0.190	0.150	2.021	0.8853	0.8852	-0.24	0.65	0.9788
8.008	0.000	0.000	0.149	0.123	0.9212	0.9212	-0.25	0.18	0.9795
8.006	0.000	0.049	0.149	0.523	0.9165	0.9164	-0.18	0.29	0.9794
8.005	0.000	0.095	0.149	1.024	0.9177	0.9177	-0.18	0.55	0.9792
8.007	0.000	0.142	0.149	1.516	0.9173	0.9173	-0.17	0.43	0.9790
8.012	0.000	0.171	0.149	1.825	0.9151	0.9150	-0.18	0.28	0.9784
10.006	0.000	0.000	0.149	0.098	0.9398	0.9397	-0.19	0.17	0.9784
10.004	0.000	0.048	0.149	0.514	0.9356	0.9356	-0.21	0.36	0.9785
10.004	0.000	0.095	0.149	1.017	0.9358	0.9358	-0.23	0.45	0.9782
10.011	0.000	0.136	0.149	1.446	0.9330	0.9330	-0.25	0.26	0.9776

Table 21. Internal Static Performance of Configuration 19

[$\varepsilon = 2.405$; forward slot injection; short Coanda flaps; $\phi_l = -10^\circ$; $\phi_r = 30^\circ$]

NPR	ω_{st}	ω_c	$p_{t,st}/p_{t,j}$	$p_{t,c}/p_{t,j}$	F_p/F_i	F_d/F_i	δ_p	δ_v	w_p/w_i
2.005	0.000	0.000	0.486	0.490	0.9269	0.9269	-0.23	-0.07	0.9720
1.996	0.000	0.050	0.488	0.579	0.9198	0.9198	-0.35	-0.40	0.9715
1.996	0.000	0.099	0.489	1.050	0.9017	0.9011	-0.53	-1.97	0.9717
1.996	0.000	0.148	0.489	1.574	0.8976	0.8960	-0.44	-3.41	0.9714
1.995	0.000	0.196	0.489	2.078	0.8939	0.8910	-0.76	-4.52	0.9709
4.002	0.000	0.000	0.151	0.243	0.8317	0.8316	-0.44	0.47	0.9798
4.002	0.000	0.050	0.150	0.534	0.8347	0.8346	-0.44	0.34	0.9801
4.004	0.000	0.097	0.151	1.044	0.8350	0.8349	-0.60	-0.67	0.9799
4.006	0.000	0.144	0.150	1.546	0.8402	0.8401	-0.60	-0.72	0.9798
4.015	0.000	0.191	0.151	2.046	0.8440	0.8438	-0.61	-1.10	0.9792
6.003	0.000	0.000	0.149	0.162	0.8842	0.8842	-0.25	0.28	0.9795
6.009	0.000	0.049	0.149	0.524	0.8805	0.8804	-0.22	0.41	0.9798
6.011	0.000	0.096	0.149	1.027	0.8821	0.8821	-0.28	-0.22	0.9795
6.013	0.000	0.142	0.149	1.520	0.8818	0.8817	-0.26	-0.55	0.9790
6.014	0.000	0.189	0.149	2.011	0.8804	0.8802	-0.33	-0.94	0.9789
8.008	0.000	0.000	0.149	0.122	0.9212	0.9212	-0.18	0.17	0.9796
8.008	0.000	0.048	0.149	0.520	0.9175	0.9175	-0.20	0.09	0.9794
8.011	0.000	0.094	0.149	1.011	0.9171	0.9171	-0.25	-0.28	0.9790
8.012	0.000	0.142	0.149	1.511	0.9130	0.9130	-0.24	-0.72	0.9788
8.013	0.000	0.171	0.149	1.817	0.9095	0.9093	-0.25	-1.03	0.9786
9.969	0.000	0.000	0.149	0.100	0.9394	0.9394	-0.16	0.04	0.9790
9.984	0.000	0.048	0.149	0.522	0.9351	0.9351	-0.22	-0.11	0.9790
9.988	0.000	0.095	0.149	1.020	0.9330	0.9329	-0.27	-0.45	0.9786
9.995	0.000	0.136	0.149	1.450	0.9283	0.9282	-0.26	-0.84	0.9783

Table 22. Internal Static Performance of Configuration 20

[$\varepsilon = 2.405$; forward slot injection; short Coanda flaps; $\phi_l = -10^\circ$; $\phi_r = 45^\circ$]

NPR	ω_{si}	ω_c	$P_{t,s}/P_{t,j}$	$P_{t,c}/P_{t,j}$	F_r/F_i	F_d/F_i	δ_p	δ_y	w_p/w_i
2.009	0.000	0.000	0.485	0.489	0.9292	0.9292	-0.09	0.05	0.9724
2.009	0.000	0.051	0.485	0.577	0.9204	0.9203	-0.44	-0.42	0.9722
2.009	0.000	0.100	0.485	1.058	0.9011	0.9005	-0.63	-1.99	0.9720
2.009	0.000	0.148	0.485	1.580	0.8874	0.8855	-0.88	-3.68	0.9720
2.010	0.000	0.195	0.485	2.079	0.8810	0.8776	-1.08	-4.96	0.9720
4.023	0.000	0.000	0.150	0.242	0.8317	0.8316	-0.57	0.58	0.9803
4.030	0.000	0.050	0.150	0.535	0.8342	0.8342	-0.68	0.47	0.9805
3.991	0.000	0.097	0.151	1.042	0.8353	0.8352	-0.84	-0.11	0.9801
3.992	0.000	0.144	0.151	1.545	0.8425	0.8424	-0.83	-0.07	0.9797
3.995	0.000	0.191	0.151	2.039	0.8459	0.8458	-0.84	-0.53	0.9795
5.998	0.000	0.000	0.149	0.163	0.8842	0.8842	-0.30	0.34	0.9795
5.997	0.000	0.049	0.149	0.523	0.8797	0.8797	-0.30	0.58	0.9796
5.998	0.000	0.096	0.149	1.031	0.8823	0.8823	-0.36	0.05	0.9795
6.000	0.000	0.143	0.149	1.526	0.8822	0.8821	-0.43	-0.24	0.9793
6.003	0.000	0.189	0.149	2.010	0.8804	0.8803	-0.37	-0.62	0.9789
7.984	0.000	0.000	0.149	0.123	0.9212	0.9212	-0.19	0.13	0.9789
8.001	0.000	0.048	0.149	0.519	0.9168	0.9167	-0.18	0.21	0.9794
8.005	0.000	0.095	0.149	1.017	0.9176	0.9176	-0.22	-0.06	0.9791
8.009	0.000	0.142	0.149	1.510	0.9137	0.9136	-0.26	-0.50	0.9787
8.012	0.000	0.170	0.149	1.812	0.9110	0.9109	-0.28	-0.80	0.9784
10.027	0.000	0.000	0.149	0.099	0.9398	0.9398	-0.18	0.06	0.9787
10.030	0.000	0.048	0.149	0.514	0.9367	0.9367	-0.24	0.05	0.9788
10.035	0.000	0.095	0.149	1.015	0.9339	0.9339	-0.26	-0.37	0.9784
10.038	0.000	0.135	0.149	1.439	0.9288	0.9287	-0.28	-0.70	0.9781

Table 23. Internal Static Performance of Configuration 21

[$\epsilon = 2.405$; forward slot injection; long Coanda flaps; $\phi_l = 0^\circ$; $\phi_r = 0^\circ$]

NPR	$\omega_{s,i}$	ω_i	$p_{t,s,i}/p_{t,j}$	$p_{t,i}/p_{t,j}$	F_r/F_i	F_d/F_i	δ_p	δ_v	w_p/w_i
2.005	0.000	0.000	0.486	0.490	0.9329	0.9329	-0.05	0.46	0.9725
1.999	0.000	0.050	0.487	0.576	0.9247	0.9246	-0.43	0.62	0.9713
2.001	0.000	0.100	0.486	1.064	0.9122	0.9120	-0.80	0.65	0.9718
2.002	0.000	0.148	0.486	1.574	0.9128	0.9125	-1.01	0.75	0.9719
2.003	0.000	0.196	0.486	2.086	0.9159	0.9156	-1.15	0.51	0.9715
3.992	0.000	0.000	0.151	0.215	0.8366	0.8365	-0.48	-0.35	0.9804
3.995	0.000	0.049	0.151	0.526	0.8368	0.8368	-0.43	0.33	0.9800
3.983	0.000	0.098	0.151	1.048	0.8432	0.8431	-0.68	0.41	0.9798
3.984	0.000	0.145	0.151	1.554	0.8488	0.8487	-0.70	0.38	0.9795
3.985	0.000	0.193	0.151	2.063	0.8511	0.8510	-0.71	0.31	0.9795
6.007	0.000	0.000	0.150	0.151	0.8870	0.8870	-0.04	0.06	0.9803
6.011	0.000	0.049	0.150	0.523	0.8836	0.8836	-0.16	-0.14	0.9798
6.012	0.000	0.096	0.150	1.035	0.8879	0.8878	-0.32	0.69	0.9794
6.014	0.000	0.143	0.150	1.529	0.8898	0.8898	-0.32	0.72	0.9793
6.016	0.000	0.190	0.150	2.029	0.8890	0.8889	-0.27	0.85	0.9790
8.010	0.000	0.000	0.148	0.112	0.9236	0.9236	-0.07	-0.08	0.9794
7.999	0.000	0.049	0.149	0.526	0.9208	0.9208	-0.24	0.02	0.9794
7.996	0.000	0.096	0.149	1.029	0.9220	0.9219	-0.28	0.73	0.9791
8.043	0.000	0.142	0.149	1.519	0.9215	0.9214	-0.22	0.72	0.9786
7.992	0.000	0.171	0.149	1.820	0.9182	0.9181	-0.23	0.83	0.9785
9.989	0.000	0.000	0.149	0.094	0.9418	0.9418	-0.14	0.14	0.9788
9.995	0.000	0.049	0.149	0.522	0.9397	0.9397	-0.26	0.22	0.9786
10.002	0.000	0.096	0.149	1.029	0.9386	0.9386	-0.25	0.27	0.9781
10.007	0.000	0.136	0.149	1.450	0.9370	0.9370	-0.23	0.19	0.9777

Table 24. Internal Static Performance of Configuration 22

[$\epsilon = 2.405$; forward slot injection; long Coanda flaps; $\phi_l = 0^\circ$; $\phi_r = 30^\circ$]

NPR	ω_{si}	ω_c	$p_{t,si}/p_{t,j}$	$p_{t,c}/p_{t,j}$	F_t/F_i	F_a/F_i	δ_p	δ_y	w_p/w_i
2.017	0.000	0.000	0.482	0.484	0.9282	0.9282	-0.60	0.11	0.9728
2.008	0.000	0.052	0.487	0.580	0.8901	0.8857	5.54	-1.32	0.9751
2.011	0.000	0.101	0.487	1.073	0.8725	0.8674	5.57	-2.75	0.9749
2.011	0.000	0.150	0.487	1.588	0.8661	0.8607	5.19	-3.72	0.9750
2.008	0.000	0.198	0.488	2.110	0.8653	0.8600	4.57	-4.41	0.9745
3.999	0.000	0.000	0.152	0.234	0.8355	0.8345	-0.35	2.78	0.9800
4.003	0.000	0.050	0.152	0.534	0.8318	0.8317	-0.35	0.54	0.9801
4.003	0.000	0.099	0.153	1.057	0.8327	0.8327	-0.48	-0.53	0.9798
4.000	0.000	0.147	0.153	1.569	0.8341	0.8340	-0.56	-0.69	0.9795
4.000	0.000	0.192	0.152	2.058	0.8369	0.8367	-0.64	-0.77	0.9795
6.001	0.000	0.000	0.150	0.158	0.8861	0.8860	-0.04	0.98	0.9800
5.997	0.000	0.050	0.151	0.534	0.8787	0.8783	-0.09	1.64	0.9799
5.998	0.000	0.097	0.151	1.036	0.8810	0.8806	-0.28	1.66	0.9797
6.000	0.000	0.144	0.150	1.534	0.8801	0.8799	-0.31	1.04	0.9795
6.003	0.000	0.191	0.150	2.039	0.8748	0.8748	-0.27	0.03	0.9790
8.011	0.000	0.000	0.149	0.118	0.9221	0.9221	-0.07	0.61	0.9794
8.025	0.000	0.049	0.149	0.525	0.9171	0.9168	-0.16	1.56	0.9792
8.017	0.000	0.098	0.149	1.047	0.9165	0.9161	-0.26	1.57	0.9788
8.016	0.000	0.141	0.149	1.509	0.9136	0.9135	-0.23	0.68	0.9787
8.018	0.000	0.170	0.149	1.810	0.9103	0.9103	-0.17	0.36	0.9786
9.990	0.000	0.000	0.149	0.097	0.9408	0.9408	-0.08	0.40	0.9788
9.997	0.000	0.051	0.149	0.541	0.9350	0.9348	-0.15	1.26	0.9786
10.004	0.000	0.097	0.149	1.040	0.9346	0.9344	-0.22	1.15	0.9781
10.010	0.000	0.136	0.149	1.445	0.9303	0.9302	-0.20	0.87	0.9777

Table 25. Internal Static Performance of Configuration 23

[$\epsilon = 2.405$; forward slot injection; long Coanda flaps; $\phi_l = 0^\circ$; $\phi_r = 45^\circ$]

NPR	ω_{si}	ω_c	$p_{t,si}/p_{t,j}$	$p_{t,c}/p_{t,j}$	F_r/F_i	F_d/F_i	δ_p	δ_y	w_p/w_i
2.010	0.000	0.000	0.484	0.487	0.9304	0.9303	-0.76	-0.02	0.9710
2.011	0.000	0.050	0.484	0.571	0.9242	0.9240	-0.99	-0.16	0.9711
2.011	0.000	0.101	0.484	1.074	0.9001	0.8997	-0.77	-1.60	0.9710
2.011	0.000	0.150	0.484	1.588	0.8888	0.8877	-1.12	-2.64	0.9709
2.011	0.000	0.199	0.483	2.109	0.8846	0.8829	-1.04	-3.41	0.9711
3.999	0.000	0.000	0.150	0.234	0.8372	0.8361	-0.57	2.93	0.9797
4.000	0.000	0.050	0.152	0.532	0.8338	0.8337	-0.42	0.88	0.9793
4.000	0.000	0.099	0.152	1.064	0.8342	0.8342	-0.54	0.04	0.9791
3.998	0.000	0.145	0.152	1.547	0.8408	0.8407	-0.61	0.65	0.9794
4.000	0.000	0.192	0.151	2.047	0.8481	0.8480	-0.68	0.80	0.9790
6.018	0.000	0.000	0.149	0.158	0.8862	0.8861	-0.08	1.12	0.9798
6.003	0.000	0.049	0.151	0.527	0.8816	0.8812	-0.20	1.85	0.9797
6.003	0.000	0.097	0.151	1.041	0.8835	0.8829	-0.26	2.15	0.9795
6.006	0.000	0.143	0.150	1.524	0.8839	0.8835	-0.34	1.71	0.9792
6.008	0.000	0.191	0.150	2.032	0.8858	0.8855	-0.31	1.25	0.9789
7.997	0.000	0.000	0.149	0.118	0.9226	0.9225	-0.10	0.75	0.9794
7.992	0.000	0.050	0.150	0.532	0.9182	0.9177	-0.18	1.74	0.9791
7.998	0.000	0.097	0.149	1.035	0.9188	0.9183	-0.27	1.86	0.9789
8.001	0.000	0.143	0.149	1.529	0.9179	0.9177	-0.26	1.14	0.9787
8.010	0.000	0.171	0.149	1.822	0.9157	0.9156	-0.24	0.97	0.9783
10.006	0.000	0.000	0.148	0.097	0.9408	0.9408	-0.10	0.51	0.9785
10.007	0.000	0.050	0.149	0.536	0.9377	0.9374	-0.20	1.58	0.9783
10.010	0.000	0.096	0.149	1.028	0.9368	0.9364	-0.27	1.45	0.9781
10.017	0.000	0.137	0.149	1.455	0.9335	0.9332	-0.26	1.28	0.9777

Table 26. Internal Static Performance of Configuration 24

[$\varepsilon = 2.405$; forward slot injection; long Coanda flaps; $\phi_l = -10^\circ$; $\phi_r = 30^\circ$]

NPR	ω_{si}	ω_c	$p_{t,sl}/p_{t,j}$	$p_{t,cl}/p_{t,j}$	F_r/F_i	F_d/F_i	δ_p	δ_y	w_p/w_i
1.990	0.000	0.000	0.489	0.495	0.9228	0.9226	-0.38	-1.17	0.9704
1.988	0.000	0.052	0.490	0.584	0.9199	0.9196	-0.33	-1.29	0.9707
2.002	0.000	0.101	0.487	1.077	0.9015	0.9003	-0.43	-2.83	0.9708
2.002	0.000	0.146	0.487	1.549	0.8980	0.8957	-0.73	-4.07	0.9704
2.002	0.000	0.195	0.487	2.065	0.8968	0.8931	-0.92	-5.16	0.9705
4.018	0.000	0.000	0.151	0.232	0.8398	0.8387	-0.56	2.78	0.9792
4.022	0.000	0.049	0.152	0.526	0.8359	0.8358	-0.39	-0.12	0.9793
3.995	0.000	0.096	0.153	1.034	0.8333	0.8328	-0.49	-2.09	0.9790
3.992	0.000	0.146	0.152	1.558	0.8324	0.8313	-0.72	-2.90	0.9788
3.991	0.000	0.191	0.152	2.039	0.8329	0.8315	-0.79	-3.18	0.9786
6.000	0.000	0.000	0.150	0.156	0.8880	0.8878	-0.15	1.08	0.9791
5.996	0.000	0.049	0.151	0.520	0.8856	0.8852	-0.10	1.61	0.9789
5.997	0.000	0.096	0.150	1.030	0.8854	0.8853	-0.21	0.95	0.9788
5.995	0.000	0.143	0.150	1.527	0.8821	0.8821	-0.31	0.33	0.9786
5.996	0.000	0.190	0.150	2.025	0.8751	0.8751	-0.29	-0.62	0.9783
7.998	0.000	0.000	0.149	0.117	0.9249	0.9248	-0.09	0.60	0.9789
7.999	0.000	0.049	0.150	0.530	0.9211	0.9210	-0.16	0.71	0.9789
8.000	0.000	0.096	0.149	1.030	0.9181	0.9181	-0.23	0.25	0.9783
8.006	0.000	0.144	0.149	1.535	0.9128	0.9127	-0.29	-0.30	0.9779
8.012	0.000	0.171	0.149	1.814	0.9081	0.9080	-0.22	-0.66	0.9777
10.009	0.000	0.000	0.148	0.093	0.9420	0.9419	-0.14	0.44	0.9777
10.009	0.000	0.048	0.149	0.517	0.9373	0.9373	-0.20	0.12	0.9777
10.018	0.000	0.096	0.149	1.022	0.9335	0.9335	-0.29	-0.34	0.9773
10.025	0.000	0.137	0.149	1.455	0.9281	0.9280	-0.28	-0.70	0.9769

Table 27. Internal Static Performance of Configuration 25

[$\epsilon = 2.405$; forward slot injection; long Coanda flaps; $\phi_l = -10^\circ$; $\phi_r = 45^\circ$]

NPR	ω_{si}	ω_c	$p_{t,si}/p_{t,j}$	$p_{t,c}/p_{t,j}$	F_r/F_i	F_d/F_i	δ_ρ	δ_y	w_p/w_i
2.004	0.000	0.000	0.484	0.490	0.9240	0.9236	-1.27	-1.13	0.9712
2.008	0.000	0.050	0.485	0.577	0.9203	0.9199	-1.11	-1.30	0.9708
2.008	0.000	0.099	0.485	1.053	0.8990	0.8979	-0.62	-2.84	0.9711
2.008	0.000	0.150	0.485	1.587	0.8885	0.8857	-0.86	-4.49	0.9708
2.009	0.000	0.200	0.485	2.115	0.8834	0.8789	-1.01	-5.70	0.9709
4.005	0.000	0.000	0.151	0.232	0.8401	0.8390	-0.36	2.94	0.9791
4.008	0.000	0.050	0.152	0.535	0.8350	0.8350	-0.27	0.08	0.9789
4.008	0.000	0.098	0.151	1.052	0.8339	0.8336	-0.50	-1.45	0.9790
4.010	0.000	0.146	0.151	1.566	0.8398	0.8395	-0.54	-1.38	0.9786
4.008	0.000	0.194	0.151	2.068	0.8438	0.8435	-0.46	-1.54	0.9783
6.009	0.000	0.000	0.150	0.156	0.8880	0.8878	0.06	1.28	0.9789
5.999	0.000	0.050	0.150	0.533	0.8872	0.8868	-0.04	1.74	0.9787
6.001	0.000	0.098	0.150	1.047	0.8876	0.8874	-0.17	1.30	0.9786
6.039	0.000	0.143	0.149	1.532	0.8868	0.8866	-0.20	1.02	0.9785
6.031	0.000	0.191	0.149	2.034	0.8841	0.8841	-0.13	0.69	0.9779
8.005	0.000	0.000	0.149	0.117	0.9236	0.9236	-0.01	0.73	0.9785
7.995	0.000	0.048	0.149	0.518	0.9218	0.9217	0.00	0.90	0.9784
7.993	0.000	0.097	0.149	1.035	0.9197	0.9196	-0.17	0.57	0.9783
7.995	0.000	0.141	0.149	1.506	0.9161	0.9161	-0.16	0.30	0.9780
7.995	0.000	0.171	0.149	1.821	0.9128	0.9128	-0.15	0.03	0.9776
10.007	0.000	0.000	0.148	0.093	0.9407	0.9407	0.01	0.54	0.9774
10.008	0.000	0.049	0.149	0.525	0.9384	0.9384	-0.06	0.37	0.9776
10.010	0.000	0.096	0.149	1.030	0.9351	0.9351	-0.15	0.02	0.9770
10.017	0.000	0.137	0.149	1.459	0.9303	0.9303	-0.18	-0.30	0.9766

Table 28. Internal Static Performance of Configuration 26

[$\epsilon = 2.405$; forward slot injection; long Coanda flaps; $\phi_l = 0^\circ$; $\phi_r = 0^\circ$]

NPR	ω_{si}	ω_c	$p_{t,s}/p_{t,j}$	$p_{t,c}/p_{t,j}$	F_i/F_i	F_d/F_i	δ_p	δ_y	w_p/w_i
2.042	0.000	0.000	0.475	0.480	0.9297	0.9296	-0.47	0.74	0.9739
1.998	0.000	0.051	0.485	0.583	0.9246	0.9245	-0.42	0.66	0.9709
1.995	0.000	0.101	0.487	1.071	0.9133	0.9132	-0.43	0.57	0.9709
1.994	0.000	0.151	0.488	1.600	0.9117	0.9116	-0.45	0.63	0.9706
1.990	0.000	0.198	0.489	2.088	0.9134	0.9133	-0.34	0.49	0.9703
4.001	0.000	0.000	0.151	0.201	0.8349	0.8349	-0.39	0.12	0.9796
4.006	0.000	0.049	0.156	0.524	0.8354	0.8353	-0.42	0.12	0.9800
4.009	0.000	0.098	0.160	1.043	0.8420	0.8420	-0.38	0.31	0.9798
4.011	0.000	0.145	0.161	1.548	0.8457	0.8456	-0.46	0.39	0.9795
4.001	0.000	0.191	0.159	2.036	0.8490	0.8489	-0.54	0.33	0.9793
6.020	0.000	0.000	0.150	0.152	0.8829	0.8829	0.03	0.18	0.9798
6.009	0.000	0.048	0.155	0.516	0.8800	0.8799	-0.18	-0.56	0.9797
5.994	0.000	0.097	0.156	1.032	0.8844	0.8844	-0.11	0.34	0.9793
5.994	0.000	0.144	0.154	1.538	0.8845	0.8844	-0.24	0.76	0.9792
5.998	0.000	0.191	0.151	2.034	0.8833	0.8832	-0.15	0.87	0.9790
7.997	0.000	0.000	0.148	0.116	0.9175	0.9175	-0.03	0.10	0.9797
8.005	0.000	0.050	0.153	0.536	0.9156	0.9156	-0.18	-0.76	0.9796
8.009	0.000	0.096	0.152	1.023	0.9160	0.9160	-0.19	0.74	0.9793
7.998	0.000	0.145	0.149	1.542	0.9128	0.9127	-0.22	0.85	0.9789
8.001	0.000	0.171	0.149	1.820	0.9106	0.9104	-0.19	0.91	0.9787
9.988	0.000	0.000	0.148	0.091	0.9322	0.9322	-0.15	0.11	0.9782
9.990	0.000	0.050	0.151	0.533	0.9295	0.9295	-0.24	0.35	0.9784
10.002	0.000	0.095	0.149	1.021	0.9278	0.9278	-0.27	0.36	0.9781
10.008	0.000	0.137	0.149	1.462	0.9234	0.9233	-0.27	0.59	0.9780

Table 29. Internal Static Performance of Configuration 27

[$\varepsilon = 2.405$; forward slot injection; long Coanda flaps; $\phi_l = 0^\circ$; $\phi_r = 30^\circ$]

NPR	ω_{s_i}	ω_i	$p_{t,s_i}/p_{t,j}$	$p_{t,c}/p_{t,j}$	F_r/F_i	F_d/F_i	δ_p	δ_v	w_p/w_i
2.006	0.000	0.000	0.483	0.486	0.9261	0.9260	-0.97	-0.08	0.9719
2.007	0.000	0.052	0.483	0.578	0.9220	0.9219	-0.93	-0.19	0.9721
2.004	0.000	0.103	0.485	1.088	0.9043	0.9040	-0.66	-1.31	0.9714
2.005	0.000	0.150	0.485	1.592	0.8987	0.8978	-0.99	-2.35	0.9717
2.005	0.000	0.200	0.485	2.120	0.8905	0.8890	-0.63	-3.28	0.9714
3.990	0.000	0.000	0.151	0.229	0.8329	0.8313	-0.38	3.50	0.9800
3.992	0.000	0.050	0.158	0.535	0.8300	0.8299	-0.54	0.54	0.9799
3.992	0.000	0.096	0.163	1.027	0.8285	0.8284	-0.47	-0.58	0.9800
3.991	0.000	0.146	0.163	1.561	0.8277	0.8274	-0.60	-1.21	0.9795
3.992	0.000	0.193	0.162	2.059	0.8282	0.8279	-0.68	-1.34	0.9796
6.011	0.000	0.000	0.150	0.157	0.8782	0.8781	-0.03	0.58	0.9800
5.999	0.000	0.050	0.156	0.532	0.8766	0.8764	-0.09	1.12	0.9801
5.997	0.000	0.097	0.158	1.041	0.8760	0.8757	-0.14	1.51	0.9796
6.003	0.000	0.144	0.155	1.537	0.8787	0.8784	-0.25	1.46	0.9795
5.994	0.000	0.190	0.150	2.021	0.8772	0.8772	-0.21	0.73	0.9791
7.995	0.000	0.000	0.148	0.119	0.9154	0.9154	0.05	0.35	0.9794
7.996	0.000	0.048	0.153	0.515	0.9111	0.9111	-0.09	0.56	0.9796
8.001	0.000	0.096	0.153	1.022	0.9153	0.9147	-0.15	2.11	0.9792
8.009	0.000	0.142	0.150	1.510	0.9102	0.9101	-0.20	1.02	0.9791
7.996	0.000	0.169	0.149	1.802	0.9069	0.9068	-0.08	0.74	0.9786
10.002	0.000	0.000	0.148	0.095	0.9308	0.9308	-0.10	0.15	0.9785
10.008	0.000	0.047	0.152	0.507	0.9288	0.9285	-0.19	1.47	0.9783
10.013	0.000	0.096	0.150	1.023	0.9285	0.9282	-0.24	1.35	0.9784
9.986	0.000	0.138	0.149	1.465	0.9230	0.9230	-0.18	0.76	0.9776

Table 30. Internal Static Performance of Configuration 28

[$\epsilon = 2.405$; forward slot injection; long Coanda flaps; $\phi_l = 0^\circ$; $\phi_r = 45^\circ$]

NPR	ω_{si}	ω_c	$p_{t,si}/p_{t,j}$	$p_{t,c}/p_{t,j}$	F_p/F_i	F_d/F_i	δ_p	δ_y	w_p/w_i
2.009	0.000	0.000	0.486	0.486	0.8949	0.8941	2.43	0.63	0.9737
2.001	0.000	0.051	0.487	0.575	0.8886	0.8878	2.46	0.34	0.9729
2.004	0.000	0.100	0.485	1.065	0.8917	0.8914	-0.33	-1.42	0.9720
2.002	0.000	0.149	0.486	1.581	0.8561	0.8549	1.75	-2.36	0.9731
2.004	0.000	0.197	0.487	2.090	0.8484	0.8466	1.58	-3.44	0.9729
3.999	0.000	0.000	0.156	0.227	0.8310	0.8292	-0.52	3.80	0.9797
4.002	0.000	0.049	0.156	0.527	0.8296	0.8293	-0.53	1.27	0.9799
4.002	0.000	0.098	0.156	1.052	0.8245	0.8244	-0.50	-0.04	0.9800
4.008	0.000	0.146	0.156	1.562	0.8442	0.8439	-0.74	1.33	0.9796
4.005	0.000	0.191	0.154	2.037	0.8463	0.8461	-0.79	1.14	0.9792
5.994	0.000	0.000	0.150	0.159	0.8783	0.8782	-0.04	0.90	0.9799
5.996	0.000	0.049	0.154	0.529	0.8759	0.8757	-0.12	1.34	0.9800
6.002	0.000	0.096	0.155	1.030	0.8827	0.8820	-0.20	2.41	0.9798
6.009	0.000	0.142	0.152	1.517	0.8832	0.8827	-0.32	2.00	0.9793
6.007	0.000	0.191	0.149	2.027	0.8814	0.8812	-0.27	1.32	0.9791
7.990	0.000	0.000	0.148	0.119	0.9148	0.9148	-0.02	0.50	0.9795
7.995	0.000	0.048	0.153	0.510	0.9135	0.9134	-0.11	0.90	0.9795
8.011	0.000	0.093	0.151	0.998	0.9168	0.9161	-0.24	2.36	0.9792
8.004	0.000	0.142	0.149	1.510	0.9119	0.9116	-0.24	1.34	0.9788
8.002	0.000	0.171	0.149	1.817	0.9087	0.9086	-0.23	1.02	0.9785
10.008	0.000	0.000	0.148	0.094	0.9309	0.9308	-0.10	0.35	0.9789
10.006	0.000	0.048	0.153	0.515	0.9305	0.9301	-0.23	1.77	0.9787
10.076	0.000	0.096	0.150	1.021	0.9296	0.9293	-0.31	1.53	0.9784
10.003	0.000	0.136	0.149	1.448	0.9246	0.9244	-0.26	1.15	0.9778

Table 31. Internal Static Performance of Configuration 29

[$\epsilon = 2.405$; forward slot injection; long Coanda flaps; $\phi_l = -10^\circ$; $\phi_r = 30^\circ$]

NPR	ω_{si}	ω_c	$P_{t,si}/P_{t,j}$	$P_{t,c}/P_{t,j}$	F_r/F_i	F_d/F_i	δ_p	δ_y	w_p/w_i
1.992	0.000	0.000	0.489	0.493	0.9418	0.9415	-0.55	-1.22	0.9549
1.991	0.000	0.053	0.489	0.587	0.9383	0.9379	-0.58	-1.58	0.9551
1.992	0.000	0.104	0.489	1.084	0.9158	0.9148	-0.60	-2.66	0.9549
1.995	0.000	0.153	0.488	1.588	0.9075	0.9051	-0.66	-4.14	0.9544
1.994	0.000	0.203	0.488	2.109	0.9019	0.8981	-0.58	-5.27	0.9548
3.996	0.000	0.000	0.150	0.229	0.8432	0.8420	-0.52	3.12	0.9718
4.003	0.000	0.051	0.151	0.536	0.8390	0.8389	-0.55	-0.36	0.9719
4.004	0.000	0.100	0.151	1.057	0.8354	0.8348	-0.67	-2.13	0.9717
4.004	0.000	0.148	0.150	1.564	0.8321	0.8308	-0.63	-3.15	0.9715
4.006	0.000	0.194	0.150	2.054	0.8372	0.8361	-0.70	-2.77	0.9712
5.996	0.000	0.000	0.150	0.147	0.8828	0.8826	-0.05	1.29	0.9744
6.002	0.000	0.049	0.150	0.525	0.8864	0.8859	-0.18	2.02	0.9746
6.002	0.000	0.098	0.150	1.040	0.8848	0.8846	-0.23	1.26	0.9744
6.003	0.000	0.145	0.150	1.537	0.8821	0.8820	-0.33	0.80	0.9740
6.007	0.000	0.192	0.149	2.023	0.8787	0.8787	-0.29	0.36	0.9738
8.009	0.000	0.000	0.148	0.108	0.9169	0.9168	-0.03	0.69	0.9758
8.013	0.000	0.049	0.149	0.525	0.9157	0.9156	-0.11	0.68	0.9755
8.023	0.000	0.097	0.149	1.032	0.9144	0.9144	-0.20	0.32	0.9753
8.031	0.000	0.144	0.149	1.518	0.9093	0.9093	-0.25	-0.13	0.9748
8.034	0.000	0.170	0.148	1.789	0.9064	0.9064	-0.17	-0.33	0.9745
10.002	0.000	0.000	0.148	0.086	0.9312	0.9311	-0.15	0.29	0.9759
10.007	0.000	0.049	0.149	0.527	0.9298	0.9297	-0.18	-0.16	0.9756
10.012	0.000	0.096	0.149	1.022	0.9256	0.9256	-0.26	-0.52	0.9753
10.020	0.000	0.136	0.149	1.434	0.9205	0.9204	-0.25	-0.86	0.9748

Table 32. Internal Static Performance of Configuration 30

[$\epsilon = 2.405$; forward slot injection; long Coanda flaps; $\phi_l = -10^\circ$; $\phi_r = 45^\circ$]

NPR	ω_{si}	ω_c	$p_{t,s}/p_{t,j}$	$p_{t,c}/p_{t,j}$	F_r/F_i	F_d/F_i	δ_p	δ_s	w_p/w_i
2.003	0.000	0.000	0.486	0.491	0.9393	0.9391	-0.62	-1.10	0.9554
1.999	0.000	0.051	0.487	0.576	0.9338	0.9335	-0.55	-1.25	0.9545
1.998	0.000	0.102	0.487	1.060	0.9093	0.9082	-0.27	-2.84	0.9544
1.998	0.000	0.154	0.487	1.602	0.8937	0.8907	-0.70	-4.63	0.9545
2.001	0.000	0.200	0.486	2.088	0.8847	0.8797	-0.85	-6.07	0.9541
4.017	0.000	0.000	0.150	0.228	0.8424	0.8409	-0.56	3.35	0.9715
4.018	0.000	0.050	0.150	0.530	0.8391	0.8390	-0.70	0.45	0.9715
4.018	0.000	0.098	0.150	1.044	0.8332	0.8328	-0.62	-1.57	0.9715
4.020	0.000	0.147	0.150	1.560	0.8487	0.8485	-0.84	-0.70	0.9713
4.021	0.000	0.194	0.150	2.045	0.8477	0.8474	-0.79	-1.26	0.9710
6.009	0.000	0.000	0.149	0.148	0.8834	0.8831	-0.15	1.58	0.9750
6.011	0.000	0.050	0.150	0.533	0.8890	0.8883	-0.20	2.28	0.9746
6.012	0.000	0.097	0.150	1.029	0.8909	0.8905	-0.30	1.76	0.9744
6.015	0.000	0.143	0.149	1.515	0.8869	0.8867	-0.39	1.19	0.9740
6.018	0.000	0.191	0.149	2.018	0.8827	0.8826	-0.35	0.72	0.9736
8.003	0.000	0.000	0.149	0.109	0.9171	0.9170	-0.10	0.83	0.9759
8.004	0.000	0.049	0.149	0.526	0.9171	0.9169	-0.21	1.03	0.9756
8.002	0.000	0.097	0.149	1.026	0.9151	0.9150	-0.29	0.47	0.9754
8.010	0.000	0.143	0.149	1.510	0.9103	0.9103	-0.29	0.04	0.9751
8.017	0.000	0.172	0.149	1.817	0.9067	0.9067	-0.21	-0.23	0.9745
10.012	0.000	0.000	0.148	0.086	0.9319	0.9319	-0.19	0.46	0.9756
10.012	0.000	0.049	0.149	0.528	0.9308	0.9308	-0.22	0.05	0.9758
10.017	0.000	0.097	0.149	1.029	0.9265	0.9264	-0.30	-0.44	0.9754
10.023	0.000	0.137	0.149	1.444	0.9214	0.9213	-0.28	-0.73	0.9750

Table 33. Internal Static Performance of Configuration 31

[$\epsilon = 1.502$; forward slot injection; long Coanda flaps; $\phi_l = 0^\circ$; $\phi_r = 0^\circ$]

NPR	ω_{s_i}	ω_c	$P_{t,s_i}/P_{t,j}$	$P_{t,c}/P_{t,j}$	F_r/F_i	F_d/F_i	δ_p	δ_y	w_p/w_i
1.993	0.000	0.000	0.310	0.499	0.8835	0.8821	3.08	0.64	0.9800
2.003	0.025	0.000	0.735	0.495	0.9063	0.8882	11.47	0.29	0.9802
2.004	0.049	0.000	1.102	0.493	0.9083	0.8990	8.22	0.17	0.9773
2.003	0.075	0.000	1.644	0.491	0.9166	0.9083	7.72	0.21	0.9602
2.009	0.103	0.000	2.166	0.488	0.9243	0.9160	7.69	0.39	0.9274
4.010	0.000	0.000	0.294	0.238	0.9513	0.9513	0.21	0.12	0.9790
4.004	0.025	0.000	0.680	0.232	0.9433	0.9422	2.76	0.03	0.9786
4.014	0.050	0.000	1.112	0.233	0.9361	0.9361	-0.33	0.02	0.9790
4.011	0.073	0.000	1.627	0.232	0.9269	0.9256	-3.12	-0.13	0.9787
4.002	0.098	0.000	2.157	0.226	0.9363	0.9356	-2.23	-0.04	0.9762
6.007	0.000	0.000	0.294	0.153	0.9731	0.9731	0.33	0.02	0.9785
6.019	0.024	0.000	0.668	0.148	0.9625	0.9619	2.01	0.00	0.9786
6.022	0.049	0.000	1.092	0.149	0.9552	0.9552	-0.63	-0.03	0.9786
6.003	0.073	0.000	1.613	0.150	0.9456	0.9442	-3.17	-0.09	0.9787
6.023	0.097	0.000	2.127	0.146	0.9372	0.9344	-4.39	-0.12	0.9786
8.025	0.000	0.000	0.294	0.114	0.9763	0.9763	0.11	0.03	0.9779
8.011	0.025	0.000	0.667	0.112	0.9652	0.9648	1.66	0.01	0.9776
8.020	0.049	0.000	1.078	0.112	0.9557	0.9556	-0.84	0.03	0.9779
8.019	0.073	0.000	1.595	0.113	0.9461	0.9448	-3.09	0.05	0.9779
8.020	0.096	0.000	2.096	0.111	0.9385	0.9358	-4.32	0.12	0.9773
10.016	0.000	0.000	0.295	0.092	0.9735	0.9735	0.00	0.14	0.9766
10.013	0.024	0.000	0.661	0.090	0.9629	0.9625	1.54	0.13	0.9766
10.025	0.049	0.000	1.078	0.091	0.9529	0.9528	-0.92	0.09	0.9766
10.027	0.072	0.000	1.583	0.092	0.9431	0.9418	-3.06	0.12	0.9765
10.050	0.096	0.000	2.093	0.091	0.9344	0.9317	-4.34	0.17	0.9748

Table 36. Internal Static Performance of Configuration 34

[$\epsilon = 1.944$; forward slot injection; long Coanda flaps; $\phi_l = 0^\circ$; $\phi_r = 0^\circ$]

NPR	ω_{si}	ω_c	$p_{t,si}/p_{t,j}$	$p_{t,c}/p_{t,j}$	F_r/F_i	F_u/F_i	δ_p	δ_y	w_p/w_i
2.009	0.000	0.000	0.247	0.488	0.8536	0.8220	-15.46	-2.51	0.9651
2.009	0.026	0.000	0.682	0.492	0.8876	0.8381	19.23	-0.15	0.9652
2.010	0.050	0.000	1.143	0.491	0.9066	0.8625	17.94	0.28	0.9630
2.009	0.076	0.000	1.713	0.493	0.9150	0.8772	16.52	0.28	0.9583
2.003	0.102	0.000	2.257	0.494	0.9223	0.8799	17.45	0.26	0.9508
3.997	0.000	0.000	0.216	0.221	0.9062	0.9062	0.09	0.31	0.9732
3.998	0.025	0.000	0.621	0.225	0.9053	0.9042	2.84	0.33	0.9735
4.001	0.050	0.000	1.136	0.230	0.9310	0.9137	11.03	0.23	0.9734
4.001	0.074	0.000	1.670	0.230	0.9422	0.9159	13.58	0.36	0.9734
4.004	0.098	0.000	2.202	0.234	0.9451	0.9207	13.04	0.43	0.9733
6.003	0.000	0.000	0.208	0.138	0.9520	0.9520	0.08	-0.11	0.9761
5.981	0.025	0.000	0.607	0.141	0.9464	0.9456	2.31	-0.21	0.9763
5.996	0.049	0.000	1.117	0.142	0.9331	0.9303	4.42	-0.18	0.9764
6.008	0.073	0.000	1.660	0.145	0.9216	0.9154	6.64	-0.03	0.9766
6.004	0.097	0.000	2.181	0.141	0.9449	0.9343	8.62	-0.21	0.9767
8.000	0.000	0.000	0.206	0.096	0.9713	0.9713	-0.01	-0.15	0.9770
8.010	0.025	0.000	0.598	0.100	0.9626	0.9620	2.08	-0.24	0.9774
7.998	0.048	0.000	1.097	0.104	0.9491	0.9467	4.08	-0.18	0.9775
7.999	0.072	0.000	1.615	0.105	0.9392	0.9346	5.69	-0.29	0.9776
7.998	0.096	0.000	2.154	0.106	0.9311	0.9264	5.76	-0.29	0.9777
9.994	0.000	0.000	0.206	0.078	0.9781	0.9780	-0.06	-0.23	0.9766
10.002	0.025	0.000	0.593	0.081	0.9686	0.9681	1.83	-0.16	0.9769
10.002	0.048	0.000	1.096	0.084	0.9554	0.9531	3.95	-0.15	0.9773
10.004	0.072	0.000	1.629	0.083	0.9406	0.9365	5.34	-0.21	0.9773
10.006	0.096	0.000	2.153	0.084	0.9353	0.9312	5.34	-0.23	0.9775

Table 39. Internal Static Performance of Configuration 37

[$\epsilon = 2.405$; forward slot injection; long Coanda flaps; $\phi_l = 0^\circ$; $\phi_r = 0^\circ$]

NPR	ω_M	ω_t	$p_{t,s}/p_{t,j}$	$p_{t,c}/p_{t,j}$	F_r/F_t	F_d/F_t	δ_p	δ_v	w_p/w_i
2.012	0.000	0.000	0.483	0.489	0.9311	0.9310	-0.87	0.46	0.9723
2.009	0.025	0.000	0.682	0.488	0.9026	0.9024	-1.11	0.38	0.9731
2.009	0.050	0.000	1.170	0.488	0.8713	0.8711	-1.09	0.58	0.9737
2.002	0.074	0.000	1.736	0.488	0.8644	0.8516	9.88	0.47	0.9701
2.003	0.098	0.000	2.301	0.487	0.8659	0.8179	19.17	0.26	0.9702
4.006	0.000	0.000	0.232	0.213	0.8412	0.8412	0.36	0.00	0.9801
4.007	0.025	0.000	0.591	0.218	0.8810	0.8735	7.49	0.06	0.9801
4.006	0.049	0.000	1.173	0.225	0.8943	0.8768	11.35	0.56	0.9803
4.007	0.072	0.000	1.706	0.223	0.8975	0.8703	14.12	0.72	0.9805
4.012	0.096	0.000	2.265	0.219	0.9024	0.8615	17.30	0.89	0.9806
6.003	0.000	0.000	0.234	0.151	0.8879	0.8879	0.12	0.05	0.9802
6.000	0.025	0.000	0.609	0.141	0.8857	0.8850	2.28	0.18	0.9802
6.001	0.049	0.000	1.151	0.144	0.8815	0.8780	5.07	0.11	0.9805
6.004	0.073	0.000	1.702	0.130	0.9140	0.8966	11.20	0.24	0.9804
6.009	0.096	0.000	2.241	0.128	0.9170	0.8906	13.77	0.29	0.9805
7.993	0.000	0.000	0.225	0.112	0.9238	0.9238	0.03	-0.13	0.9798
7.995	0.025	0.000	0.588	0.104	0.9202	0.9196	2.01	-0.26	0.9801
7.993	0.049	0.000	1.151	0.103	0.9121	0.9096	4.23	-0.05	0.9802
7.996	0.073	0.000	1.706	0.107	0.9080	0.9020	6.58	0.07	0.9802
7.997	0.097	0.000	2.265	0.108	0.9208	0.9053	10.52	0.11	0.9802
9.997	0.000	0.000	0.212	0.094	0.9435	0.9435	-0.06	0.11	0.9788
10.015	0.024	0.000	0.577	0.078	0.9373	0.9368	1.84	-0.03	0.9791
10.011	0.049	0.000	1.141	0.078	0.9291	0.9267	4.04	0.04	0.9793
10.014	0.072	0.000	1.688	0.080	0.9206	0.9158	5.82	0.24	0.9793
9.995	0.091	0.000	2.112	0.081	0.9143	0.9070	7.25	0.26	0.9794
10.001	0.096	0.000	2.222	0.082	0.9135	0.9055	7.62	0.24	0.9794

Table 49. Concluded

[$\epsilon = 1.944$; aft slot injection; long Coanda flaps; $\phi_f = 0^\circ$; $\phi_r = 45^\circ$]

NPR	ω_{sl}	ω_c	$P_{t,sl}/P_{t,j}$	$P_{t,c}/P_{t,j}$	F_r/F_i	F_u/F_i	δ_ρ	δ_y	w_p/w_i
5.993	0.093	0.141	2.118	1.500	0.9314	0.9144	10.98	0.01	0.9740
5.994	0.093	0.189	2.129	2.001	0.9360	0.9206	10.41	0.18	0.9738
8.002	0.000	0.049	0.164	0.525	0.9692	0.9691	-0.10	0.62	0.9739
8.006	0.000	0.094	0.163	1.006	0.9668	0.9667	-0.10	0.82	0.9739
8.007	0.000	0.142	0.163	1.512	0.9643	0.9642	-0.10	0.86	0.9738
8.013	0.000	0.172	0.162	1.819	0.9619	0.9618	-0.16	0.85	0.9736
8.008	0.024	0.048	0.568	0.511	0.9627	0.9621	1.95	0.39	0.9744
8.012	0.023	0.096	0.558	1.020	0.9611	0.9606	1.80	0.48	0.9742
8.016	0.024	0.142	0.567	1.508	0.9591	0.9586	1.73	0.59	0.9739
8.003	0.023	0.170	0.559	1.798	0.9568	0.9564	1.62	0.64	0.9738
8.002	0.047	0.048	1.081	0.511	0.9502	0.9479	3.97	0.23	0.9741
8.003	0.047	0.095	1.082	1.009	0.9486	0.9466	3.75	0.32	0.9741
8.004	0.047	0.141	1.086	1.498	0.9465	0.9447	3.54	0.33	0.9739
8.006	0.047	0.168	1.073	1.777	0.9454	0.9437	3.43	0.35	0.9737
8.005	0.071	0.047	1.631	0.506	0.9481	0.9399	7.55	0.16	0.9742
8.005	0.070	0.094	1.596	1.004	0.9462	0.9393	6.93	0.13	0.9741
8.007	0.070	0.141	1.602	1.496	0.9439	0.9375	6.64	0.25	0.9740
8.008	0.070	0.166	1.596	1.756	0.9421	0.9362	6.42	0.23	0.9738
8.007	0.095	0.048	2.155	0.514	0.9406	0.9263	10.02	-0.07	0.9742
8.008	0.093	0.094	2.126	1.007	0.9407	0.9280	9.45	-0.04	0.9742
8.008	0.093	0.141	2.120	1.496	0.9390	0.9275	8.97	0.03	0.9740
8.010	0.092	0.164	2.101	1.738	0.9369	0.9260	8.75	0.05	0.9738
9.981	0.000	0.048	0.163	0.513	0.9764	0.9764	-0.12	0.37	0.9736
10.008	0.000	0.094	0.162	1.007	0.9741	0.9741	-0.14	0.45	0.9736
10.006	0.000	0.140	0.162	1.487	0.9697	0.9697	-0.16	0.47	0.9737
9.996	0.024	0.048	0.562	0.516	0.9696	0.9691	1.78	0.08	0.9741
9.997	0.024	0.094	0.567	1.006	0.9678	0.9673	1.72	0.20	0.9741
9.996	0.024	0.138	0.570	1.459	0.9638	0.9634	1.63	0.22	0.9739
9.990	0.047	0.047	1.083	0.506	0.9553	0.9532	3.77	-0.07	0.9741
9.989	0.047	0.095	1.085	1.014	0.9540	0.9522	3.54	-0.02	0.9742
9.986	0.047	0.136	1.088	1.439	0.9508	0.9491	3.42	-0.04	0.9742
9.985	0.070	0.048	1.598	0.510	0.9470	0.9418	6.01	-0.13	0.9745
9.989	0.071	0.095	1.609	1.012	0.9459	0.9411	5.77	-0.11	0.9742
9.988	0.070	0.132	1.605	1.398	0.9428	0.9384	5.52	-0.13	0.9741
9.992	0.094	0.048	2.131	0.516	0.9400	0.9291	8.73	-0.32	0.9744
9.995	0.094	0.095	2.142	1.014	0.9398	0.9297	8.37	-0.26	0.9743
9.993	0.094	0.128	2.127	1.357	0.9384	0.9291	8.05	-0.24	0.9741

Table 50. Concluded

[$\epsilon = 1.944$; aft slot injection; long Coanda flaps; $\phi_i = -10^\circ$; $\phi_r = 45^\circ$]

NPR	ω_{st}	ω_c	$p_{t,s}/p_{t,j}$	$p_{t,c}/p_{t,j}$	F_r/F_i	F_d/F_i	δ_p	δ_v	w_p/w_i
6.002	0.094	0.142	2.133	1.511	0.9266	0.9091	10.98	-2.09	0.9742
6.002	0.093	0.189	2.125	2.009	0.9242	0.9084	10.43	-2.06	0.9742
8.002	0.000	0.048	0.162	0.512	0.9657	0.9657	-0.16	-0.48	0.9742
8.008	0.000	0.095	0.162	1.015	0.9615	0.9614	-0.20	-0.81	0.9742
8.010	0.000	0.143	0.162	1.515	0.9582	0.9580	-0.19	-0.97	0.9741
8.012	0.000	0.172	0.162	1.820	0.9540	0.9539	-0.21	-1.03	0.9738
8.005	0.024	0.048	0.564	0.518	0.9583	0.9577	1.85	-0.85	0.9745
8.007	0.024	0.094	0.567	1.005	0.9550	0.9544	1.78	-1.20	0.9745
8.007	0.024	0.142	0.564	1.507	0.9503	0.9497	1.65	-1.28	0.9743
8.009	0.023	0.169	0.555	1.795	0.9482	0.9476	1.59	-1.33	0.9741
8.005	0.047	0.048	1.089	0.517	0.9442	0.9418	3.89	-1.05	0.9745
8.009	0.047	0.094	1.091	1.007	0.9420	0.9398	3.73	-1.39	0.9744
8.008	0.047	0.142	1.079	1.504	0.9388	0.9368	3.46	-1.53	0.9743
8.010	0.047	0.168	1.083	1.778	0.9364	0.9344	3.41	-1.55	0.9742
8.007	0.070	0.048	1.610	0.514	0.9407	0.9330	7.25	-1.39	0.9744
8.005	0.071	0.094	1.615	1.004	0.9383	0.9309	6.95	-1.81	0.9745
8.008	0.070	0.141	1.598	1.494	0.9349	0.9283	6.55	-1.81	0.9745
8.008	0.070	0.167	1.590	1.771	0.9330	0.9269	6.32	-1.88	0.9743
8.007	0.094	0.048	2.139	0.509	0.9338	0.9194	9.93	-1.77	0.9748
8.007	0.094	0.094	2.139	1.002	0.9326	0.9194	9.45	-2.02	0.9746
8.010	0.091	0.142	2.080	1.507	0.9293	0.9179	8.77	-2.07	0.9746
8.011	0.093	0.167	2.121	1.764	0.9273	0.9158	8.78	-2.11	0.9743
10.004	0.000	0.048	0.162	0.509	0.9725	0.9723	-0.19	-0.87	0.9743
10.005	0.000	0.095	0.162	1.018	0.9677	0.9675	-0.21	-1.10	0.9743
10.011	0.000	0.140	0.162	1.488	0.9629	0.9626	-0.19	-1.29	0.9741
10.003	0.024	0.047	0.565	0.508	0.9646	0.9639	1.76	-1.22	0.9746
10.004	0.023	0.095	0.553	1.012	0.9617	0.9610	1.61	-1.45	0.9745
10.007	0.024	0.137	0.572	1.453	0.9551	0.9544	1.61	-1.57	0.9744
10.005	0.047	0.048	1.070	0.513	0.9507	0.9485	3.65	-1.44	0.9747
10.004	0.047	0.094	1.084	1.003	0.9474	0.9452	3.48	-1.72	0.9745
10.009	0.047	0.134	1.069	1.420	0.9432	0.9412	3.32	-1.79	0.9744
10.009	0.070	0.048	1.591	0.513	0.9408	0.9355	5.86	-1.63	0.9746
10.011	0.070	0.095	1.606	1.011	0.9381	0.9330	5.69	-1.85	0.9747
10.011	0.071	0.132	1.609	1.397	0.9350	0.9301	5.49	-1.95	0.9743
10.011	0.094	0.047	2.126	0.504	0.9359	0.9249	8.62	-1.89	0.9745
10.012	0.094	0.094	2.142	0.999	0.9330	0.9226	8.31	-2.09	0.9746
10.012	0.094	0.130	2.132	1.381	0.9302	0.9205	8.01	-2.19	0.9743

Table 51. Concluded

[$\epsilon = 1.944$; aft slot injection; long Coanda flaps; $\phi_l = -10^\circ$; $\phi_r = 30^\circ$]

NPR	ω_{si}	ω_c	$p_{t,si}/p_{t,j}$	$p_{t,c}/p_{t,j}$	F_r/F_i	F_a/F_i	δ_p	δ_y	w_p/w_i
5.995	0.094	0.141	2.134	1.504	0.9227	0.9043	11.10	-2.88	0.9742
5.994	0.093	0.187	2.127	1.981	0.9185	0.9019	10.58	-2.70	0.9741
7.987	0.000	0.048	0.162	0.515	0.9636	0.9634	-0.07	-1.00	0.9746
7.991	0.000	0.094	0.162	1.005	0.9589	0.9587	-0.11	-1.27	0.9745
7.992	0.000	0.141	0.162	1.504	0.9491	0.9486	-0.12	-1.85	0.9743
7.995	0.000	0.174	0.162	1.845	0.9444	0.9438	-0.13	-2.16	0.9742
7.990	0.024	0.047	0.562	0.506	0.9569	0.9561	1.95	-1.28	0.9748
7.993	0.023	0.094	0.560	1.009	0.9525	0.9517	1.82	-1.63	0.9745
7.994	0.023	0.141	0.553	1.499	0.9446	0.9435	1.74	-2.12	0.9743
7.996	0.023	0.170	0.555	1.807	0.9396	0.9385	1.63	-2.22	0.9742
7.992	0.047	0.048	1.070	0.515	0.9431	0.9405	3.92	-1.57	0.9746
7.993	0.047	0.094	1.070	1.003	0.9389	0.9364	3.71	-1.95	0.9747
7.995	0.047	0.140	1.075	1.493	0.9326	0.9301	3.57	-2.25	0.9746
7.995	0.046	0.167	1.068	1.771	0.9296	0.9271	3.41	-2.38	0.9746
7.997	0.070	0.048	1.595	0.511	0.9396	0.9315	7.29	-1.93	0.9747
7.996	0.070	0.094	1.597	1.003	0.9345	0.9269	6.95	-2.36	0.9748
7.998	0.070	0.140	1.595	1.490	0.9314	0.9243	6.62	-2.50	0.9746
8.001	0.070	0.166	1.600	1.762	0.9282	0.9213	6.51	-2.54	0.9746
8.002	0.093	0.048	2.111	0.514	0.9331	0.9186	9.84	-2.31	0.9749
8.004	0.093	0.093	2.114	1.001	0.9306	0.9172	9.38	-2.70	0.9749
8.006	0.093	0.140	2.111	1.494	0.9246	0.9122	8.98	-2.76	0.9747
8.009	0.093	0.165	2.125	1.752	0.9239	0.9120	8.81	-2.61	0.9746
10.013	0.000	0.048	0.162	0.515	0.9687	0.9684	-0.16	-1.28	0.9739
10.020	0.000	0.094	0.162	1.001	0.9639	0.9635	-0.14	-1.58	0.9740
10.009	0.000	0.139	0.162	1.471	0.9552	0.9546	-0.13	-2.00	0.9736
10.004	0.023	0.048	0.559	0.517	0.9622	0.9613	1.78	-1.65	0.9745
10.003	0.023	0.094	0.557	1.001	0.9581	0.9572	1.69	-1.80	0.9743
10.007	0.024	0.136	0.563	1.447	0.9505	0.9494	1.64	-2.12	0.9741
10.001	0.046	0.048	1.065	0.516	0.9484	0.9459	3.68	-1.90	0.9745
10.001	0.047	0.093	1.077	0.997	0.9451	0.9427	3.51	-1.98	0.9743
10.005	0.047	0.135	1.081	1.428	0.9380	0.9354	3.45	-2.45	0.9742
10.003	0.070	0.047	1.587	0.507	0.9378	0.9321	5.96	-2.18	0.9744
10.002	0.070	0.094	1.590	0.999	0.9348	0.9295	5.65	-2.30	0.9744
10.004	0.070	0.132	1.606	1.397	0.9299	0.9247	5.54	-2.48	0.9740
10.003	0.093	0.048	2.118	0.512	0.9309	0.9193	8.70	-2.53	0.9744
10.005	0.093	0.094	2.117	0.998	0.9274	0.9166	8.29	-2.86	0.9743
10.003	0.093	0.127	2.115	1.347	0.9252	0.9152	7.99	-2.73	0.9742

Table 52. Concluded

[$\varepsilon = 1.499$; aft slot injection; long Coanda flaps; $\phi_i = 0^\circ$; $\phi_r = 45^\circ$]

NPR	ω_{st}	ω_c	$p_{t,st}/p_{t,j}$	$p_{t,c}/p_{t,j}$	F_r/F_i	F_a/F_i	δ_p	δ_y	w_p/w_i
6.006	0.096	0.144	2.139	1.498	0.9486	0.9245	12.93	0.35	0.9554
6.002	0.094	0.191	2.092	1.980	0.9433	0.9217	12.28	0.51	0.9560
7.994	0.000	0.050	0.328	0.523	0.9712	0.9280	17.16	0.02	0.9582
7.991	0.000	0.097	0.328	1.022	0.9699	0.9310	16.28	0.26	0.9581
7.999	0.000	0.143	0.327	1.487	0.9637	0.9282	15.59	0.32	0.9581
8.005	0.000	0.174	0.328	1.805	0.9591	0.9256	15.16	0.50	0.9578
8.006	0.024	0.047	0.714	0.499	0.9656	0.9208	17.52	0.18	0.9581
8.005	0.023	0.093	0.704	0.981	0.9637	0.9226	16.78	0.26	0.9585
8.005	0.024	0.144	0.713	1.498	0.9572	0.9203	15.95	0.38	0.9585
8.007	0.024	0.172	0.709	1.785	0.9534	0.9187	15.49	0.53	0.9583
8.009	0.048	0.050	1.110	0.530	0.9535	0.9192	15.41	-0.32	0.9584
8.009	0.048	0.096	1.096	1.006	0.9558	0.9246	14.69	0.05	0.9584
8.011	0.046	0.144	1.074	1.499	0.9517	0.9229	14.14	0.16	0.9585
8.013	0.048	0.170	1.110	1.766	0.9469	0.9203	13.61	-0.29	0.9583
8.000	0.072	0.050	1.600	0.527	0.9459	0.9208	13.21	-0.31	0.9584
8.006	0.073	0.096	1.619	1.002	0.9476	0.9253	12.46	-0.02	0.9585
8.003	0.070	0.145	1.572	1.511	0.9441	0.9233	12.07	0.08	0.9583
7.987	0.070	0.169	1.564	1.759	0.9420	0.9220	11.82	0.18	0.9582
8.018	0.094	0.048	2.075	0.510	0.9448	0.9195	13.29	-0.18	0.9566
8.003	0.095	0.093	2.100	0.978	0.9472	0.9242	12.65	0.08	0.9562
8.000	0.094	0.144	2.078	1.498	0.9434	0.9226	12.05	0.19	0.9565
8.007	0.095	0.167	2.113	1.734	0.9408	0.9210	11.78	0.26	0.9561
10.010	0.000	0.048	0.339	0.505	0.9698	0.9295	16.56	-0.13	0.9575
9.994	0.000	0.096	0.339	1.006	0.9668	0.9306	15.73	0.03	0.9578
9.998	0.000	0.141	0.338	1.470	0.9600	0.9271	15.06	0.17	0.9577
9.992	0.025	0.047	0.729	0.490	0.9583	0.9166	16.96	-0.42	0.9584
10.017	0.024	0.094	0.719	0.987	0.9592	0.9217	16.07	0.07	0.9586
10.022	0.024	0.139	0.709	1.448	0.9533	0.9186	15.50	0.21	0.9584
9.996	0.047	0.049	1.077	0.516	0.9507	0.9179	15.09	-0.49	0.9586
9.998	0.048	0.096	1.095	0.999	0.9520	0.9228	14.23	-0.06	0.9585
10.007	0.048	0.137	1.102	1.426	0.9469	0.9201	13.67	0.07	0.9584
10.003	0.070	0.048	1.563	0.507	0.9424	0.9183	12.99	-0.57	0.9583
10.006	0.071	0.095	1.588	0.994	0.9444	0.9231	12.19	-0.21	0.9585
10.002	0.071	0.135	1.587	1.400	0.9410	0.9214	11.70	-0.13	0.9584
9.995	0.096	0.048	2.118	0.502	0.9408	0.9174	12.81	-0.46	0.9558
9.990	0.095	0.098	2.100	1.019	0.9426	0.9215	12.14	-0.13	0.9562
9.990	0.095	0.131	2.099	1.354	0.9399	0.9202	11.76	-0.07	0.9563

Table 53. Concluded

[$\epsilon = 1.499$; aft slot injection; long Coanda flaps; $\phi_l = -10^\circ$; $\phi_r = 45^\circ$]

NPR	ω_{sl}	ω_c	$p_{t,sl}/p_{t,j}$	$p_{t,c}/p_{t,j}$	F_r/F_i	F_a/F_i	δ_p	δ_y	w_p/w_i
6.011	0.097	0.145	2.144	1.520	0.9449	0.9207	12.92	-1.46	0.9559
6.032	0.097	0.192	2.146	2.001	0.9398	0.9176	12.40	-1.47	0.9556
7.991	0.000	0.048	0.325	0.506	0.9693	0.9257	17.21	-1.29	0.9587
7.991	0.000	0.098	0.324	1.034	0.9660	0.9267	16.35	-1.36	0.9588
7.993	0.000	0.145	0.324	1.517	0.9589	0.9232	15.62	-1.42	0.9588
7.995	0.000	0.168	0.323	1.749	0.9553	0.9210	15.33	-1.40	0.9584
7.992	0.023	0.050	0.703	0.522	0.9646	0.9190	17.66	-1.13	0.9590
8.019	0.025	0.097	0.720	1.015	0.9604	0.9196	16.72	-1.29	0.9592
8.001	0.024	0.147	0.712	1.537	0.9523	0.9155	15.94	-1.32	0.9589
8.009	0.024	0.165	0.716	1.722	0.9501	0.9145	15.68	-1.31	0.9586
8.008	0.048	0.049	1.099	0.518	0.9526	0.9173	15.57	-1.56	0.9592
8.002	0.048	0.098	1.111	1.028	0.9521	0.9207	14.68	-1.51	0.9591
8.009	0.049	0.146	1.121	1.529	0.9461	0.9177	13.98	-1.55	0.9588
8.004	0.048	0.168	1.107	1.751	0.9425	0.9151	13.78	-1.49	0.9587
8.005	0.073	0.048	1.618	0.506	0.9438	0.9186	13.19	-1.54	0.9589
8.001	0.071	0.098	1.583	1.029	0.9444	0.9211	12.65	-1.62	0.9590
8.005	0.073	0.145	1.626	1.516	0.9388	0.9182	11.94	-1.61	0.9588
8.007	0.072	0.167	1.605	1.738	0.9369	0.9167	11.81	-1.65	0.9588
8.010	0.094	0.049	2.079	0.517	0.9432	0.9177	13.28	-1.38	0.9570
8.013	0.098	0.097	2.159	1.017	0.9439	0.9207	12.65	-1.43	0.9562
8.015	0.097	0.145	2.138	1.512	0.9391	0.9178	12.15	-1.48	0.9561
8.002	0.096	0.165	2.117	1.713	0.9366	0.9162	11.90	-1.48	0.9562
9.991	0.000	0.049	0.314	0.514	0.9675	0.9271	16.56	-1.45	0.9579
9.994	0.000	0.097	0.314	1.016	0.9629	0.9263	15.77	-1.54	0.9581
9.998	0.000	0.139	0.314	1.454	0.9550	0.9215	15.16	-1.58	0.9580
9.993	0.024	0.050	0.716	0.527	0.9573	0.9152	16.99	-1.63	0.9586
9.997	0.024	0.098	0.707	1.025	0.9557	0.9174	16.23	-1.45	0.9585
10.004	0.025	0.137	0.723	1.427	0.9493	0.9142	15.56	-1.48	0.9584
10.006	0.049	0.049	1.118	0.522	0.9476	0.9153	14.91	-1.79	0.9586
10.000	0.048	0.097	1.095	1.019	0.9481	0.9185	14.26	-1.67	0.9585
10.007	0.048	0.134	1.092	1.401	0.9426	0.9150	13.82	-1.64	0.9584
10.010	0.073	0.049	1.613	0.514	0.9398	0.9163	12.71	-1.85	0.9585
10.015	0.073	0.097	1.620	1.020	0.9397	0.9185	12.08	-1.81	0.9586
10.011	0.072	0.132	1.593	1.374	0.9352	0.9149	11.82	-1.88	0.9585
10.007	0.098	0.048	2.159	0.503	0.9385	0.9150	12.74	-1.72	0.9555
10.006	0.097	0.098	2.140	1.021	0.9386	0.9172	12.14	-1.66	0.9559
10.006	0.096	0.129	2.118	1.344	0.9351	0.9150	11.81	-1.71	0.9561

Table 54. Concluded

[$\varepsilon = 1.499$; aft slot injection; long Coanda flaps; $\phi_i = -10^\circ$; $\phi_r = 30^\circ$]

NPR	ω_{si}	ω_c	$p_{1,si}/p_{1,j}$	$p_{1,c}/p_{1,j}$	F_i/F_i	F_d/F_i	δ_p	δ_v	w_p/w_i
5.994	0.095	0.144	2.117	1.499	0.9397	0.9149	13.06	-2.01	0.9555
5.997	0.097	0.192	2.140	1.993	0.9358	0.9131	12.54	-1.82	0.9551
7.982	0.000	0.048	0.316	0.505	0.9683	0.9240	17.34	-1.59	0.9579
7.990	0.000	0.096	0.314	1.002	0.9595	0.9192	16.54	-2.12	0.9579
7.986	0.000	0.144	0.314	1.497	0.9546	0.9184	15.73	-1.84	0.9579
7.985	0.000	0.177	0.314	1.838	0.9496	0.9160	15.21	-1.76	0.9577
7.980	0.024	0.048	0.708	0.505	0.9618	0.9158	17.72	-1.62	0.9584
7.984	0.024	0.096	0.712	1.003	0.9521	0.9101	16.94	-2.31	0.9585
7.983	0.024	0.143	0.714	1.489	0.9507	0.9130	16.13	-1.67	0.9583
7.987	0.024	0.175	0.709	1.817	0.9455	0.9100	15.67	-1.59	0.9584
7.989	0.047	0.049	1.090	0.517	0.9534	0.9180	15.58	-1.71	0.9583
7.989	0.047	0.096	1.086	1.011	0.9444	0.9112	15.04	-2.52	0.9585
7.991	0.047	0.143	1.088	1.489	0.9427	0.9130	14.30	-2.01	0.9582
7.990	0.047	0.172	1.086	1.786	0.9393	0.9113	13.92	-1.83	0.9583
7.991	0.072	0.049	1.598	0.513	0.9444	0.9187	13.31	-1.70	0.9583
7.988	0.071	0.096	1.589	1.004	0.9354	0.9113	12.79	-2.56	0.9585
7.992	0.071	0.143	1.592	1.488	0.9343	0.9127	12.16	-2.21	0.9582
7.991	0.071	0.170	1.588	1.764	0.9325	0.9119	11.90	-2.05	0.9582
8.008	0.095	0.049	2.099	0.510	0.9443	0.9186	13.32	-1.52	0.9559
8.008	0.095	0.096	2.106	1.004	0.9356	0.9115	12.83	-2.39	0.9559
8.009	0.096	0.144	2.114	1.497	0.9344	0.9128	12.21	-1.94	0.9558
8.008	0.095	0.166	2.108	1.719	0.9322	0.9115	11.97	-1.87	0.9558
9.993	0.000	0.049	0.314	0.516	0.9647	0.9238	16.63	-1.93	0.9574
9.987	0.000	0.096	0.314	1.004	0.9590	0.9219	15.88	-1.93	0.9577
9.983	0.000	0.141	0.314	1.463	0.9518	0.9179	15.23	-1.89	0.9576
9.996	0.024	0.048	0.709	0.511	0.9574	0.9146	17.11	-1.87	0.9582
10.006	0.024	0.096	0.709	1.005	0.9530	0.9141	16.32	-1.86	0.9580
10.005	0.024	0.139	0.707	1.444	0.9466	0.9109	15.69	-1.81	0.9578
9.997	0.048	0.049	1.101	0.515	0.9490	0.9161	15.02	-1.95	0.9581
9.997	0.048	0.096	1.102	1.000	0.9411	0.9109	14.37	-2.42	0.9582
9.998	0.048	0.136	1.098	1.415	0.9371	0.9092	13.83	-2.30	0.9581
9.995	0.071	0.049	1.589	0.515	0.9405	0.9164	12.86	-2.02	0.9582
9.993	0.071	0.096	1.580	0.999	0.9334	0.9109	12.37	-2.63	0.9582
9.991	0.072	0.134	1.590	1.386	0.9307	0.9100	11.87	-2.46	0.9579
10.000	0.096	0.048	2.113	0.509	0.9402	0.9165	12.79	-1.82	0.9557
10.002	0.095	0.096	2.101	0.999	0.9335	0.9114	12.28	-2.36	0.9559
9.997	0.095	0.131	2.099	1.360	0.9290	0.9081	11.95	-2.38	0.9560

Table 60. Coanda Flap Static Pressure Ratios $p/p_{t,j}$ for Configuration 6

[$\epsilon = 1.502$; long Coanda flaps; $\phi_l = 0^\circ$; $\phi_r = 0^\circ$]

			$p/p_{t,j}$ for---									
			Left Coanda flap at---					Right Coanda flap at---				
			x_c/R of---					x_c/R of---				
NPR	$\omega_{s,l}$	ω_c	-0.785	-0.524	0.000	0.560	1.140	-0.785	-0.524	0.000	0.560	1.140
2.003	0.0000	0.0000	0.497	0.497	0.495	0.512	0.526	0.498	0.498	0.496	0.530	0.532
1.991	0.0000	0.0480	0.499	0.499	0.512	0.517	0.513	0.502	0.501	0.511	0.520	0.515
1.994	0.0000	0.0967	0.466	0.459	0.489	0.545	0.508	0.477	0.452	0.500	0.536	0.510
1.998	0.0000	0.1456	0.449	0.439	0.459	0.546	0.513	0.460	0.419	0.454	0.531	0.507
1.998	0.0000	0.1928	0.427	0.412	0.449	0.471	0.499	0.464	0.429	0.545	0.490	0.517
4.006	0.0000	0.0000	0.237	0.234	0.236	0.239	0.239	0.243	0.237	0.235	0.237	0.238
4.001	0.0000	0.0495	0.209	0.197	0.214	0.235	0.255	0.224	0.192	0.198	0.238	0.258
3.995	0.0000	0.0980	0.190	0.169	0.160	0.191	0.256	0.229	0.208	0.148	0.185	0.258
3.992	0.0000	0.1456	0.222	0.216	0.234	0.131	0.201	0.246	0.243	0.218	0.128	0.179
4.014	0.0000	0.1900	0.239	0.237	0.307	0.179	0.126	0.249	0.249	0.283	0.145	0.074
5.996	0.0000	0.0000	0.155	0.151	0.153	0.154	0.151	0.160	0.153	0.149	0.150	0.150
5.995	0.0000	0.0494	0.131	0.120	0.135	0.143	0.155	0.147	0.122	0.075	0.147	0.161
6.007	0.0000	0.0966	0.148	0.144	0.150	0.087	0.140	0.164	0.162	0.145	0.134	0.151
6.008	0.0000	0.1443	0.163	0.162	0.239	0.137	0.111	0.166	0.164	0.215	0.102	0.120
6.000	0.0000	0.1914	0.166	0.166	0.321	0.187	0.126	0.166	0.162	0.276	0.119	0.088
7.985	0.0000	0.0000	0.116	0.114	0.116	0.118	0.117	0.120	0.115	0.113	0.114	0.115
8.011	0.0000	0.0490	0.099	0.093	0.104	0.113	0.117	0.115	0.105	0.075	0.138	0.133
7.982	0.0000	0.0973	0.121	0.120	0.158	0.092	0.131	0.125	0.125	0.145	0.145	0.149
8.005	0.0000	0.1439	0.125	0.124	0.242	0.141	0.114	0.124	0.121	0.208	0.100	0.126
7.993	0.0000	0.1770	0.125	0.123	0.293	0.178	0.118	0.123	0.117	0.251	0.107	0.098
10.002	0.0000	0.0000	0.093	0.091	0.093	0.095	0.095	0.096	0.093	0.092	0.093	0.097
10.040	0.0000	0.0494	0.087	0.085	0.094	0.104	0.110	0.096	0.093	0.076	0.137	0.130
10.008	0.0000	0.0970	0.099	0.098	0.163	0.094	0.131	0.099	0.099	0.143	0.148	0.148
10.009	0.0000	0.1409	0.100	0.098	0.233	0.141	0.114	0.098	0.094	0.200	0.123	0.135

Table 65. Coanda Flap Static Pressure Ratios $p^i/p_{t,i}$ for Configuration 11

[$\varepsilon = 1.944$; long Coanda flaps; $\phi_l = 0^\circ$; $\phi_r = 0^\circ$]

			$p^i/p_{t,i}$ for---									
			Left Coanda flap at---					Right Coanda flap at---				
			x_i/R of---					x_i/R of---				
NPR	ω_{x_i}	ω_{ϕ_i}	-0.785	-0.524	0.000	0.560	1.140	-0.785	-0.524	0.000	0.560	1.140
2.010	0.0000	0.0000	0.483	0.482	0.485	0.486	0.484	0.495	0.491	0.484	0.504	0.526
2.009	0.0000	0.0517	0.474	0.469	0.473	0.480	0.489	0.497	0.495	0.493	0.516	0.520
2.010	0.0000	0.1008	0.425	0.416	0.438	0.468	0.486	0.480	0.436	0.477	0.540	0.536
2.010	0.0000	0.1505	0.408	0.399	0.427	0.449	0.478	0.476	0.422	0.404	0.548	0.534
2.011	0.0000	0.1989	0.385	0.370	0.402	0.411	0.482	0.481	0.444	0.365	0.525	0.560
3.992	0.0000	0.0000	0.219	0.213	0.221	0.226	0.237	0.244	0.228	0.216	0.222	0.238
3.996	0.0000	0.0000	0.219	0.213	0.221	0.225	0.236	0.244	0.228	0.216	0.221	0.238
3.999	0.0000	0.0511	0.203	0.197	0.212	0.225	0.251	0.237	0.202	0.163	0.212	0.240
4.000	0.0000	0.0993	0.199	0.196	0.213	0.209	0.206	0.242	0.223	0.122	0.199	0.223
4.001	0.0000	0.1484	0.219	0.216	0.270	0.112	0.222	0.249	0.249	0.186	0.201	0.202
4.002	0.0000	0.1944	0.239	0.238	0.326	0.141	0.188	0.248	0.242	0.239	0.106	0.195
6.008	0.0000	0.0000	0.142	0.139	0.145	0.147	0.150	0.161	0.147	0.133	0.136	0.135
6.007	0.0000	0.0501	0.109	0.093	0.107	0.116	0.141	0.158	0.136	0.061	0.074	0.100
6.009	0.0000	0.0964	0.144	0.142	0.175	0.069	0.073	0.166	0.166	0.124	0.058	0.063
6.011	0.0000	0.1455	0.162	0.162	0.247	0.109	0.038	0.163	0.160	0.182	0.078	0.032
6.012	0.0000	0.1900	0.165	0.165	0.352	0.151	0.052	0.162	0.155	0.236	0.099	0.080
7.990	0.0000	0.0000	0.102	0.099	0.105	0.107	0.109	0.120	0.106	0.091	0.093	0.095
7.991	0.0000	0.0494	0.091	0.084	0.083	0.055	0.090	0.121	0.112	0.061	0.072	0.079
7.990	0.0000	0.0947	0.119	0.119	0.162	0.070	0.071	0.124	0.122	0.118	0.054	0.069
7.984	0.0000	0.1434	0.125	0.124	0.266	0.114	0.065	0.122	0.117	0.178	0.075	0.031
7.981	0.0000	0.1719	0.125	0.123	0.322	0.140	0.047	0.122	0.111	0.212	0.089	0.036
9.996	0.0000	0.0000	0.078	0.075	0.081	0.083	0.085	0.096	0.085	0.073	0.075	0.076
10.024	0.0000	0.0509	0.082	0.080	0.086	0.040	0.083	0.099	0.097	0.065	0.070	0.078
9.983	0.0000	0.0961	0.098	0.098	0.171	0.074	0.075	0.098	0.096	0.120	0.053	0.067
9.982	0.0000	0.1371	0.100	0.098	0.257	0.111	0.075	0.097	0.089	0.169	0.071	0.031

Table 66. Coanda Flap Static Pressure Ratios $p/p_{t,j}$ for Configuration 12

[$\epsilon = 1.944$; long Coanda flaps; $\phi_j = 0^\circ$; $\phi_r = 30^\circ$]

			$p/p_{t,j}$ for---									
			Left Coanda flap at---					Right Coanda flap at---				
			x_i/R of---					x_r/R of---				
NPR	$\omega_{s,i}$	ω_r	-0.785	-0.524	0.000	0.560	1.140	-0.785	-0.524	0.000	0.560	1.140
1.999	0.0000	0.0000	0.491	0.490	0.490	0.512	0.515	0.449	0.444	0.456	0.466	0.482
1.995	0.0000	0.0530	0.497	0.497	0.506	0.514	0.508	0.460	0.429	0.466	0.484	0.490
1.995	0.0000	0.1036	0.458	0.454	0.472	0.525	0.502	0.330	0.341	0.410	0.476	0.504
1.995	0.0000	0.1531	0.446	0.443	0.458	0.505	0.508	0.350	0.310	0.342	0.440	0.504
1.996	0.0000	0.2017	0.422	0.415	0.445	0.451	0.529	0.431	0.357	0.313	0.396	0.471
4.014	0.0000	0.0000	0.218	0.211	0.221	0.224	0.234	0.229	0.224	0.231	0.244	0.246
4.018	0.0000	0.0506	0.202	0.196	0.211	0.224	0.249	0.190	0.216	0.225	0.223	0.237
4.014	0.0000	0.0997	0.199	0.196	0.213	0.209	0.204	0.215	0.179	0.202	0.199	0.211
4.017	0.0000	0.1457	0.217	0.213	0.265	0.109	0.222	0.241	0.256	0.192	0.190	0.200
4.017	0.0000	0.1951	0.238	0.237	0.326	0.139	0.191	0.269	0.339	0.234	0.230	0.233
6.019	0.0000	0.0000	0.142	0.138	0.146	0.147	0.150	0.160	0.159	0.156	0.158	0.161
6.022	0.0000	0.0510	0.108	0.092	0.100	0.111	0.139	0.121	0.106	0.128	0.126	0.141
6.023	0.0000	0.0974	0.145	0.142	0.179	0.068	0.072	0.162	0.172	0.129	0.125	0.139
6.023	0.0000	0.1450	0.161	0.161	0.248	0.107	0.053	0.192	0.249	0.141	0.140	0.145
6.028	0.0000	0.1907	0.165	0.164	0.354	0.149	0.055	0.240	0.313	0.136	0.137	0.141
8.013	0.0000	0.0000	0.106	0.103	0.108	0.110	0.112	0.120	0.119	0.114	0.113	0.118
8.011	0.0000	0.0489	0.090	0.083	0.083	0.056	0.090	0.107	0.089	0.106	0.094	0.104
8.014	0.0000	0.0955	0.119	0.119	0.163	0.068	0.071	0.134	0.166	0.111	0.106	0.109
8.022	0.0000	0.1426	0.124	0.124	0.265	0.111	0.072	0.181	0.232	0.113	0.112	0.115
8.015	0.0000	0.1707	0.124	0.122	0.320	0.136	0.049	0.215	0.276	0.111	0.112	0.115
10.031	0.0000	0.0000	0.085	0.083	0.088	0.088	0.089	0.096	0.096	0.093	0.092	0.093
9.981	0.0000	0.0496	0.081	0.078	0.084	0.046	0.082	0.096	0.088	0.083	0.079	0.086
9.985	0.0000	0.0960	0.098	0.098	0.170	0.073	0.076	0.124	0.161	0.091	0.086	0.088
9.989	0.0000	0.1375	0.100	0.098	0.257	0.109	0.079	0.174	0.222	0.091	0.093	0.095

Table 67. Coanda Flap Static Pressure Ratios $p/p_{t,j}$ for Configuration 13

[$\epsilon = 1.944$; long Coanda flaps; $\phi_l = 0^\circ$; $\phi_r = 45^\circ$]

		$p/p_{t,j}$ for---										
		Left Coanda flap at---					Right Coanda flap at---					
		x_c/R of---										
NPR	ω_{st}	ω_t	-0.785	-0.524	0.000	0.560	1.140	-0.785	-0.524	0.000	0.560	1.140
1.997	0.0000	0.0000	0.491	0.490	0.491	0.513	0.515	0.445	0.448	0.454	0.469	0.490
1.996	0.0000	0.0511	0.497	0.497	0.506	0.513	0.507	0.455	0.462	0.483	0.485	0.487
1.997	0.0000	0.0998	0.461	0.457	0.475	0.522	0.502	0.390	0.410	0.440	0.475	0.497
1.997	0.0000	0.1500	0.446	0.442	0.458	0.506	0.508	0.341	0.306	0.368	0.430	0.485
1.997	0.0000	0.1966	0.423	0.416	0.444	0.448	0.531	0.421	0.309	0.359	0.410	0.456
3.996	0.0000	0.0000	0.220	0.213	0.223	0.227	0.237	0.236	0.232	0.242	0.247	0.248
3.995	0.0000	0.0506	0.204	0.198	0.213	0.226	0.252	0.216	0.228	0.229	0.238	0.246
3.995	0.0000	0.0978	0.199	0.196	0.213	0.209	0.209	0.220	0.193	0.216	0.223	0.234
3.995	0.0000	0.1453	0.217	0.213	0.261	0.114	0.224	0.310	0.231	0.241	0.243	0.245
3.995	0.0000	0.1912	0.238	0.237	0.320	0.135	0.191	0.406	0.224	0.245	0.247	0.247
5.994	0.0000	0.0000	0.141	0.138	0.146	0.146	0.149	0.164	0.163	0.163	0.164	0.165
5.992	0.0000	0.0495	0.109	0.092	0.105	0.115	0.140	0.145	0.154	0.142	0.153	0.160
5.998	0.0000	0.0972	0.145	0.142	0.177	0.068	0.074	0.207	0.155	0.161	0.162	0.164
6.000	0.0000	0.1442	0.162	0.162	0.244	0.106	0.056	0.307	0.141	0.162	0.164	0.165
6.002	0.0000	0.1892	0.165	0.165	0.348	0.148	0.053	0.392	0.092	0.161	0.164	0.164
8.007	0.0000	0.0000	0.104	0.101	0.108	0.108	0.110	0.123	0.122	0.121	0.121	0.122
7.998	0.0000	0.0493	0.091	0.084	0.083	0.052	0.090	0.116	0.120	0.120	0.121	0.123
7.984	0.0000	0.0965	0.120	0.119	0.163	0.069	0.072	0.206	0.113	0.123	0.124	0.124
7.986	0.0000	0.1421	0.124	0.124	0.262	0.111	0.070	0.295	0.069	0.122	0.123	0.123
7.987	0.0000	0.1735	0.125	0.123	0.326	0.140	0.049	0.349	0.082	0.121	0.123	0.124
9.993	0.0000	0.0000	0.085	0.083	0.088	0.088	0.090	0.098	0.098	0.097	0.098	0.098
10.000	0.0000	0.0483	0.080	0.077	0.081	0.053	0.082	0.105	0.093	0.097	0.098	0.099
10.001	0.0000	0.0960	0.098	0.098	0.169	0.072	0.075	0.204	0.075	0.098	0.098	0.099
10.004	0.0000	0.1385	0.099	0.098	0.260	0.110	0.077	0.278	0.066	0.097	0.098	0.098

Table 68. Coanda Flap Static Pressure Ratios $p/p_{t,j}$ for Configuration 14

[$\epsilon = 1.944$; long Coanda flaps; $\phi_l = -10^\circ$; $\phi_r = 45^\circ$]

NPR	ω_{s_i}	ω_r	$p/p_{t,j}$ for---									
			Left Coanda flap at---					Right Coanda flap at---				
			x_c/R of---					x_c/R of---				
			-0.785	-0.524	0.000	0.560	1.140	-0.785	-0.524	0.000	0.560	1.140
1.994	0.0000	0.0000	0.497	0.496	0.495	0.534	0.536	0.447	0.449	0.455	0.471	0.490
1.988	0.0000	0.0522	0.502	0.502	0.522	0.536	0.523	0.458	0.466	0.486	0.489	0.491
1.990	0.0000	0.1006	0.490	0.488	0.488	0.571	0.511	0.392	0.411	0.440	0.478	0.498
1.991	0.0000	0.1505	0.483	0.482	0.479	0.607	0.506	0.345	0.309	0.369	0.435	0.488
1.992	0.0000	0.2001	0.474	0.472	0.477	0.539	0.550	0.427	0.316	0.364	0.414	0.457
4.030	0.0000	0.0000	0.221	0.215	0.219	0.223	0.233	0.236	0.231	0.239	0.245	0.246
4.017	0.0000	0.0511	0.213	0.206	0.214	0.202	0.254	0.215	0.227	0.228	0.237	0.244
4.018	0.0000	0.0984	0.216	0.211	0.223	0.197	0.248	0.220	0.194	0.214	0.223	0.232
4.021	0.0000	0.1471	0.241	0.240	0.273	0.214	0.223	0.310	0.230	0.240	0.242	0.243
4.023	0.0000	0.1935	0.247	0.248	0.395	0.281	0.134	0.407	0.221	0.243	0.246	0.246
6.013	0.0000	0.0000	0.144	0.140	0.145	0.148	0.151	0.163	0.161	0.162	0.164	0.165
6.009	0.0000	0.0494	0.141	0.136	0.144	0.084	0.151	0.145	0.153	0.141	0.152	0.160
6.010	0.0000	0.0980	0.161	0.161	0.177	0.143	0.118	0.208	0.154	0.160	0.162	0.163
6.010	0.0000	0.1455	0.166	0.166	0.305	0.213	0.117	0.308	0.140	0.162	0.164	0.164
6.013	0.0000	0.1909	0.166	0.165	0.476	0.289	0.149	0.395	0.092	0.161	0.163	0.164
8.020	0.0000	0.0000	0.110	0.108	0.111	0.113	0.115	0.122	0.121	0.121	0.121	0.122
8.028	0.0000	0.0493	0.106	0.103	0.109	0.072	0.136	0.116	0.119	0.120	0.121	0.122
8.026	0.0000	0.0948	0.124	0.124	0.189	0.137	0.145	0.202	0.113	0.123	0.123	0.123
8.029	0.0000	0.1433	0.125	0.124	0.360	0.217	0.117	0.297	0.069	0.121	0.123	0.123
8.030	0.0000	0.1717	0.124	0.124	0.491	0.262	0.132	0.347	0.082	0.121	0.122	0.123
9.987	0.0000	0.0000	0.091	0.090	0.092	0.094	0.095	0.098	0.098	0.097	0.098	0.098
9.983	0.0000	0.0495	0.093	0.092	0.095	0.070	0.134	0.107	0.094	0.098	0.098	0.099
9.984	0.0000	0.0962	0.100	0.100	0.213	0.143	0.139	0.203	0.075	0.098	0.099	0.099
9.988	0.0000	0.1380	0.100	0.100	0.396	0.212	0.110	0.279	0.066	0.097	0.098	0.099

Table 69. Coanda Flap Static Pressure Ratios $p/p_{t,j}$ for Configuration 15

[$\epsilon = 1.944$; long Coanda flaps; $\phi_l = -10^\circ$; $\phi_r = 30^\circ$]

NPR	ω_{st}	ω_t	$p/p_{t,j}$ for---									
			Left Coanda flap at---					Right Coanda flap at---				
			x_c/R of---					x_c/R of---				
			-0.785	-0.524	0.000	0.560	1.140	-0.785	-0.524	0.000	0.560	1.140
2.012	0.0000	0.0000	0.493	0.492	0.492	0.512	0.533	0.482	0.481	0.484	0.486	0.485
2.003	0.0000	0.0505	0.498	0.499	0.522	0.527	0.520	0.475	0.457	0.476	0.494	0.499
2.002	0.0000	0.1028	0.484	0.483	0.482	0.577	0.511	0.364	0.387	0.420	0.493	0.505
2.002	0.0000	0.1505	0.480	0.479	0.476	0.613	0.509	0.364	0.428	0.354	0.453	0.506
2.003	0.0000	0.1999	0.473	0.471	0.476	0.560	0.543	0.422	0.374	0.336	0.397	0.459
4.002	0.0000	0.0000	0.222	0.215	0.219	0.224	0.233	0.230	0.225	0.232	0.244	0.247
4.007	0.0000	0.0505	0.214	0.206	0.215	0.206	0.255	0.195	0.216	0.225	0.224	0.237
4.009	0.0000	0.1000	0.216	0.212	0.224	0.198	0.249	0.213	0.189	0.201	0.199	0.212
4.011	0.0000	0.1455	0.241	0.240	0.267	0.221	0.224	0.236	0.269	0.192	0.190	0.197
4.012	0.0000	0.1953	0.248	0.248	0.398	0.297	0.136	0.250	0.359	0.228	0.222	0.226
6.010	0.0000	0.0000	0.144	0.140	0.145	0.148	0.151	0.161	0.160	0.156	0.158	0.162
6.006	0.0000	0.0500	0.141	0.136	0.144	0.083	0.153	0.121	0.120	0.130	0.127	0.142
6.010	0.0000	0.0972	0.161	0.160	0.175	0.147	0.117	0.158	0.181	0.126	0.124	0.135
6.005	0.0000	0.1448	0.166	0.166	0.302	0.221	0.115	0.173	0.265	0.135	0.135	0.140
6.008	0.0000	0.1908	0.166	0.165	0.476	0.300	0.150	0.194	0.332	0.130	0.135	0.138
8.028	0.0000	0.0000	0.109	0.106	0.110	0.112	0.114	0.118	0.117	0.110	0.112	0.118
8.016	0.0000	0.0487	0.106	0.103	0.109	0.077	0.134	0.105	0.093	0.104	0.093	0.103
8.022	0.0000	0.0954	0.124	0.124	0.194	0.146	0.139	0.124	0.176	0.101	0.096	0.099
8.019	0.0000	0.1430	0.125	0.124	0.359	0.225	0.119	0.146	0.249	0.106	0.105	0.107
8.028	0.0000	0.1728	0.124	0.124	0.499	0.277	0.133	0.162	0.293	0.104	0.105	0.107
10.032	0.0000	0.0000	0.091	0.089	0.092	0.093	0.094	0.096	0.096	0.093	0.092	0.093
10.033	0.0000	0.0494	0.093	0.092	0.095	0.073	0.132	0.094	0.092	0.079	0.076	0.083
10.043	0.0000	0.0938	0.099	0.099	0.207	0.144	0.140	0.105	0.168	0.078	0.071	0.075
10.047	0.0000	0.1377	0.099	0.099	0.401	0.219	0.113	0.130	0.234	0.083	0.082	0.084

Table 70. Coanda Flap Static Pressure Ratios $p/p_{t,j}$ for Configuration 16

[$\epsilon = 2.405$; short Coanda flaps; $\phi_l = 0^\circ$; $\phi_r = 0^\circ$]

NPR	ω_{st}	ω_c	$p/p_{t,j}$ for---									
			Left Coanda flap at---					Right Coanda flap at---				
			x_c/R of---					x_c/R of---				
			-0.785	-0.524	0.000	0.560	1.140	-0.785	-0.524	0.000	0.560	1.140
2.002	0.0000	0.0000	0.488	0.486	0.488	0.486	0.501	0.494	0.491	0.490	0.500	0.512
2.007	0.0000	0.0506	0.489	0.488	0.490	0.501	0.500	0.496	0.493	0.496	0.507	0.502
2.005	0.0000	0.1007	0.449	0.445	0.460	0.534	0.503	0.459	0.420	0.467	0.526	0.500
2.008	0.0000	0.1508	0.438	0.435	0.453	0.509	0.533	0.446	0.394	0.438	0.553	0.504
2.008	0.0000	0.2012	0.408	0.401	0.432	0.471	0.522	0.453	0.410	0.337	0.559	0.513
4.005	0.0000	0.0000	0.242	0.242	0.242	0.239	0.236	0.245	0.241	0.240	0.238	0.237
4.006	0.0000	0.0513	0.189	0.180	0.200	0.206	0.231	0.216	0.174	0.155	0.200	0.230
3.998	0.0000	0.0993	0.178	0.166	0.164	0.125	0.198	0.226	0.202	0.151	0.137	0.206
4.019	0.0000	0.1456	0.213	0.210	0.252	0.141	0.187	0.244	0.240	0.226	0.112	0.191
3.987	0.0000	0.1914	0.237	0.236	0.338	0.194	0.207	0.251	0.250	0.293	0.125	0.205
5.987	0.0000	0.0000	0.162	0.163	0.162	0.159	0.156	0.165	0.163	0.162	0.159	0.159
5.983	0.0000	0.0492	0.128	0.127	0.132	0.134	0.151	0.148	0.132	0.136	0.144	0.136
5.984	0.0000	0.0967	0.143	0.141	0.168	0.094	0.116	0.164	0.161	0.149	0.104	0.141
5.986	0.0000	0.1434	0.162	0.161	0.251	0.149	0.146	0.167	0.166	0.219	0.092	0.140
5.990	0.0000	0.1890	0.165	0.165	0.348	0.201	0.140	0.166	0.162	0.280	0.120	0.151
7.996	0.0000	0.0000	0.122	0.122	0.122	0.121	0.119	0.124	0.123	0.122	0.120	0.118
7.999	0.0000	0.0485	0.101	0.101	0.104	0.105	0.103	0.113	0.101	0.075	0.084	0.109
8.003	0.0000	0.0959	0.119	0.118	0.167	0.096	0.105	0.125	0.125	0.147	0.062	0.108
8.009	0.0000	0.1417	0.124	0.124	0.260	0.151	0.105	0.124	0.122	0.210	0.090	0.113
8.018	0.0000	0.1686	0.124	0.124	0.310	0.182	0.085	0.123	0.119	0.247	0.106	0.112
10.003	0.0000	0.0000	0.098	0.098	0.098	0.097	0.096	0.099	0.098	0.097	0.096	0.095
9.990	0.0000	0.0489	0.083	0.084	0.092	0.089	0.088	0.095	0.091	0.076	0.064	0.078
9.993	0.0000	0.0952	0.098	0.098	0.171	0.101	0.089	0.100	0.099	0.144	0.061	0.081
9.990	0.0000	0.1349	0.100	0.099	0.248	0.146	0.070	0.099	0.096	0.198	0.085	0.090

Table 71. Coanda Flap Static Pressure Ratios $p/p_{t,j}$ for Configuration 17

[$\epsilon = 2.405$; short Coanda flaps; $\phi_f = 0^\circ$; $\phi_r = 30^\circ$]

NPR	ω_{st}	ω_c	$p/p_{t,j}$ for---									
			Left Coanda flap at---					Right Coanda flap at---				
			x_c/R of---					x_r/R of---				
			-0.785	-0.524	0.000	0.560	1.140	-0.785	-0.524	0.000	0.560	1.140
1.994	0.0000	0.0000	0.489	0.489	0.491	0.492	0.501	0.489	0.489	0.490	0.492	0.494
1.997	0.0000	0.0507	0.490	0.489	0.492	0.503	0.503	0.478	0.455	0.488	0.499	0.500
1.998	0.0000	0.1001	0.453	0.449	0.464	0.533	0.510	0.347	0.378	0.434	0.501	0.506
2.002	0.0000	0.1492	0.439	0.436	0.455	0.505	0.534	0.337	0.329	0.372	0.471	0.519
2.002	0.0000	0.1951	0.411	0.403	0.432	0.465	0.519	0.413	0.369	0.334	0.427	0.490
4.011	0.0000	0.0000	0.243	0.243	0.243	0.240	0.238	0.245	0.244	0.243	0.241	0.241
4.015	0.0000	0.0501	0.188	0.178	0.199	0.204	0.229	0.185	0.213	0.221	0.228	0.243
4.017	0.0000	0.0973	0.175	0.163	0.160	0.125	0.203	0.211	0.196	0.216	0.211	0.230
4.018	0.0000	0.1444	0.213	0.210	0.251	0.141	0.184	0.236	0.282	0.231	0.230	0.227
4.020	0.0000	0.1900	0.235	0.234	0.334	0.192	0.203	0.243	0.375	0.237	0.241	0.238
6.026	0.0000	0.0000	0.161	0.161	0.161	0.159	0.158	0.164	0.164	0.163	0.157	0.158
6.023	0.0000	0.0484	0.127	0.126	0.134	0.135	0.153	0.141	0.151	0.157	0.157	0.162
6.029	0.0000	0.0965	0.143	0.140	0.167	0.093	0.124	0.157	0.189	0.153	0.159	0.156
6.031	0.0000	0.1409	0.160	0.160	0.246	0.146	0.144	0.167	0.276	0.153	0.155	0.153
6.017	0.0000	0.1883	0.165	0.164	0.345	0.200	0.140	0.182	0.351	0.142	0.155	0.153
8.028	0.0000	0.0000	0.122	0.122	0.122	0.121	0.120	0.124	0.123	0.123	0.118	0.118
8.026	0.0000	0.0479	0.100	0.100	0.104	0.105	0.103	0.110	0.107	0.119	0.120	0.120
8.020	0.0000	0.0956	0.118	0.118	0.165	0.096	0.105	0.122	0.189	0.118	0.120	0.118
8.025	0.0000	0.1404	0.124	0.123	0.257	0.150	0.107	0.136	0.262	0.109	0.118	0.117
8.026	0.0000	0.1686	0.124	0.123	0.309	0.182	0.085	0.146	0.311	0.111	0.115	0.114
10.021	0.0000	0.0000	0.098	0.097	0.098	0.097	0.096	0.099	0.099	0.099	0.095	0.096
10.020	0.0000	0.0485	0.085	0.085	0.090	0.090	0.089	0.093	0.094	0.092	0.097	0.096
10.028	0.0000	0.0950	0.098	0.098	0.170	0.099	0.088	0.104	0.183	0.095	0.097	0.096
10.035	0.0000	0.1357	0.099	0.099	0.250	0.146	0.067	0.117	0.249	0.087	0.094	0.094

Table 72. Coanda Flap Static Pressure Ratios $p/p_{t,j}$ for Configuration 18

[$\epsilon = 2.405$; short Coanda flaps; $\phi_l = 0^\circ$; $\phi_r = 45^\circ$]

		$p/p_{t,j}$ for---										
		Left Coanda flap at---					Right Coanda flap at---					
		x_c/R of---					x_c/R of---					
NPR	$\omega_{s,l}$	ω_c	-0.785	-0.524	0.000	0.560	1.140	-0.785	-0.524	0.000	0.560	1.140
2.007	0.0000	0.0000	0.486	0.485	0.488	0.488	0.497	0.486	0.486	0.488	0.489	0.492
2.007	0.0000	0.0501	0.488	0.486	0.490	0.499	0.499	0.460	0.466	0.490	0.492	0.494
2.006	0.0000	0.1009	0.448	0.438	0.461	0.524	0.505	0.388	0.409	0.440	0.493	0.503
2.007	0.0000	0.1495	0.434	0.425	0.452	0.495	0.525	0.340	0.337	0.385	0.458	0.504
2.008	0.0000	0.1972	0.406	0.387	0.429	0.462	0.513	0.427	0.360	0.389	0.424	0.470
4.005	0.0000	0.0000	0.244	0.244	0.243	0.240	0.239	0.246	0.246	0.246	0.246	0.246
4.007	0.0000	0.0496	0.192	0.175	0.200	0.202	0.229	0.216	0.228	0.227	0.241	0.245
4.009	0.0000	0.0976	0.183	0.162	0.150	0.121	0.200	0.228	0.230	0.230	0.237	0.234
4.011	0.0000	0.1446	0.219	0.214	0.238	0.128	0.201	0.310	0.227	0.242	0.243	0.242
4.012	0.0000	0.1906	0.238	0.237	0.310	0.174	0.201	0.410	0.221	0.243	0.245	0.245
5.986	0.0000	0.0000	0.162	0.162	0.162	0.160	0.159	0.165	0.165	0.164	0.163	0.163
5.983	0.0000	0.0491	0.133	0.131	0.136	0.138	0.140	0.152	0.161	0.162	0.165	0.165
5.985	0.0000	0.0966	0.147	0.144	0.156	0.085	0.109	0.208	0.107	0.163	0.162	0.162
5.989	0.0000	0.1433	0.163	0.163	0.239	0.134	0.144	0.308	0.139	0.162	0.163	0.163
5.987	0.0000	0.1895	0.166	0.166	0.315	0.181	0.147	0.396	0.093	0.161	0.162	0.163
8.008	0.0000	0.0000	0.122	0.122	0.122	0.121	0.120	0.124	0.123	0.123	0.121	0.121
8.006	0.0000	0.0486	0.105	0.105	0.109	0.110	0.107	0.107	0.114	0.121	0.122	0.122
8.005	0.0000	0.0955	0.120	0.120	0.156	0.087	0.104	0.206	0.106	0.121	0.122	0.122
8.007	0.0000	0.1419	0.124	0.124	0.236	0.136	0.110	0.296	0.070	0.120	0.121	0.121
8.012	0.0000	0.1714	0.125	0.122	0.281	0.166	0.092	0.347	0.083	0.120	0.121	0.120
10.006	0.0000	0.0000	0.098	0.098	0.098	0.097	0.096	0.099	0.099	0.099	0.097	0.097
10.004	0.0000	0.0477	0.087	0.086	0.092	0.091	0.088	0.104	0.093	0.098	0.098	0.098
10.004	0.0000	0.0950	0.099	0.099	0.160	0.089	0.088	0.202	0.077	0.097	0.098	0.098
10.011	0.0000	0.1357	0.100	0.098	0.223	0.131	0.075	0.275	0.065	0.097	0.098	0.098

Table 73. Coanda Flap Static Pressure Ratios $p/p_{t,j}$ for Configuration 19

[$\epsilon = 2.405$; short Coanda flaps; $\phi_f = -10^\circ$; $\phi_r = 30^\circ$]

NPR	ω_{xi}	ω_c	$p/p_{t,j}$ for---									
			Left Coanda flap at---					Right Coanda flap at---				
			x_c/R of---					x_c/R of---				
			-0.785	-0.524	0.000	0.560	1.140	-0.785	-0.524	0.000	0.560	1.140
2.005	0.0000	0.0000	0.495	0.495	0.492	0.497	0.521	0.480	0.479	0.481	0.489	0.495
1.996	0.0000	0.0505	0.501	0.501	0.518	0.534	0.522	0.473	0.452	0.485	0.493	0.501
1.996	0.0000	0.0989	0.485	0.484	0.486	0.604	0.530	0.357	0.402	0.428	0.472	0.508
1.996	0.0000	0.1484	0.480	0.479	0.483	0.670	0.547	0.330	0.290	0.368	0.435	0.510
1.995	0.0000	0.1956	0.473	0.472	0.479	0.629	0.659	0.410	0.385	0.336	0.394	0.471
4.002	0.0000	0.0000	0.241	0.241	0.243	0.240	0.239	0.245	0.245	0.244	0.243	0.243
4.002	0.0000	0.0498	0.202	0.190	0.203	0.184	0.220	0.189	0.213	0.225	0.229	0.242
4.004	0.0000	0.0973	0.206	0.198	0.213	0.181	0.262	0.208	0.200	0.211	0.206	0.231
4.006	0.0000	0.1443	0.239	0.238	0.248	0.273	0.189	0.237	0.284	0.232	0.229	0.225
4.015	0.0000	0.1914	0.247	0.247	0.330	0.357	0.134	0.239	0.378	0.237	0.241	0.238
6.003	0.0000	0.0000	0.160	0.159	0.161	0.160	0.159	0.164	0.164	0.163	0.161	0.161
6.009	0.0000	0.0488	0.139	0.135	0.145	0.145	0.143	0.140	0.149	0.155	0.157	0.163
6.011	0.0000	0.0957	0.160	0.159	0.167	0.181	0.148	0.158	0.187	0.156	0.159	0.158
6.013	0.0000	0.1422	0.166	0.165	0.207	0.265	0.139	0.163	0.279	0.156	0.158	0.157
6.014	0.0000	0.1886	0.166	0.166	0.296	0.355	0.074	0.171	0.359	0.141	0.157	0.156
8.008	0.0000	0.0000	0.121	0.121	0.122	0.121	0.120	0.124	0.124	0.124	0.118	0.119
8.008	0.0000	0.0483	0.102	0.097	0.106	0.087	0.110	0.110	0.107	0.120	0.120	0.120
8.011	0.0000	0.0942	0.124	0.124	0.155	0.176	0.046	0.120	0.187	0.120	0.120	0.119
8.012	0.0000	0.1416	0.125	0.124	0.223	0.266	0.055	0.128	0.270	0.106	0.119	0.117
8.013	0.0000	0.1707	0.125	0.123	0.325	0.329	0.065	0.131	0.317	0.110	0.115	0.114
9.969	0.0000	0.0000	0.099	0.098	0.099	0.099	0.099	0.100	0.100	0.100	0.096	0.096
9.984	0.0000	0.0485	0.091	0.090	0.093	0.089	0.086	0.093	0.096	0.091	0.097	0.096
9.988	0.0000	0.0953	0.100	0.099	0.139	0.177	0.050	0.100	0.187	0.094	0.097	0.096
9.995	0.0000	0.1362	0.100	0.098	0.260	0.262	0.052	0.106	0.253	0.087	0.094	0.094

Table 74. Coanda Flap Static Pressure Ratios $p/p_{t,j}$ for Configuration 20

[$\epsilon = 2.405$; short Coanda flaps; $\phi_l = -10^\circ$; $\phi_r = 45^\circ$]

		$p/p_{t,j}$ for---										
		Left Coanda flap at---					Right Coanda flap at---					
		x_c/R of---										
NPR	ω_{st}	ω_c	-0.785	-0.524	0.000	0.560	1.140	-0.785	-0.524	0.000	0.560	1.140
2.009	0.0000	0.0000	0.493	0.493	0.491	0.496	0.520	0.480	0.483	0.480	0.491	0.492
2.009	0.0000	0.0505	0.497	0.498	0.514	0.531	0.519	0.458	0.475	0.485	0.491	0.494
2.009	0.0000	0.0995	0.481	0.480	0.482	0.602	0.527	0.401	0.420	0.434	0.474	0.499
2.009	0.0000	0.1484	0.477	0.476	0.480	0.665	0.547	0.328	0.381	0.387	0.411	0.494
2.010	0.0000	0.1953	0.470	0.468	0.475	0.611	0.628	0.420	0.344	0.364	0.394	0.474
4.023	0.0000	0.0000	0.240	0.240	0.242	0.239	0.238	0.244	0.245	0.245	0.244	0.244
4.030	0.0000	0.0499	0.201	0.189	0.201	0.181	0.218	0.215	0.226	0.224	0.239	0.243
3.991	0.0000	0.0970	0.206	0.197	0.212	0.178	0.267	0.226	0.229	0.229	0.237	0.235
3.992	0.0000	0.1441	0.240	0.239	0.249	0.273	0.188	0.308	0.229	0.243	0.244	0.243
3.995	0.0000	0.1907	0.248	0.248	0.333	0.356	0.133	0.410	0.221	0.244	0.246	0.246
5.998	0.0000	0.0000	0.160	0.159	0.161	0.161	0.161	0.165	0.164	0.164	0.163	0.163
5.997	0.0000	0.0486	0.140	0.136	0.145	0.145	0.144	0.151	0.160	0.161	0.165	0.165
5.998	0.0000	0.0961	0.160	0.159	0.168	0.180	0.148	0.207	0.106	0.162	0.161	0.162
6.000	0.0000	0.1427	0.166	0.165	0.207	0.266	0.140	0.305	0.137	0.162	0.162	0.163
6.003	0.0000	0.1887	0.167	0.166	0.293	0.353	0.074	0.392	0.092	0.161	0.162	0.162
7.984	0.0000	0.0000	0.122	0.122	0.123	0.123	0.122	0.124	0.124	0.123	0.121	0.121
8.001	0.0000	0.0482	0.103	0.098	0.106	0.087	0.111	0.104	0.112	0.121	0.122	0.122
8.005	0.0000	0.0949	0.124	0.124	0.156	0.178	0.044	0.204	0.107	0.122	0.123	0.122
8.009	0.0000	0.1416	0.125	0.125	0.225	0.266	0.056	0.294	0.070	0.121	0.122	0.121
8.012	0.0000	0.1703	0.125	0.123	0.323	0.328	0.065	0.343	0.082	0.121	0.121	0.121
10.027	0.0000	0.0000	0.098	0.098	0.098	0.098	0.098	0.099	0.099	0.099	0.097	0.097
10.030	0.0000	0.0477	0.090	0.088	0.092	0.087	0.087	0.104	0.092	0.097	0.098	0.098
10.035	0.0000	0.0948	0.100	0.099	0.140	0.177	0.049	0.200	0.076	0.097	0.098	0.098
10.038	0.0000	0.1353	0.099	0.098	0.258	0.260	0.051	0.272	0.065	0.096	0.097	0.097

Table 75. Coanda Flap Static Pressure Ratios $p/p_{t,j}$ for Configuration 21

[$\epsilon = 2.405$; long Coanda flaps; $\phi_l = 0^\circ$; $\phi_r = 0^\circ$]

			$p/p_{t,j}$ for---									
			Left Coanda flap at---					Right Coanda flap at---				
			x_c/R of---					x_c/R of---				
NPR	$\omega_{s,i}$	ω_c	-0.785	-0.524	0.000	0.560	1.140	-0.785	-0.524	0.000	0.560	1.140
2.005	0.0000	0.0000	0.490	0.488	0.491	0.491	0.502	0.495	0.491	0.491	0.496	0.506
1.999	0.0000	0.0496	0.492	0.490	0.494	0.505	0.506	0.499	0.498	0.499	0.511	0.508
2.001	0.0000	0.0998	0.454	0.445	0.466	0.532	0.518	0.461	0.421	0.462	0.539	0.513
2.002	0.0000	0.1478	0.439	0.430	0.455	0.503	0.541	0.451	0.401	0.441	0.567	0.510
2.003	0.0000	0.1961	0.411	0.393	0.434	0.464	0.529	0.454	0.408	0.337	0.534	0.520
3.992	0.0000	0.0000	0.214	0.207	0.220	0.220	0.223	0.231	0.213	0.208	0.216	0.229
3.995	0.0000	0.0490	0.190	0.172	0.198	0.201	0.228	0.217	0.175	0.156	0.199	0.226
3.983	0.0000	0.0976	0.183	0.163	0.150	0.126	0.203	0.227	0.202	0.150	0.116	0.205
3.984	0.0000	0.1449	0.219	0.214	0.233	0.132	0.169	0.246	0.242	0.231	0.119	0.174
3.985	0.0000	0.1928	0.240	0.239	0.305	0.181	0.163	0.251	0.250	0.309	0.131	0.185
6.007	0.0000	0.0000	0.152	0.150	0.154	0.153	0.153	0.159	0.153	0.151	0.150	0.151
6.011	0.0000	0.0487	0.111	0.088	0.077	0.106	0.102	0.144	0.117	0.074	0.064	0.085
6.012	0.0000	0.0965	0.147	0.143	0.154	0.087	0.069	0.163	0.160	0.152	0.063	0.105
6.014	0.0000	0.1430	0.162	0.162	0.233	0.137	0.122	0.166	0.164	0.229	0.096	0.131
6.016	0.0000	0.1902	0.165	0.165	0.320	0.186	0.125	0.165	0.162	0.290	0.125	0.148
8.010	0.0000	0.0000	0.114	0.112	0.115	0.114	0.113	0.119	0.113	0.112	0.108	0.106
7.999	0.0000	0.0489	0.092	0.082	0.076	0.043	0.045	0.113	0.101	0.075	0.031	0.048
7.996	0.0000	0.0962	0.120	0.120	0.151	0.090	0.026	0.125	0.125	0.154	0.065	0.082
8.043	0.0000	0.1423	0.124	0.123	0.240	0.140	0.072	0.123	0.121	0.217	0.093	0.108
7.992	0.0000	0.1709	0.125	0.123	0.286	0.171	0.046	0.122	0.118	0.258	0.110	0.105
9.989	0.0000	0.0000	0.095	0.094	0.095	0.094	0.093	0.097	0.095	0.095	0.094	0.093
9.995	0.0000	0.0485	0.081	0.077	0.075	0.043	0.043	0.095	0.091	0.077	0.032	0.046
10.002	0.0000	0.0961	0.099	0.098	0.161	0.093	0.026	0.099	0.099	0.150	0.064	0.022
10.007	0.0000	0.1362	0.100	0.098	0.227	0.136	0.036	0.098	0.094	0.207	0.088	0.031

Table 76. Coanda Flap Static Pressure Ratios $p/p_{t,j}$ for Configuration 22

[$\epsilon = 2.405$; long Coanda flaps; $\phi_l = 0^\circ$; $\phi_r = 30^\circ$]

			$p/p_{t,j}$ for---									
			Left Coanda flap at---					Right Coanda flap at---				
			x_c/R of---					x_c/R of---				
NPR	ω_{si}	ω_c	-0.785	-0.524	0.000	0.560	1.140	-0.785	-0.524	0.000	0.560	1.140
2.017	0.0000	0.0000	0.486	0.485	0.487	0.488	0.498	0.478	0.477	0.479	0.487	0.492
2.008	0.0000	0.0521	0.488	0.487	0.491	0.503	0.504	0.474	0.452	0.484	0.495	0.496
2.011	0.0000	0.1006	0.448	0.440	0.461	0.529	0.516	0.342	0.373	0.429	0.499	0.503
2.011	0.0000	0.1496	0.435	0.426	0.452	0.500	0.539	0.328	0.346	0.373	0.479	0.515
2.008	0.0000	0.1984	0.407	0.389	0.433	0.466	0.528	0.409	0.378	0.336	0.439	0.489
3.999	0.0000	0.0000	0.215	0.207	0.220	0.222	0.225	0.246	0.246	0.245	0.246	0.246
4.003	0.0000	0.0499	0.189	0.171	0.197	0.199	0.227	0.183	0.212	0.215	0.228	0.241
4.003	0.0000	0.0988	0.184	0.164	0.153	0.116	0.194	0.205	0.190	0.200	0.201	0.222
4.000	0.0000	0.1468	0.220	0.215	0.237	0.134	0.162	0.234	0.297	0.198	0.197	0.209
4.000	0.0000	0.1925	0.239	0.238	0.305	0.181	0.165	0.239	0.394	0.213	0.212	0.220
6.001	0.0000	0.0000	0.152	0.151	0.155	0.154	0.154	0.164	0.164	0.163	0.163	0.163
5.997	0.0000	0.0499	0.112	0.089	0.077	0.105	0.102	0.135	0.146	0.150	0.156	0.163
5.998	0.0000	0.0967	0.147	0.143	0.152	0.087	0.084	0.157	0.196	0.154	0.155	0.160
6.000	0.0000	0.1435	0.163	0.162	0.235	0.138	0.123	0.161	0.291	0.156	0.157	0.156
6.003	0.0000	0.1913	0.166	0.165	0.321	0.187	0.127	0.163	0.366	0.130	0.138	0.138
8.011	0.0000	0.0000	0.114	0.112	0.115	0.114	0.113	0.123	0.123	0.122	0.122	0.121
8.025	0.0000	0.0490	0.092	0.081	0.076	0.043	0.045	0.108	0.105	0.118	0.119	0.121
8.017	0.0000	0.0979	0.120	0.120	0.155	0.092	0.027	0.120	0.200	0.119	0.120	0.121
8.016	0.0000	0.1414	0.124	0.124	0.238	0.139	0.075	0.122	0.271	0.110	0.118	0.118
8.018	0.0000	0.1700	0.124	0.122	0.283	0.170	0.046	0.127	0.324	0.107	0.113	0.114
9.990	0.0000	0.0000	0.095	0.095	0.096	0.095	0.094	0.099	0.099	0.098	0.098	0.097
9.997	0.0000	0.0505	0.083	0.079	0.077	0.045	0.042	0.094	0.100	0.092	0.095	0.096
10.004	0.0000	0.0973	0.099	0.099	0.164	0.095	0.026	0.097	0.192	0.095	0.096	0.097
10.010	0.0000	0.1357	0.100	0.098	0.227	0.136	0.036	0.102	0.259	0.087	0.093	0.095

Table 77. Coanda Flap Static Pressure Ratios $p/p_{t,j}$ for Configuration 23

[$\epsilon = 2.405$; long Coanda flaps; $\phi_f = 0^\circ$; $\phi_r = 45^\circ$]

		$p/p_{t,j}$ for---										
		Left Coanda flap at---						Right Coanda flap at---				
		x_c/R of---										
NPR	ω_{st}	ω_c	-0.785	-0.524	0.000	0.560	1.140	-0.785	-0.524	0.000	0.560	1.140
2.010	0.0000	0.0000	0.488	0.487	0.490	0.490	0.501	0.482	0.484	0.481	0.492	0.493
2.011	0.0000	0.0503	0.489	0.488	0.491	0.503	0.503	0.457	0.475	0.484	0.492	0.495
2.011	0.0000	0.1015	0.450	0.442	0.462	0.529	0.517	0.400	0.419	0.434	0.472	0.500
2.011	0.0000	0.1503	0.437	0.427	0.453	0.501	0.538	0.332	0.386	0.389	0.410	0.492
2.011	0.0000	0.1989	0.408	0.389	0.431	0.468	0.529	0.431	0.347	0.365	0.394	0.469
3.999	0.0000	0.0000	0.215	0.207	0.220	0.222	0.225	0.246	0.246	0.247	0.248	0.248
4.000	0.0000	0.0498	0.190	0.172	0.197	0.200	0.227	0.216	0.227	0.225	0.240	0.245
4.000	0.0000	0.0995	0.185	0.166	0.154	0.115	0.193	0.224	0.225	0.223	0.233	0.238
3.998	0.0000	0.1448	0.220	0.214	0.235	0.133	0.166	0.309	0.228	0.243	0.245	0.246
4.000	0.0000	0.1918	0.239	0.238	0.304	0.181	0.165	0.410	0.219	0.244	0.247	0.247
6.018	0.0000	0.0000	0.151	0.150	0.154	0.154	0.154	0.164	0.164	0.164	0.164	0.165
6.003	0.0000	0.0493	0.112	0.089	0.078	0.106	0.103	0.150	0.159	0.161	0.164	0.165
6.003	0.0000	0.0972	0.147	0.144	0.155	0.088	0.075	0.208	0.118	0.164	0.164	0.164
6.006	0.0000	0.1427	0.162	0.162	0.234	0.137	0.124	0.305	0.137	0.163	0.164	0.164
6.008	0.0000	0.1906	0.166	0.165	0.322	0.187	0.125	0.396	0.094	0.161	0.164	0.164
7.997	0.0000	0.0000	0.114	0.113	0.116	0.115	0.114	0.123	0.123	0.123	0.124	0.124
7.992	0.0000	0.0497	0.093	0.083	0.077	0.044	0.045	0.111	0.117	0.121	0.123	0.123
7.998	0.0000	0.0968	0.120	0.120	0.153	0.092	0.027	0.208	0.106	0.122	0.123	0.124
8.001	0.0000	0.1434	0.124	0.124	0.242	0.141	0.073	0.298	0.071	0.121	0.123	0.123
8.010	0.0000	0.1713	0.125	0.122	0.286	0.172	0.046	0.345	0.083	0.121	0.122	0.122
10.006	0.0000	0.0000	0.095	0.095	0.096	0.095	0.094	0.099	0.098	0.098	0.098	0.098
10.007	0.0000	0.0500	0.083	0.079	0.077	0.045	0.042	0.108	0.093	0.098	0.099	0.099
10.010	0.0000	0.0962	0.099	0.098	0.162	0.094	0.026	0.203	0.074	0.097	0.098	0.099
10.017	0.0000	0.1366	0.100	0.098	0.229	0.137	0.037	0.275	0.066	0.097	0.098	0.098

Table 78. Coanda Flap Static Pressure Ratios $p/p_{t,j}$ for Configuration 24

[$\varepsilon = 2.405$; long Coanda flaps; $\phi_l = -10^\circ$; $\phi_r = 30^\circ$]

		$p/p_{t,j}$ for---										
		Left Coanda flap at---					Right Coanda flap at---					
		x_c/R of---										
NPR	$\omega_{s,l}$	ω_c	-0.785	-0.524	0.000	0.560	1.140	-0.785	-0.524	0.000	0.560	1.140
1.990	0.0000	0.0000	0.501	0.499	0.496	0.504	0.554	0.486	0.484	0.487	0.493	0.499
1.988	0.0000	0.0515	0.502	0.502	0.526	0.542	0.545	0.475	0.452	0.487	0.496	0.503
2.002	0.0000	0.1014	0.485	0.484	0.486	0.611	0.551	0.353	0.401	0.424	0.465	0.510
2.002	0.0000	0.1463	0.480	0.479	0.483	0.669	0.551	0.327	0.319	0.371	0.431	0.514
2.002	0.0000	0.1950	0.474	0.473	0.479	0.625	0.665	0.406	0.356	0.330	0.399	0.473
4.018	0.0000	0.0000	0.212	0.203	0.210	0.216	0.226	0.245	0.245	0.243	0.245	0.245
4.022	0.0000	0.0491	0.203	0.191	0.202	0.183	0.221	0.186	0.213	0.219	0.228	0.240
3.995	0.0000	0.0965	0.208	0.200	0.213	0.186	0.259	0.204	0.182	0.202	0.202	0.225
3.992	0.0000	0.1458	0.241	0.240	0.250	0.295	0.097	0.238	0.286	0.198	0.196	0.209
3.991	0.0000	0.1911	0.248	0.248	0.333	0.382	0.142	0.239	0.386	0.210	0.208	0.218
6.000	0.0000	0.0000	0.144	0.142	0.149	0.146	0.148	0.164	0.164	0.163	0.163	0.163
5.996	0.0000	0.0488	0.138	0.132	0.141	0.092	0.091	0.136	0.146	0.151	0.156	0.163
5.997	0.0000	0.0962	0.160	0.160	0.168	0.193	0.039	0.159	0.189	0.155	0.156	0.160
5.995	0.0000	0.1430	0.166	0.166	0.207	0.287	0.057	0.161	0.286	0.157	0.158	0.157
5.996	0.0000	0.1902	0.167	0.166	0.302	0.382	0.075	0.161	0.359	0.131	0.138	0.138
7.998	0.0000	0.0000	0.110	0.108	0.113	0.110	0.109	0.123	0.123	0.122	0.122	0.122
7.999	0.0000	0.0495	0.104	0.099	0.107	0.092	0.091	0.109	0.105	0.116	0.119	0.122
8.000	0.0000	0.0964	0.124	0.124	0.149	0.193	0.039	0.119	0.194	0.120	0.121	0.121
8.006	0.0000	0.1442	0.125	0.124	0.232	0.290	0.057	0.121	0.271	0.110	0.117	0.118
8.012	0.0000	0.1706	0.125	0.123	0.327	0.350	0.066	0.124	0.318	0.105	0.112	0.112
10.009	0.0000	0.0000	0.085	0.083	0.088	0.086	0.088	0.099	0.099	0.098	0.098	0.097
10.009	0.0000	0.0483	0.091	0.089	0.093	0.094	0.087	0.092	0.091	0.093	0.096	0.097
10.018	0.0000	0.0958	0.100	0.099	0.142	0.191	0.044	0.098	0.187	0.095	0.096	0.097
10.025	0.0000	0.1368	0.099	0.098	0.265	0.282	0.053	0.101	0.254	0.088	0.094	0.095

Table 79. Coanda Flap Static Pressure Ratios $p/p_{t,j}$ for Configuration 25

[$\epsilon = 2.405$; long Coanda flaps; $\phi_l = -10^\circ$; $\phi_r = 45^\circ$]

			$p/p_{t,j}$ for---									
			Left Coanda flap at---					Right Coanda flap at---				
			x_c/R of---					x_c/R of---				
NPR	ω_{si}	ω_c	-0.785	-0.524	0.000	0.560	1.140	-0.785	-0.524	0.000	0.560	1.140
2.004	0.0000	0.0000	0.497	0.495	0.493	0.500	0.548	0.484	0.486	0.484	0.494	0.495
2.008	0.0000	0.0503	0.498	0.497	0.520	0.538	0.540	0.461	0.479	0.486	0.493	0.495
2.008	0.0000	0.0992	0.485	0.484	0.485	0.604	0.550	0.402	0.421	0.434	0.475	0.500
2.008	0.0000	0.1498	0.478	0.478	0.481	0.670	0.554	0.340	0.383	0.390	0.409	0.492
2.009	0.0000	0.1995	0.471	0.469	0.476	0.604	0.599	0.408	0.348	0.365	0.395	0.467
4.005	0.0000	0.0000	0.211	0.203	0.210	0.217	0.226	0.246	0.245	0.246	0.247	0.247
4.008	0.0000	0.0500	0.204	0.192	0.203	0.184	0.221	0.217	0.228	0.224	0.239	0.244
4.008	0.0000	0.0983	0.208	0.201	0.214	0.190	0.255	0.216	0.229	0.224	0.233	0.238
4.010	0.0000	0.1462	0.240	0.239	0.249	0.294	0.097	0.323	0.232	0.243	0.245	0.245
4.008	0.0000	0.1936	0.248	0.248	0.334	0.387	0.146	0.431	0.217	0.243	0.246	0.247
6.009	0.0000	0.0000	0.144	0.142	0.149	0.144	0.148	0.164	0.164	0.164	0.165	0.165
5.999	0.0000	0.0497	0.137	0.131	0.140	0.093	0.088	0.150	0.160	0.161	0.164	0.165
6.001	0.0000	0.0978	0.161	0.160	0.169	0.197	0.039	0.213	0.119	0.164	0.164	0.164
6.039	0.0000	0.1433	0.165	0.165	0.205	0.284	0.056	0.319	0.132	0.162	0.163	0.163
6.031	0.0000	0.1911	0.166	0.165	0.305	0.383	0.075	0.398	0.096	0.161	0.163	0.163
8.005	0.0000	0.0000	0.110	0.108	0.113	0.110	0.110	0.123	0.123	0.123	0.123	0.124
7.995	0.0000	0.0484	0.102	0.097	0.105	0.089	0.093	0.103	0.118	0.121	0.123	0.124
7.993	0.0000	0.0968	0.124	0.124	0.148	0.193	0.039	0.216	0.102	0.123	0.124	0.124
7.995	0.0000	0.1412	0.125	0.125	0.223	0.282	0.055	0.296	0.072	0.121	0.123	0.123
7.995	0.0000	0.1712	0.125	0.124	0.329	0.352	0.066	0.351	0.084	0.122	0.123	0.123
10.007	0.0000	0.0000	0.085	0.083	0.087	0.086	0.088	0.099	0.098	0.098	0.098	0.098
10.008	0.0000	0.0490	0.091	0.090	0.094	0.095	0.086	0.104	0.095	0.098	0.099	0.099
10.010	0.0000	0.0964	0.100	0.099	0.143	0.192	0.043	0.208	0.065	0.098	0.099	0.099
10.017	0.0000	0.1371	0.100	0.098	0.267	0.282	0.053	0.280	0.067	0.097	0.098	0.098

Table 80. Coanda Flap Static Pressure Ratios $p/p_{t,j}$ for Configuration 26

[$\epsilon = 2.405$; long Coanda flaps; $\phi_l = 0^\circ$; $\phi_r = 0^\circ$]

			$p/p_{t,j}$ for---									
			Left Coanda flap at---					Right Coanda flap at---				
			x_c/R of---					x_c/R of---				
NPR	$\omega_{s,i}$	ω_c	-0.785	-0.524	0.000	0.560	1.140	-0.785	-0.524	0.000	0.560	1.140
2.042	0.0000	0.0000	0.480	0.478	0.481	0.481	0.490	0.485	0.481	0.481	0.486	0.497
1.998	0.0000	0.0514	0.493	0.491	0.494	0.505	0.506	0.499	0.497	0.499	0.512	0.509
1.995	0.0000	0.1013	0.454	0.445	0.466	0.533	0.520	0.460	0.422	0.459	0.542	0.517
1.994	0.0000	0.1513	0.438	0.429	0.456	0.503	0.545	0.450	0.401	0.433	0.572	0.515
1.990	0.0000	0.1976	0.411	0.394	0.436	0.466	0.533	0.455	0.409	0.335	0.544	0.532
4.001	0.0000	0.0000	0.199	0.189	0.206	0.210	0.214	0.225	0.204	0.196	0.204	0.208
4.006	0.0000	0.0490	0.190	0.171	0.197	0.198	0.223	0.213	0.172	0.145	0.188	0.215
4.009	0.0000	0.0976	0.183	0.162	0.150	0.113	0.192	0.224	0.201	0.154	0.103	0.208
4.011	0.0000	0.1449	0.220	0.215	0.225	0.130	0.162	0.244	0.240	0.229	0.111	0.164
4.001	0.0000	0.1908	0.240	0.239	0.298	0.176	0.169	0.250	0.249	0.299	0.126	0.175
6.020	0.0000	0.0000	0.154	0.152	0.154	0.152	0.151	0.159	0.154	0.153	0.151	0.150
6.009	0.0000	0.0482	0.125	0.120	0.131	0.134	0.136	0.142	0.115	0.071	0.054	0.127
5.994	0.0000	0.0967	0.148	0.144	0.152	0.086	0.128	0.163	0.160	0.152	0.065	0.110
5.994	0.0000	0.1442	0.164	0.163	0.234	0.136	0.131	0.167	0.165	0.225	0.095	0.133
5.998	0.0000	0.1911	0.166	0.165	0.320	0.184	0.138	0.166	0.163	0.288	0.124	0.149
7.997	0.0000	0.0000	0.118	0.116	0.117	0.115	0.114	0.120	0.117	0.116	0.114	0.112
8.005	0.0000	0.0501	0.105	0.104	0.110	0.111	0.108	0.113	0.102	0.079	0.056	0.099
8.009	0.0000	0.0957	0.120	0.119	0.149	0.089	0.029	0.125	0.124	0.151	0.063	0.076
7.998	0.0000	0.1448	0.124	0.124	0.243	0.140	0.076	0.124	0.122	0.218	0.094	0.107
8.001	0.0000	0.1711	0.124	0.123	0.284	0.170	0.046	0.123	0.119	0.253	0.108	0.102
9.988	0.0000	0.0000	0.093	0.091	0.092	0.092	0.090	0.096	0.092	0.091	0.090	0.088
9.990	0.0000	0.0496	0.083	0.079	0.076	0.044	0.042	0.095	0.091	0.078	0.032	0.044
10.002	0.0000	0.0954	0.098	0.098	0.161	0.092	0.026	0.099	0.099	0.146	0.062	0.022
10.008	0.0000	0.1372	0.100	0.098	0.228	0.136	0.037	0.098	0.095	0.203	0.087	0.033

Table 81. Coanda Flap Static Pressure Ratios $p/p_{t,j}$ for Configuration 27

[$\epsilon = 2.405$; long Coanda flaps; $\phi_l = 0^\circ$; $\phi_r = 30^\circ$]

			$p/p_{t,j}$ for---									
			Left Coanda flap at---					Right Coanda flap at---				
			x_c/R of---					x_c/R of---				
NPR	ω_{si}	ω_c	-0.785	-0.524	0.000	0.560	1.140	-0.785	-0.524	0.000	0.560	1.140
2.006	0.0000	0.0000	0.489	0.487	0.489	0.491	0.500	0.481	0.479	0.482	0.489	0.495
2.007	0.0000	0.0519	0.490	0.488	0.491	0.503	0.504	0.469	0.445	0.481	0.492	0.499
2.004	0.0000	0.1029	0.449	0.440	0.461	0.530	0.519	0.353	0.400	0.423	0.467	0.511
2.005	0.0000	0.1504	0.435	0.426	0.453	0.500	0.541	0.331	0.309	0.373	0.434	0.518
2.005	0.0000	0.1999	0.406	0.388	0.431	0.467	0.531	0.411	0.372	0.328	0.390	0.475
3.990	0.0000	0.0000	0.202	0.191	0.211	0.211	0.217	0.248	0.247	0.247	0.248	0.247
3.992	0.0000	0.0500	0.190	0.171	0.197	0.198	0.224	0.190	0.212	0.219	0.222	0.234
3.992	0.0000	0.0960	0.182	0.160	0.147	0.120	0.198	0.202	0.182	0.201	0.198	0.205
3.991	0.0000	0.1460	0.222	0.216	0.228	0.131	0.162	0.239	0.291	0.186	0.186	0.184
3.992	0.0000	0.1927	0.241	0.240	0.303	0.179	0.170	0.238	0.398	0.200	0.196	0.194
6.011	0.0000	0.0000	0.154	0.152	0.154	0.153	0.152	0.162	0.162	0.160	0.158	0.158
5.999	0.0000	0.0496	0.127	0.123	0.131	0.136	0.138	0.138	0.151	0.160	0.158	0.157
5.997	0.0000	0.0973	0.149	0.145	0.153	0.087	0.129	0.159	0.195	0.153	0.151	0.150
6.003	0.0000	0.1440	0.163	0.163	0.234	0.136	0.132	0.161	0.295	0.156	0.156	0.157
5.994	0.0000	0.1897	0.166	0.166	0.318	0.183	0.139	0.158	0.369	0.150	0.155	0.155
7.995	0.0000	0.0000	0.117	0.116	0.117	0.115	0.114	0.122	0.122	0.121	0.120	0.119
7.996	0.0000	0.0481	0.105	0.104	0.109	0.110	0.108	0.105	0.098	0.117	0.119	0.119
8.001	0.0000	0.0955	0.120	0.119	0.148	0.089	0.029	0.119	0.197	0.119	0.120	0.120
8.009	0.0000	0.1416	0.124	0.124	0.238	0.137	0.078	0.119	0.275	0.112	0.117	0.118
7.996	0.0000	0.1693	0.125	0.123	0.279	0.166	0.046	0.119	0.325	0.107	0.116	0.116
10.002	0.0000	0.0000	0.093	0.091	0.093	0.092	0.090	0.098	0.098	0.097	0.092	0.090
10.008	0.0000	0.0473	0.081	0.076	0.073	0.041	0.045	0.092	0.090	0.075	0.092	0.094
10.013	0.0000	0.0957	0.098	0.098	0.159	0.091	0.025	0.097	0.193	0.094	0.095	0.095
9.986	0.0000	0.1376	0.100	0.098	0.228	0.136	0.037	0.096	0.262	0.089	0.093	0.093

Table 82. Coanda Flap Static Pressure Ratios $p/p_{t,j}$ for Configuration 28

[$\epsilon = 2.405$; long Coanda flaps; $\phi_l = 0^\circ$; $\phi_r = 45^\circ$]

		$p/p_{t,j}$ for---										
		Left Coanda flap at---					Right Coanda flap at---					
		x_c/R of---										
NPR	$\omega_{s,j}$	ω_c	-0.785	-0.524	0.000	0.560	1.140	-0.785	-0.524	0.000	0.560	1.140
2.009	0.0000	0.0000	0.489	0.487	0.489	0.489	0.508	0.480	0.482	0.480	0.491	0.493
2.001	0.0000	0.0507	0.494	0.493	0.498	0.510	0.508	0.454	0.471	0.480	0.493	0.499
2.004	0.0000	0.1005	0.452	0.443	0.464	0.529	0.517	0.403	0.420	0.434	0.468	0.503
2.002	0.0000	0.1490	0.436	0.428	0.454	0.511	0.532	0.387	0.405	0.398	0.413	0.491
2.004	0.0000	0.1969	0.410	0.394	0.437	0.461	0.532	0.417	0.313	0.373	0.374	0.455
3.999	0.0000	0.0000	0.201	0.192	0.209	0.211	0.215	0.247	0.247	0.248	0.248	0.248
4.002	0.0000	0.0493	0.190	0.171	0.197	0.198	0.223	0.212	0.225	0.230	0.236	0.241
4.002	0.0000	0.0983	0.184	0.163	0.151	0.111	0.191	0.210	0.206	0.206	0.205	0.212
4.008	0.0000	0.1462	0.220	0.215	0.227	0.130	0.161	0.330	0.226	0.245	0.246	0.246
4.005	0.0000	0.1910	0.240	0.239	0.300	0.177	0.169	0.444	0.215	0.245	0.247	0.247
5.994	0.0000	0.0000	0.155	0.152	0.155	0.154	0.153	0.164	0.164	0.164	0.163	0.162
5.996	0.0000	0.0494	0.128	0.124	0.132	0.137	0.138	0.150	0.159	0.163	0.163	0.163
6.002	0.0000	0.0962	0.148	0.144	0.152	0.086	0.133	0.214	0.155	0.164	0.165	0.165
6.009	0.0000	0.1422	0.163	0.162	0.231	0.134	0.131	0.330	0.132	0.162	0.164	0.164
6.007	0.0000	0.1906	0.165	0.165	0.319	0.184	0.138	0.424	0.100	0.161	0.164	0.164
7.990	0.0000	0.0000	0.118	0.116	0.117	0.116	0.114	0.123	0.122	0.122	0.121	0.121
7.995	0.0000	0.0477	0.105	0.104	0.108	0.110	0.108	0.101	0.112	0.122	0.123	0.123
8.011	0.0000	0.0934	0.119	0.119	0.144	0.086	0.028	0.218	0.102	0.122	0.123	0.123
8.004	0.0000	0.1419	0.124	0.124	0.238	0.137	0.080	0.316	0.074	0.121	0.122	0.123
8.002	0.0000	0.1712	0.124	0.123	0.285	0.170	0.046	0.369	0.087	0.120	0.122	0.123
10.008	0.0000	0.0000	0.093	0.091	0.093	0.092	0.090	0.097	0.097	0.096	0.095	0.094
10.006	0.0000	0.0480	0.082	0.077	0.075	0.043	0.044	0.103	0.093	0.097	0.098	0.098
10.076	0.0000	0.0958	0.098	0.098	0.162	0.093	0.026	0.217	0.058	0.097	0.098	0.097
10.003	0.0000	0.1365	0.100	0.098	0.227	0.136	0.036	0.293	0.069	0.096	0.098	0.098

Table 83. Coanda Flap Static Pressure Ratios $p/p_{t,j}$ for Configuration 29

[$\epsilon = 2.405$; long Coanda flaps; $\phi_l = -10^\circ$; $\phi_r = 30^\circ$]

NPR	$p/p_{t,j}$ for---											
	ω_{N_i}	ω_i	Left Coanda flap at---					Right Coanda flap at---				
			x_c/R of---					x_c/R of---				
			-0.785	-0.524	0.000	0.560	1.140	-0.785	-0.524	0.000	0.560	1.140
1.992	0.0000	0.0000	0.501	0.500	0.495	0.503	0.548	0.485	0.483	0.486	0.493	0.499
1.991	0.0000	0.0527	0.502	0.502	0.527	0.539	0.540	0.473	0.446	0.485	0.496	0.504
1.992	0.0000	0.1044	0.489	0.486	0.489	0.609	0.548	0.355	0.400	0.426	0.473	0.515
1.995	0.0000	0.1527	0.484	0.481	0.485	0.663	0.547	0.336	0.304	0.376	0.440	0.524
1.994	0.0000	0.2025	0.477	0.473	0.480	0.614	0.596	0.418	0.360	0.331	0.392	0.478
3.996	0.0000	0.0000	0.207	0.194	0.202	0.216	0.220	0.247	0.247	0.246	0.247	0.247
4.003	0.0000	0.0507	0.208	0.191	0.201	0.177	0.217	0.188	0.213	0.219	0.221	0.233
4.004	0.0000	0.0998	0.215	0.203	0.216	0.171	0.260	0.210	0.182	0.201	0.199	0.206
4.004	0.0000	0.1477	0.242	0.240	0.292	0.254	0.090	0.237	0.288	0.186	0.186	0.184
4.006	0.0000	0.1943	0.248	0.248	0.438	0.338	0.134	0.241	0.384	0.225	0.218	0.216
5.996	0.0000	0.0000	0.137	0.126	0.131	0.139	0.142	0.162	0.162	0.160	0.158	0.158
6.002	0.0000	0.0493	0.128	0.109	0.120	0.079	0.088	0.136	0.151	0.159	0.158	0.158
6.002	0.0000	0.0978	0.161	0.160	0.180	0.169	0.037	0.158	0.191	0.157	0.158	0.158
6.003	0.0000	0.1452	0.166	0.165	0.341	0.255	0.053	0.164	0.284	0.157	0.158	0.158
6.007	0.0000	0.1916	0.166	0.164	0.570	0.338	0.069	0.170	0.353	0.151	0.157	0.158
8.009	0.0000	0.0000	0.107	0.096	0.096	0.098	0.098	0.121	0.120	0.119	0.117	0.116
8.013	0.0000	0.0491	0.107	0.099	0.107	0.078	0.085	0.106	0.093	0.114	0.118	0.119
8.023	0.0000	0.0971	0.124	0.123	0.207	0.170	0.038	0.121	0.193	0.119	0.120	0.120
8.031	0.0000	0.1436	0.124	0.123	0.429	0.253	0.052	0.127	0.265	0.113	0.118	0.119
8.034	0.0000	0.1696	0.124	0.121	0.561	0.301	0.061	0.135	0.312	0.111	0.118	0.119
10.002	0.0000	0.0000	0.085	0.075	0.073	0.074	0.075	0.098	0.097	0.097	0.091	0.089
10.007	0.0000	0.0492	0.091	0.088	0.095	0.082	0.081	0.094	0.094	0.094	0.096	0.096
10.012	0.0000	0.0963	0.100	0.099	0.251	0.169	0.042	0.100	0.185	0.095	0.096	0.096
10.020	0.0000	0.1358	0.099	0.097	0.449	0.241	0.049	0.109	0.250	0.091	0.094	0.095

Table 84. Coanda Flap Static Pressure Ratios $p/p_{t,j}$ for Configuration 30

[$\epsilon = 2.405$; long Coanda flaps; $\phi_l = -10^\circ$; $\phi_r = 45^\circ$]

			$p/p_{t,j}$ for---									
			Left Coanda flap at---					Right Coanda flap at---				
			x_c/R of---					x_c/R of---				
NPR	ω_{x_i}	ω_c	-0.785	-0.524	0.000	0.560	1.140	-0.785	-0.524	0.000	0.560	1.140
2.003	0.0000	0.0000	0.498	0.497	0.493	0.501	0.545	0.483	0.485	0.483	0.494	0.496
1.999	0.0000	0.0507	0.500	0.500	0.525	0.536	0.537	0.457	0.474	0.482	0.494	0.501
1.998	0.0000	0.1021	0.489	0.486	0.489	0.602	0.546	0.404	0.421	0.434	0.470	0.504
1.998	0.0000	0.1539	0.484	0.481	0.485	0.663	0.549	0.379	0.407	0.402	0.412	0.490
2.001	0.0000	0.2005	0.476	0.472	0.478	0.621	0.628	0.425	0.317	0.375	0.375	0.456
4.017	0.0000	0.0000	0.206	0.193	0.201	0.215	0.218	0.246	0.245	0.246	0.247	0.247
4.018	0.0000	0.0499	0.207	0.190	0.200	0.177	0.217	0.215	0.229	0.229	0.236	0.241
4.018	0.0000	0.0985	0.213	0.201	0.214	0.168	0.260	0.215	0.215	0.212	0.209	0.213
4.020	0.0000	0.1473	0.241	0.240	0.290	0.253	0.090	0.314	0.226	0.244	0.246	0.246
4.021	0.0000	0.1936	0.247	0.247	0.435	0.336	0.134	0.415	0.222	0.244	0.246	0.246
6.009	0.0000	0.0000	0.138	0.126	0.131	0.138	0.141	0.164	0.163	0.163	0.162	0.162
6.011	0.0000	0.0500	0.128	0.109	0.120	0.080	0.088	0.150	0.160	0.163	0.164	0.164
6.012	0.0000	0.0968	0.160	0.159	0.175	0.167	0.036	0.207	0.153	0.163	0.165	0.165
6.015	0.0000	0.1430	0.166	0.165	0.336	0.251	0.053	0.308	0.142	0.162	0.164	0.164
6.018	0.0000	0.1911	0.165	0.164	0.569	0.338	0.069	0.400	0.094	0.161	0.164	0.164
8.003	0.0000	0.0000	0.107	0.096	0.096	0.098	0.098	0.122	0.121	0.121	0.120	0.119
8.004	0.0000	0.0493	0.108	0.099	0.107	0.078	0.085	0.107	0.109	0.122	0.123	0.123
8.002	0.0000	0.0966	0.124	0.124	0.205	0.170	0.038	0.207	0.111	0.122	0.123	0.123
8.010	0.0000	0.1428	0.124	0.123	0.426	0.252	0.052	0.298	0.070	0.121	0.122	0.122
8.017	0.0000	0.1722	0.124	0.122	0.575	0.308	0.062	0.350	0.083	0.121	0.122	0.122
10.012	0.0000	0.0000	0.084	0.075	0.073	0.074	0.075	0.097	0.097	0.095	0.095	0.094
10.012	0.0000	0.0494	0.091	0.088	0.096	0.082	0.081	0.106	0.094	0.098	0.099	0.098
10.017	0.0000	0.0970	0.100	0.099	0.257	0.172	0.040	0.206	0.077	0.097	0.098	0.098
10.023	0.0000	0.1369	0.099	0.097	0.456	0.244	0.049	0.277	0.066	0.097	0.098	0.098

Table 85. Static Pressure Ratios $p/p_{t,j}$ Upstream and Downstream of the Slot for Configuration 31

[$\epsilon = 1.502$; forward slot injection; $\phi_l = 0^\circ$; $\phi_r = 0^\circ$]

NPR	ω_{si}	ω_c	$p/p_{t,j}$ for---							
			Upstream lateral row at---				Downstream lateral row at---			
			y/y_l of---				y/y_l of---			
			0.056	0.204	0.352	0.500	0.056	0.204	0.352	0.500
1.993	0.0000	0.0000	0.337	0.329	0.325	0.325	0.462	0.477	0.479	0.478
2.003	0.0245	0.0000	0.525	0.555	0.561	0.563	0.463	0.468	0.472	0.473
2.004	0.0491	0.0000	0.552	0.577	0.564	0.571	0.428	0.448	0.464	0.464
2.003	0.0753	0.0000	0.667	0.687	0.678	0.679	0.448	0.469	0.477	0.477
2.009	0.1028	0.0000	0.756	0.775	0.765	0.768	0.472	0.477	0.483	0.483
4.010	0.0000	0.0000	0.336	0.325	0.323	0.321	0.239	0.252	0.240	0.241
4.004	0.0251	0.0000	0.351	0.478	0.480	0.491	0.221	0.219	0.214	0.228
4.014	0.0496	0.0000	0.559	0.572	0.586	0.576	0.139	0.114	0.136	0.117
4.011	0.0735	0.0000	0.619	0.578	0.556	0.574	0.049	0.047	0.048	0.045
4.002	0.0980	0.0000	0.633	0.637	0.635	0.654	0.142	0.160	0.178	0.185
6.007	0.0000	0.0000	0.335	0.322	0.321	0.320	0.239	0.251	0.239	0.241
6.019	0.0245	0.0000	0.360	0.479	0.476	0.484	0.222	0.221	0.214	0.223
6.022	0.0489	0.0000	0.543	0.548	0.554	0.568	0.144	0.110	0.130	0.117
6.003	0.0732	0.0000	0.597	0.579	0.642	0.634	0.057	0.048	0.044	0.043
6.023	0.0970	0.0000	0.622	0.609	0.625	0.628	0.026	0.042	0.057	0.056
8.025	0.0000	0.0000	0.334	0.322	0.320	0.319	0.239	0.251	0.239	0.241
8.011	0.0248	0.0000	0.375	0.481	0.481	0.484	0.223	0.223	0.214	0.224
8.020	0.0486	0.0000	0.522	0.525	0.525	0.533	0.150	0.110	0.113	0.109
8.019	0.0725	0.0000	0.553	0.552	0.573	0.574	0.063	0.051	0.049	0.048
8.020	0.0957	0.0000	0.575	0.590	0.594	0.601	0.025	0.039	0.048	0.048
10.016	0.0000	0.0000	0.333	0.321	0.319	0.318	0.239	0.251	0.238	0.241
10.013	0.0244	0.0000	0.367	0.477	0.476	0.479	0.225	0.224	0.214	0.225
10.025	0.0487	0.0000	0.516	0.522	0.516	0.526	0.149	0.114	0.103	0.102
10.027	0.0722	0.0000	0.525	0.534	0.537	0.553	0.057	0.052	0.050	0.050
10.050	0.0962	0.0000	0.552	0.570	0.571	0.579	0.026	0.035	0.044	0.045

Table 86. Static Pressure Ratios $p/p_{t,j}$ Upstream and Downstream of the Slot for Configuration 32

[$\epsilon = 1.502$; forward slot injection; $\phi_l = 0^\circ$; $\phi_r = 0^\circ$]

			$p/p_{t,j}$ for---							
			Upstream lateral row at---				Downstream lateral row at---			
			y/y_t of---				y/y_t of---			
NPR	ω_{s_i}	ω_c	0.056	0.204	0.352	0.500	0.056	0.204	0.352	0.500
2.001	0.0000	0.0497	0.337	0.328	0.325	0.325	0.451	0.474	0.476	0.476
2.002	0.0000	0.0973	0.338	0.328	0.325	0.325	0.450	0.474	0.476	0.475
2.003	0.0249	0.0491	0.528	0.558	0.563	0.565	0.464	0.469	0.472	0.473
1.999	0.0246	0.0975	0.526	0.557	0.561	0.563	0.465	0.470	0.473	0.474
2.006	0.0489	0.0493	0.551	0.576	0.564	0.571	0.427	0.447	0.464	0.463
2.000	0.0488	0.0979	0.552	0.576	0.564	0.571	0.429	0.449	0.465	0.465
2.006	0.0729	0.0507	0.659	0.678	0.672	0.675	0.443	0.467	0.474	0.475
1.996	0.0732	0.0984	0.662	0.681	0.674	0.677	0.446	0.470	0.477	0.478
1.999	0.1032	0.0526	0.761	0.781	0.771	0.774	0.474	0.479	0.485	0.486
2.002	0.1024	0.1028	0.760	0.779	0.769	0.773	0.474	0.479	0.485	0.485
3.990	0.0000	0.0494	0.337	0.325	0.323	0.321	0.239	0.251	0.240	0.241
4.017	0.0000	0.0964	0.337	0.325	0.323	0.321	0.239	0.251	0.240	0.241
3.994	0.0238	0.0491	0.342	0.461	0.458	0.479	0.223	0.220	0.216	0.229
4.015	0.0234	0.0975	0.341	0.455	0.450	0.473	0.224	0.221	0.217	0.230
3.990	0.0481	0.0486	0.556	0.569	0.580	0.570	0.145	0.122	0.144	0.127
4.019	0.0469	0.0969	0.553	0.566	0.573	0.565	0.150	0.130	0.152	0.136
4.005	0.0717	0.0485	0.609	0.627	0.555	0.576	0.051	0.048	0.049	0.046
4.008	0.0717	0.0967	0.610	0.628	0.555	0.576	0.051	0.048	0.048	0.046
3.996	0.0963	0.0492	0.629	0.633	0.632	0.652	0.142	0.160	0.179	0.185
3.992	0.0972	0.0975	0.633	0.638	0.636	0.656	0.144	0.163	0.181	0.187
5.994	0.0000	0.0493	0.334	0.322	0.321	0.320	0.239	0.251	0.239	0.241
6.027	0.0000	0.0957	0.334	0.322	0.321	0.320	0.239	0.251	0.239	0.241
5.985	0.0242	0.0486	0.358	0.478	0.475	0.482	0.222	0.222	0.213	0.223
5.993	0.0238	0.0963	0.352	0.474	0.471	0.478	0.223	0.222	0.214	0.223
5.990	0.0476	0.0484	0.540	0.545	0.546	0.565	0.148	0.115	0.138	0.121
6.008	0.0477	0.0963	0.540	0.545	0.546	0.565	0.147	0.114	0.136	0.120
5.990	0.0720	0.0485	0.592	0.576	0.638	0.630	0.060	0.049	0.045	0.044
6.032	0.0712	0.0960	0.589	0.574	0.636	0.629	0.062	0.050	0.046	0.044
5.992	0.0951	0.0488	0.623	0.606	0.623	0.626	0.026	0.041	0.053	0.053
5.985	0.0952	0.0969	0.623	0.606	0.623	0.626	0.026	0.041	0.054	0.053
7.990	0.0000	0.0484	0.333	0.321	0.320	0.319	0.239	0.250	0.238	0.241
8.000	0.0000	0.0963	0.333	0.321	0.320	0.319	0.239	0.250	0.238	0.241
8.000	0.0244	0.0476	0.370	0.479	0.479	0.482	0.224	0.223	0.214	0.224
7.999	0.0241	0.0959	0.364	0.476	0.476	0.480	0.224	0.223	0.215	0.224
8.035	0.0479	0.0479	0.521	0.524	0.523	0.531	0.152	0.112	0.115	0.111
7.989	0.0475	0.0963	0.521	0.524	0.523	0.531	0.155	0.116	0.119	0.115
7.987	0.0716	0.0478	0.550	0.551	0.567	0.571	0.064	0.051	0.050	0.049
7.984	0.0713	0.0959	0.550	0.551	0.566	0.571	0.064	0.052	0.050	0.049
7.991	0.0959	0.0483	0.573	0.590	0.593	0.600	0.025	0.040	0.050	0.050
8.035	0.0954	0.0960	0.572	0.589	0.591	0.598	0.025	0.040	0.050	0.050
9.993	0.0000	0.0482	0.333	0.321	0.320	0.319	0.239	0.250	0.238	0.241
10.022	0.0000	0.0953	0.333	0.321	0.320	0.319	0.239	0.250	0.238	0.241
9.996	0.0243	0.0485	0.368	0.477	0.476	0.480	0.225	0.224	0.214	0.225
10.023	0.0241	0.0956	0.365	0.476	0.475	0.479	0.225	0.224	0.214	0.225
10.026	0.0473	0.0491	0.516	0.523	0.517	0.526	0.156	0.121	0.111	0.112
10.008	0.0482	0.0962	0.516	0.523	0.517	0.526	0.151	0.116	0.106	0.105
10.004	0.0715	0.0477	0.525	0.534	0.536	0.552	0.058	0.053	0.051	0.050
10.024	0.0714	0.0966	0.524	0.534	0.536	0.552	0.059	0.053	0.052	0.051
10.021	0.0953	0.0479	0.552	0.569	0.571	0.578	0.026	0.036	0.045	0.046
10.005	0.0957	0.0963	0.553	0.570	0.571	0.579	0.026	0.036	0.046	0.047

Table 87. Static Pressure Ratios $p/p_{t,j}$ Upstream and Downstream of the Slot for Configuration 33

[$\epsilon = 1.502$; aft slot injection; $\phi_t = 0^\circ$; $\phi_r = 0^\circ$]

$p/p_{t,j}$ for---										
		Upstream lateral row at---					Downstream lateral row at---			
		y/y_t of---					y/y_t of---			
NPR	$\omega_{s,i}$	ω_c	0.056	0.204	0.352	0.500	0.056	0.204	0.352	0.500
1.999	0.0000	0.0497	0.422	0.433	0.448	0.454	0.464	0.466	0.469	0.469
2.004	0.0000	0.0996	0.421	0.430	0.447	0.453	0.463	0.466	0.468	0.468
1.995	0.0249	0.0488	0.503	0.512	0.519	0.520	0.485	0.493	0.495	0.495
2.007	0.0244	0.0989	0.500	0.509	0.517	0.517	0.483	0.490	0.492	0.492
2.004	0.0491	0.0491	0.555	0.570	0.579	0.584	0.459	0.484	0.487	0.487
1.999	0.0487	0.0988	0.556	0.569	0.579	0.584	0.460	0.486	0.488	0.488
2.010	0.0735	0.0495	0.636	0.629	0.611	0.616	0.459	0.478	0.482	0.482
2.009	0.0731	0.1003	0.636	0.628	0.610	0.615	0.459	0.478	0.482	0.482
2.006	0.0984	0.0500	0.709	0.709	0.695	0.707	0.471	0.480	0.482	0.482
1.998	0.0988	0.0992	0.712	0.711	0.698	0.710	0.473	0.481	0.484	0.484
3.996	0.0000	0.0494	0.247	0.261	0.251	0.249	0.185	0.175	0.175	0.173
4.003	0.0000	0.0980	0.246	0.261	0.251	0.249	0.185	0.175	0.175	0.173
4.008	0.0243	0.0494	0.259	0.368	0.393	0.403	0.161	0.166	0.160	0.167
4.006	0.0245	0.0978	0.259	0.371	0.396	0.405	0.161	0.166	0.160	0.167
4.005	0.0486	0.0494	0.459	0.494	0.496	0.498	0.184	0.208	0.214	0.217
4.009	0.0479	0.0978	0.457	0.492	0.494	0.496	0.183	0.205	0.212	0.214
4.005	0.0722	0.0496	0.502	0.527	0.533	0.535	0.225	0.236	0.239	0.239
4.004	0.0719	0.0966	0.502	0.527	0.532	0.535	0.225	0.236	0.239	0.239
4.008	0.0962	0.0487	0.547	0.565	0.574	0.578	0.232	0.239	0.240	0.241
4.007	0.0964	0.0963	0.548	0.566	0.574	0.579	0.232	0.239	0.241	0.241
6.019	0.0000	0.0513	0.249	0.261	0.250	0.248	0.185	0.175	0.173	0.173
6.017	0.0000	0.0997	0.249	0.260	0.250	0.248	0.185	0.175	0.173	0.173
6.016	0.0244	0.0504	0.268	0.372	0.394	0.401	0.165	0.163	0.159	0.166
6.014	0.0250	0.0978	0.278	0.380	0.400	0.405	0.164	0.162	0.159	0.165
6.011	0.0489	0.0497	0.442	0.478	0.480	0.480	0.105	0.073	0.072	0.066
6.010	0.0479	0.0982	0.440	0.476	0.478	0.478	0.108	0.076	0.075	0.069
6.007	0.0724	0.0491	0.486	0.515	0.519	0.519	0.113	0.140	0.143	0.145
6.011	0.0722	0.0959	0.486	0.514	0.519	0.519	0.114	0.140	0.143	0.145
6.010	0.0964	0.0478	0.516	0.541	0.548	0.548	0.120	0.144	0.147	0.148
6.012	0.0958	0.0960	0.515	0.540	0.547	0.547	0.121	0.144	0.147	0.148
7.986	0.0000	0.0493	0.248	0.260	0.249	0.247	0.188	0.176	0.173	0.173
8.001	0.0000	0.0962	0.248	0.260	0.249	0.247	0.189	0.176	0.173	0.173
8.024	0.0242	0.0490	0.272	0.365	0.389	0.396	0.167	0.162	0.158	0.165
8.015	0.0237	0.0961	0.266	0.357	0.384	0.392	0.167	0.162	0.159	0.166
8.017	0.0471	0.0480	0.436	0.475	0.474	0.476	0.109	0.076	0.075	0.069
7.997	0.0477	0.0951	0.437	0.476	0.475	0.476	0.107	0.075	0.073	0.068
8.012	0.0718	0.0484	0.478	0.511	0.510	0.512	0.044	0.050	0.050	0.050
8.012	0.0698	0.0943	0.476	0.509	0.507	0.509	0.046	0.043	0.044	0.043
8.007	0.0951	0.0479	0.501	0.532	0.531	0.534	0.064	0.081	0.088	0.088
8.010	0.0947	0.0767	0.501	0.532	0.531	0.534	0.064	0.080	0.087	0.088
9.995	0.0000	0.0490	0.249	0.260	0.249	0.247	0.189	0.176	0.173	0.173
10.023	0.0000	0.0955	0.249	0.260	0.249	0.247	0.189	0.176	0.173	0.173
9.998	0.0242	0.0479	0.274	0.360	0.386	0.394	0.168	0.160	0.159	0.166
10.017	0.0243	0.0955	0.275	0.361	0.387	0.395	0.168	0.160	0.158	0.165
9.986	0.0479	0.0486	0.438	0.476	0.476	0.478	0.107	0.074	0.072	0.068
9.997	0.0481	0.0906	0.439	0.476	0.476	0.478	0.106	0.073	0.072	0.067
9.999	0.0711	0.0481	0.478	0.510	0.509	0.512	0.044	0.036	0.036	0.036
9.989	0.0719	0.0665	0.479	0.510	0.510	0.513	0.043	0.036	0.036	0.036
9.996	0.0906	0.0478	0.498	0.527	0.527	0.531	0.028	0.049	0.058	0.058

Table 88. Static Pressure Ratios $p/p_{t,j}$ Upstream and Downstream of the Slot for Configuration 34

[$\epsilon = 1.944$; forward slot injection; $\phi_l = 0^\circ$; $\phi_r = 0^\circ$]

NPR	ω_{si}	ω_c	$p/p_{t,j}$ for---							
			Upstream lateral row at---				Downstream lateral row at---			
			y/y_i of---				y/y_i of---			
			0.056	0.204	0.352	0.500	0.056	0.204	0.352	0.500
2.009	0.0000	0.0000	0.237	0.222	0.224	0.236	0.407	0.387	0.397	0.388
2.009	0.0258	0.0000	0.420	0.457	0.456	0.458	0.419	0.477	0.488	0.488
2.010	0.0505	0.0000	0.484	0.513	0.493	0.491	0.475	0.480	0.487	0.486
2.009	0.0763	0.0000	0.526	0.565	0.543	0.538	0.480	0.485	0.491	0.491
2.003	0.1015	0.0000	0.573	0.617	0.593	0.588	0.483	0.486	0.492	0.493
3.997	0.0000	0.0000	0.237	0.221	0.226	0.231	0.174	0.189	0.183	0.179
3.998	0.0251	0.0000	0.237	0.377	0.379	0.385	0.167	0.169	0.173	0.164
4.001	0.0499	0.0000	0.369	0.386	0.379	0.397	0.162	0.175	0.185	0.199
4.001	0.0738	0.0000	0.419	0.439	0.451	0.467	0.218	0.228	0.232	0.235
4.004	0.0978	0.0000	0.466	0.486	0.497	0.517	0.233	0.237	0.240	0.240
6.003	0.0000	0.0000	0.235	0.221	0.224	0.229	0.182	0.186	0.181	0.179
5.981	0.0249	0.0000	0.235	0.377	0.385	0.387	0.172	0.166	0.172	0.156
5.996	0.0492	0.0000	0.434	0.441	0.429	0.438	0.114	0.076	0.068	0.058
6.008	0.0734	0.0000	0.456	0.459	0.432	0.441	0.035	0.034	0.038	0.037
6.004	0.0967	0.0000	0.461	0.484	0.463	0.467	0.131	0.140	0.151	0.153
8.000	0.0000	0.0000	0.234	0.219	0.224	0.228	0.183	0.188	0.181	0.179
8.010	0.0248	0.0000	0.254	0.379	0.378	0.382	0.166	0.168	0.163	0.166
7.998	0.0484	0.0000	0.384	0.395	0.389	0.397	0.111	0.073	0.063	0.056
7.999	0.0715	0.0000	0.383	0.410	0.393	0.391	0.036	0.035	0.039	0.039
7.998	0.0956	0.0000	0.400	0.444	0.426	0.421	0.018	0.025	0.035	0.035
9.994	0.0000	0.0000	0.237	0.218	0.224	0.228	0.176	0.191	0.180	0.179
10.002	0.0246	0.0000	0.253	0.377	0.375	0.379	0.164	0.169	0.162	0.167
10.002	0.0485	0.0000	0.376	0.386	0.371	0.377	0.105	0.070	0.054	0.055
10.004	0.0723	0.0000	0.376	0.408	0.391	0.387	0.034	0.034	0.037	0.036
10.006	0.0958	0.0000	0.396	0.442	0.424	0.419	0.018	0.025	0.033	0.034

Table 91. Static Pressure Ratios p/p_{1j} Upstream and Downstream of the Slot for Configuration 37

[$\varepsilon = 2.405$; forward slot injection; $\phi_l = 0^\circ$; $\phi_r = 0^\circ$]

			p/p_{1j} for---							
			Upstream lateral row at---				Downstream lateral row at---			
			y/y_l of---				y/y_r of---			
NPR	ω_{si}	ω_c	0.056	0.204	0.352	0.500	0.056	0.204	0.352	0.500
2.012	0.0000	0.0000	0.482	0.487	0.487	0.486	0.483	0.485	0.486	0.485
2.009	0.0252	0.0000	0.463	0.471	0.471	0.468	0.483	0.487	0.488	0.487
2.009	0.0496	0.0000	0.443	0.443	0.445	0.445	0.462	0.466	0.463	0.461
2.002	0.0740	0.0000	0.495	0.503	0.505	0.507	0.475	0.488	0.491	0.491
2.003	0.0982	0.0000	0.526	0.534	0.536	0.544	0.486	0.491	0.494	0.494
4.006	0.0000	0.0000	0.171	0.147	0.146	0.150	0.128	0.209	0.210	0.132
4.007	0.0246	0.0000	0.297	0.257	0.257	0.258	0.172	0.217	0.230	0.230
4.006	0.0495	0.0000	0.293	0.292	0.298	0.299	0.215	0.223	0.225	0.223
4.007	0.0723	0.0000	0.331	0.333	0.336	0.334	0.225	0.234	0.237	0.233
4.012	0.0964	0.0000	0.365	0.374	0.374	0.369	0.235	0.239	0.242	0.241
6.003	0.0000	0.0000	0.171	0.149	0.149	0.152	0.126	0.128	0.126	0.127
6.000	0.0253	0.0000	0.210	0.282	0.287	0.291	0.112	0.113	0.108	0.120
6.001	0.0488	0.0000	0.267	0.269	0.276	0.275	0.031	0.035	0.036	0.034
6.004	0.0725	0.0000	0.316	0.324	0.335	0.329	0.141	0.148	0.154	0.155
6.009	0.0957	0.0000	0.337	0.349	0.354	0.355	0.153	0.156	0.160	0.160
7.993	0.0000	0.0000	0.167	0.150	0.150	0.153	0.128	0.127	0.125	0.127
7.995	0.0246	0.0000	0.273	0.284	0.283	0.291	0.108	0.107	0.098	0.110
7.993	0.0489	0.0000	0.292	0.301	0.289	0.306	0.040	0.035	0.034	0.033
7.996	0.0729	0.0000	0.283	0.295	0.304	0.308	0.015	0.029	0.036	0.035
7.997	0.0970	0.0000	0.312	0.323	0.333	0.334	0.098	0.104	0.109	0.111
9.997	0.0000	0.0000	0.164	0.150	0.150	0.152	0.127	0.127	0.125	0.127
10.015	0.0242	0.0000	0.266	0.275	0.274	0.279	0.108	0.101	0.094	0.106
10.011	0.0486	0.0000	0.244	0.251	0.257	0.256	0.035	0.034	0.035	0.034
10.014	0.0722	0.0000	0.269	0.278	0.286	0.284	0.013	0.024	0.030	0.030
9.995	0.0908	0.0000	0.289	0.299	0.305	0.306	0.011	0.018	0.029	0.029
10.001	0.0957	0.0000	0.293	0.304	0.310	0.312	0.011	0.018	0.030	0.029

Table 101. Sidewall and Lower Divergent Flap Internal Static Pressure Ratios $p/p_{t,j}$ for Configuration 31

$[\epsilon = 1.502; \delta_{v,p} = 0^\circ; \text{forward slot injection}; \phi_f = 0^\circ; \phi_r = 0^\circ]$

NPR	ω_{si}	ω_c	$p/p_{t,j}$ for---					
			Sidewall centerline at---			Lower flap centerline at---		
			$[x - x_t]/[L_f - x_t]$ of---			$[x - x_t]/[L_f - x_t]$ of---		
			0.000	0.190	0.381	0.000	0.190	0.381
1.993	0.0000	0.0000	0.654	0.388	0.238	0.280	0.307	0.294
2.003	0.0245	0.0000	0.654	0.388	0.238	0.280	0.307	0.294
2.004	0.0491	0.0000	0.659	0.422	0.381	0.283	0.321	0.572
2.003	0.0753	0.0000	0.687	0.576	0.605	0.328	0.542	0.615
2.009	0.1028	0.0000	0.734	0.674	0.675	0.418	0.667	0.659
4.010	0.0000	0.0000	0.652	0.386	0.236	0.278	0.307	0.291
4.004	0.0251	0.0000	0.653	0.386	0.236	0.278	0.307	0.291
4.014	0.0496	0.0000	0.653	0.387	0.237	0.278	0.307	0.291
4.011	0.0735	0.0000	0.653	0.387	0.311	0.278	0.308	0.300
4.002	0.0980	0.0000	0.656	0.432	0.567	0.280	0.401	0.611
6.007	0.0000	0.0000	0.653	0.385	0.236	0.279	0.309	0.290
6.019	0.0245	0.0000	0.652	0.385	0.236	0.279	0.309	0.290
6.022	0.0489	0.0000	0.652	0.385	0.237	0.279	0.309	0.290
6.003	0.0732	0.0000	0.653	0.386	0.299	0.279	0.309	0.290
6.023	0.0970	0.0000	0.653	0.391	0.400	0.279	0.310	0.525
8.025	0.0000	0.0000	0.652	0.385	0.236	0.279	0.309	0.289
8.011	0.0248	0.0000	0.652	0.385	0.236	0.279	0.309	0.289
8.020	0.0486	0.0000	0.652	0.385	0.237	0.279	0.309	0.289
8.019	0.0725	0.0000	0.652	0.386	0.323	0.279	0.309	0.290
8.020	0.0957	0.0000	0.653	0.414	0.368	0.280	0.312	0.509
10.016	0.0000	0.0000	0.652	0.385	0.236	0.279	0.308	0.289
10.013	0.0244	0.0000	0.652	0.385	0.236	0.279	0.308	0.289
10.025	0.0487	0.0000	0.652	0.385	0.236	0.279	0.308	0.289
10.027	0.0722	0.0000	0.652	0.397	0.317	0.279	0.308	0.305
10.050	0.0962	0.0000	0.656	0.421	0.359	0.281	0.318	0.491

Table 104. Sidewall and Lower Divergent Flap Internal Static Pressure Ratios $p/p_{t,j}$ for Configuration 34

[$\epsilon = 1.944$; $\delta_{v,p} = 0^\circ$; forward slot injection; $\phi_j = 0^\circ$; $\phi_r = 0^\circ$]

NPR	ω_{si}	ω_c	$p/p_{t,j}$ for---					
			Sidewall centerline at---			Lower flap centerline at---		
			[$x - x_j$]/[$L_f - x_j$] of---			[$x - x_j$]/[$L_f - x_j$] of---		
			0.000	0.190	0.381	0.000	0.190	0.381
2.009	0.0000	0.0000	0.658	0.393	0.240	0.470	0.481	0.482
2.009	0.0258	0.0000	0.657	0.403	0.265	0.283	0.212	0.233
2.010	0.0505	0.0000	0.666	0.435	0.330	0.284	0.216	0.384
2.009	0.0763	0.0000	0.671	0.451	0.372	0.287	0.224	0.443
2.003	0.1015	0.0000	0.680	0.475	0.526	0.295	0.356	0.442
3.997	0.0000	0.0000	0.656	0.394	0.235	0.281	0.206	0.215
3.998	0.0251	0.0000	0.655	0.394	0.235	0.281	0.206	0.215
4.001	0.0499	0.0000	0.656	0.397	0.261	0.281	0.206	0.215
4.001	0.0738	0.0000	0.657	0.413	0.284	0.281	0.207	0.218
4.004	0.0978	0.0000	0.658	0.418	0.304	0.281	0.208	0.223
6.003	0.0000	0.0000	0.655	0.394	0.236	0.283	0.206	0.214
5.981	0.0249	0.0000	0.655	0.394	0.236	0.283	0.206	0.214
5.996	0.0492	0.0000	0.655	0.394	0.236	0.283	0.206	0.214
6.008	0.0734	0.0000	0.655	0.394	0.236	0.283	0.206	0.214
6.004	0.0967	0.0000	0.656	0.395	0.279	0.283	0.206	0.214
8.000	0.0000	0.0000	0.656	0.394	0.237	0.283	0.207	0.214
8.010	0.0248	0.0000	0.656	0.394	0.237	0.283	0.207	0.214
7.998	0.0484	0.0000	0.656	0.394	0.236	0.283	0.207	0.214
7.999	0.0715	0.0000	0.656	0.394	0.261	0.283	0.207	0.214
7.998	0.0956	0.0000	0.656	0.409	0.282	0.283	0.207	0.220
9.994	0.0000	0.0000	0.656	0.394	0.237	0.283	0.207	0.213
10.002	0.0246	0.0000	0.657	0.394	0.237	0.283	0.207	0.213
10.002	0.0485	0.0000	0.657	0.394	0.237	0.283	0.207	0.213
10.004	0.0723	0.0000	0.657	0.396	0.267	0.283	0.207	0.213
10.006	0.0958	0.0000	0.657	0.412	0.282	0.283	0.207	0.221

Table 107. Sidewall and Lower Divergent Flap Internal Static Pressure Ratios $p/p_{t,j}$ for Configuration 37

[$\epsilon = 2.405$; $\delta_{v,p} = 0^\circ$; forward slot injection; $\phi_f = 0^\circ$; $\phi_r = 0^\circ$]

			$p/p_{t,j}$ for---					
			Sidewall centerline at---			Lower flap centerline at---		
			[$x - x_j$]/[$L_j - x_j$] of---			[$x - x_j$]/[$L_j - x_j$] of---		
NPR	ω_v	ω_t	0.000	0.190	0.381	0.000	0.190	0.381
2.012	0.0000	0.0000	0.682	0.489	0.459	0.469	0.489	0.489
2.009	0.0252	0.0000	0.679	0.482	0.442	0.469	0.487	0.486
2.009	0.0496	0.0000	0.677	0.477	0.433	0.468	0.485	0.483
2.002	0.0740	0.0000	0.682	0.489	0.455	0.413	0.445	0.448
2.003	0.0982	0.0000	0.682	0.486	0.440	0.325	0.350	0.413
4.006	0.0000	0.0000	0.660	0.395	0.238	0.292	0.133	0.141
4.007	0.0246	0.0000	0.660	0.395	0.238	0.292	0.133	0.141
4.006	0.0495	0.0000	0.660	0.395	0.244	0.292	0.133	0.141
4.007	0.0723	0.0000	0.660	0.395	0.265	0.292	0.133	0.142
4.012	0.0964	0.0000	0.660	0.397	0.282	0.292	0.134	0.143
6.003	0.0000	0.0000	0.660	0.395	0.238	0.294	0.134	0.141
6.000	0.0253	0.0000	0.660	0.395	0.239	0.294	0.134	0.141
6.001	0.0488	0.0000	0.660	0.395	0.239	0.294	0.134	0.141
6.004	0.0725	0.0000	0.660	0.395	0.242	0.294	0.134	0.141
6.009	0.0957	0.0000	0.660	0.395	0.262	0.294	0.134	0.141
7.993	0.0000	0.0000	0.660	0.395	0.239	0.296	0.135	0.142
7.995	0.0246	0.0000	0.660	0.395	0.239	0.296	0.135	0.142
7.993	0.0489	0.0000	0.660	0.395	0.239	0.296	0.136	0.142
7.996	0.0729	0.0000	0.660	0.395	0.239	0.296	0.135	0.142
7.997	0.0970	0.0000	0.660	0.395	0.257	0.296	0.136	0.142
9.997	0.0000	0.0000	0.660	0.395	0.239	0.296	0.135	0.141
10.015	0.0242	0.0000	0.660	0.395	0.239	0.296	0.135	0.141
10.011	0.0486	0.0000	0.660	0.395	0.239	0.296	0.135	0.141
10.014	0.0722	0.0000	0.660	0.395	0.239	0.296	0.135	0.141
9.995	0.0908	0.0000	0.660	0.395	0.249	0.296	0.135	0.141
10.001	0.0957	0.0000	0.660	0.395	0.253	0.296	0.135	0.141

Table 108. Sidewall and Lower Divergent Flap Internal Static Pressure Ratios $p/p_{t,j}$ for Configuration 38

[$\epsilon = 2.405$; $\delta_{r,p} = 0^\circ$; forward slot injection; $\phi_f = 0^\circ$; $\phi_r = 0^\circ$]

			$p/p_{t,j}$ for---					
			Sidewall centerline at---			Lower flap centerline at---		
			[$x - x_f$]/[$L_f - x_f$] of---			[$x - x_f$]/[$L_f - x_f$] of---		
NPR	$\omega_{s,f}$	ω_f	0.000	0.190	0.381	0.000	0.190	0.381
2.006	0.0000	0.0491	0.682	0.490	0.461	0.471	0.490	0.490
2.006	0.0000	0.0985	0.682	0.490	0.461	0.471	0.491	0.490
2.002	0.0245	0.0495	0.680	0.483	0.447	0.472	0.490	0.489
2.003	0.0244	0.0974	0.680	0.483	0.447	0.471	0.490	0.489
2.001	0.0482	0.0486	0.678	0.476	0.433	0.469	0.487	0.485
2.002	0.0481	0.0993	0.678	0.476	0.433	0.469	0.487	0.485
2.006	0.0739	0.0482	0.684	0.490	0.455	0.420	0.448	0.449
2.005	0.0737	0.1000	0.683	0.489	0.454	0.414	0.444	0.448
2.006	0.0979	0.0500	0.682	0.485	0.439	0.330	0.355	0.407
2.006	0.0975	0.0984	0.682	0.485	0.440	0.336	0.363	0.404
3.995	0.0000	0.0493	0.660	0.395	0.238	0.292	0.133	0.141
3.997	0.0000	0.0970	0.660	0.395	0.238	0.292	0.133	0.141
3.997	0.0243	0.0481	0.660	0.395	0.238	0.292	0.133	0.141
3.998	0.0240	0.0969	0.660	0.395	0.238	0.292	0.133	0.141
3.998	0.0478	0.0483	0.660	0.395	0.240	0.292	0.133	0.141
3.999	0.0473	0.0961	0.660	0.395	0.240	0.292	0.133	0.141
3.999	0.0704	0.0492	0.660	0.395	0.266	0.292	0.133	0.142
3.999	0.0712	0.0964	0.660	0.395	0.267	0.292	0.133	0.142
3.999	0.0942	0.0481	0.660	0.397	0.283	0.292	0.133	0.143
3.999	0.0945	0.0963	0.660	0.397	0.284	0.292	0.133	0.143
5.995	0.0000	0.0474	0.660	0.395	0.238	0.294	0.134	0.141
5.996	0.0000	0.0960	0.660	0.395	0.238	0.294	0.134	0.141
5.994	0.0231	0.0476	0.660	0.395	0.238	0.294	0.134	0.141
5.996	0.0227	0.0956	0.660	0.395	0.238	0.294	0.134	0.141
5.994	0.0484	0.0488	0.660	0.395	0.239	0.294	0.134	0.141
5.994	0.0476	0.0951	0.660	0.395	0.239	0.294	0.134	0.141
5.996	0.0696	0.0479	0.660	0.395	0.240	0.294	0.134	0.141
5.998	0.0714	0.0954	0.660	0.395	0.241	0.294	0.134	0.141
5.997	0.0929	0.0486	0.660	0.395	0.258	0.294	0.134	0.141
5.998	0.0928	0.0944	0.660	0.395	0.257	0.294	0.134	0.141
8.002	0.0000	0.0481	0.660	0.395	0.239	0.296	0.136	0.142
8.006	0.0000	0.0950	0.660	0.395	0.238	0.296	0.136	0.142
8.003	0.0237	0.0484	0.660	0.395	0.239	0.296	0.136	0.142
8.003	0.0231	0.0953	0.660	0.395	0.239	0.296	0.136	0.142
8.000	0.0478	0.0479	0.660	0.395	0.239	0.296	0.136	0.142
7.999	0.0463	0.0955	0.660	0.395	0.238	0.296	0.136	0.142
7.998	0.0709	0.0476	0.660	0.395	0.239	0.296	0.136	0.142
7.998	0.0704	0.0927	0.660	0.395	0.239	0.296	0.136	0.142
7.997	0.0946	0.0469	0.660	0.395	0.256	0.296	0.136	0.142
7.998	0.0937	0.0606	0.660	0.395	0.255	0.296	0.136	0.142
9.999	0.0000	0.0475	0.660	0.395	0.239	0.296	0.135	0.141
9.999	0.0000	0.0949	0.659	0.395	0.238	0.296	0.135	0.141
9.991	0.0240	0.0469	0.660	0.395	0.239	0.296	0.135	0.141
10.001	0.0232	0.0941	0.659	0.395	0.239	0.296	0.135	0.141
10.006	0.0472	0.0926	0.659	0.395	0.239	0.296	0.135	0.141
10.010	0.0705	0.0473	0.659	0.395	0.239	0.296	0.135	0.141
9.923	0.0710	0.0611	0.660	0.395	0.239	0.296	0.135	0.141
10.007	0.0885	0.0466	0.660	0.395	0.246	0.296	0.135	0.141

Table 113. Sidewall and Lower Divergent Flap Internal Static Pressure Ratios $p/p_{t,j}$ for Configuration 43[$\epsilon = 1.952$; $\delta_{v,p} = 7.75^\circ$; forward slot injection; $\phi_l = 0^\circ$; $\phi_r = 0^\circ$]

			$p/p_{t,j}$ for---					
			Sidewall centerline at---			Lower flap centerline at---		
			[$x - x_l$]/[$L_f - x_l$] of---			[$x - x_l$]/[$L_f - x_l$] of---		
NPR	ω_{st}	ω_r	0.000	0.190	0.381	0.000	0.190	0.381
1.999	0.0000	0.0522	0.671	0.445	0.367	0.477	0.495	0.495
2.007	0.0000	0.1034	0.670	0.444	0.365	0.475	0.493	0.493
2.009	0.0261	0.1029	0.670	0.436	0.388	0.474	0.492	0.492
2.010	0.0252	0.0517	0.670	0.436	0.372	0.474	0.492	0.492
2.013	0.0511	0.0513	0.671	0.456	0.531	0.472	0.490	0.489
2.013	0.0511	0.1013	0.671	0.456	0.530	0.472	0.490	0.489
2.001	0.0756	0.0517	0.670	0.456	0.510	0.299	0.303	0.308
2.000	0.0746	0.1024	0.669	0.455	0.508	0.299	0.304	0.309
2.016	0.1008	0.0498	0.681	0.508	0.561	0.304	0.314	0.335
2.014	0.0991	0.1019	0.681	0.502	0.558	0.304	0.312	0.332
4.001	0.0000	0.0507	0.660	0.390	0.251	0.291	0.136	0.145
4.002	0.0000	0.0993	0.660	0.389	0.250	0.291	0.136	0.145
3.996	0.0250	0.0502	0.660	0.388	0.249	0.291	0.136	0.145
4.005	0.0242	0.0973	0.660	0.388	0.249	0.291	0.136	0.145
3.996	0.0480	0.0501	0.660	0.390	0.251	0.291	0.136	0.145
4.009	0.0487	0.0978	0.659	0.389	0.249	0.291	0.136	0.145
4.011	0.0722	0.0481	0.660	0.392	0.306	0.291	0.136	0.145
4.010	0.0722	0.0985	0.659	0.390	0.324	0.291	0.136	0.145
4.007	0.0964	0.0495	0.660	0.419	0.426	0.292	0.139	0.155
4.002	0.0967	0.0978	0.661	0.424	0.431	0.292	0.139	0.156
6.001	0.0000	0.0488	0.661	0.389	0.250	0.294	0.137	0.146
6.005	0.0000	0.0976	0.660	0.389	0.249	0.295	0.137	0.146
6.001	0.0244	0.0488	0.660	0.389	0.248	0.294	0.137	0.146
6.002	0.0238	0.0975	0.660	0.390	0.251	0.294	0.137	0.146
6.001	0.0474	0.0495	0.661	0.390	0.251	0.294	0.137	0.146
6.001	0.0478	0.0969	0.659	0.388	0.248	0.294	0.137	0.146
6.001	0.0712	0.0481	0.659	0.389	0.268	0.294	0.137	0.146
6.004	0.0718	0.0969	0.660	0.390	0.269	0.295	0.137	0.146
6.003	0.0949	0.0493	0.660	0.390	0.407	0.294	0.137	0.146
6.002	0.0948	0.0959	0.660	0.390	0.407	0.294	0.137	0.146
8.015	0.0000	0.0485	0.660	0.388	0.249	0.295	0.137	0.146
8.007	0.0000	0.0953	0.659	0.390	0.249	0.295	0.137	0.146
8.005	0.0235	0.0480	0.656	0.388	0.251	0.295	0.137	0.146
8.003	0.0235	0.0950	0.656	0.389	0.247	0.295	0.137	0.146
8.003	0.0469	0.0487	0.656	0.394	0.252	0.295	0.137	0.146
8.007	0.0473	0.0956	0.656	0.394	0.251	0.295	0.137	0.146
8.007	0.0708	0.0488	0.656	0.394	0.340	0.295	0.137	0.146
8.009	0.0711	0.0955	0.656	0.394	0.331	0.295	0.137	0.146
8.012	0.0942	0.0477	0.656	0.421	0.381	0.296	0.138	0.154
8.015	0.0936	0.0952	0.656	0.419	0.383	0.296	0.138	0.153
9.999	0.0000	0.0485	0.656	0.393	0.249	0.295	0.137	0.145
10.000	0.0000	0.0951	0.655	0.394	0.248	0.295	0.137	0.145
10.003	0.0241	0.0472	0.656	0.392	0.250	0.295	0.137	0.145
10.006	0.0236	0.0950	0.656	0.394	0.250	0.295	0.137	0.145
10.000	0.0475	0.0479	0.655	0.394	0.247	0.295	0.137	0.145
10.002	0.0472	0.0947	0.656	0.395	0.250	0.295	0.137	0.145
10.009	0.0703	0.0483	0.656	0.396	0.331	0.295	0.137	0.146
10.006	0.0690	0.0954	0.656	0.397	0.331	0.295	0.137	0.146
10.021	0.0945	0.0484	0.658	0.430	0.376	0.296	0.141	0.157
10.018	0.0937	0.0944	0.658	0.429	0.371	0.296	0.141	0.157

Table 114. Sidewall and Lower Divergent Flap Internal Static Pressure Ratios $p/p_{t,j}$ for Configuration 44

[$\epsilon = 1.952$; $\delta_{v,p} = 7.75^\circ$; aft slot injection; $\phi_j = 0^\circ$; $\phi_r = 0^\circ$]

$p/p_{t,j}$ for---

NPR	ω_{st}	ω_c	Sidewall centerline at---			Lower flap centerline at---		
			[$x - x_i$]/[$L_f - x_i$] of---			[$x - x_i$]/[$L_f - x_i$] of---		
			0.000	0.190	0.381	0.000	0.190	0.381
2.007	0.0000	0.0510	0.668	0.442	0.361	0.475	0.493	0.493
2.007	0.0000	0.1027	0.668	0.442	0.360	0.475	0.493	0.493
2.007	0.0256	0.0494	0.667	0.441	0.360	0.475	0.492	0.493
2.007	0.0252	0.1012	0.667	0.441	0.359	0.475	0.492	0.493
2.007	0.0511	0.0524	0.667	0.445	0.554	0.473	0.490	0.491
2.006	0.0506	0.1028	0.667	0.444	0.554	0.473	0.490	0.491
2.010	0.0755	0.0506	0.669	0.474	0.548	0.443	0.453	0.448
2.010	0.0744	0.1020	0.669	0.474	0.548	0.445	0.455	0.451
2.007	0.0991	0.0513	0.662	0.446	0.480	0.297	0.321	0.353
2.007	0.1004	0.1003	0.662	0.444	0.478	0.296	0.316	0.349
4.013	0.0000	0.0512	0.656	0.387	0.244	0.292	0.136	0.144
4.008	0.0000	0.0992	0.656	0.387	0.243	0.293	0.136	0.145
3.994	0.0244	0.0483	0.655	0.388	0.242	0.292	0.136	0.144
4.013	0.0249	0.0971	0.656	0.388	0.242	0.293	0.136	0.144
3.997	0.0488	0.0505	0.655	0.387	0.242	0.293	0.136	0.145
4.011	0.0491	0.0959	0.655	0.388	0.242	0.292	0.136	0.144
4.010	0.0720	0.0491	0.655	0.388	0.242	0.292	0.136	0.145
4.011	0.0717	0.0973	0.655	0.388	0.241	0.293	0.136	0.145
4.010	0.0976	0.0504	0.655	0.388	0.240	0.292	0.136	0.144
4.010	0.0963	0.0954	0.655	0.388	0.240	0.292	0.136	0.145
5.998	0.0000	0.0477	0.655	0.387	0.239	0.294	0.137	0.146
5.993	0.0000	0.0986	0.655	0.387	0.239	0.294	0.137	0.146
5.991	0.0245	0.0479	0.655	0.386	0.239	0.294	0.136	0.145
5.990	0.0240	0.0975	0.655	0.387	0.239	0.294	0.137	0.145
5.989	0.0486	0.0474	0.655	0.386	0.239	0.294	0.137	0.145
5.989	0.0472	0.0958	0.655	0.386	0.240	0.294	0.137	0.145
5.989	0.0718	0.0499	0.655	0.386	0.240	0.294	0.137	0.145
5.990	0.0717	0.0960	0.655	0.386	0.240	0.294	0.137	0.145
5.989	0.0953	0.0468	0.655	0.386	0.240	0.294	0.137	0.145
5.990	0.0944	0.0957	0.655	0.387	0.240	0.294	0.137	0.145
7.999	0.0000	0.0486	0.655	0.386	0.239	0.296	0.137	0.145
7.997	0.0000	0.0951	0.655	0.385	0.240	0.296	0.137	0.145
7.998	0.0239	0.0481	0.655	0.387	0.240	0.295	0.137	0.145
7.999	0.0230	0.0942	0.655	0.386	0.240	0.296	0.137	0.145
8.003	0.0469	0.0475	0.655	0.386	0.241	0.296	0.137	0.145
8.004	0.0484	0.0948	0.655	0.386	0.241	0.296	0.137	0.145
8.005	0.0701	0.0479	0.655	0.386	0.241	0.296	0.137	0.145
8.012	0.0693	0.0950	0.655	0.386	0.241	0.296	0.137	0.145
8.014	0.0921	0.0473	0.655	0.386	0.241	0.295	0.137	0.145
8.010	0.0945	0.0948	0.655	0.385	0.241	0.296	0.137	0.145
10.000	0.0000	0.0479	0.655	0.386	0.240	0.296	0.137	0.145
10.000	0.0000	0.0949	0.655	0.385	0.240	0.296	0.137	0.145
9.996	0.0236	0.0484	0.655	0.390	0.241	0.296	0.137	0.145
9.997	0.0234	0.0944	0.655	0.389	0.240	0.296	0.137	0.145
9.996	0.0464	0.0480	0.655	0.389	0.240	0.296	0.137	0.145
9.998	0.0466	0.0944	0.655	0.389	0.240	0.296	0.137	0.145
9.988	0.0709	0.0473	0.655	0.389	0.241	0.296	0.137	0.145
9.999	0.0707	0.0952	0.655	0.389	0.240	0.296	0.137	0.145
10.001	0.0948	0.0476	0.655	0.390	0.241	0.296	0.137	0.145
10.007	0.0947	0.0939	0.655	0.390	0.240	0.296	0.137	0.145

Table 115. Sidewall and Lower Divergent Flap Internal Static Pressure Ratios $p/p_{t,j}$ for Configuration 45

$[\varepsilon = 2.172; \delta_{v,p} = 4.00^\circ; \text{forward slot injection}; \phi_j = 0^\circ; \phi_r = 0^\circ]$

NPR	$\omega_{i,}$ ω_c		$p/p_{t,j}$ for---					
			Sidewall centerline at---			Lower flap centerline at---		
			[$x - x_j$]/[$L_j - x_j$] of---			[$x - x_j$]/[$L_j - x_j$] of---		
			0.000	0.190	0.381	0.000	0.190	0.381
1.993	0.0000	0.0511	0.669	0.440	0.355	0.479	0.496	0.497
2.015	0.0000	0.0997	0.667	0.438	0.351	0.473	0.491	0.491
2.014	0.0250	0.0523	0.668	0.451	0.406	0.472	0.490	0.491
2.013	0.0244	0.0999	0.668	0.450	0.406	0.473	0.490	0.491
2.007	0.0496	0.0509	0.663	0.445	0.413	0.464	0.482	0.482
2.012	0.0496	0.1016	0.673	0.477	0.514	0.469	0.487	0.487
2.013	0.0761	0.0505	0.674	0.493	0.526	0.428	0.439	0.434
2.012	0.0762	0.1012	0.674	0.493	0.527	0.428	0.439	0.434
2.008	0.0997	0.0509	0.669	0.458	0.477	0.300	0.303	0.306
2.007	0.0988	0.1006	0.668	0.457	0.475	0.300	0.303	0.305
3.995	0.0000	0.0521	0.656	0.389	0.241	0.293	0.136	0.145
3.997	0.0000	0.0985	0.655	0.389	0.240	0.293	0.136	0.145
3.997	0.0247	0.0498	0.656	0.389	0.240	0.293	0.136	0.145
3.996	0.0241	0.0984	0.655	0.389	0.240	0.293	0.136	0.145
3.997	0.0496	0.0478	0.655	0.389	0.240	0.293	0.136	0.145
3.997	0.0484	0.0977	0.655	0.389	0.240	0.293	0.136	0.145
3.998	0.0739	0.0501	0.655	0.389	0.251	0.293	0.136	0.145
4.000	0.0720	0.0970	0.655	0.389	0.248	0.293	0.136	0.145
3.993	0.0978	0.0477	0.655	0.392	0.302	0.293	0.136	0.147
3.995	0.0971	0.0975	0.655	0.391	0.301	0.293	0.136	0.147
5.992	0.0000	0.0481	0.655	0.390	0.241	0.294	0.136	0.145
6.001	0.0000	0.0970	0.655	0.390	0.240	0.294	0.136	0.146
6.003	0.0248	0.0493	0.655	0.389	0.240	0.294	0.136	0.146
6.010	0.0247	0.0972	0.655	0.391	0.238	0.294	0.136	0.146
6.008	0.0486	0.0470	0.655	0.391	0.238	0.294	0.136	0.146
6.012	0.0480	0.0969	0.654	0.390	0.238	0.294	0.136	0.146
6.012	0.0719	0.0480	0.654	0.391	0.238	0.294	0.136	0.146
6.013	0.0718	0.0954	0.654	0.390	0.238	0.294	0.136	0.146
6.014	0.0949	0.0488	0.654	0.392	0.278	0.294	0.136	0.148
6.015	0.0956	0.0961	0.654	0.392	0.280	0.294	0.137	0.148
8.011	0.0000	0.0484	0.655	0.390	0.238	0.295	0.137	0.145
8.007	0.0000	0.0940	0.655	0.390	0.239	0.295	0.137	0.145
8.002	0.0235	0.0479	0.655	0.390	0.239	0.295	0.137	0.145
8.005	0.0231	0.0941	0.655	0.390	0.239	0.295	0.137	0.145
8.010	0.0482	0.0489	0.655	0.390	0.239	0.295	0.136	0.145
8.015	0.0473	0.0946	0.655	0.390	0.239	0.295	0.137	0.145
8.019	0.0714	0.0487	0.655	0.390	0.256	0.295	0.137	0.145
8.006	0.0708	0.0961	0.655	0.390	0.256	0.295	0.137	0.145
8.008	0.0955	0.0480	0.655	0.399	0.280	0.295	0.137	0.148
8.011	0.0938	0.0946	0.655	0.397	0.279	0.295	0.137	0.147
10.005	0.0000	0.0475	0.655	0.390	0.239	0.295	0.137	0.145
10.006	0.0000	0.0954	0.655	0.389	0.239	0.295	0.137	0.145
10.003	0.0250	0.0478	0.655	0.390	0.239	0.295	0.137	0.145
10.006	0.0241	0.0945	0.655	0.391	0.239	0.295	0.137	0.145
10.012	0.0474	0.0461	0.655	0.390	0.239	0.295	0.137	0.145
10.011	0.0478	0.0950	0.655	0.390	0.239	0.295	0.137	0.145
10.016	0.0703	0.0487	0.655	0.391	0.267	0.295	0.137	0.145
10.018	0.0707	0.0951	0.655	0.391	0.267	0.295	0.137	0.145
10.017	0.0952	0.0474	0.655	0.406	0.284	0.295	0.137	0.148
10.019	0.0946	0.0939	0.655	0.406	0.284	0.295	0.137	0.148

Table 116. Sidewall and Lower Divergent Flap Internal Static Pressure Ratios $p/p_{t,j}$ for Configuration 46

[$\epsilon = 2.172$; $\delta_{v,p} = 4.00^\circ$; aft slot injection; $\phi_f = 0^\circ$; $\phi_r = 0^\circ$]

			$p/p_{t,j}$ for---					
			Sidewall centerline at---			Lower flap centerline at---		
			[$x - x_t$]/[$L_f - x_t$] of---			[$x - x_t$]/[$L_f - x_t$] of---		
NPR	$\omega_{s,i}$	ω_c	0.000	0.190	0.381	0.000	0.190	0.381
2.012	0.0000	0.0518	0.668	0.440	0.350	0.473	0.492	0.492
2.011	0.0000	0.1010	0.668	0.440	0.350	0.474	0.492	0.492
2.011	0.0259	0.0511	0.668	0.440	0.350	0.474	0.492	0.493
2.010	0.0258	0.1015	0.668	0.440	0.350	0.474	0.492	0.493
2.012	0.0520	0.0512	0.671	0.466	0.440	0.471	0.489	0.489
2.010	0.0513	0.1028	0.672	0.465	0.439	0.472	0.490	0.490
2.013	0.0756	0.0510	0.674	0.478	0.514	0.466	0.483	0.482
2.013	0.0744	0.1012	0.674	0.478	0.512	0.466	0.484	0.482
2.014	0.0989	0.0500	0.674	0.480	0.518	0.450	0.463	0.459
2.014	0.1016	0.1002	0.674	0.480	0.518	0.447	0.460	0.456
4.005	0.0000	0.0513	0.657	0.390	0.239	0.293	0.136	0.145
4.006	0.0000	0.0995	0.657	0.389	0.238	0.293	0.136	0.145
4.005	0.0250	0.0494	0.657	0.389	0.238	0.293	0.136	0.145
4.005	0.0259	0.0983	0.657	0.389	0.238	0.293	0.136	0.145
4.004	0.0488	0.0493	0.657	0.389	0.238	0.293	0.136	0.145
4.006	0.0480	0.0991	0.657	0.389	0.238	0.293	0.136	0.145
4.007	0.0730	0.0500	0.657	0.389	0.238	0.293	0.136	0.145
4.008	0.0727	0.0982	0.656	0.389	0.239	0.293	0.136	0.145
4.008	0.0979	0.0499	0.656	0.389	0.239	0.293	0.136	0.145
4.009	0.0983	0.0980	0.657	0.389	0.239	0.293	0.136	0.145
5.986	0.0000	0.0496	0.657	0.389	0.239	0.294	0.137	0.146
5.998	0.0000	0.0980	0.656	0.388	0.239	0.294	0.137	0.146
5.997	0.0243	0.0471	0.656	0.388	0.239	0.294	0.137	0.146
5.999	0.0238	0.0974	0.656	0.388	0.239	0.294	0.137	0.146
6.001	0.0480	0.0495	0.656	0.388	0.239	0.294	0.137	0.146
6.002	0.0487	0.0971	0.656	0.388	0.239	0.294	0.137	0.146
6.002	0.0713	0.0494	0.656	0.388	0.239	0.294	0.137	0.146
6.004	0.0720	0.0960	0.656	0.388	0.239	0.294	0.137	0.146
6.006	0.0958	0.0484	0.656	0.388	0.239	0.294	0.137	0.146
6.005	0.0957	0.0968	0.656	0.389	0.239	0.294	0.137	0.146
8.005	0.0000	0.0490	0.655	0.388	0.240	0.296	0.136	0.145
8.009	0.0000	0.0957	0.656	0.388	0.239	0.296	0.136	0.145
8.010	0.0242	0.0475	0.656	0.388	0.239	0.296	0.136	0.145
8.011	0.0238	0.0964	0.655	0.388	0.239	0.296	0.136	0.145
8.013	0.0488	0.0484	0.655	0.388	0.239	0.296	0.136	0.145
8.012	0.0473	0.0955	0.655	0.388	0.239	0.296	0.136	0.145
8.010	0.0712	0.0487	0.655	0.388	0.239	0.295	0.136	0.145
8.009	0.0716	0.0954	0.655	0.388	0.239	0.295	0.136	0.145
8.002	0.0951	0.0476	0.655	0.388	0.239	0.295	0.136	0.145
8.006	0.0955	0.0948	0.655	0.388	0.239	0.296	0.136	0.145
10.005	0.0000	0.0465	0.654	0.388	0.240	0.296	0.137	0.145
10.011	0.0000	0.0948	0.654	0.388	0.240	0.296	0.137	0.145
10.015	0.0233	0.0492	0.655	0.388	0.240	0.295	0.137	0.145
10.026	0.0238	0.0945	0.655	0.388	0.239	0.296	0.137	0.145
10.018	0.0480	0.0493	0.655	0.388	0.239	0.295	0.137	0.145
10.009	0.0473	0.0956	0.655	0.388	0.239	0.296	0.137	0.145
10.009	0.0706	0.0480	0.655	0.388	0.240	0.295	0.137	0.145
10.009	0.0723	0.0953	0.655	0.388	0.239	0.296	0.137	0.145
10.013	0.0955	0.0487	0.656	0.388	0.240	0.296	0.137	0.145
10.024	0.0949	0.0947	0.655	0.387	0.238	0.296	0.137	0.145

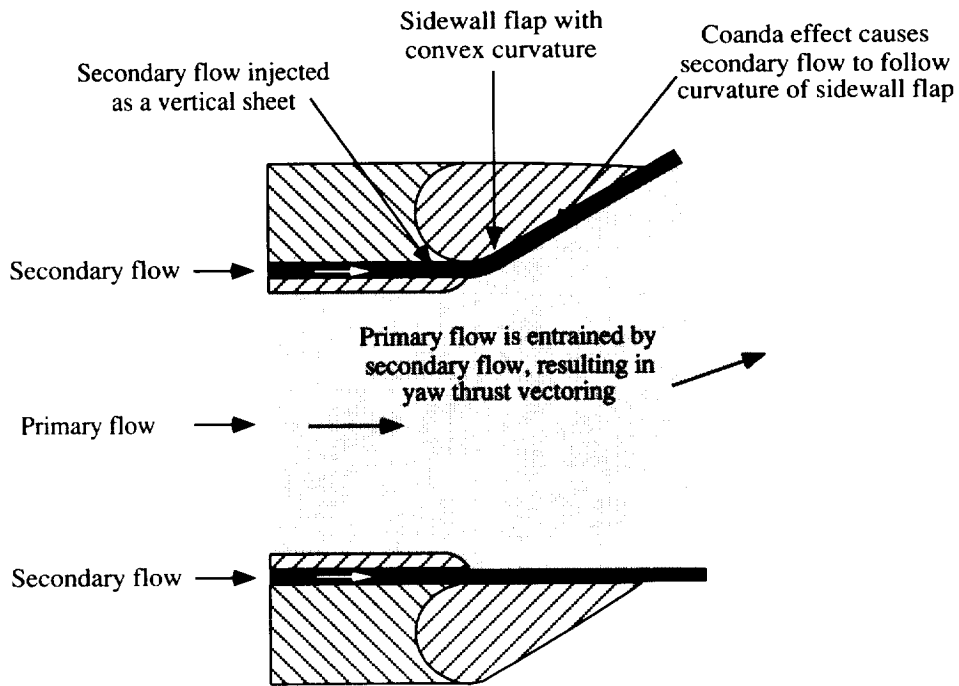


Figure 1. Top view of two-dimensional convergent-divergent nozzle using the Coanda effect to produce yaw thrust vectoring.

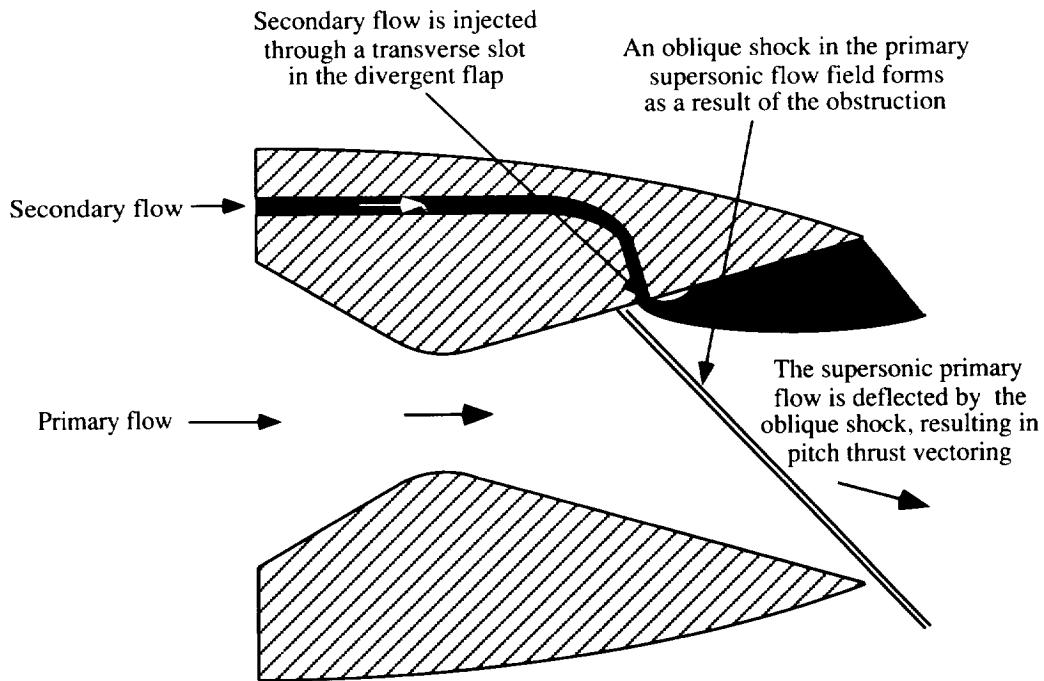
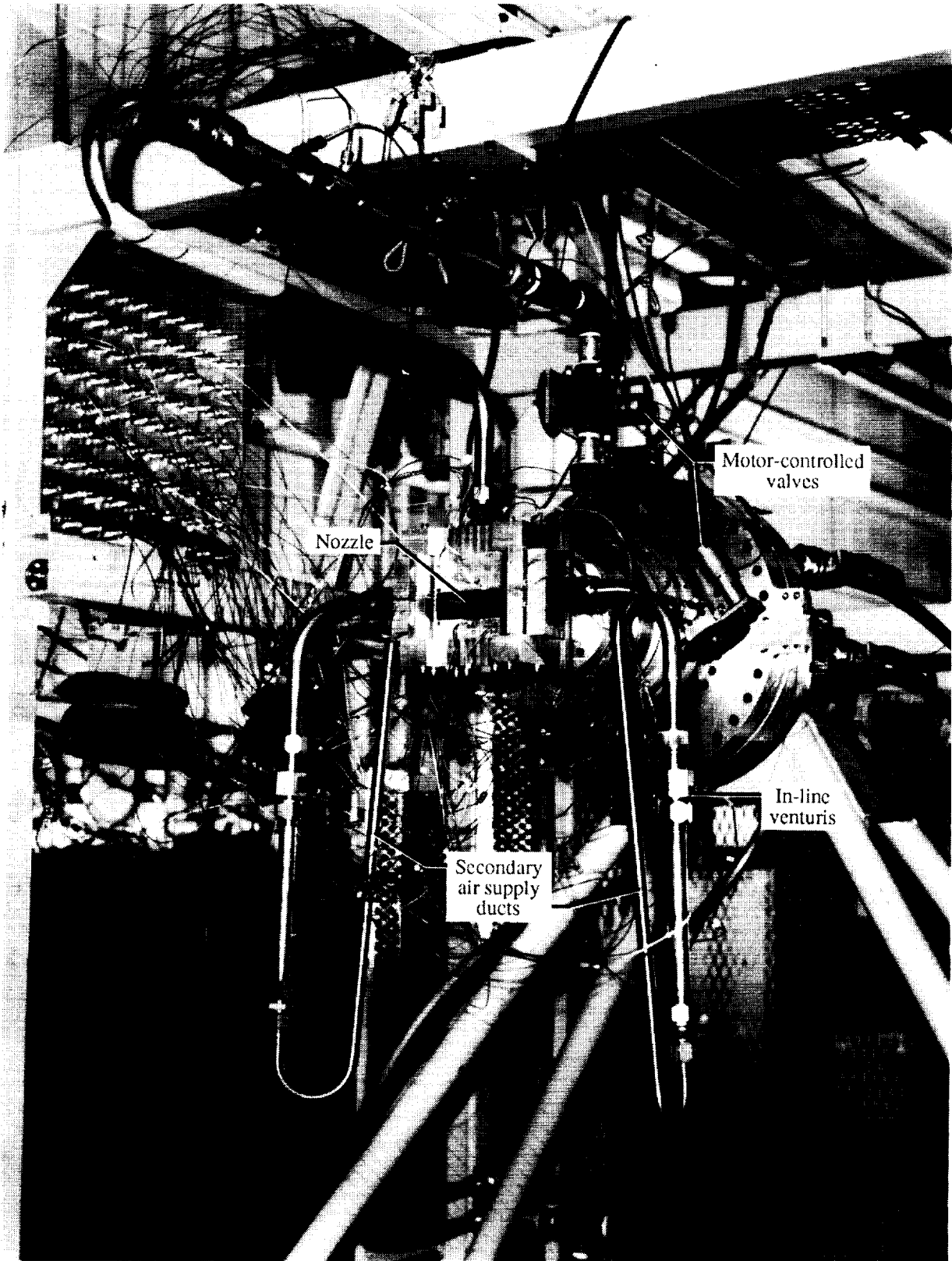


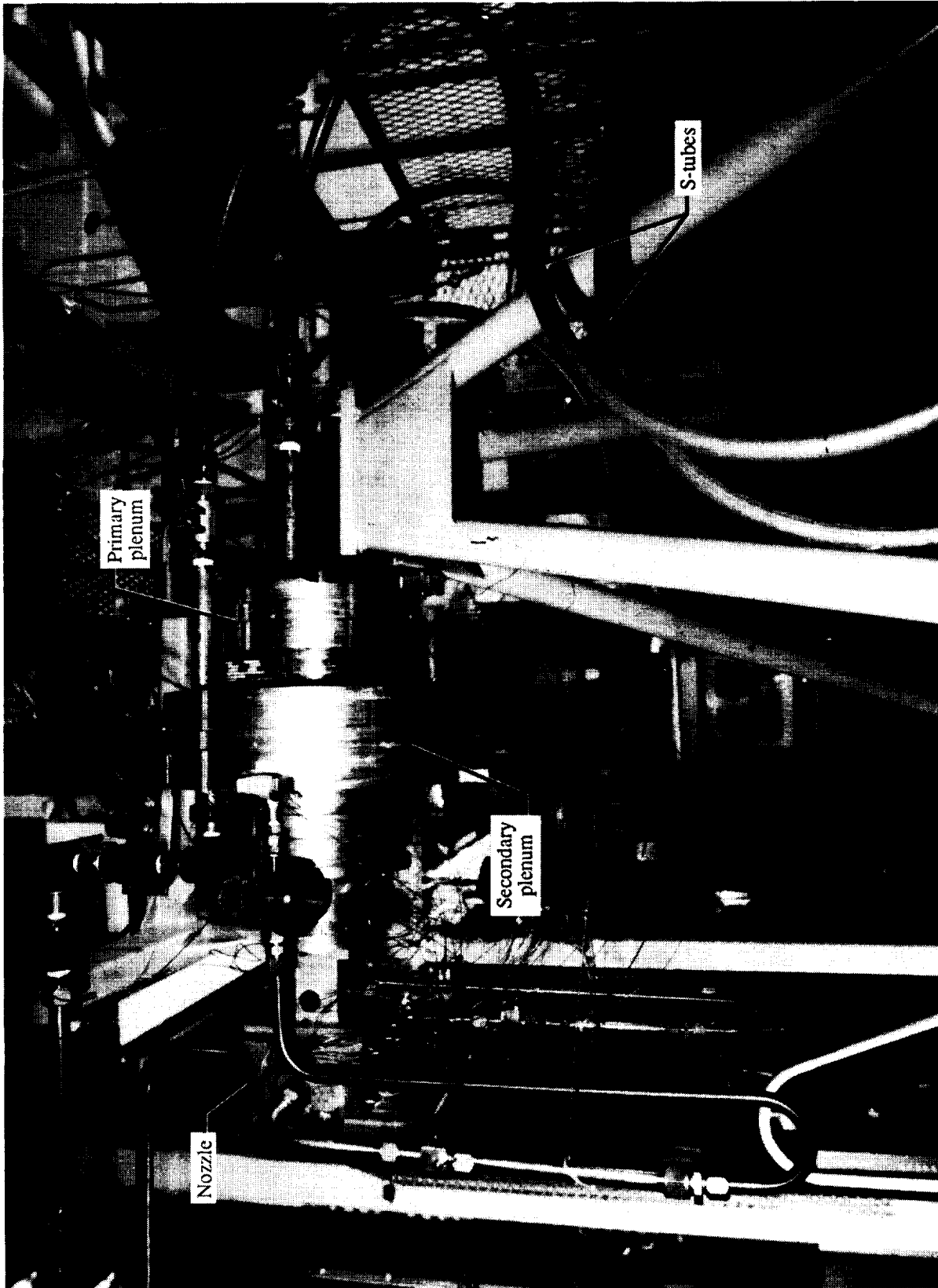
Figure 2. Side view of two-dimensional convergent-divergent nozzle using shock vector control to produce pitch thrust vectoring.



L-92-01243

(a) Quarter view showing nozzle and secondary air ducting.

Figure 3. Photographs of nozzle mounted on dual-flow static test stand.



L-92-01245

(b) Side view of dual-flow static test stand showing S-tubes and air plenums.

Figure 3. Concluded.

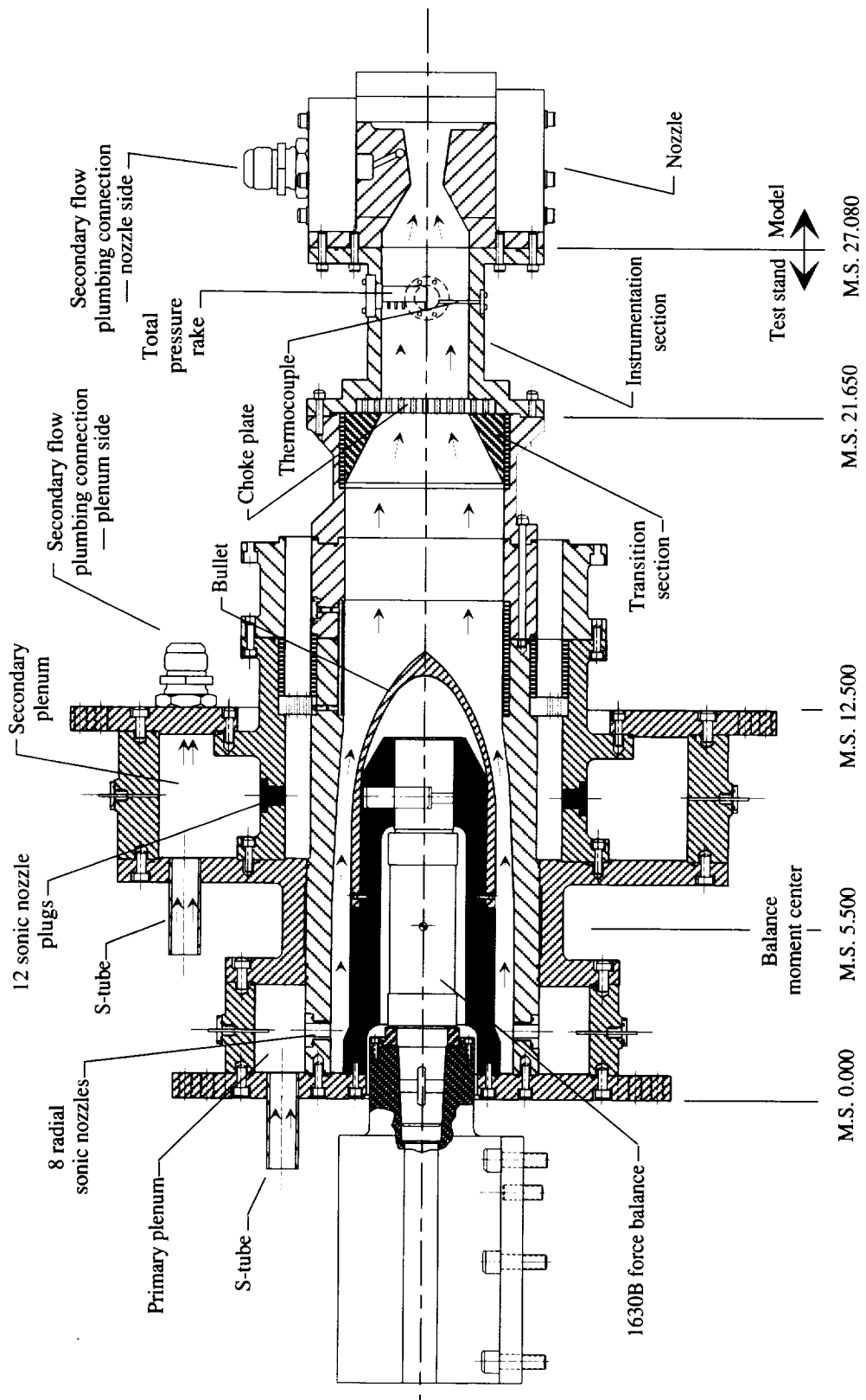
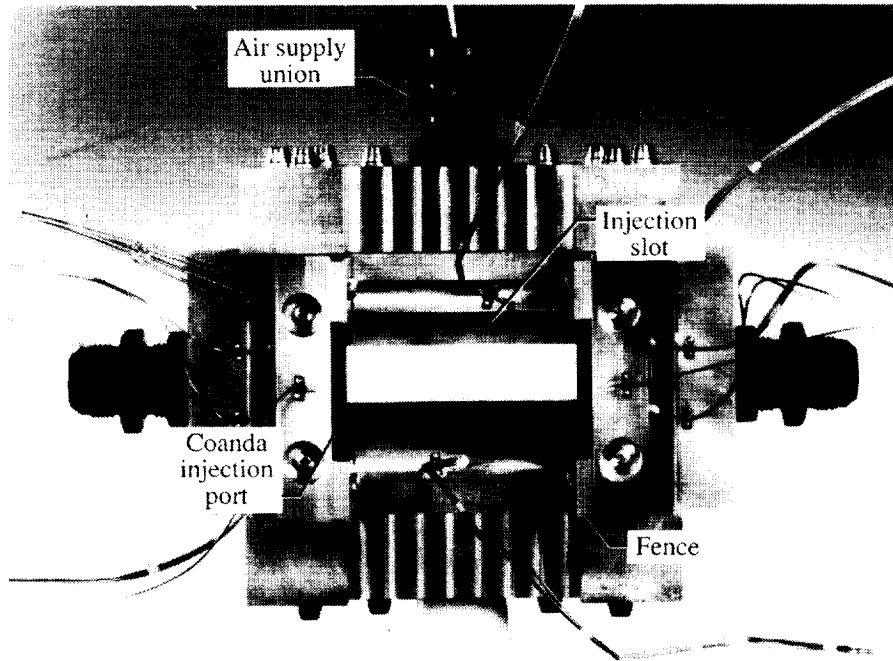
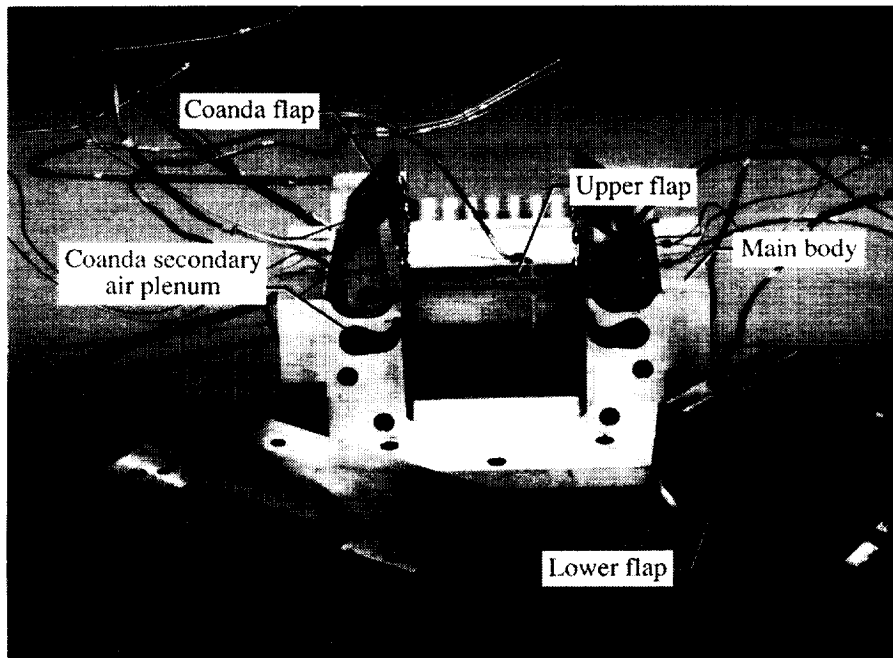


Figure 4. Sketch of dual-flow propulsion simulation system with fluidic nozzle of current investigation installed. Model stations are in inches.

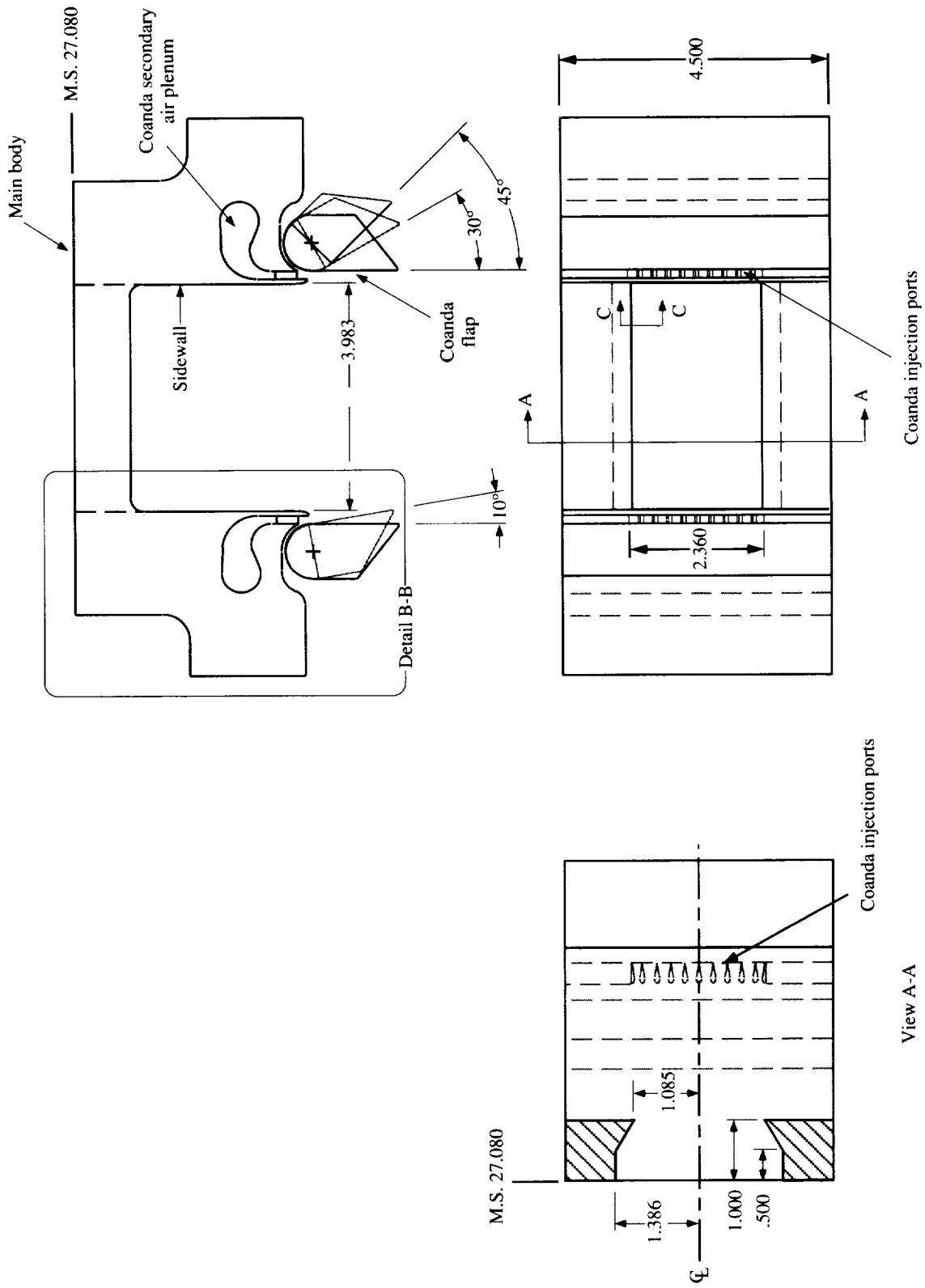


(a) Front view of model showing Coanda injection ports, injection slot, and plumbing unions.



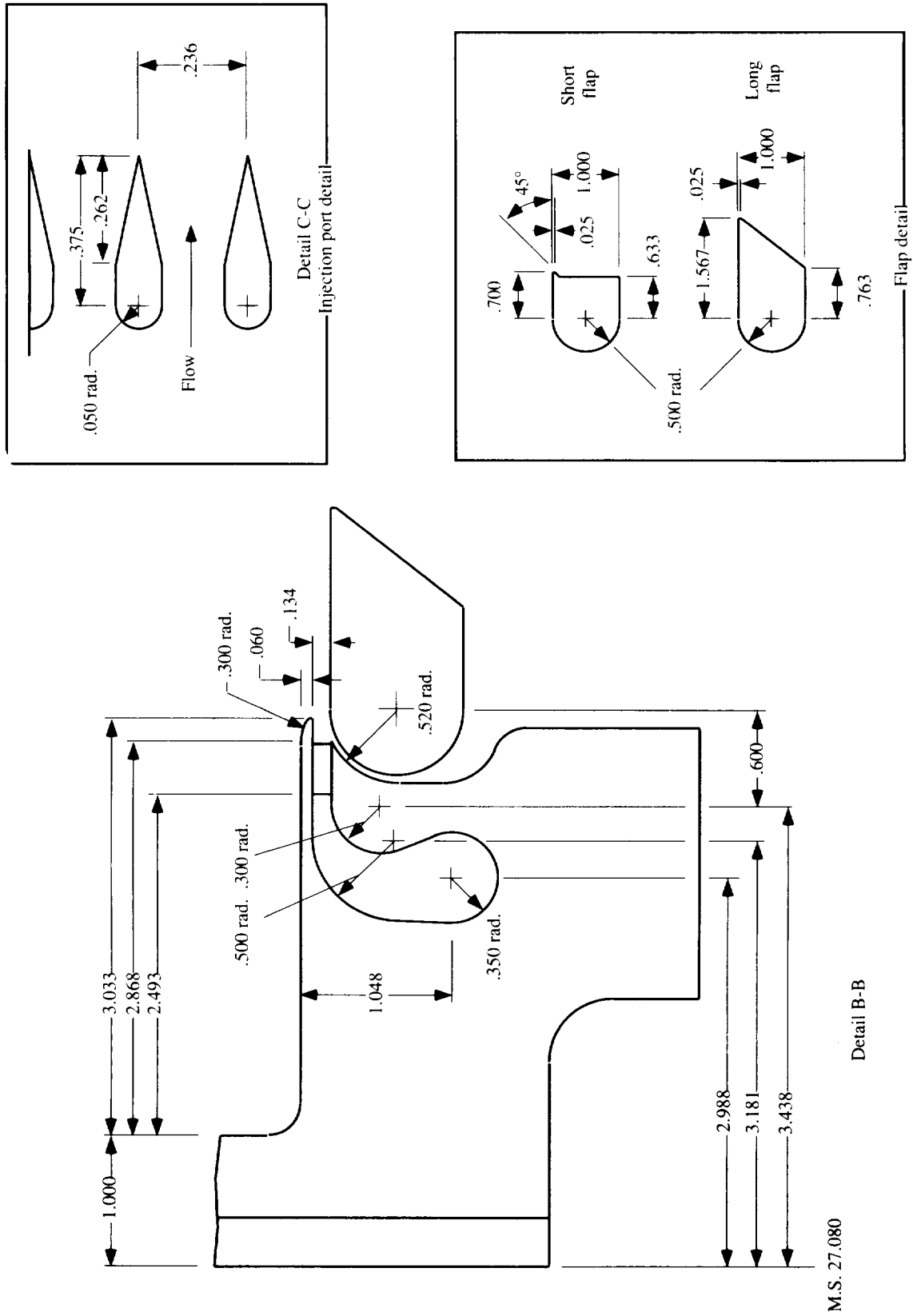
(b) Partially disassembled model showing Coanda secondary air plenums, Coanda flaps, and injection slot.

Figure 5. Photographs of fluidic vectoring nozzle showing geometric details.



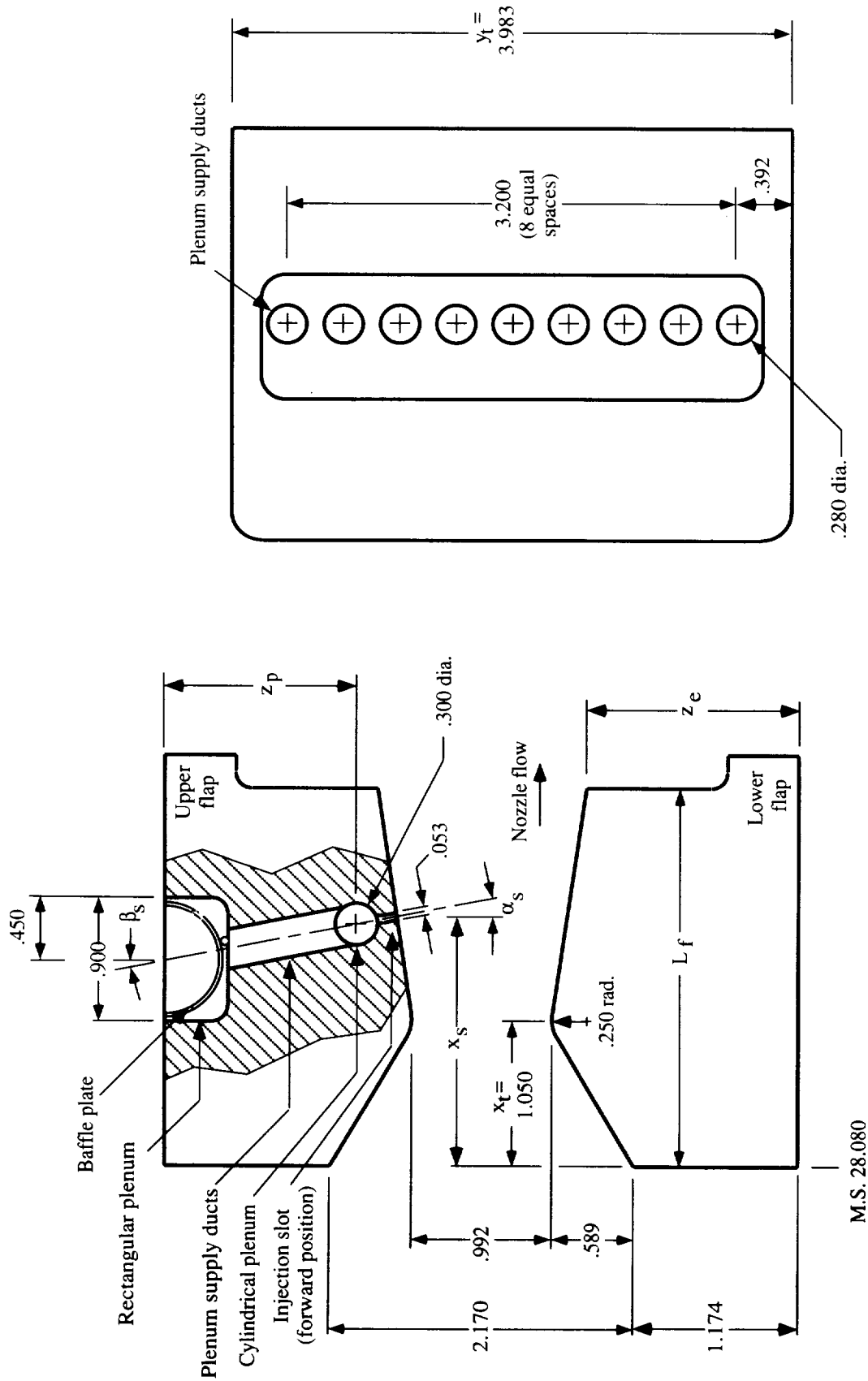
(a) Main body geometry showing Coanda injection ports and ramps. Upper and lower flaps removed.

Figure 6. Sketches of fluidic thrust-vectoring nozzle showing model geometry and pressure orifice locations. All dimensions in inches unless otherwise noted.



(b) Details of Coanda reservoir, flaps, and injection ports.

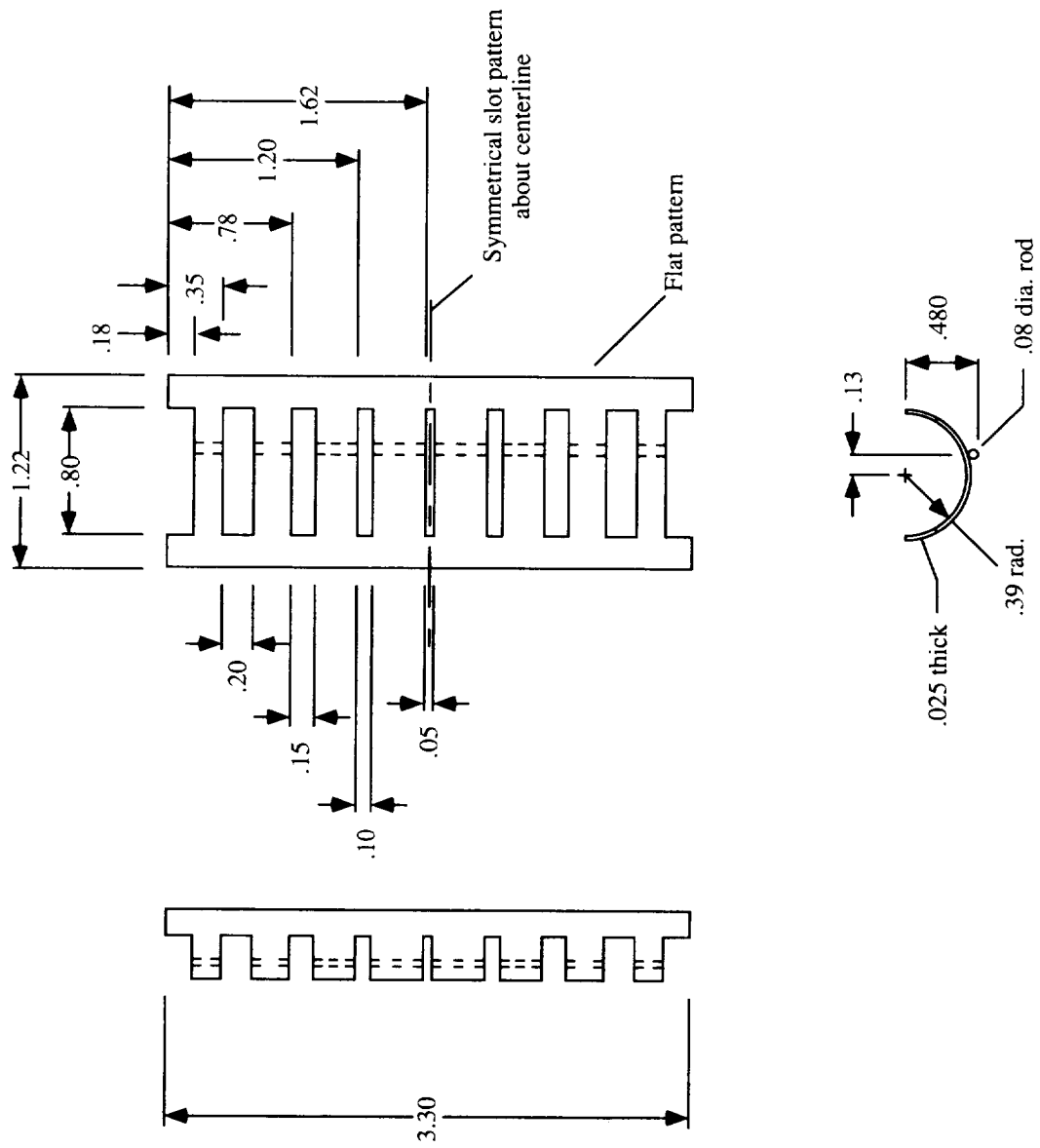
Figure 6. Continued.



Top view of upper flap

(c) Details of upper and lower flaps.

Figure 6. Continued.



(d) Rectangular plenum baffle plate.

Figure 6. Concluded.

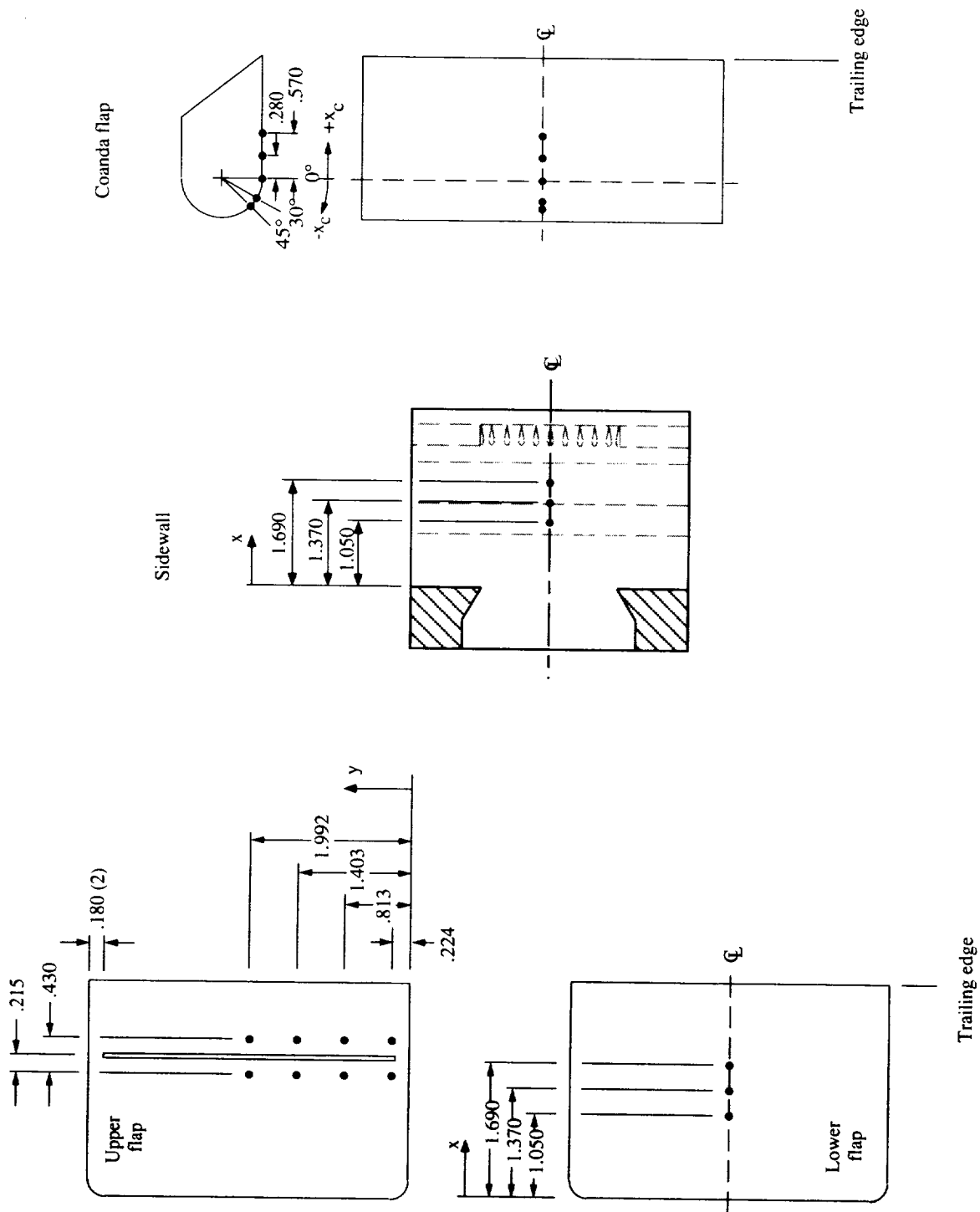


Figure 7. Sketch of upper flap, lower flap, sidewall, and Coanda flap showing locations of pressure taps. All dimensions in inches unless otherwise noted.

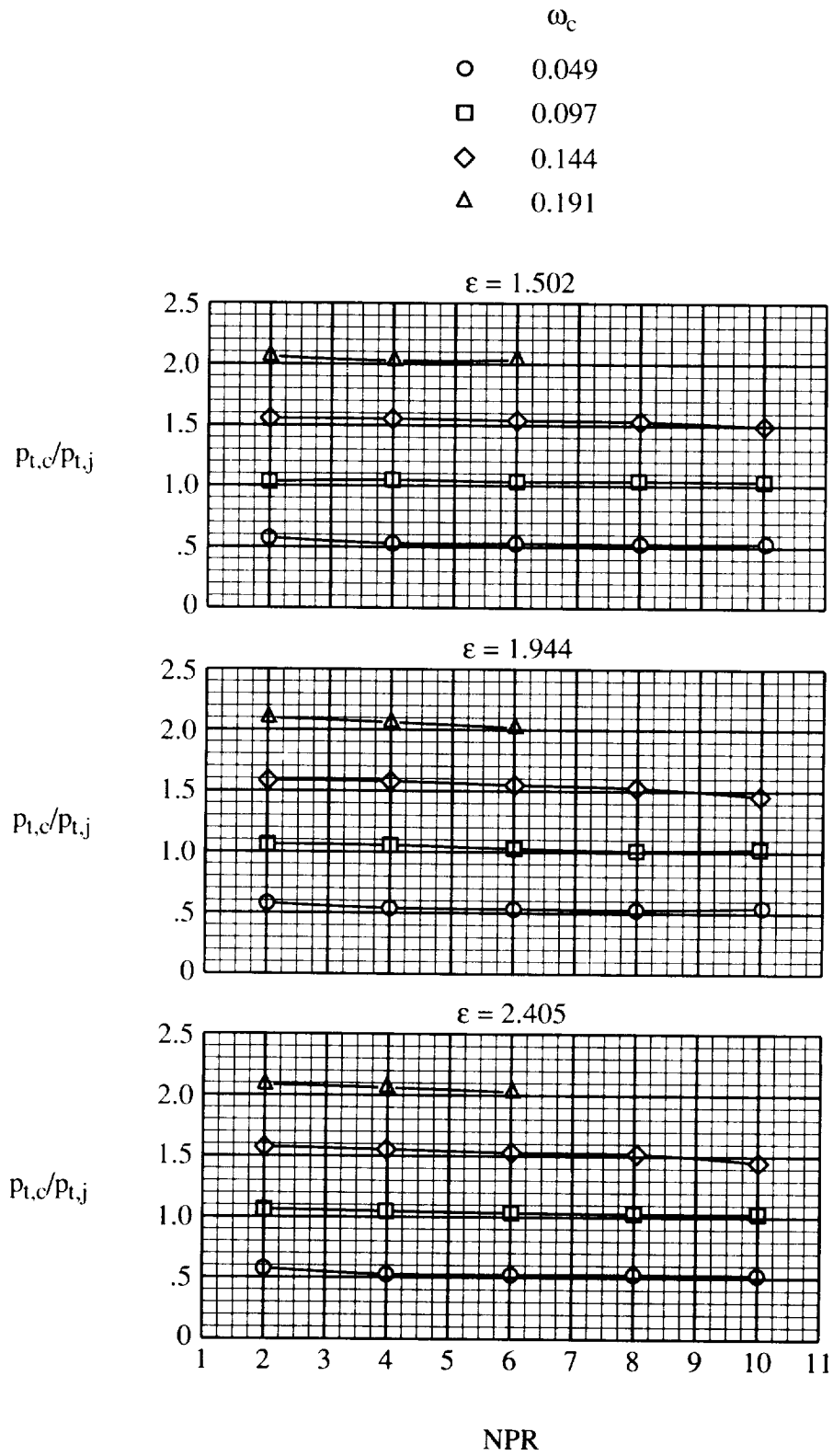
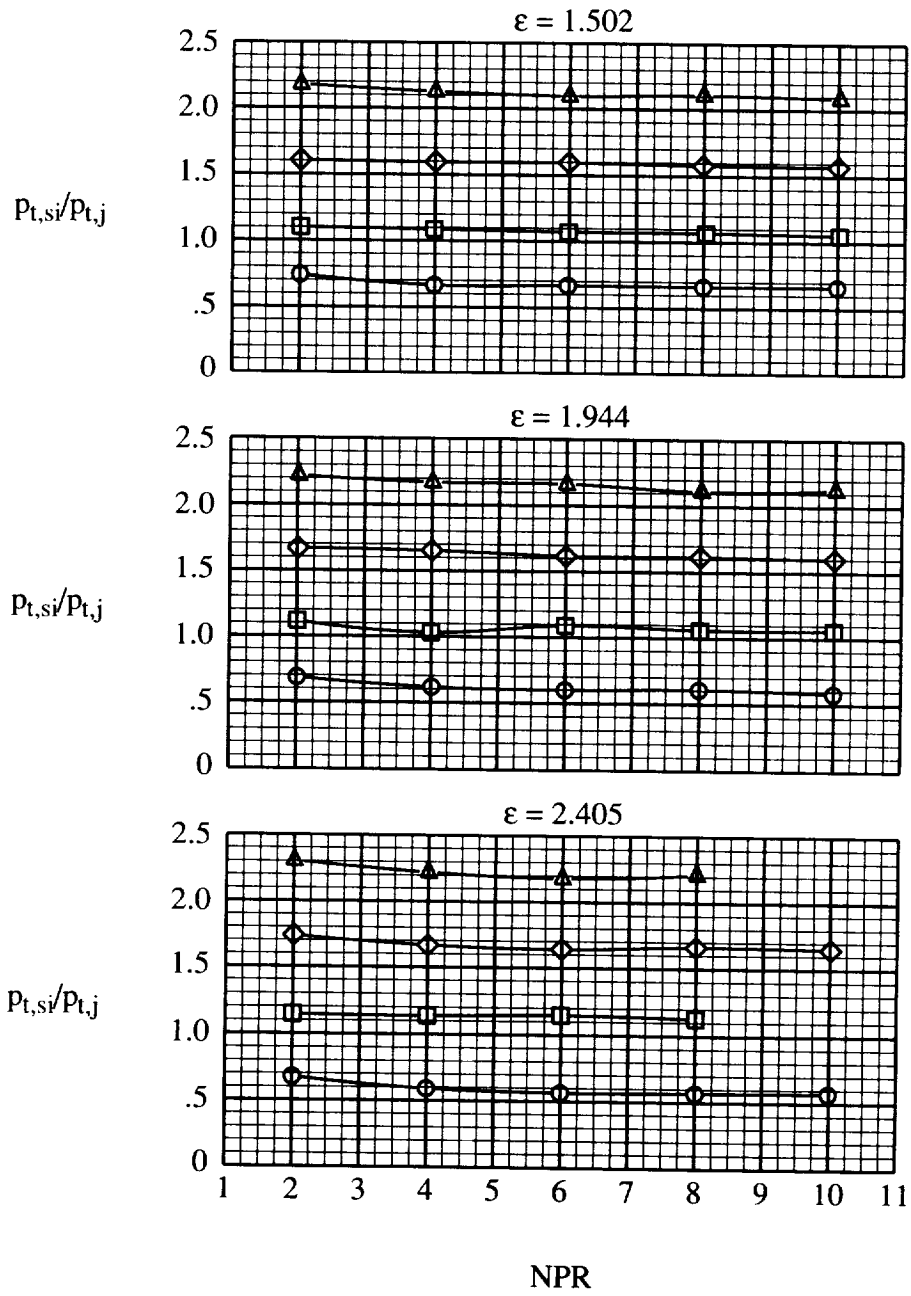


Figure 8. Supply pressure requirements for Coanda secondary flow.

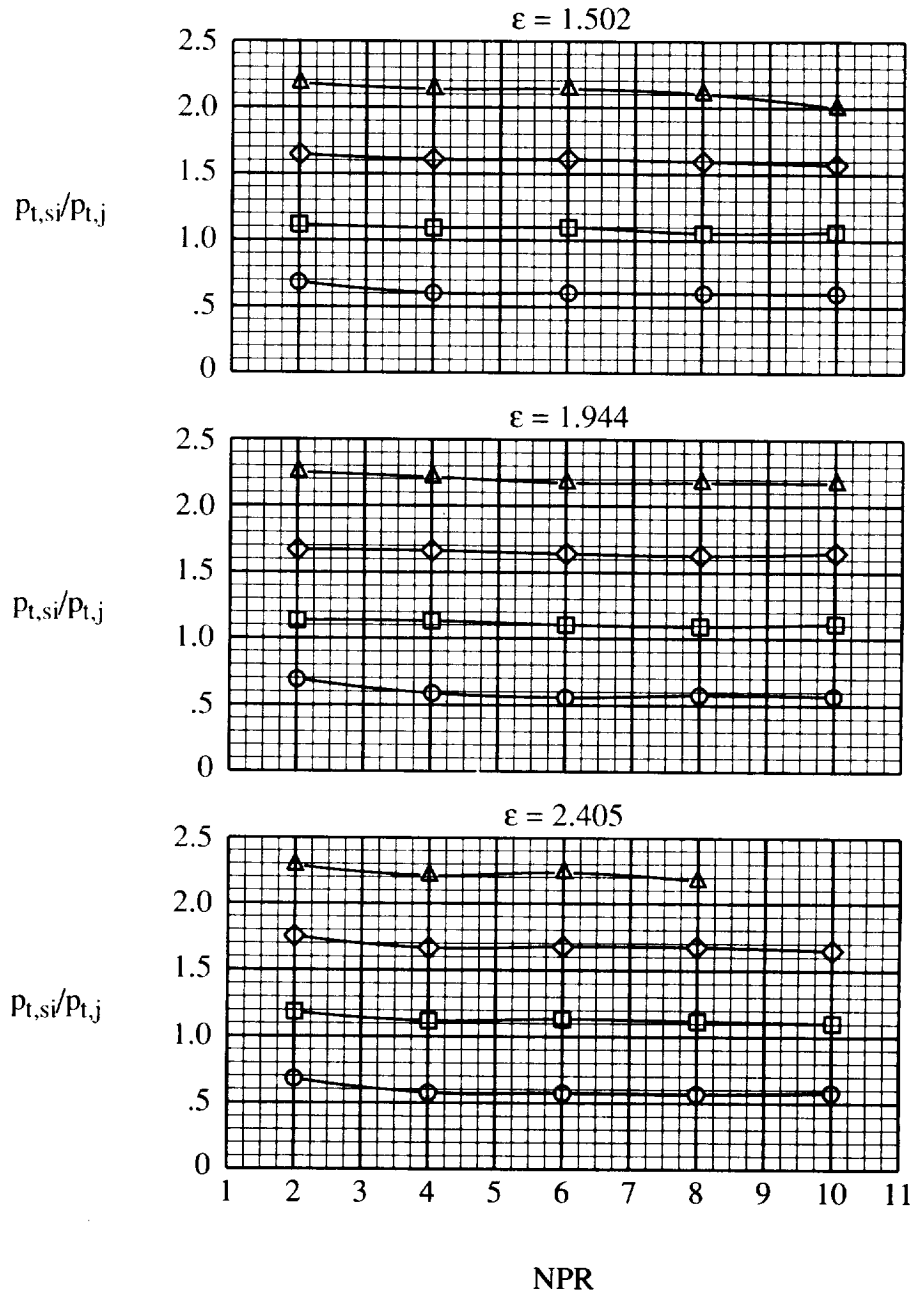
	ω_{si}
○	0.024
□	0.048
◇	0.072
△	0.097



(a) Forward slot injection.

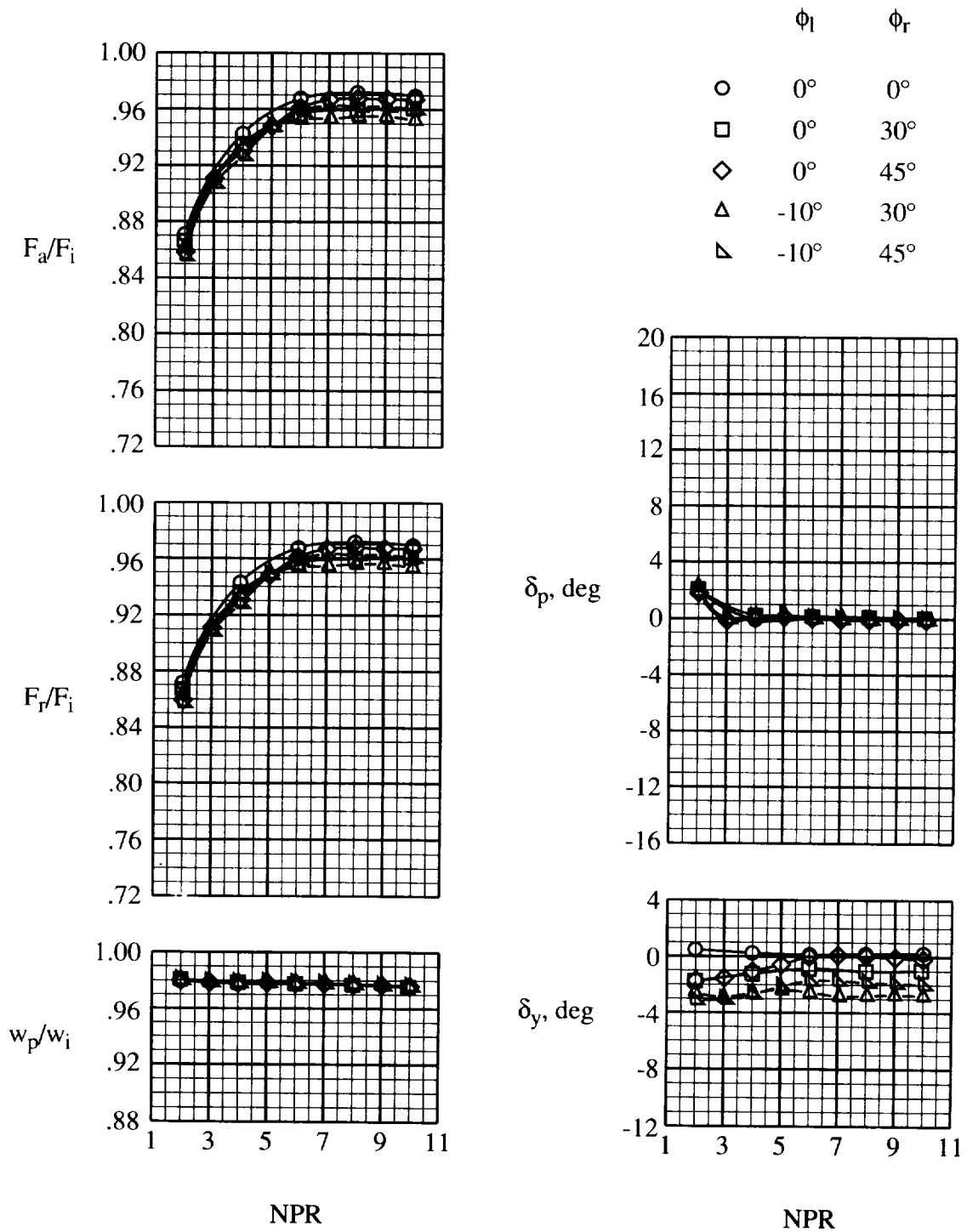
Figure 9. Supply pressure requirements for slot injection secondary flow.

- ω_{si} 0.024
- 0.048
- ◇ 0.072
- △ 0.095



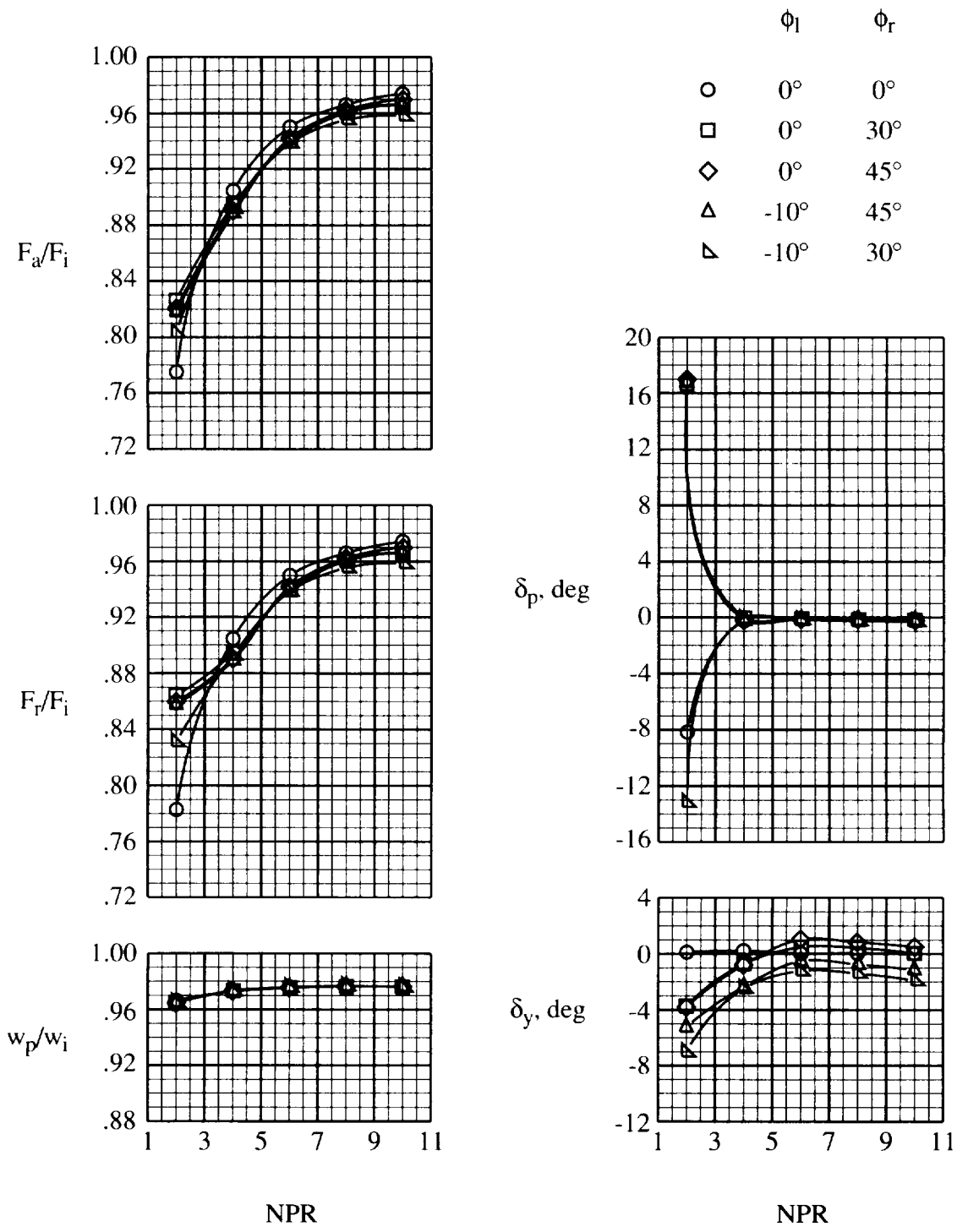
(b) Aft slot injection.

Figure 9. Concluded.



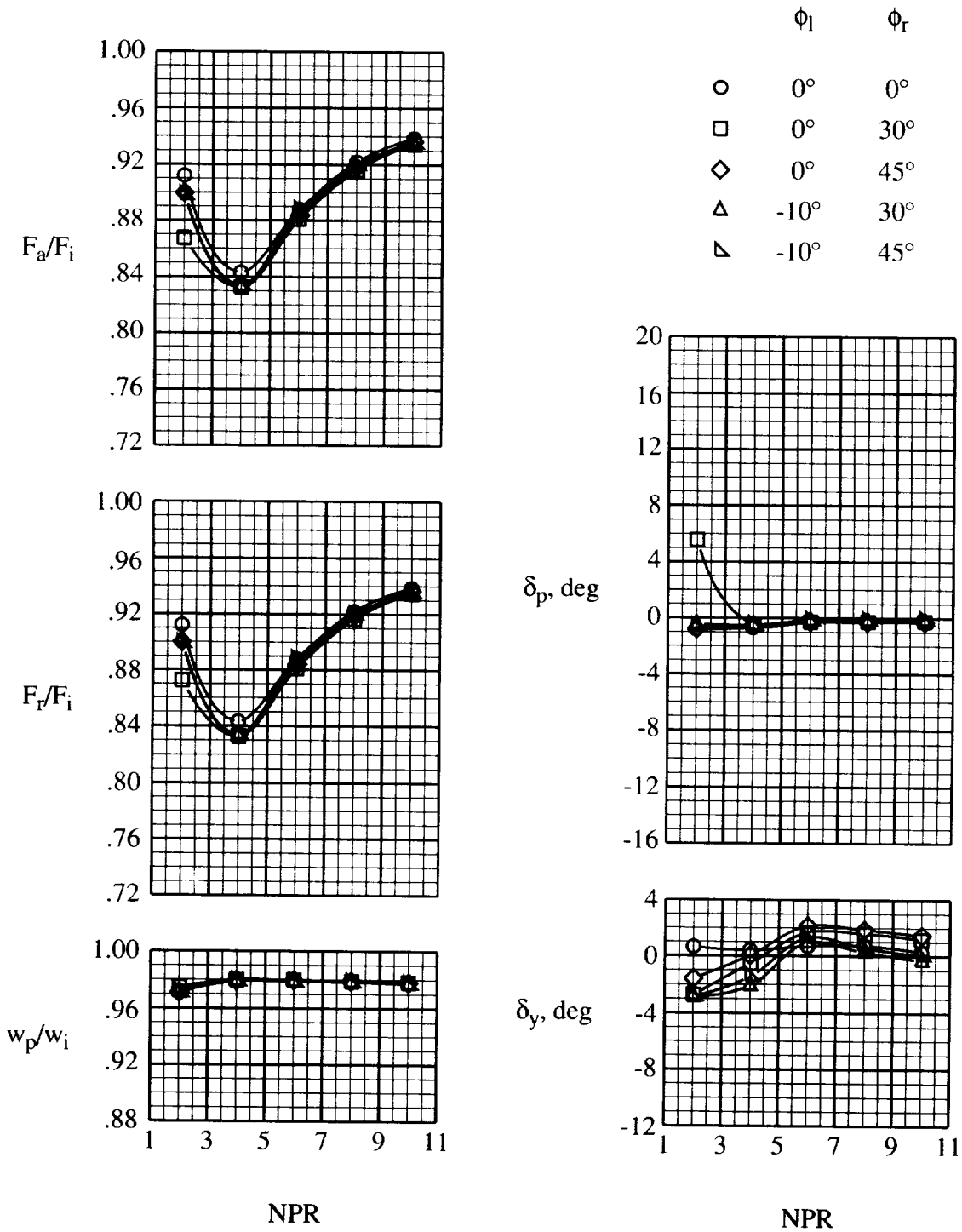
(a) $\varepsilon = 1.502$; $(NPR)_{des} = 6.26$.

Figure 10. Effect of Coanda flap angles on internal performance. Long Coanda flaps; $\omega_c = 0.10$.



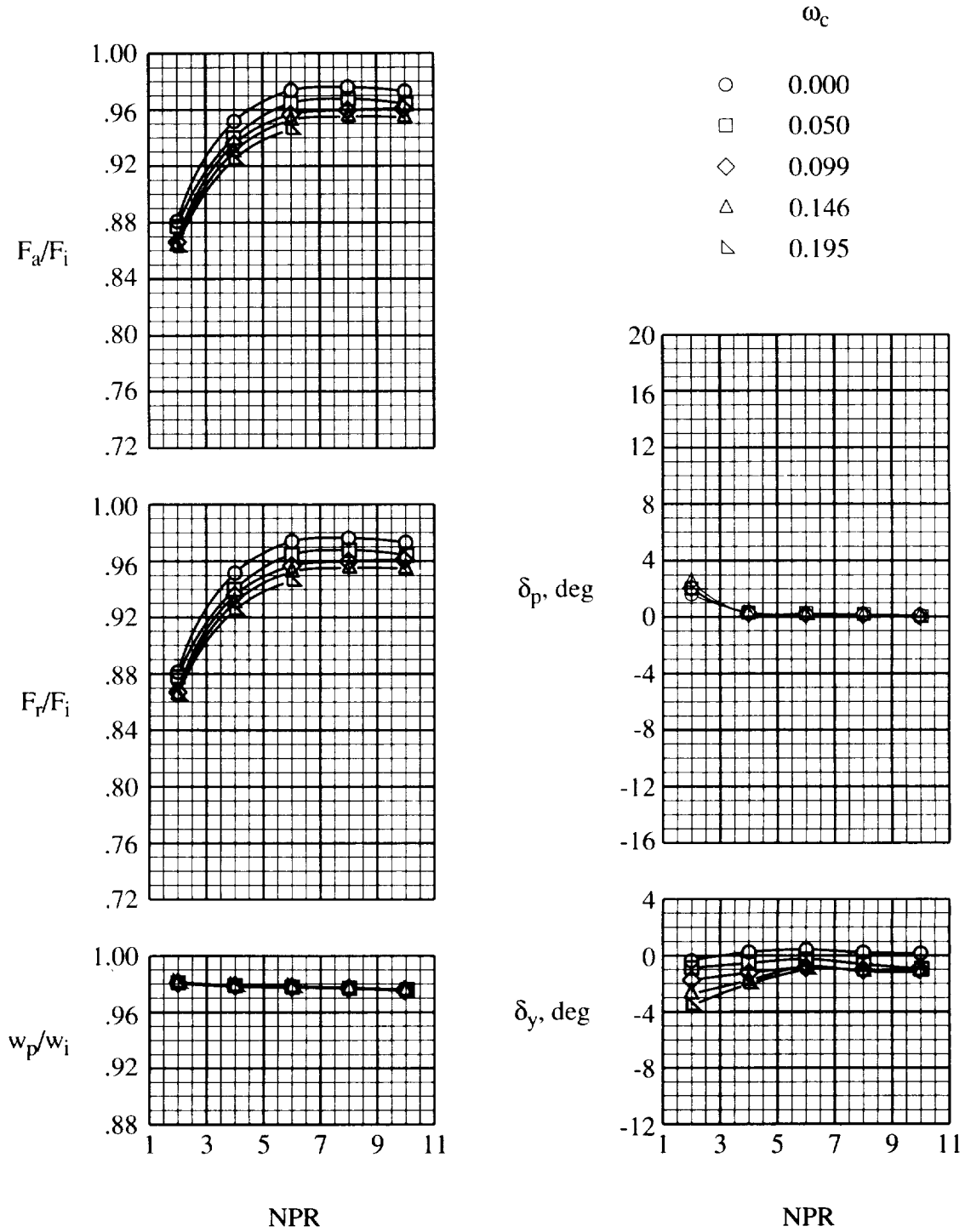
(b) $\epsilon = 1.944$; $(NPR)_{des} = 10.12$.

Figure 10. Continued.



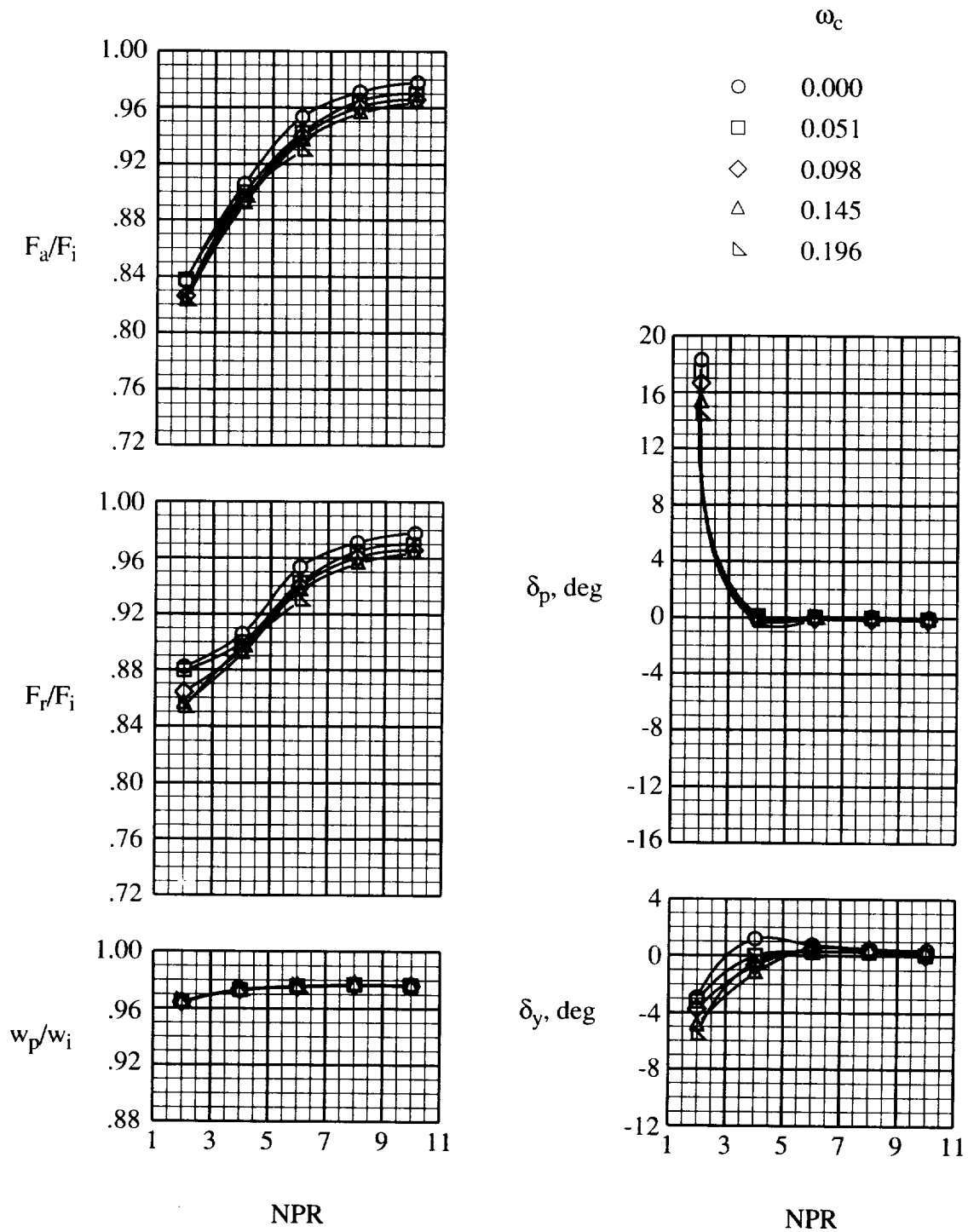
(c) $\varepsilon = 2.405$; $(NPR)_{des} = 14.64$.

Figure 10. Concluded.



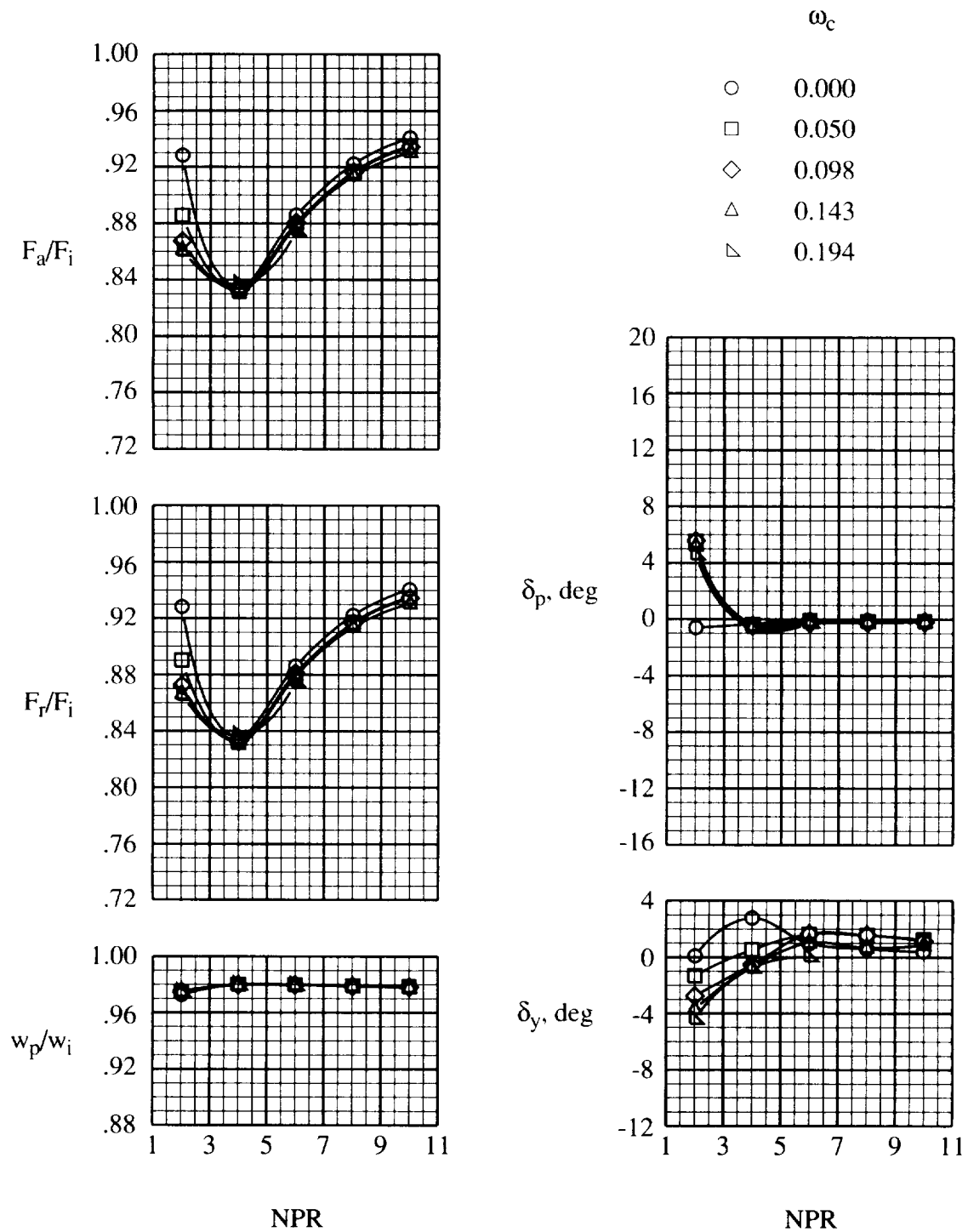
(a) $\epsilon = 1.502$; $(NPR)_{des} = 6.26$.

Figure 11. Effect of Coanda corrected weight flow ratio on internal performance. Long Coanda flaps; $\phi_l = 0^\circ$; $\phi_r = 30^\circ$



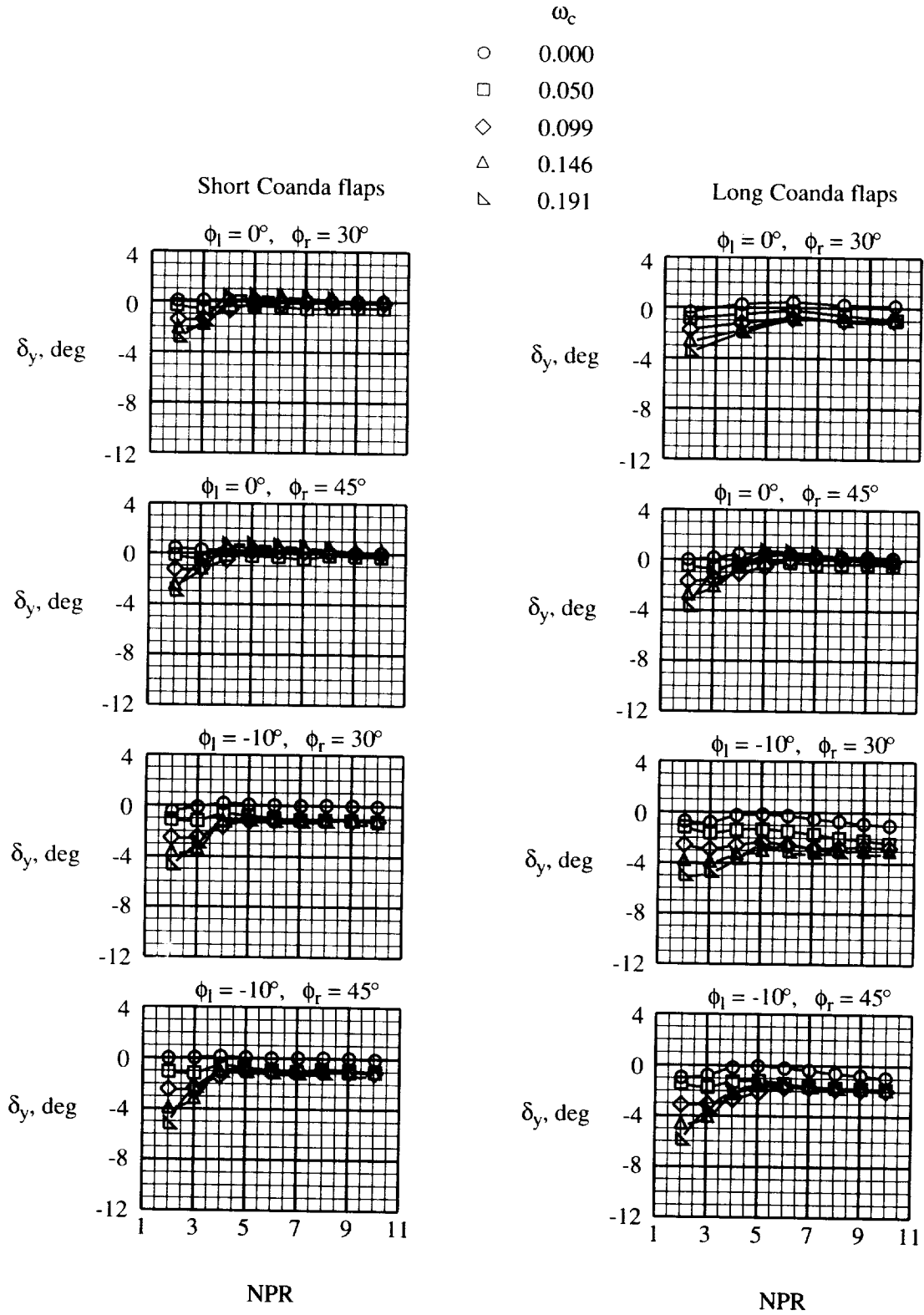
(b) $\varepsilon = 1.944$; $(\text{NPR})_{\text{des}} = 10.12$.

Figure 11. Continued.



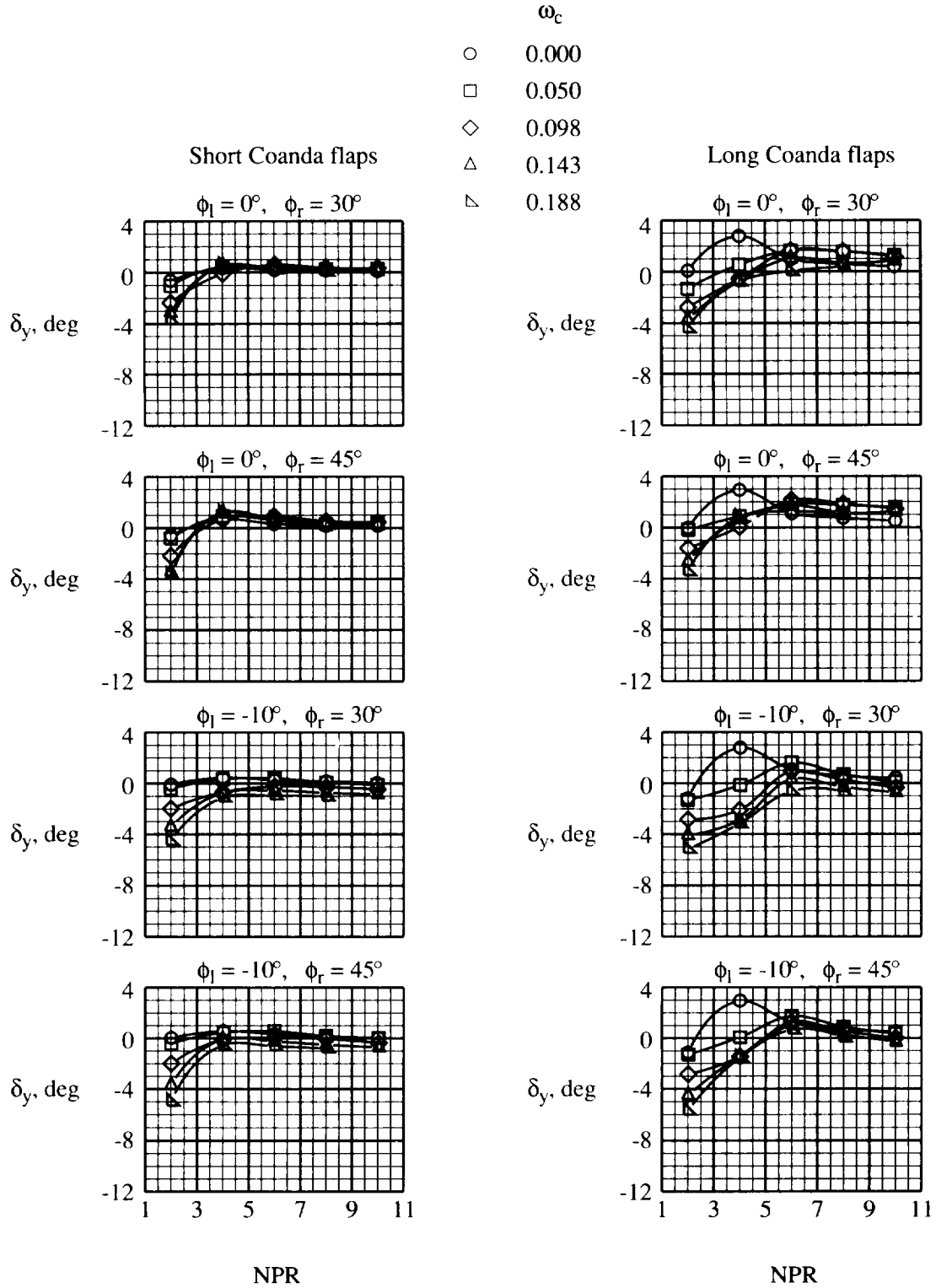
(c) $\varepsilon = 2.405$; $(NPR)_{des} = 14.64$.

Figure 11. Concluded.



(a) $\varepsilon = 1.502$; $(NPR)_{des} = 6.26$.

Figure 12. Effect of Coanda flap length, flap angle, and corrected weight flow ratio on yaw thrust vector angle.



(b) $\varepsilon = 2.405$; $(NPR)_{des} = 14.64$.

Figure 12. Concluded.

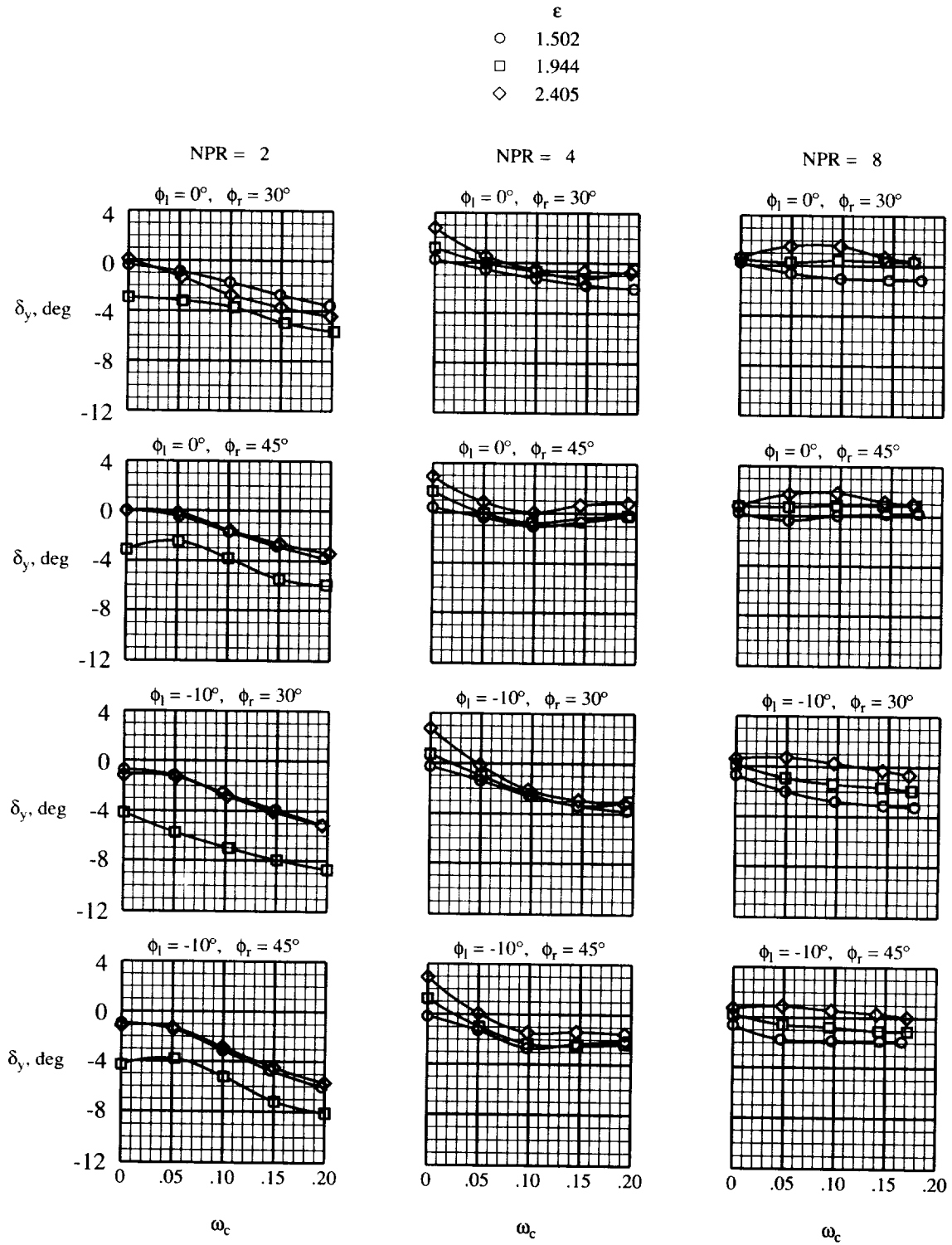
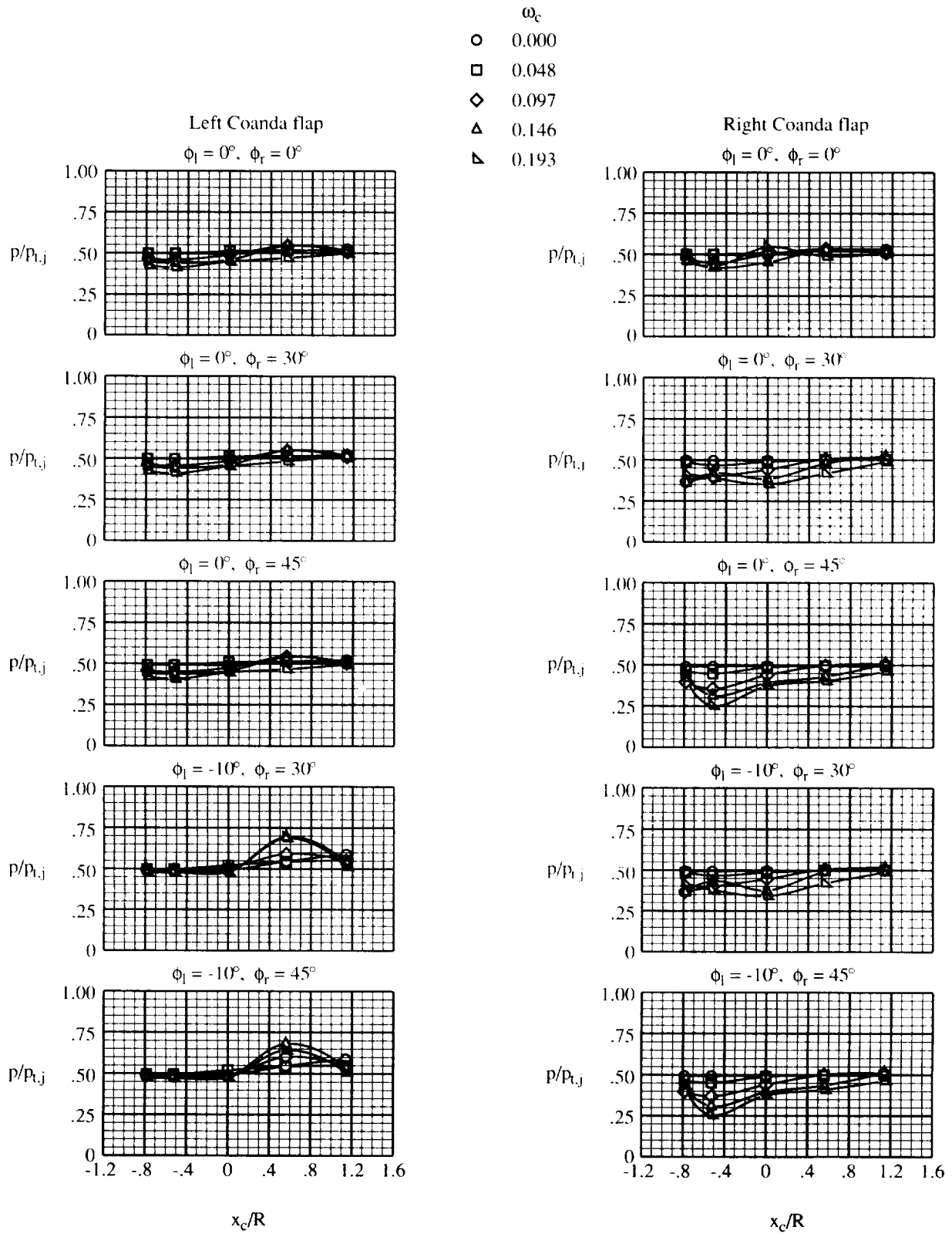
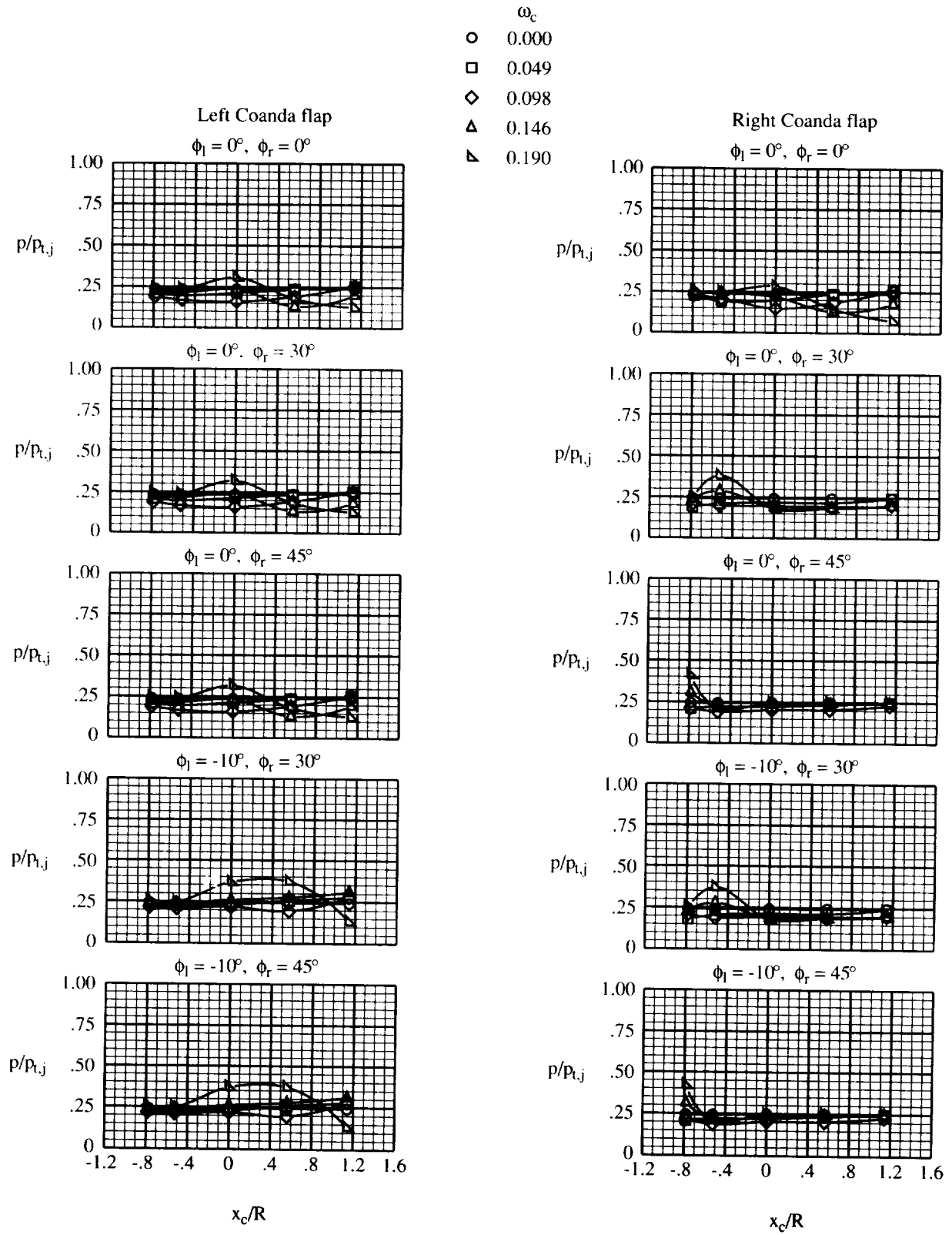


Figure 13. Yaw thrust vector angle as a function of Coanda corrected weight flow ratio at different Coanda flap angles and jet nozzle pressure ratios; long Coanda flaps.



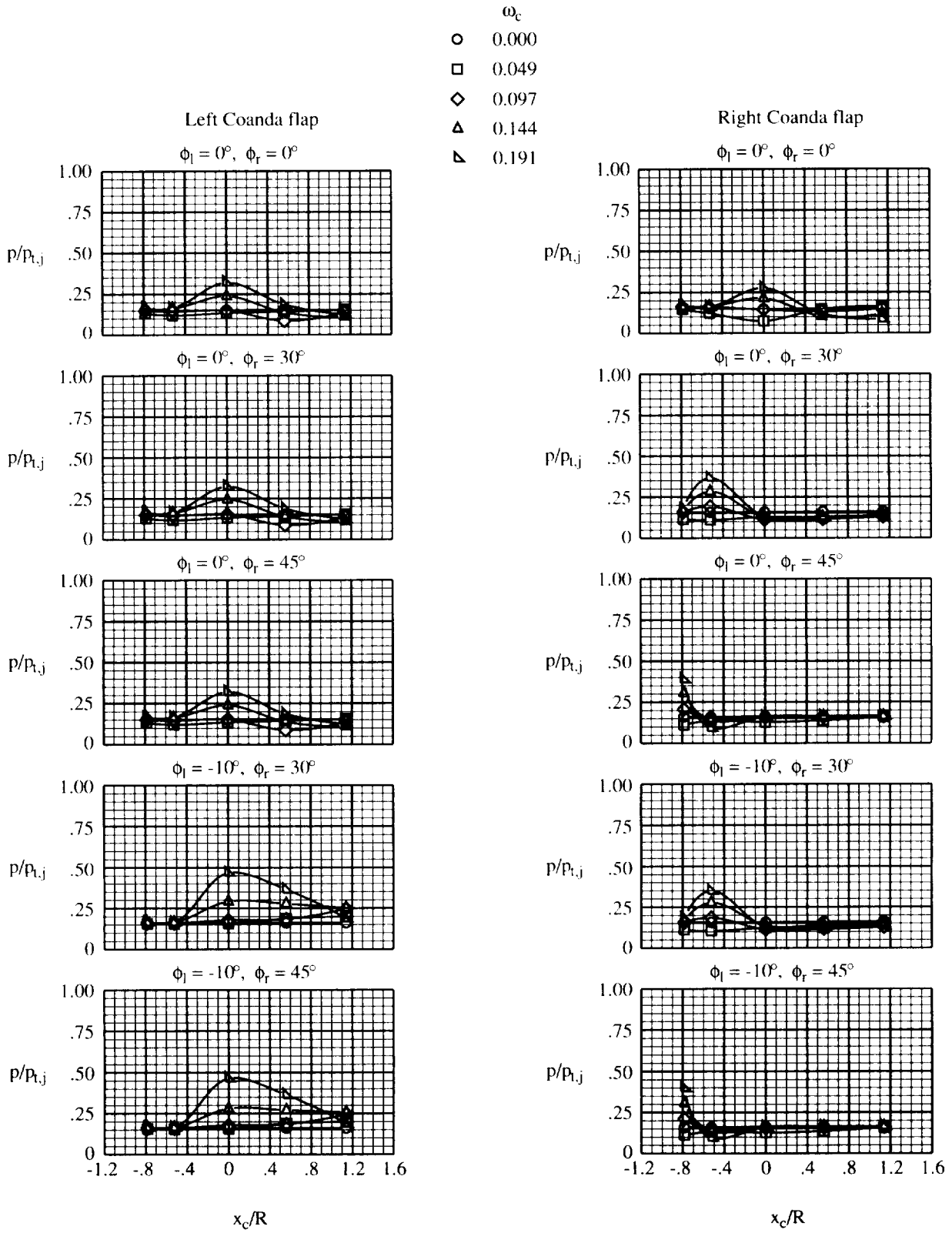
(a) NPR = 2.

Figure 14. Coanda flap static pressure ratio distributions. $\varepsilon = 1.502$; long Coanda flaps.



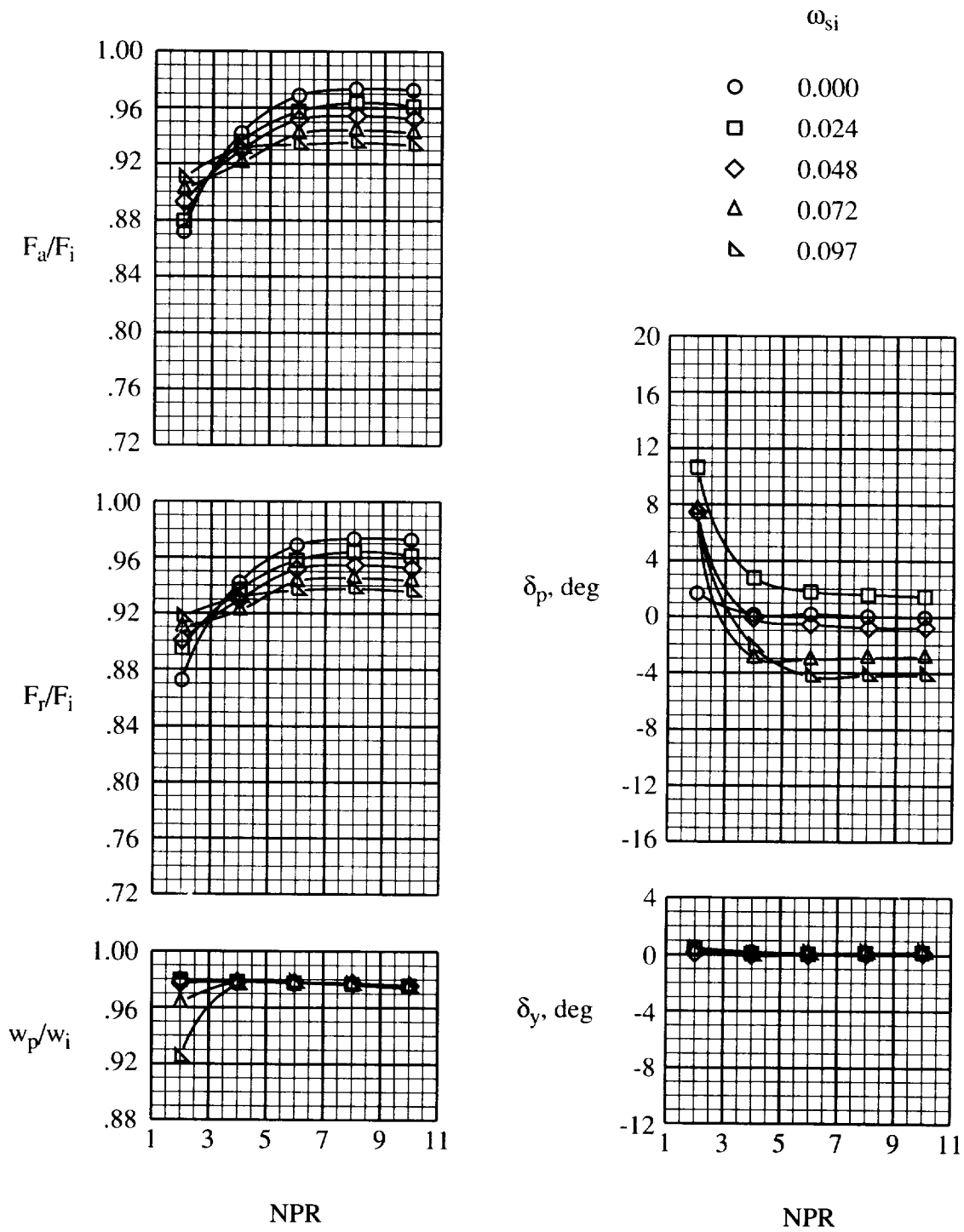
(b) NPR = 4.

Figure 14. Continued.



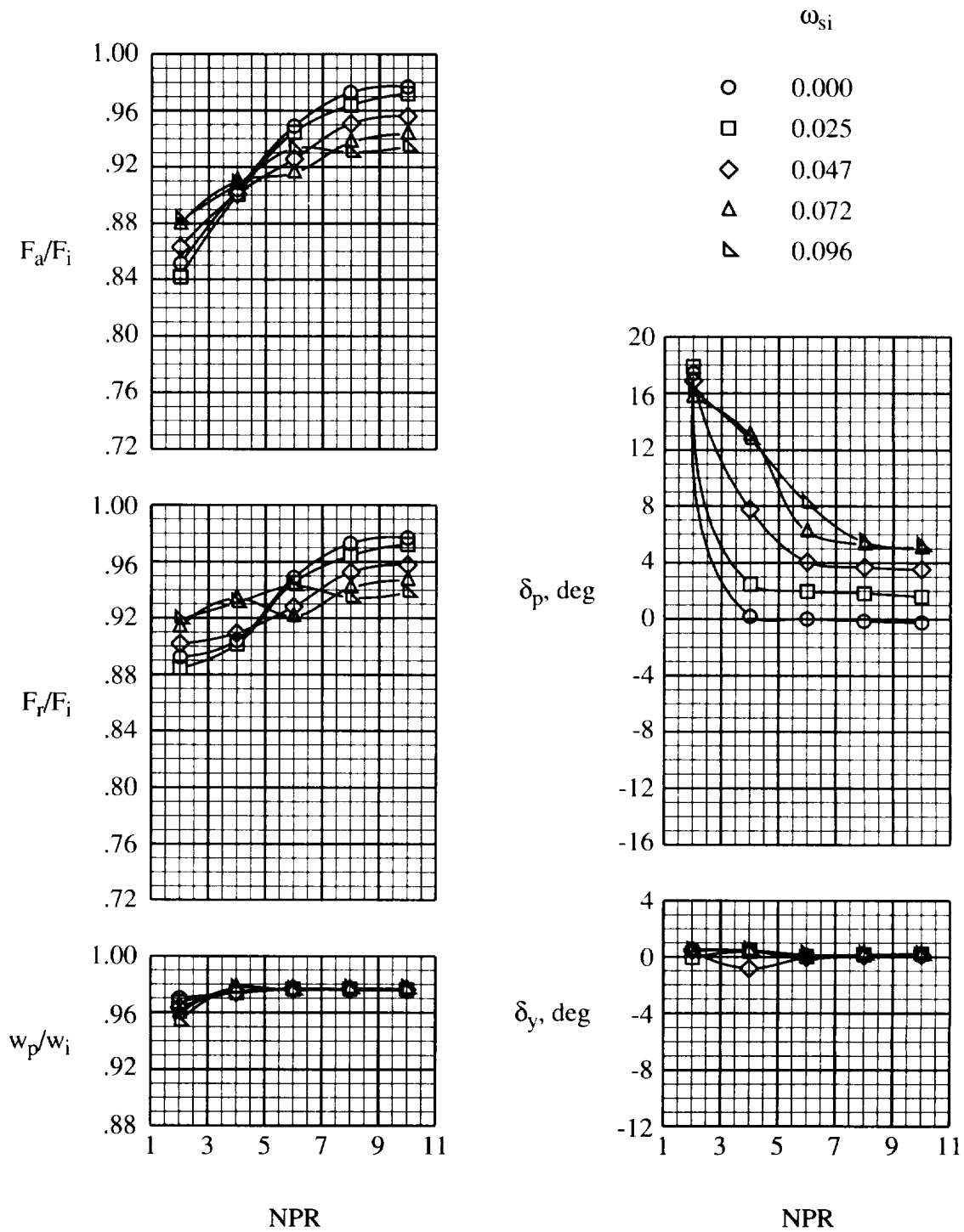
(c) NPR = 6.

Figure 14. Concluded.



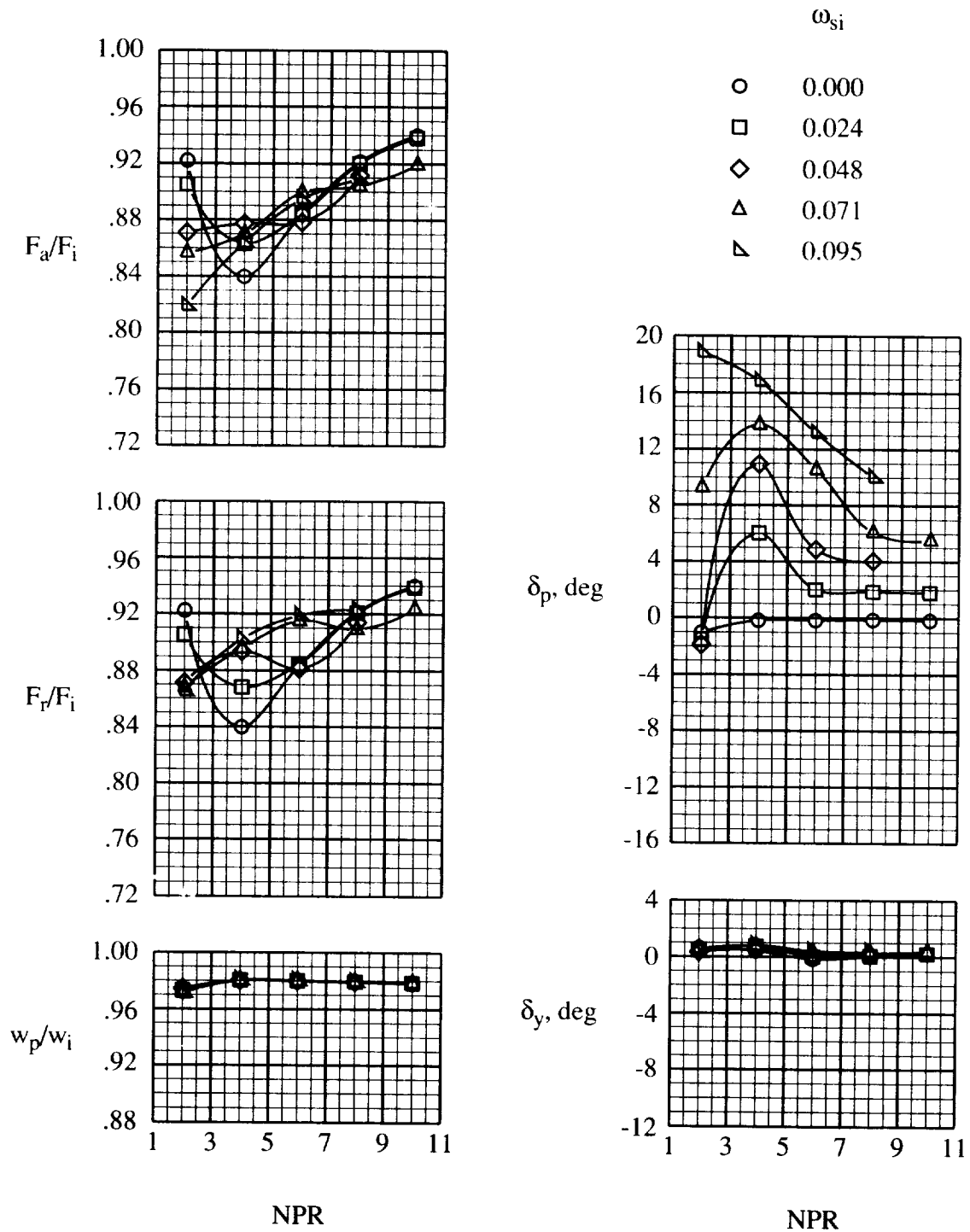
(a) $\epsilon = 1.502$; $(NPR)_{des} = 6.26$.

Figure 15. Effect of slot injection on internal performance. Forward slot injection; $\phi_l = 0^\circ$; $\phi_r = 0^\circ$; $\omega_c = 0.05$.



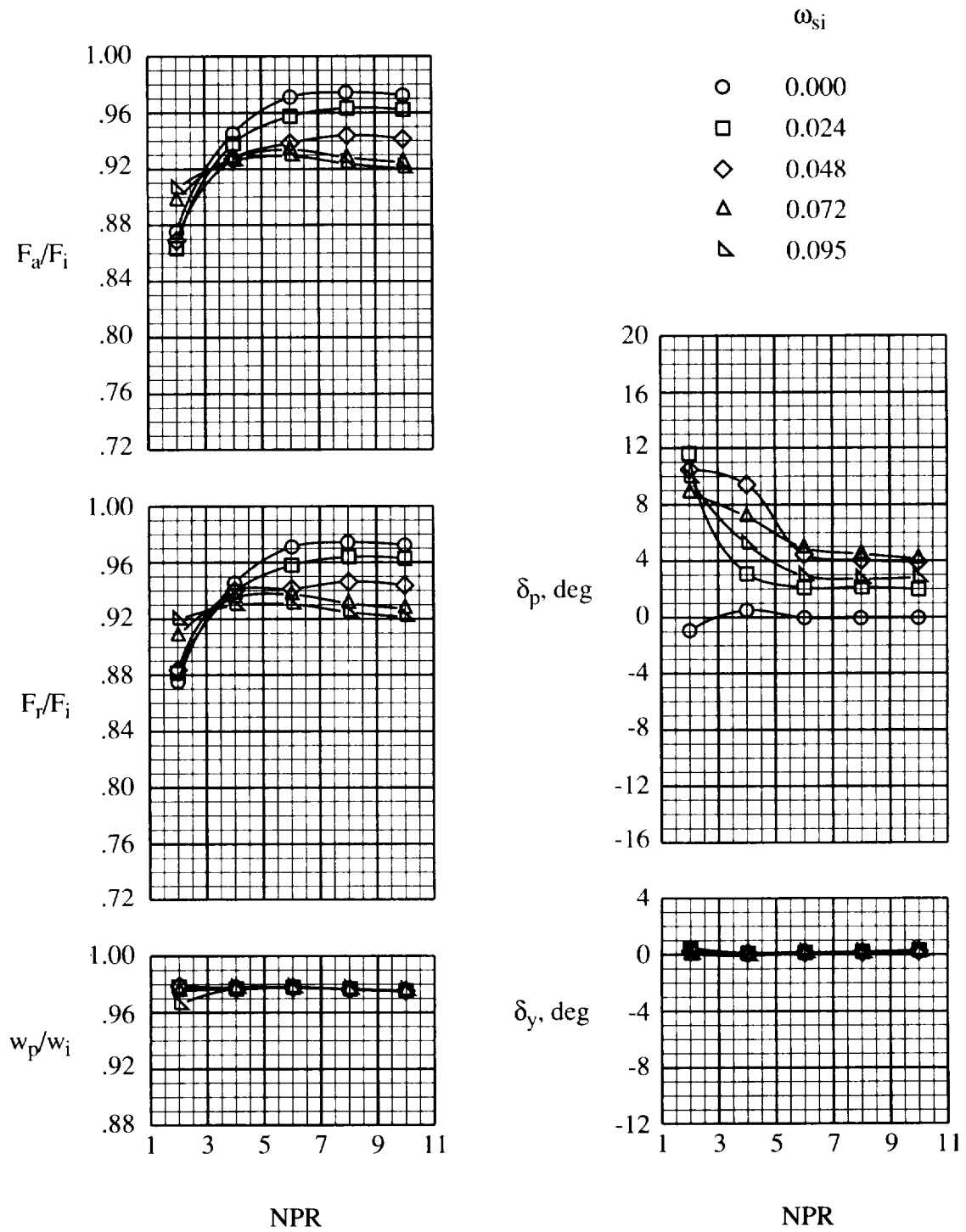
(b) $\varepsilon = 1.944$; $(NPR)_{des} = 10.12$.

Figure 15. Continued.



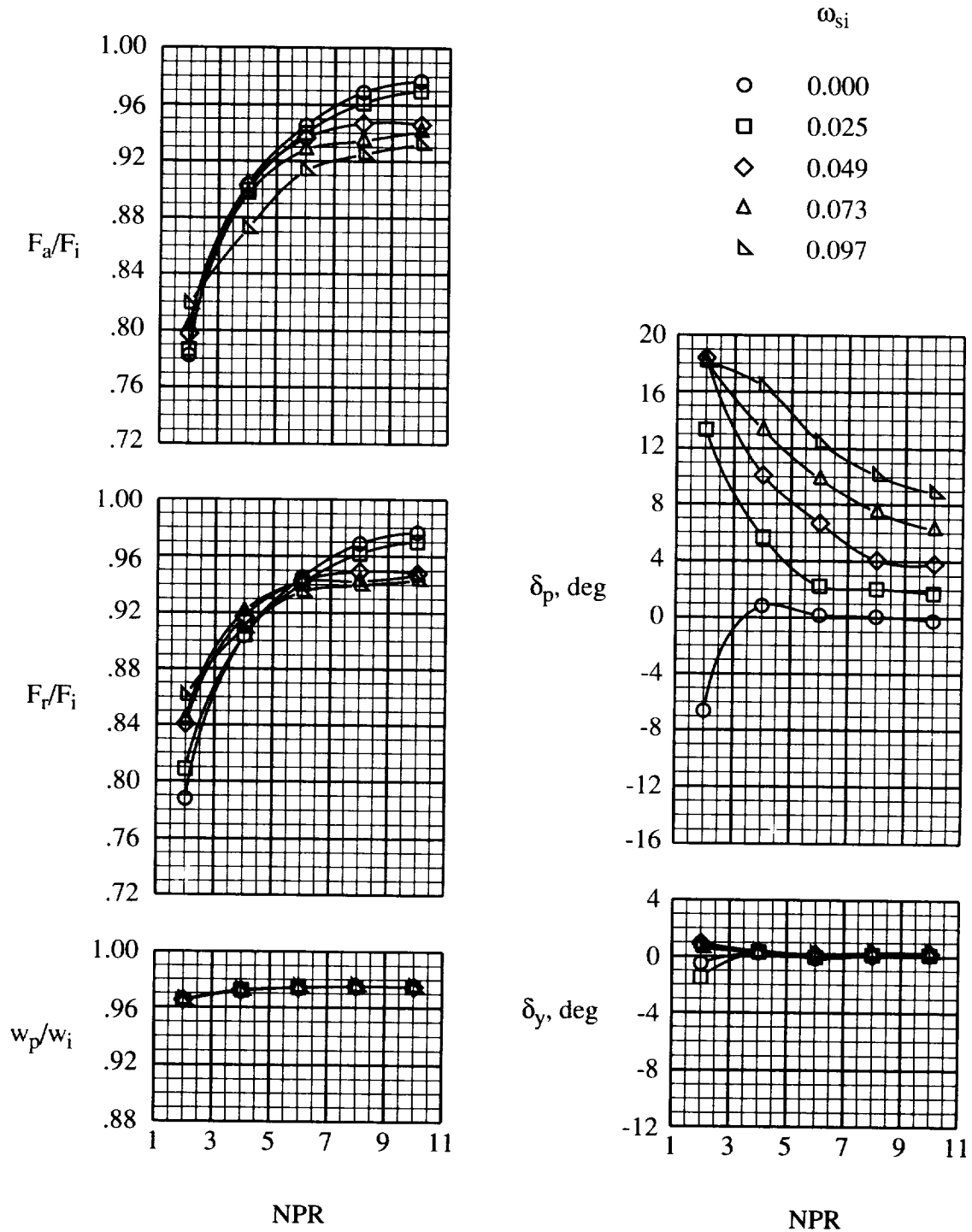
(c) $\varepsilon = 2.405$; $(NPR)_{des} = 14.64$.

Figure 15. Concluded.



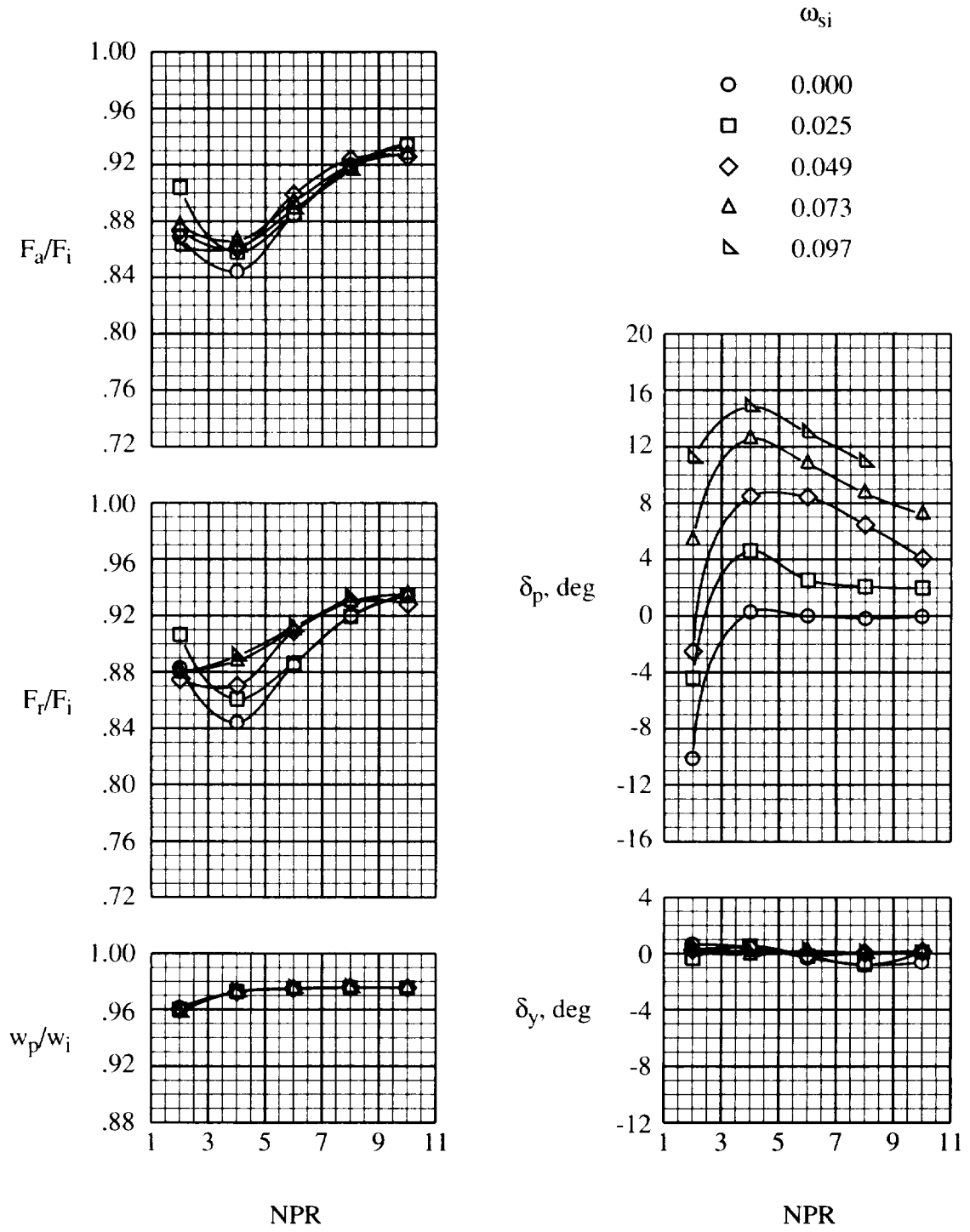
(a) $\varepsilon = 1.502$; $(NPR)_{des} = 6.26$.

Figure 16. Effect of slot injection on internal performance. Aft slot injection; $\phi_l = 0^\circ$; $\phi_r = 0^\circ$; $\omega_c = 0.05$.



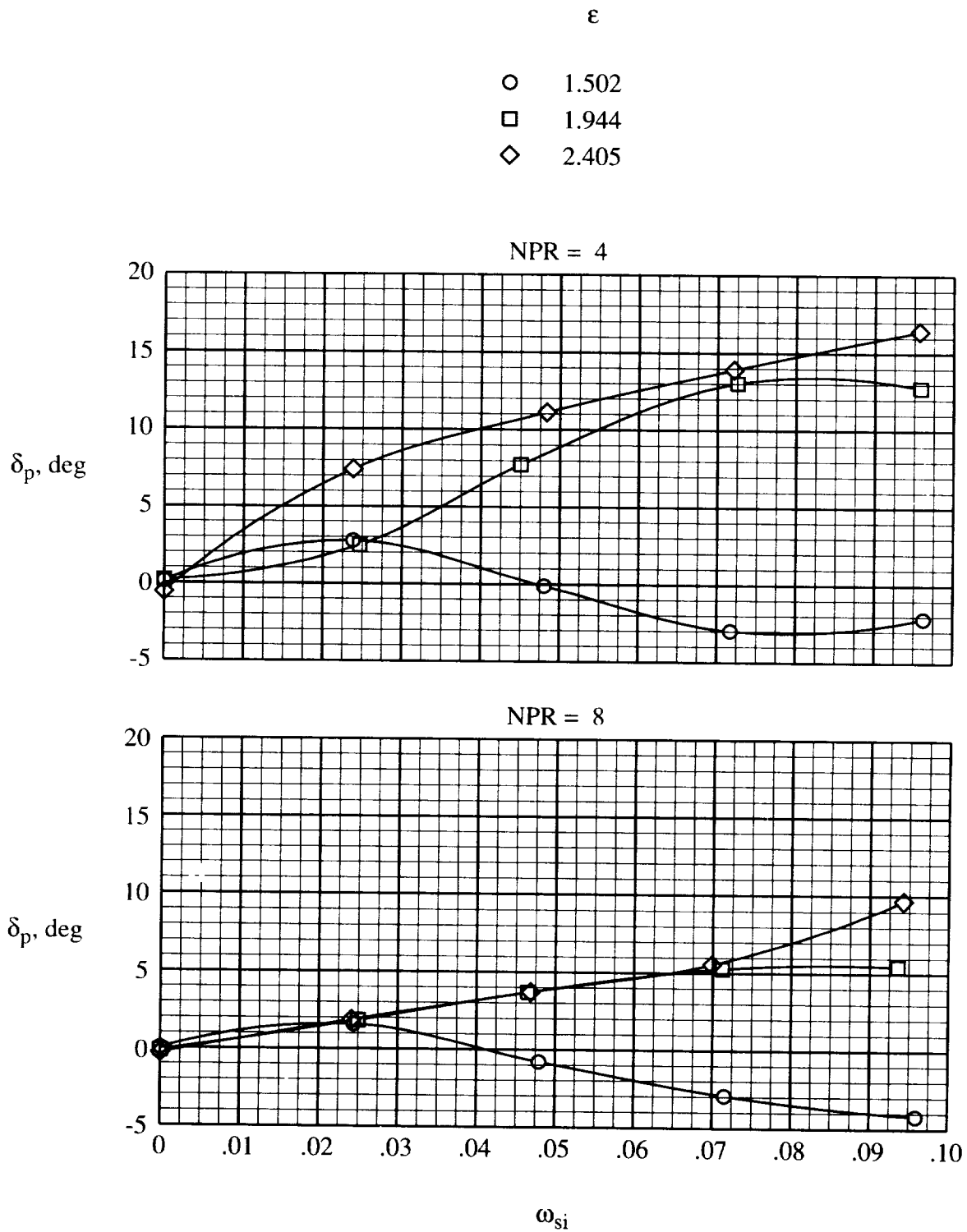
(b) $\varepsilon = 1.944$; $(NPR)_{des} = 10.12$.

Figure 16. Continued.



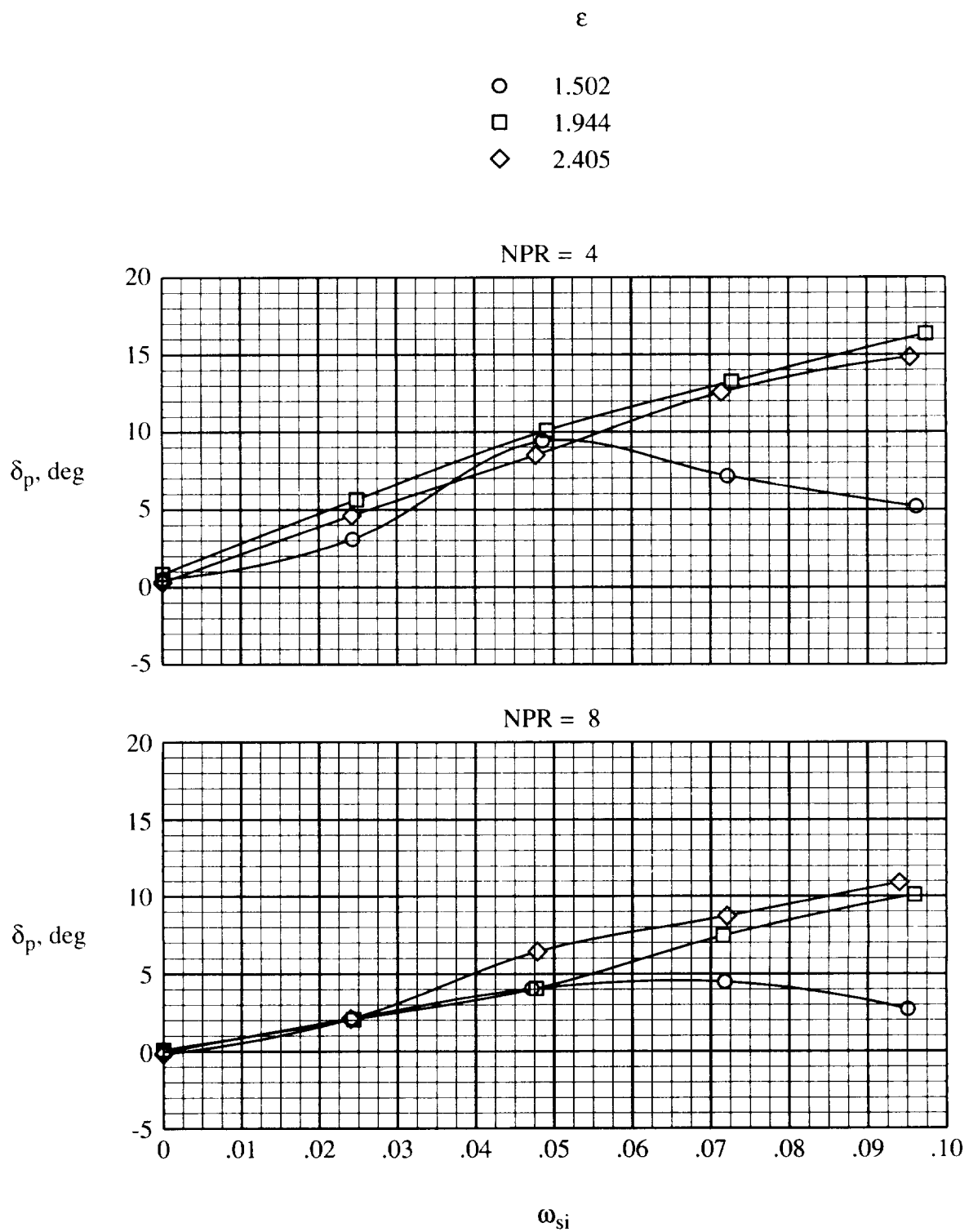
(c) $\varepsilon = 2.405$; $(NPR)_{des} = 14.64$.

Figure 16. Concluded.



(a) Forward slot injection.

Figure 17. Effect of slot injection corrected weight flow ratio on pitch thrust vector angle. $\phi_l = 0^\circ$; $\phi_r = 0^\circ$; $\omega_c = 0.05$.



(b) Aft slot injection.

Figure 17. Concluded.

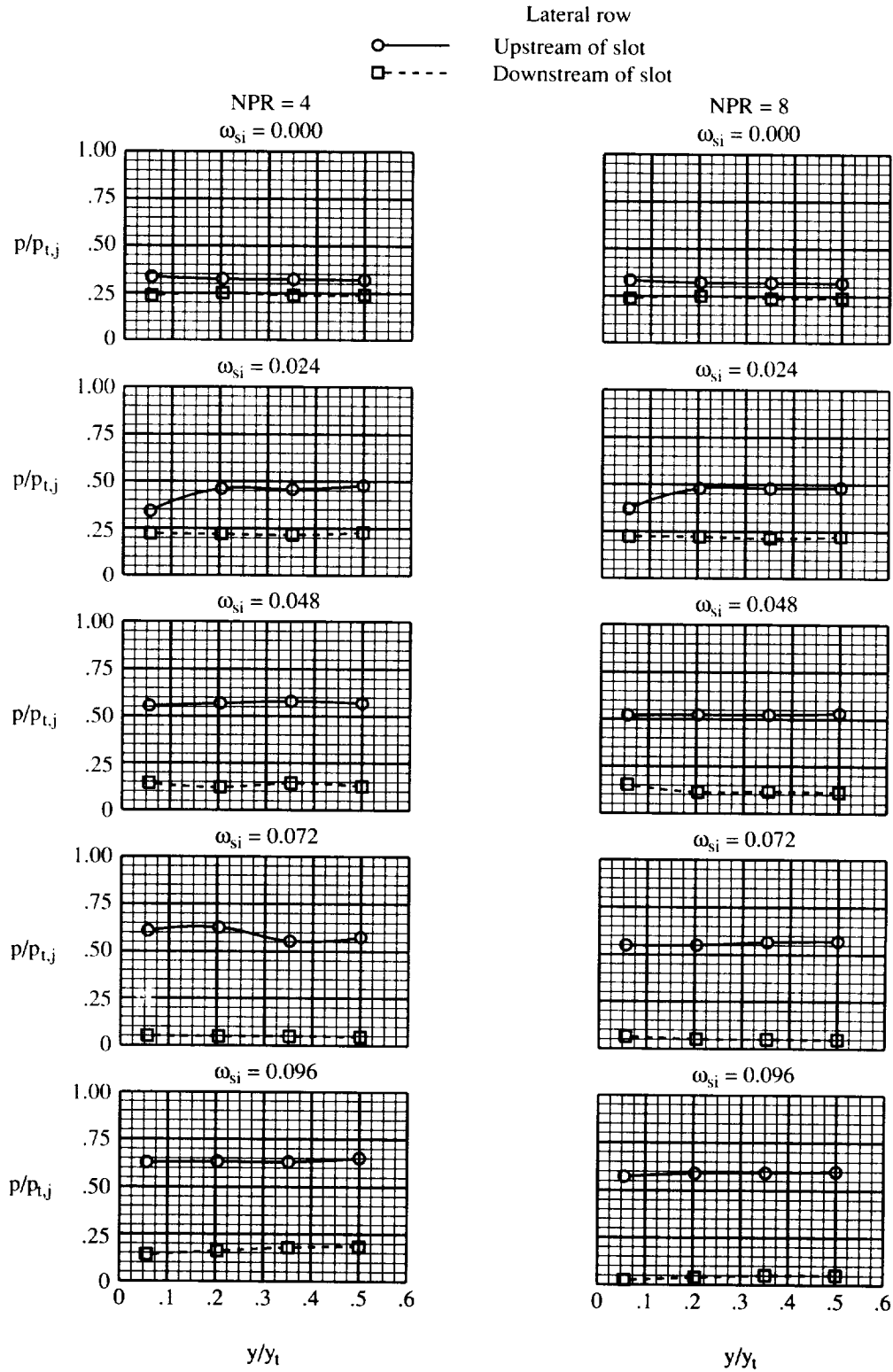
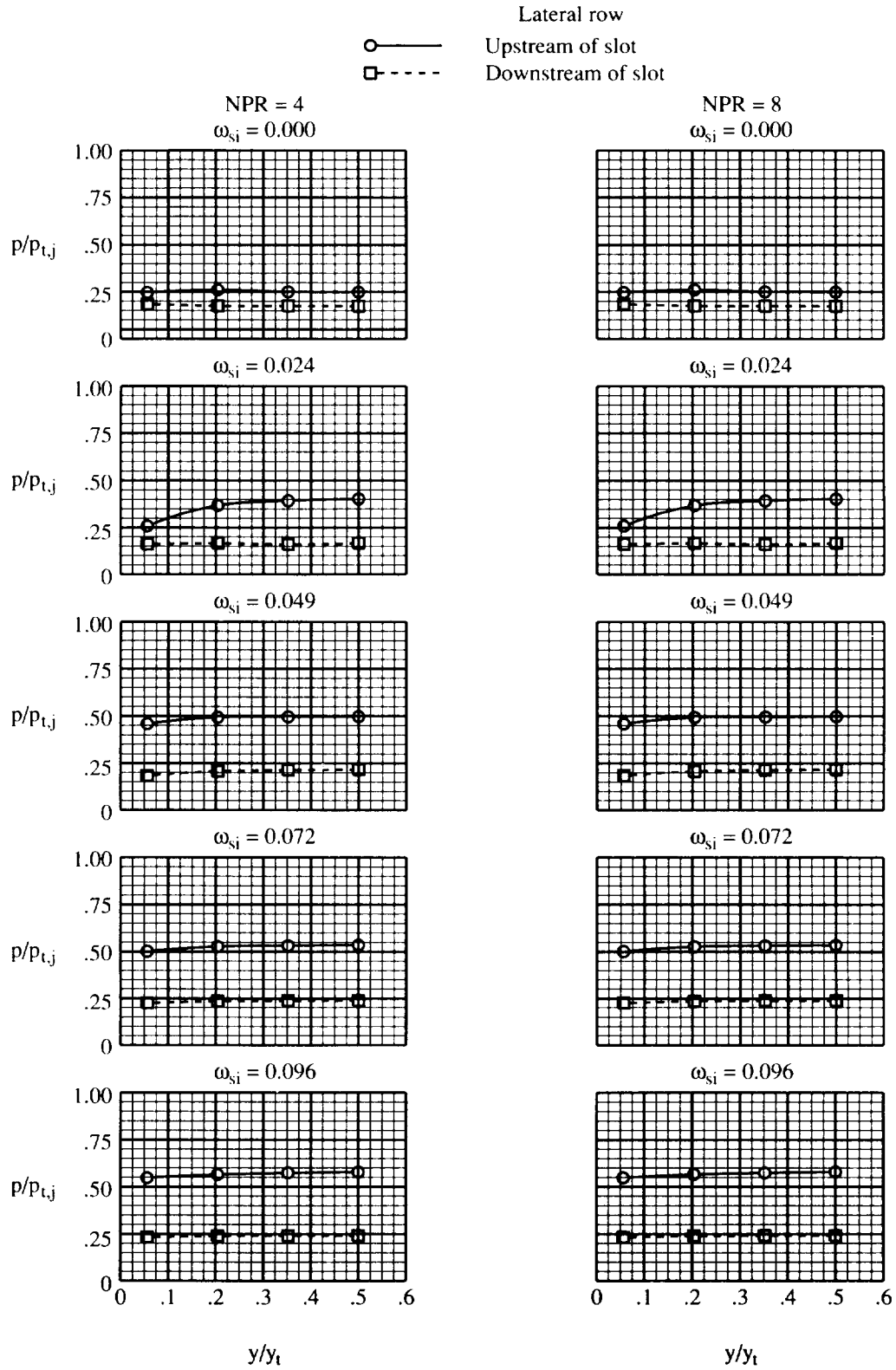
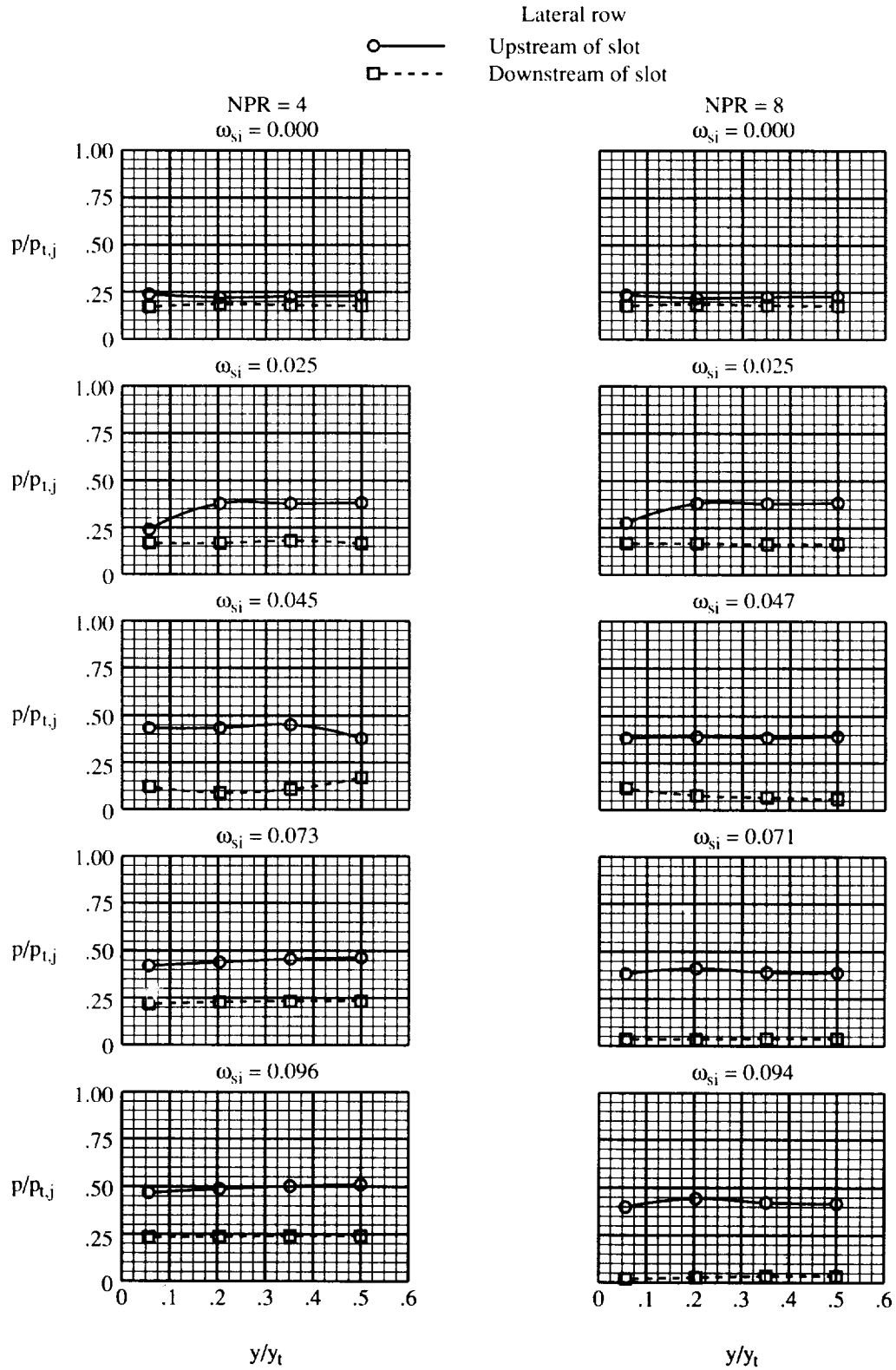


Figure 18. Lateral static pressure ratio distributions on upstream and downstream sides of injection slot.
 $\phi_l = 0^\circ$; $\phi_r = 0^\circ$; $\omega_c = 0.05$.



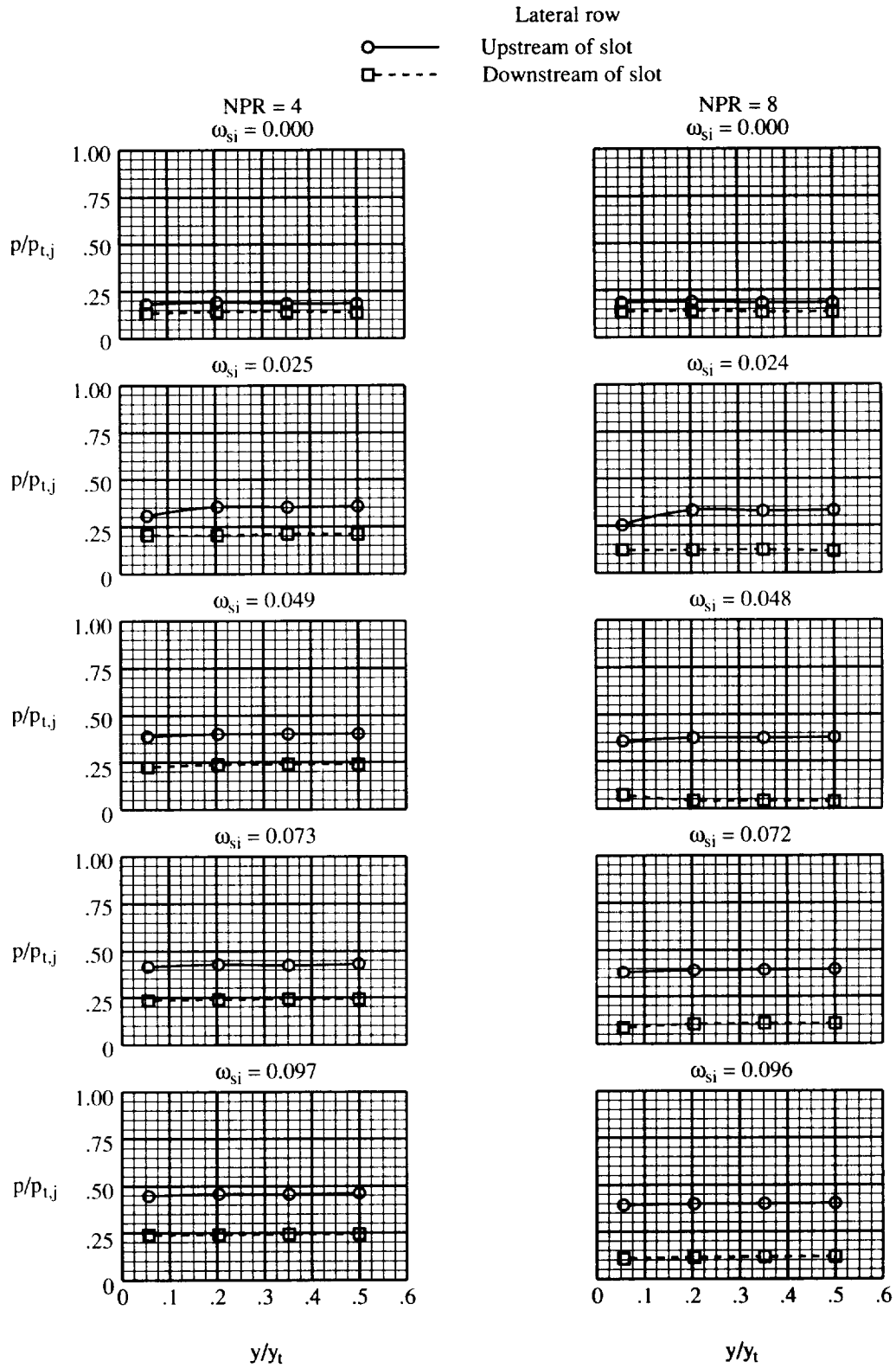
(b) $\epsilon = 1.502$; aft slot injection.

Figure 18. Continued.



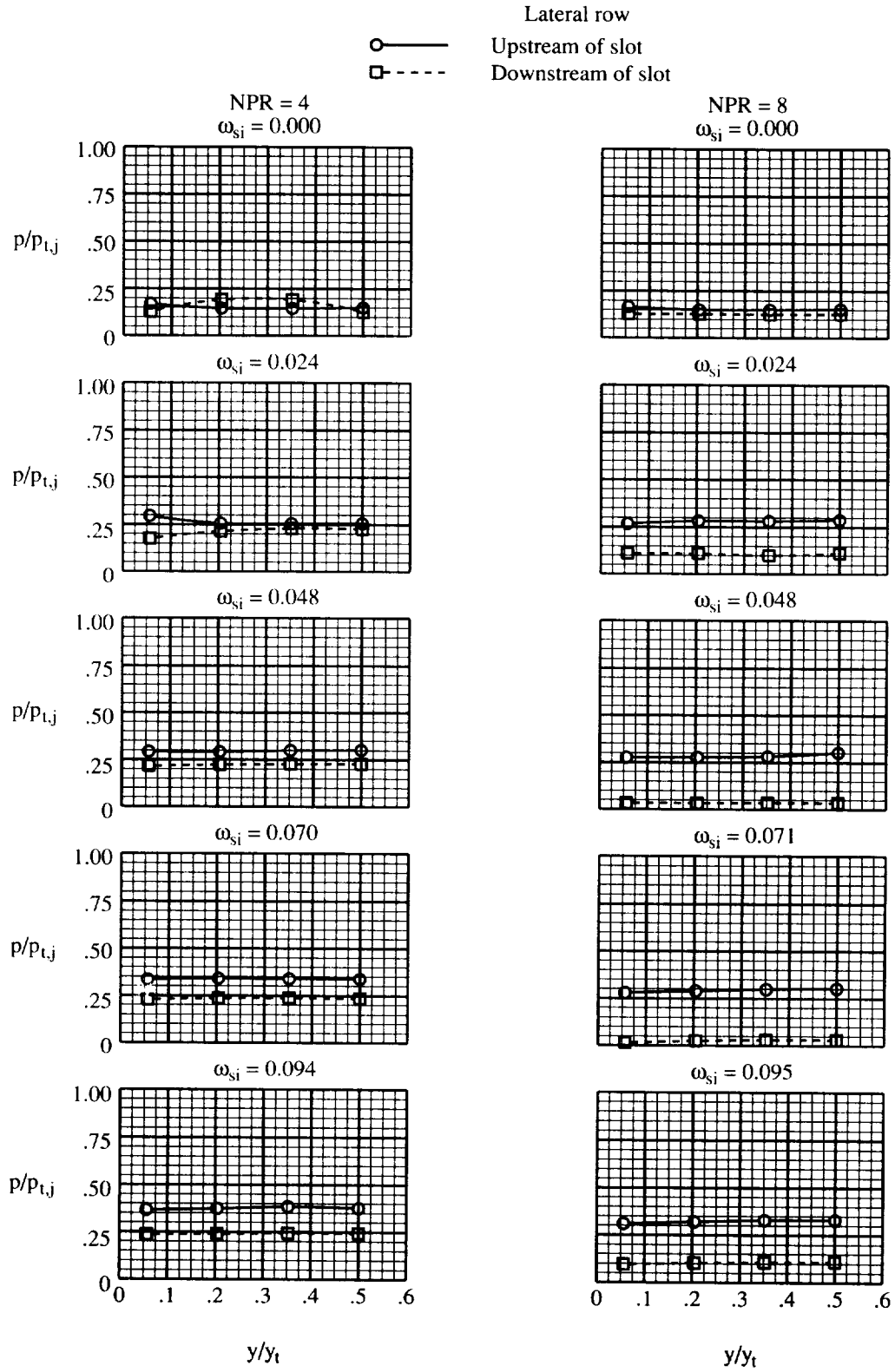
(c) $\varepsilon = 1.944$; forward slot injection.

Figure 18. Continued.



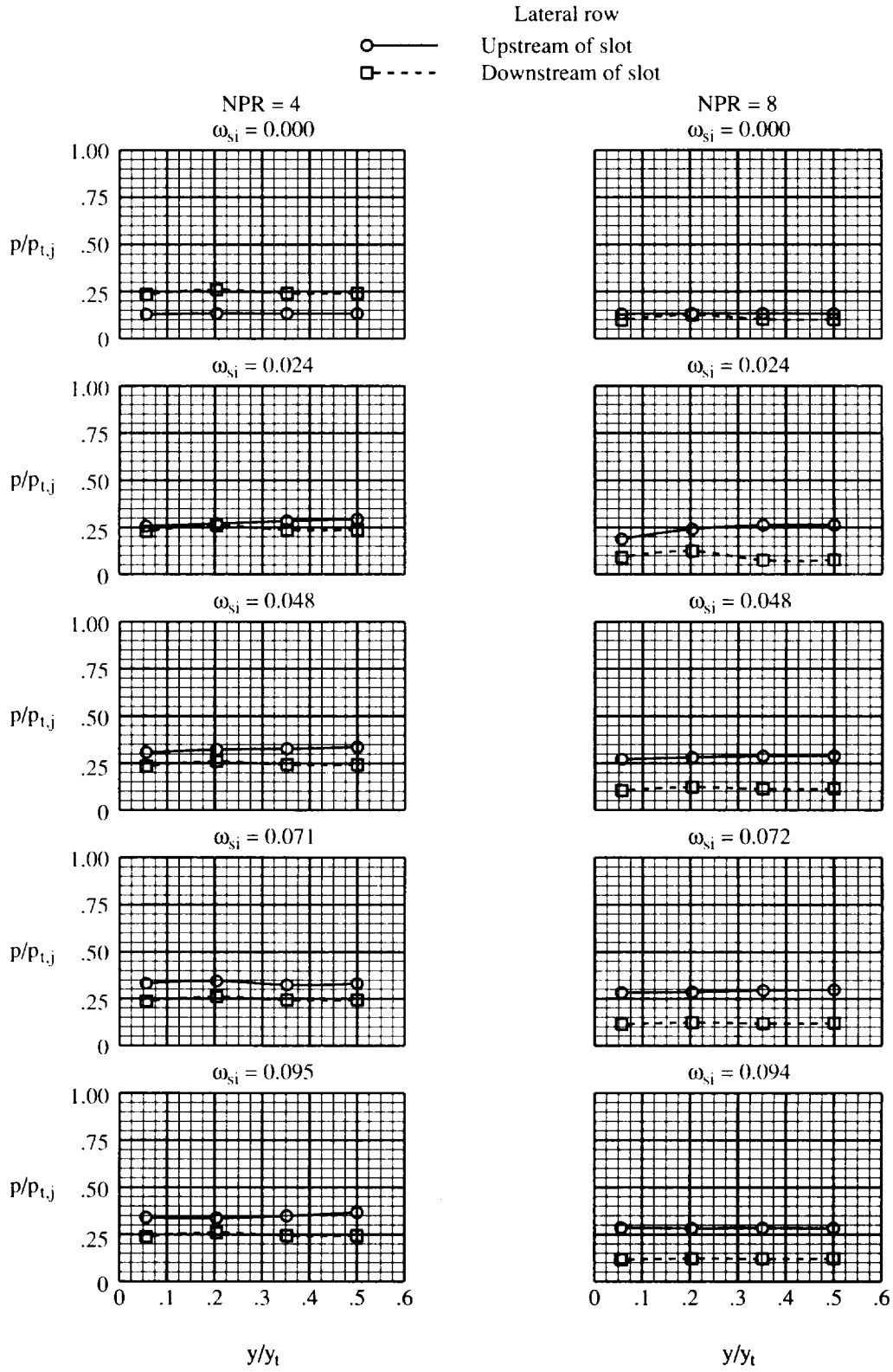
(d) $\varepsilon = 1.944$; aft slot injection.

Figure 18. Continued.



(e) $\epsilon = 2.405$; forward slot injection.

Figure 18. Continued.



(f) $\varepsilon = 2.405$; aft slot injection.

Figure 18. Concluded.

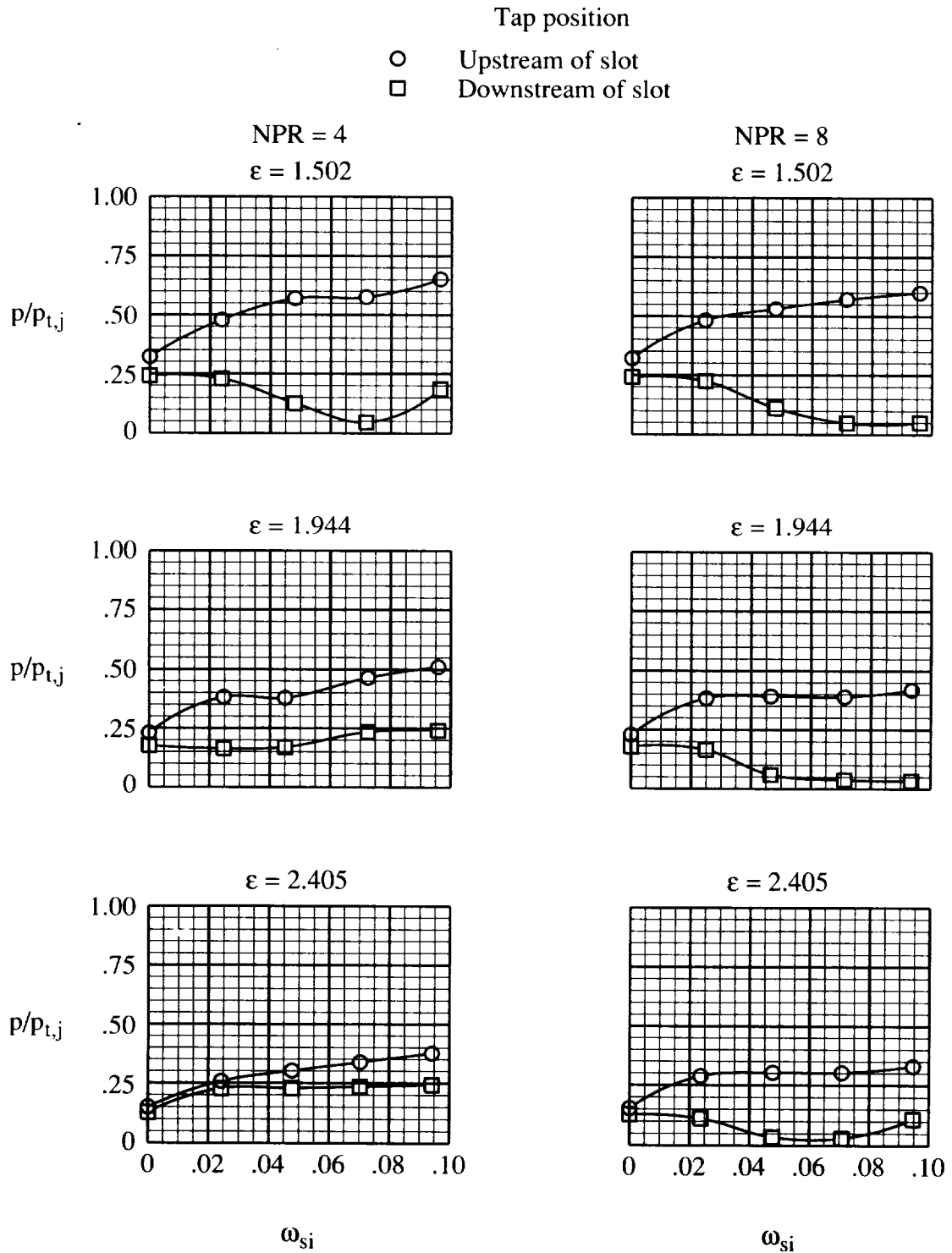
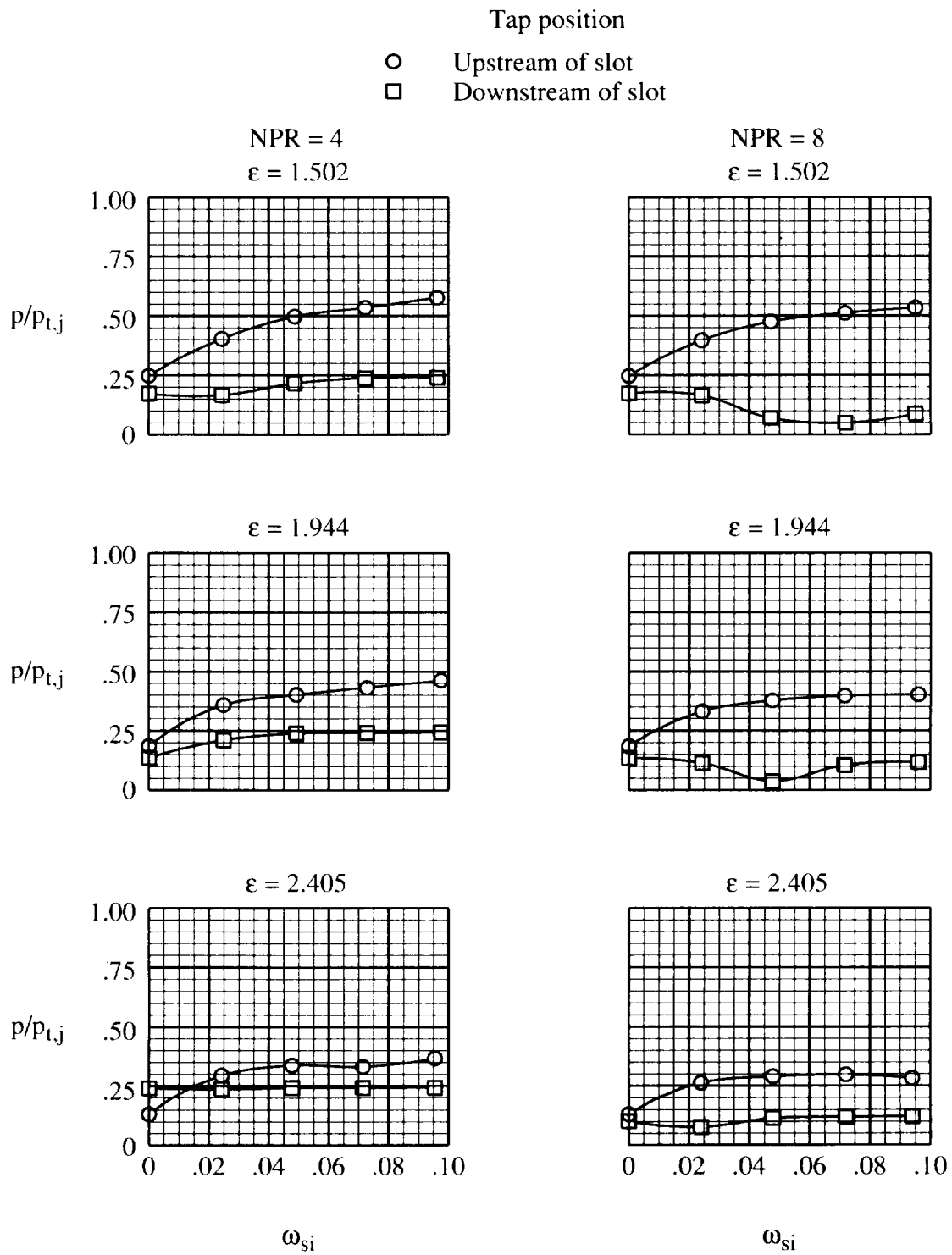
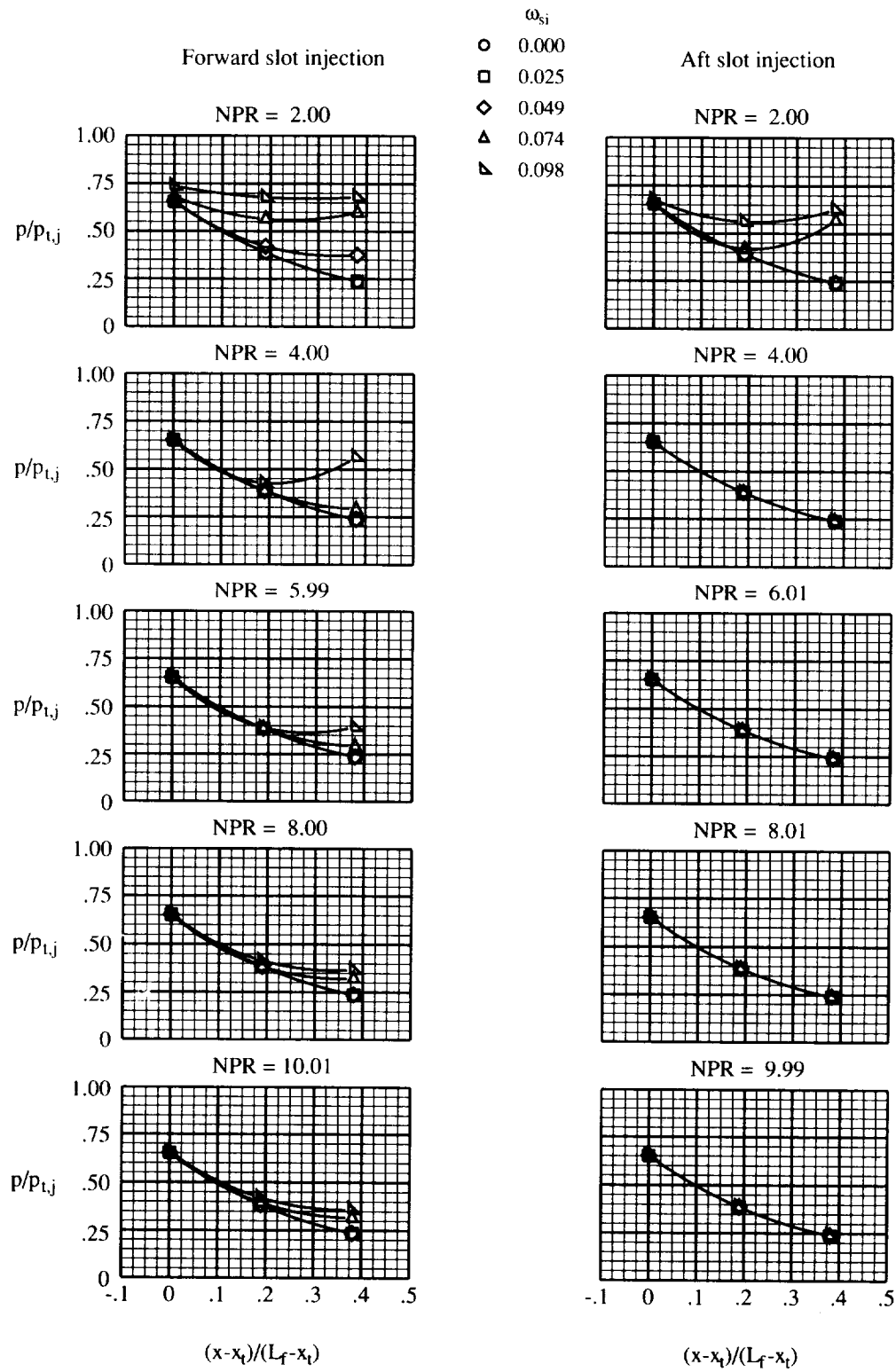


Figure 19. Upper flap centerline static pressure ratios upstream and downstream of injection slot. $\phi_l = 0^\circ$; $\phi_r = 0^\circ$; $\omega_c = 0.05$.



(b) Aft slot injection.

Figure 19. Concluded.



(a) $\epsilon = 1.502$.

Figure 20. Sidewall static pressure ratio distributions between nozzle geometric throat and injection slot.
 $\phi_l = 0^\circ$; $\phi_r = 0^\circ$; $\omega_c = 0.05$.

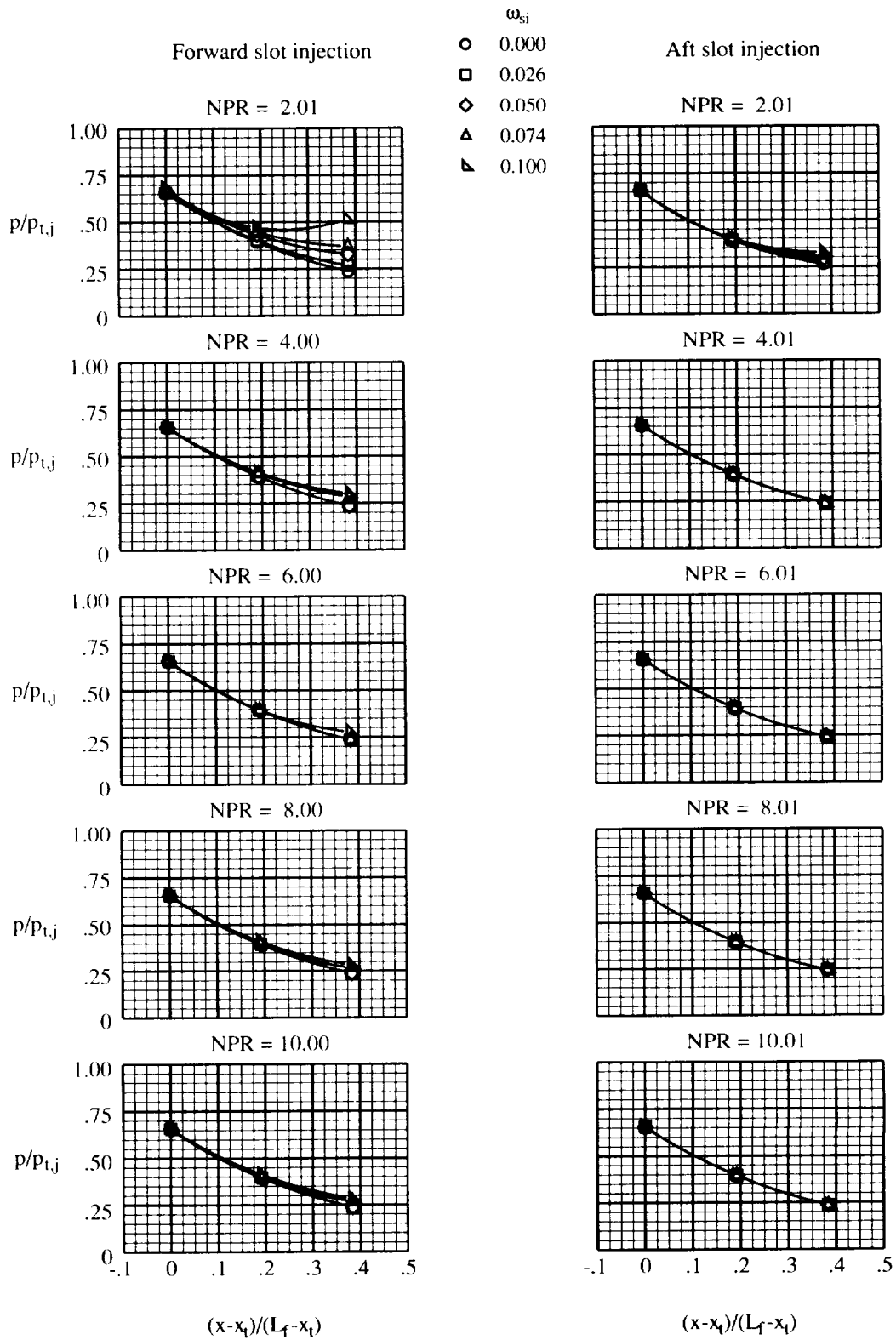


Figure 20. Continued.

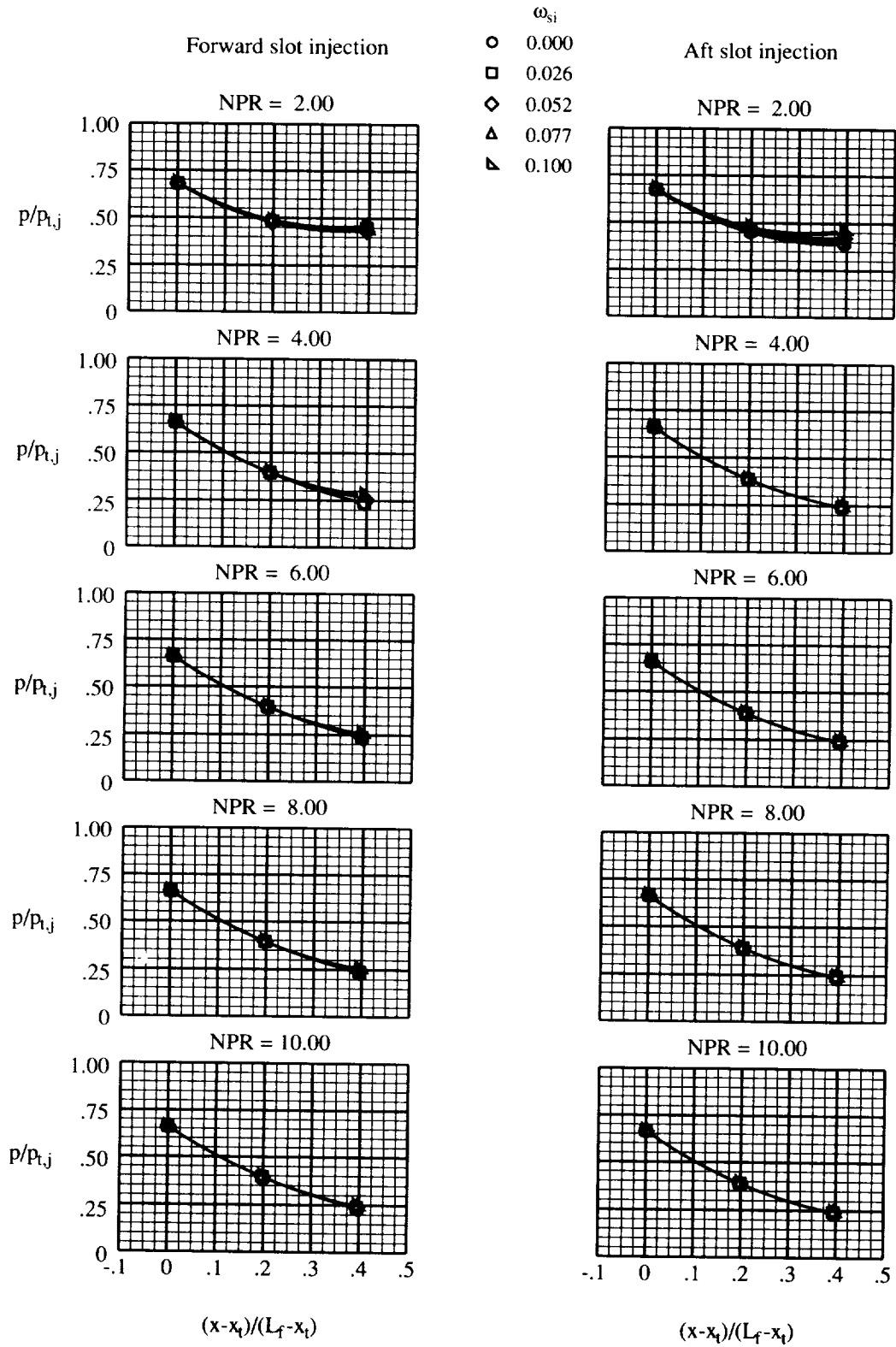
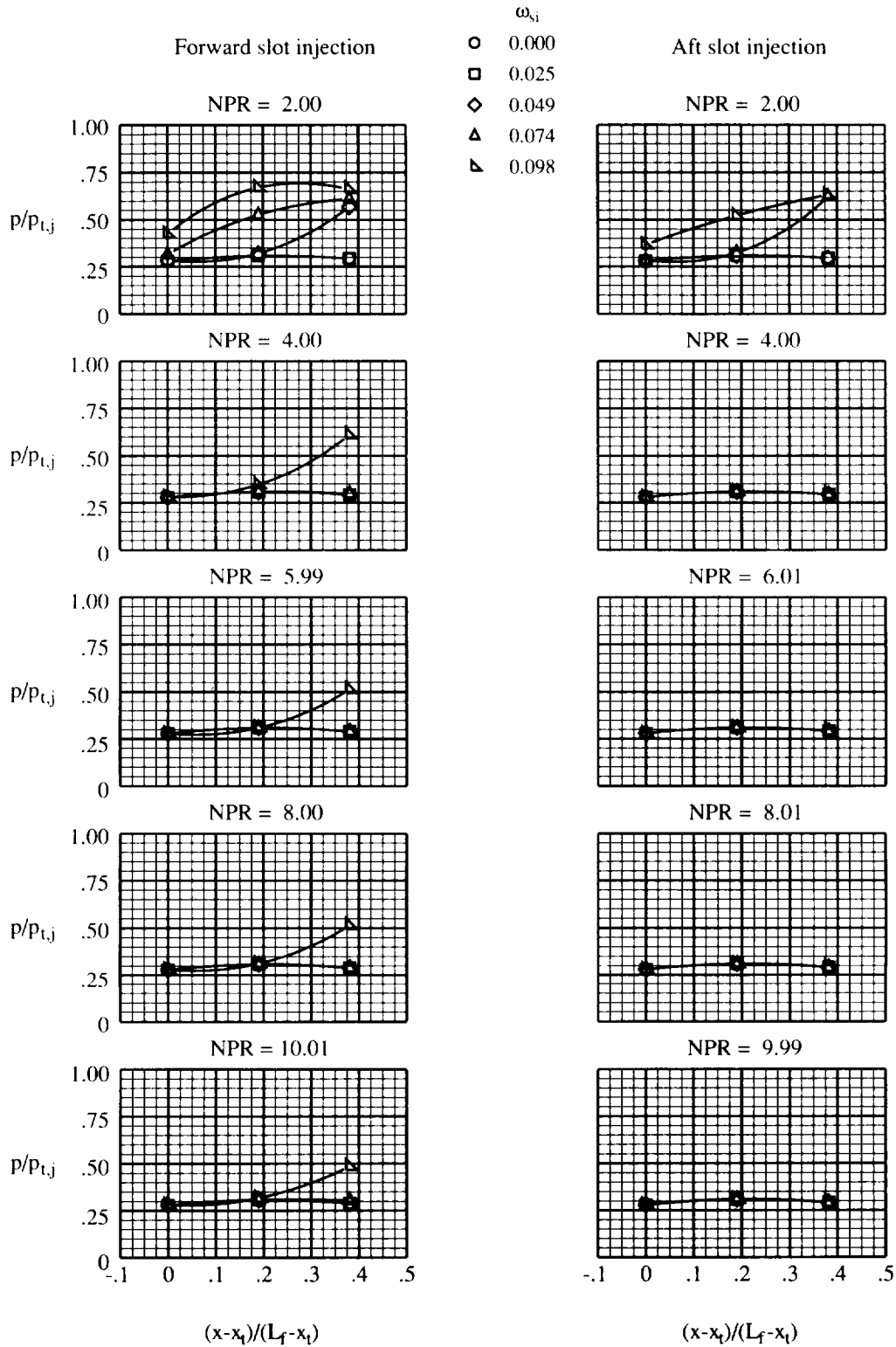
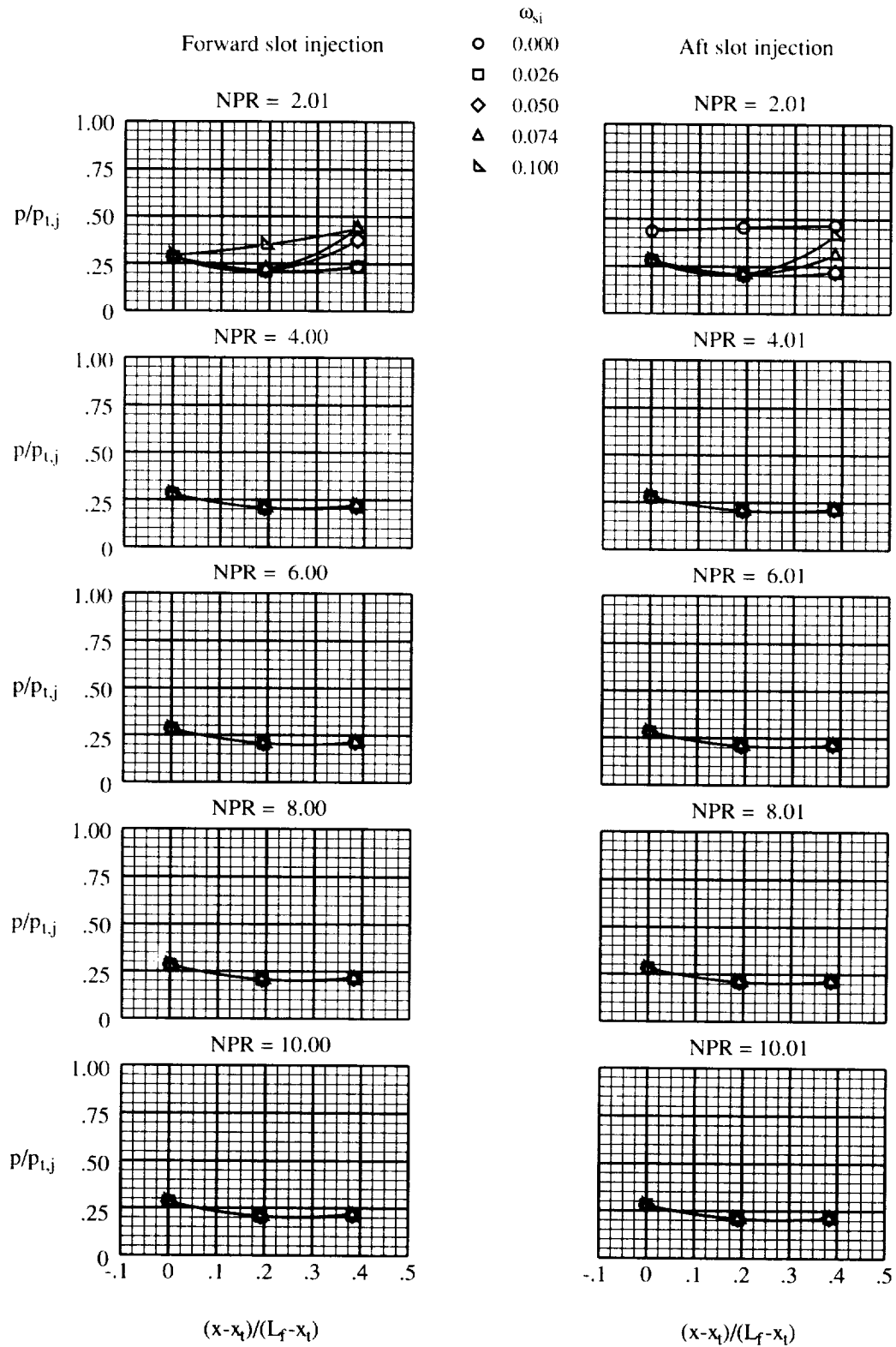


Figure 20. Concluded.



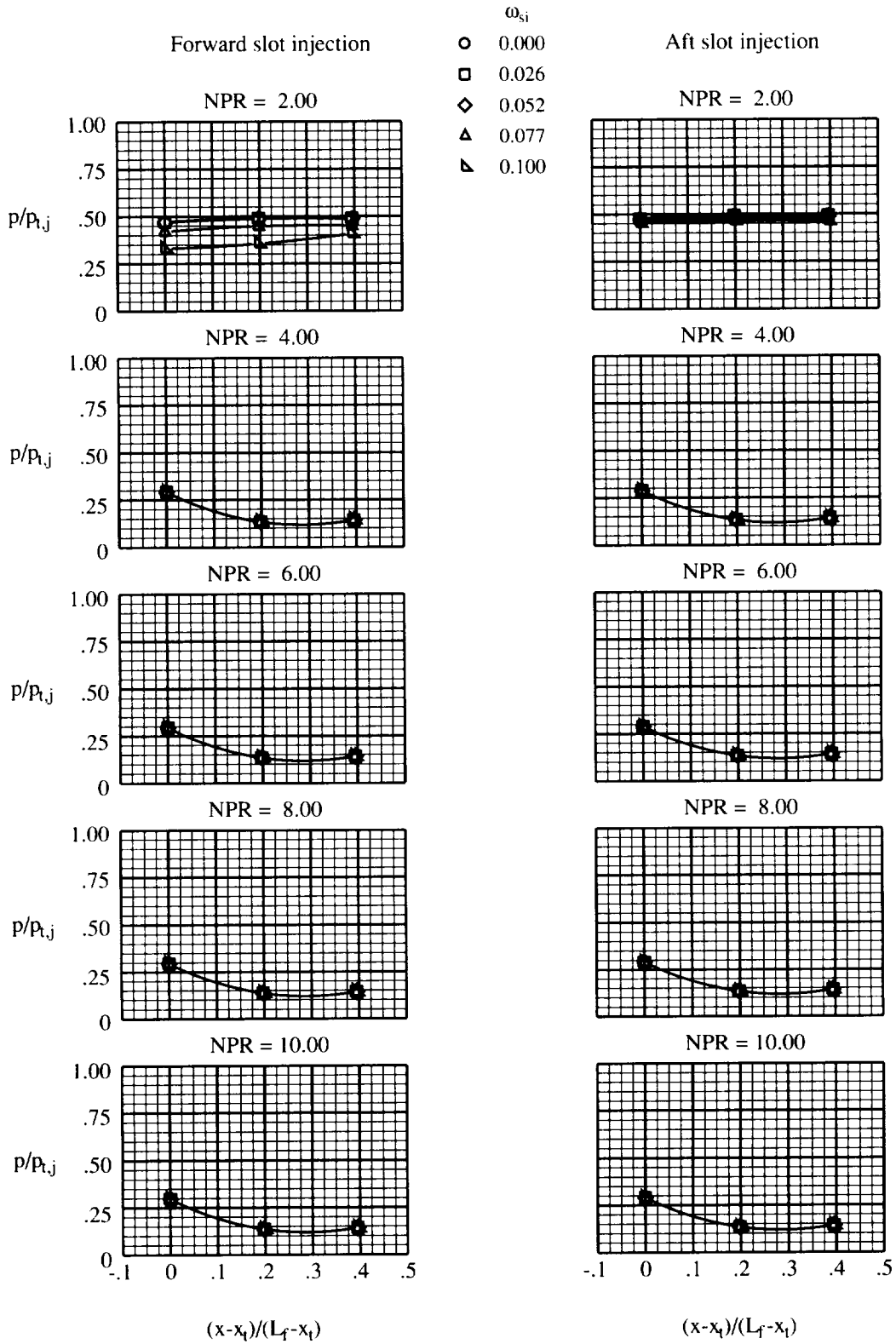
(a) $\varepsilon = 1.502$.

Figure 21. Lower flap static pressure ratio distributions between nozzle geometric throat and injection slot.
 $\phi_l = 0^\circ$; $\phi_r = 0^\circ$; $\omega_c = 0.05$.



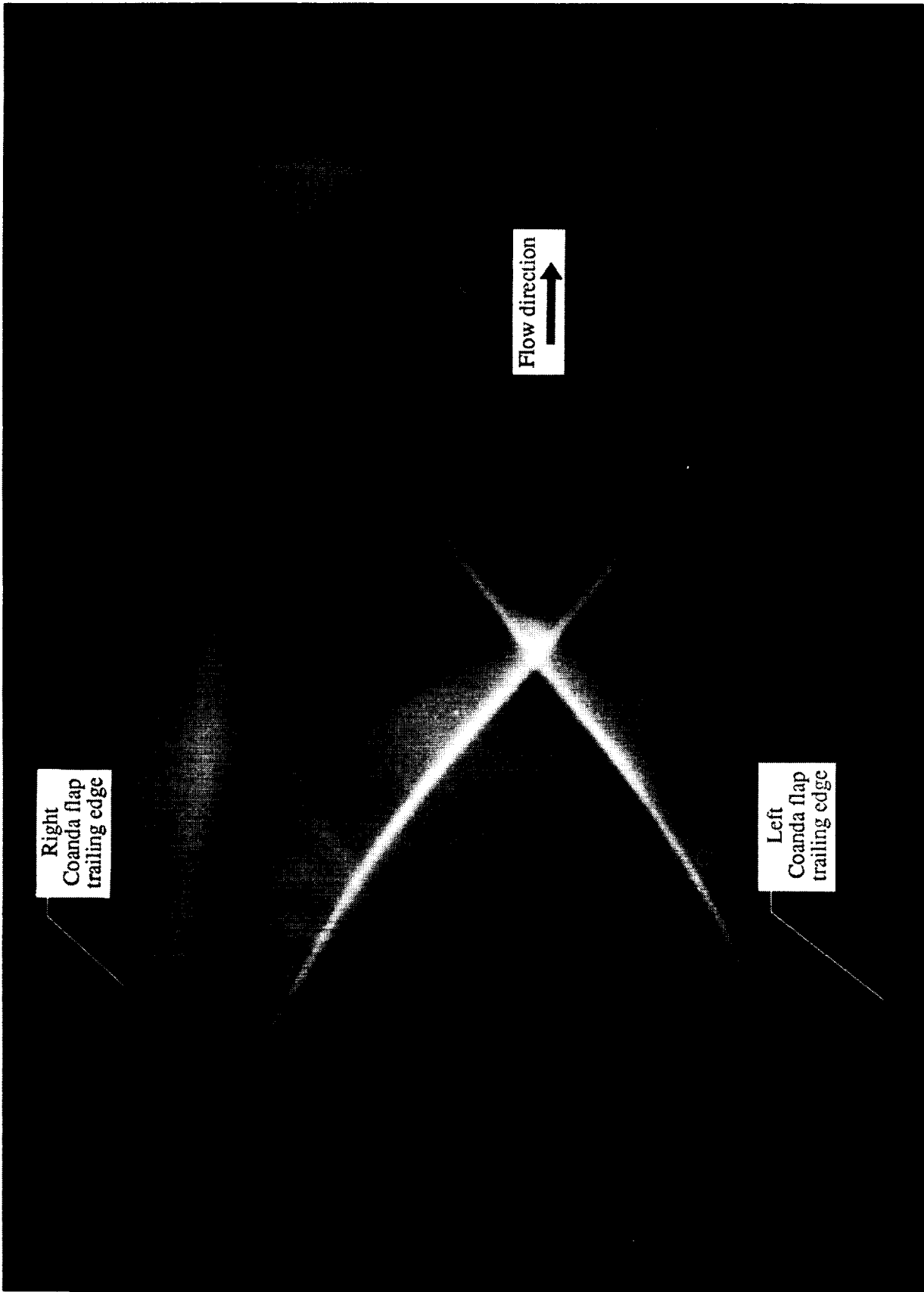
(b) $\varepsilon = 1.9 \cdot 4$.

Figure 21. Continued.



(c) $\varepsilon = 2.405$.

Figure 21. Concluded.



(a) $\phi_l = 0^\circ$; $\phi_r = 0^\circ$; $\omega_c = 0$.

Figure 22. Focusing schlieren photographs of Coanda thrust-vectoring configuration. $\epsilon = 1.502$; NPR = 6.4.



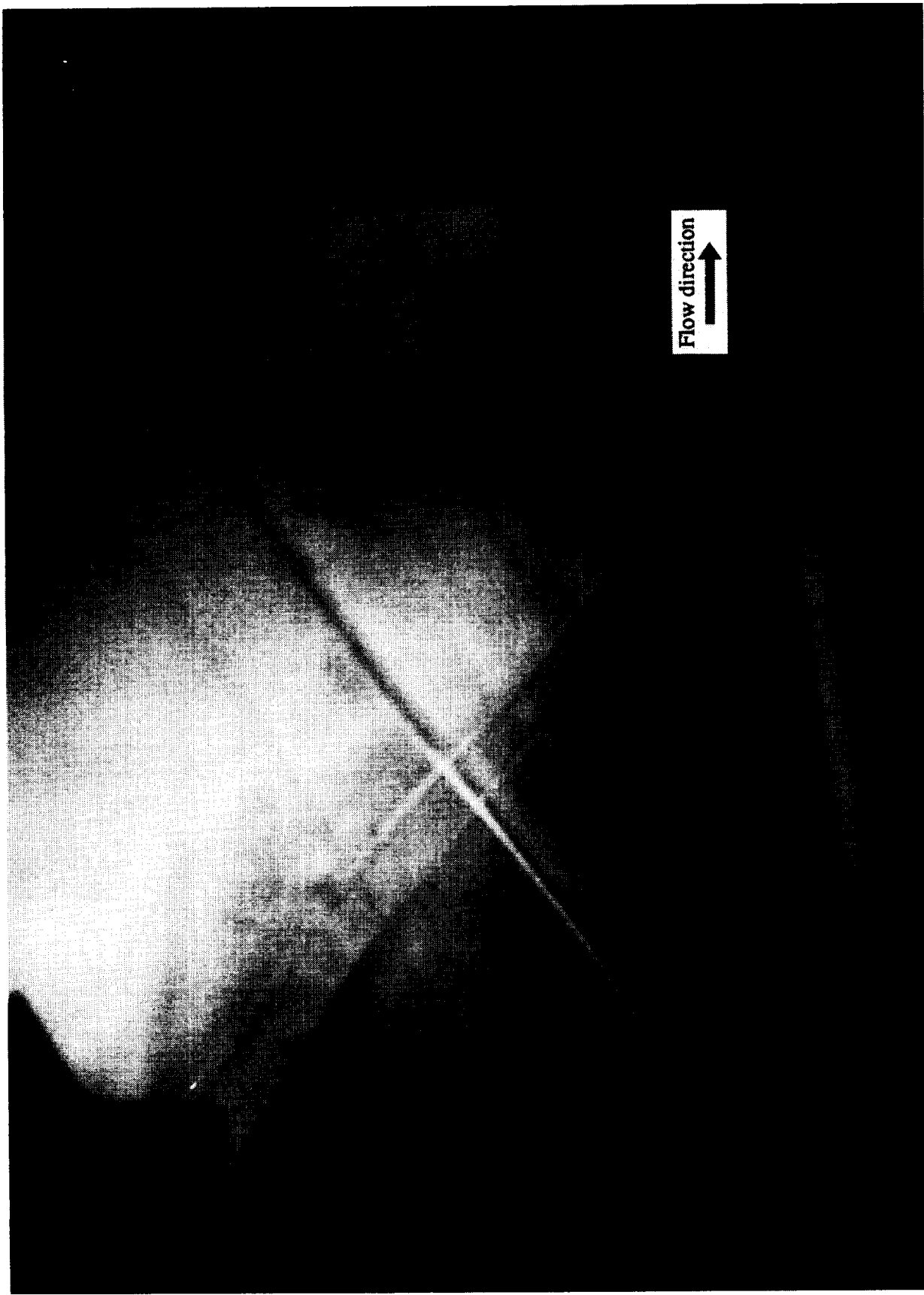
(b) $\phi_l = 0^\circ$; $\phi_r = 0^\circ$; $\omega_c = 0.20$.

Figure 22. Continued.



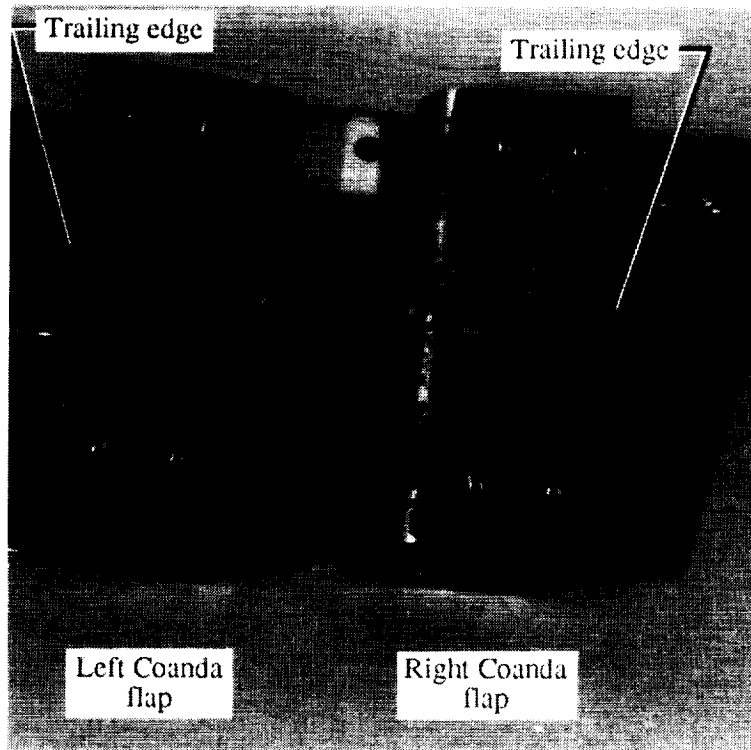
(c) $\phi_l = 0^\circ$; $\phi_r = 30^\circ$; $\omega_c = 0.20$.

Figure 22. Continued.



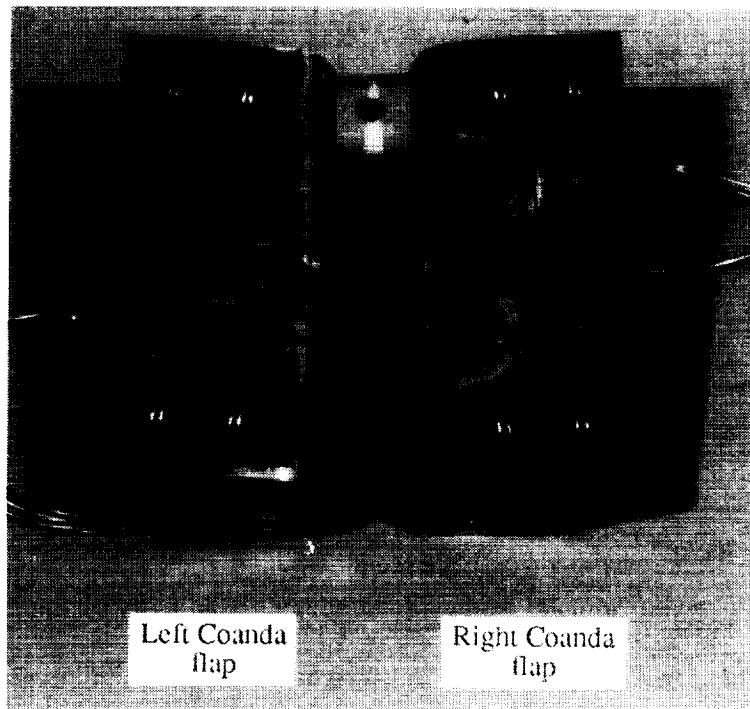
(d) $\phi_l = -10^\circ$; $\phi_r = 30^\circ$; $\omega_c = 0.20$.

Figure 22. Concluded.



L-92-01841

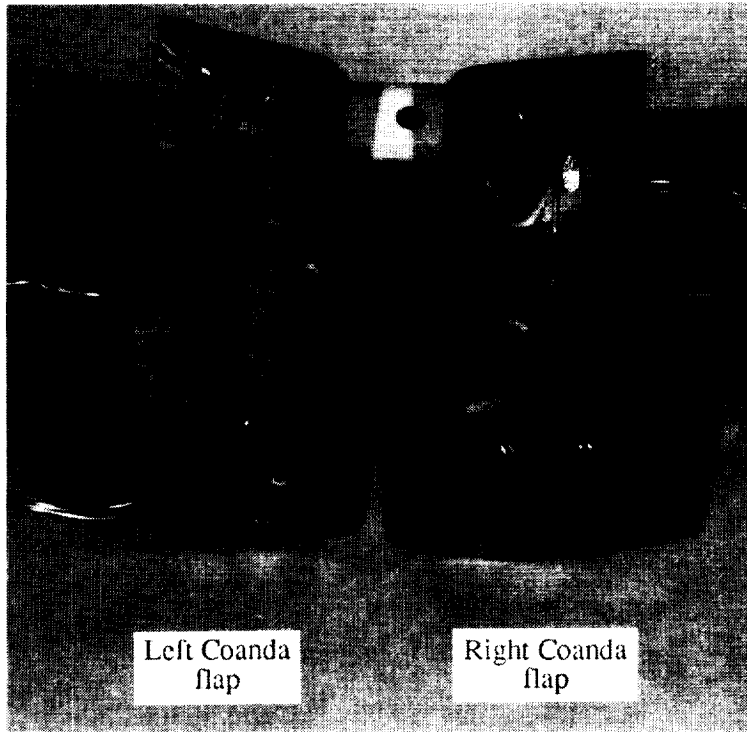
(a) $\phi_l = 0^\circ$; $\phi_r = 0^\circ$.



L-92-01840

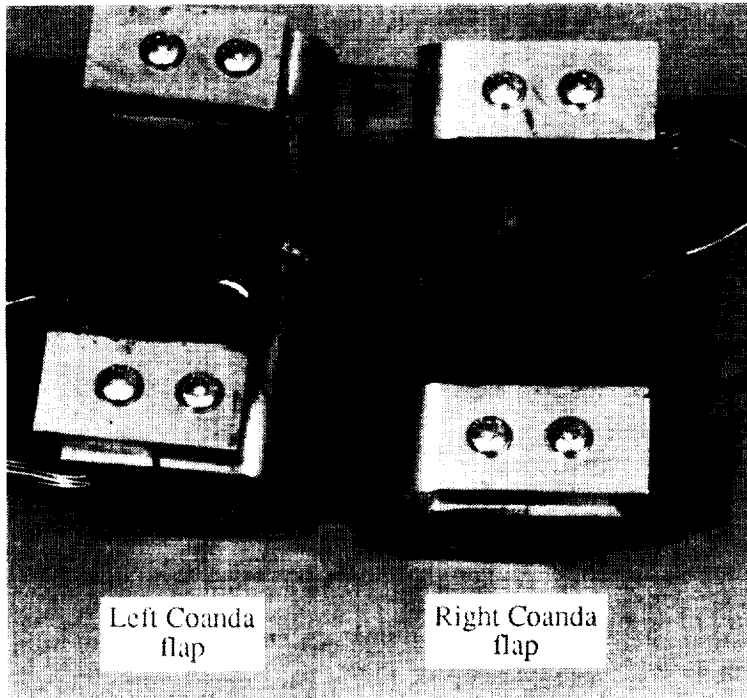
(b) $\phi_l = 0^\circ$; $\phi_r = 30^\circ$

Figure 23. Photographs showing surface flow patterns on Coanda flaps. $\varepsilon = 1.502$; $\text{NPR} = 6.4$; $\omega_c = 0.20$.



L-92-01834

(c) $\phi_l = -10^\circ$; $\phi_r = 30^\circ$.



L-92-01837

(d) $\phi_l = -10^\circ$; $\phi_r = 30^\circ$; fences installed.

Figure 23. Concluded.



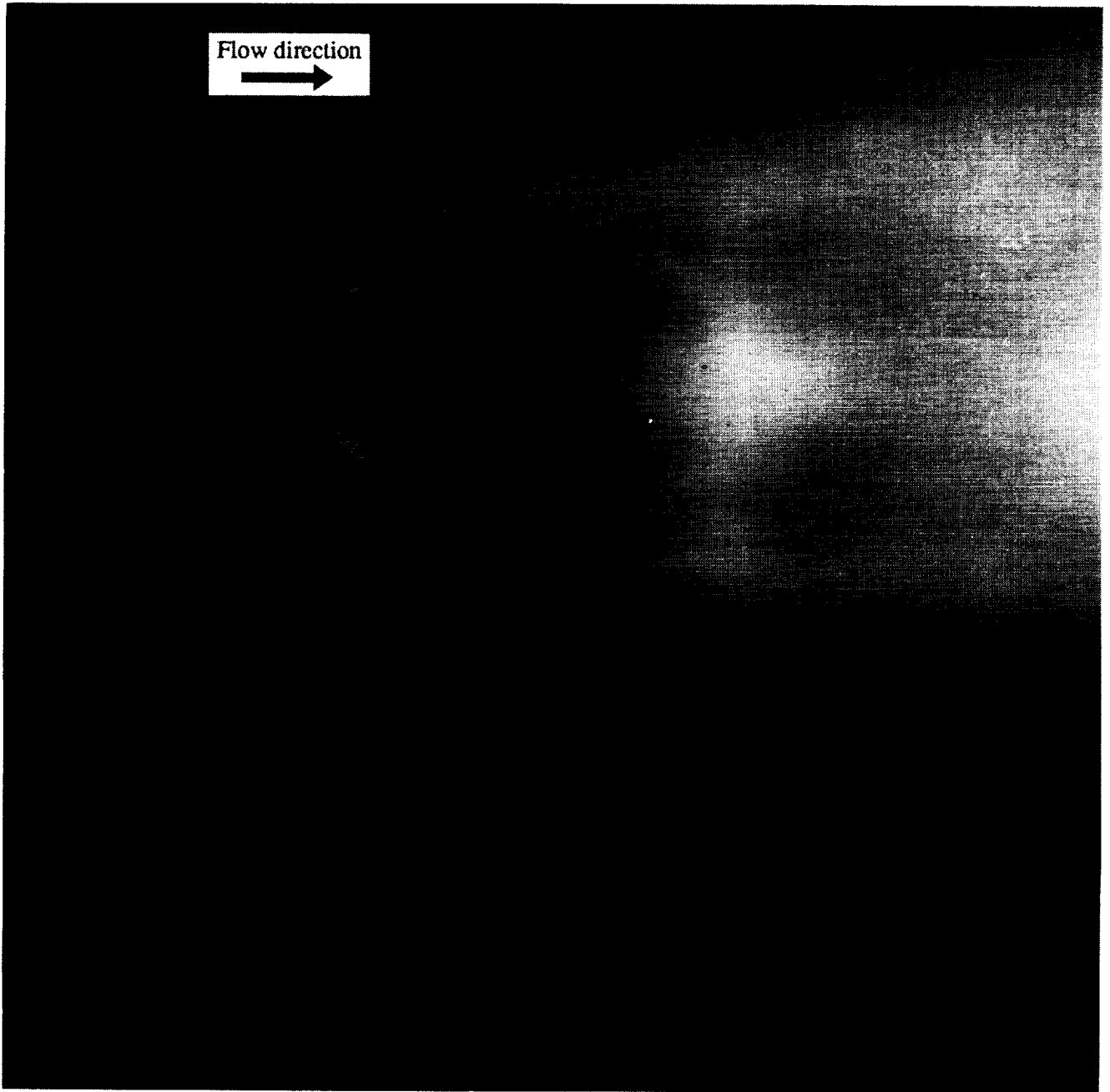
(a) $\varepsilon = 1.944$; $\omega_{si} = 0$.

Figure 24. Focusing schlieren photographs of the slot injection thrust-vectoring configuration. Forward injection; NPR = 10.4.



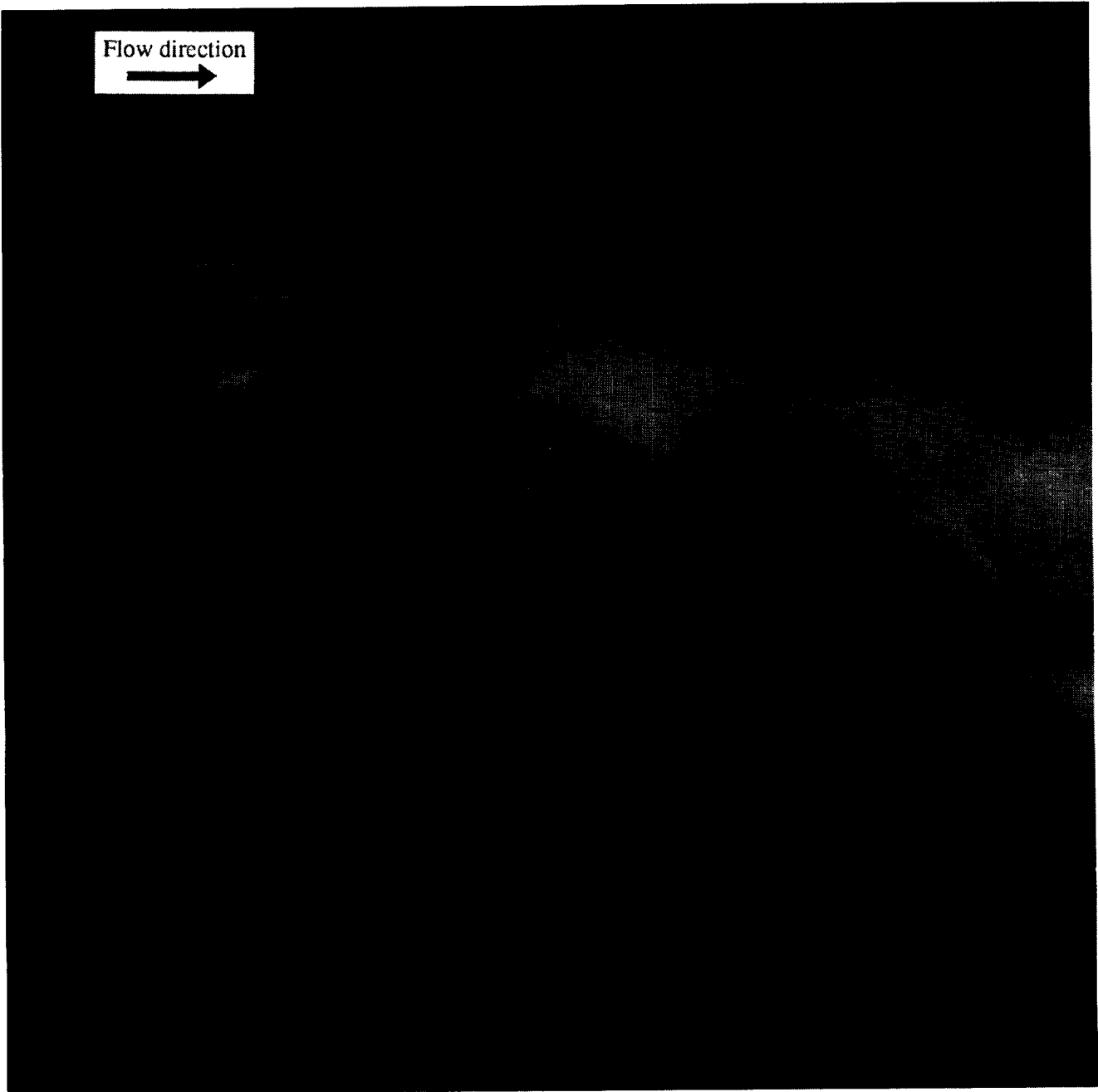
(b) $\varepsilon = 1.944$; $\omega_{si} = 0.10$.

Figure 24. Continued.



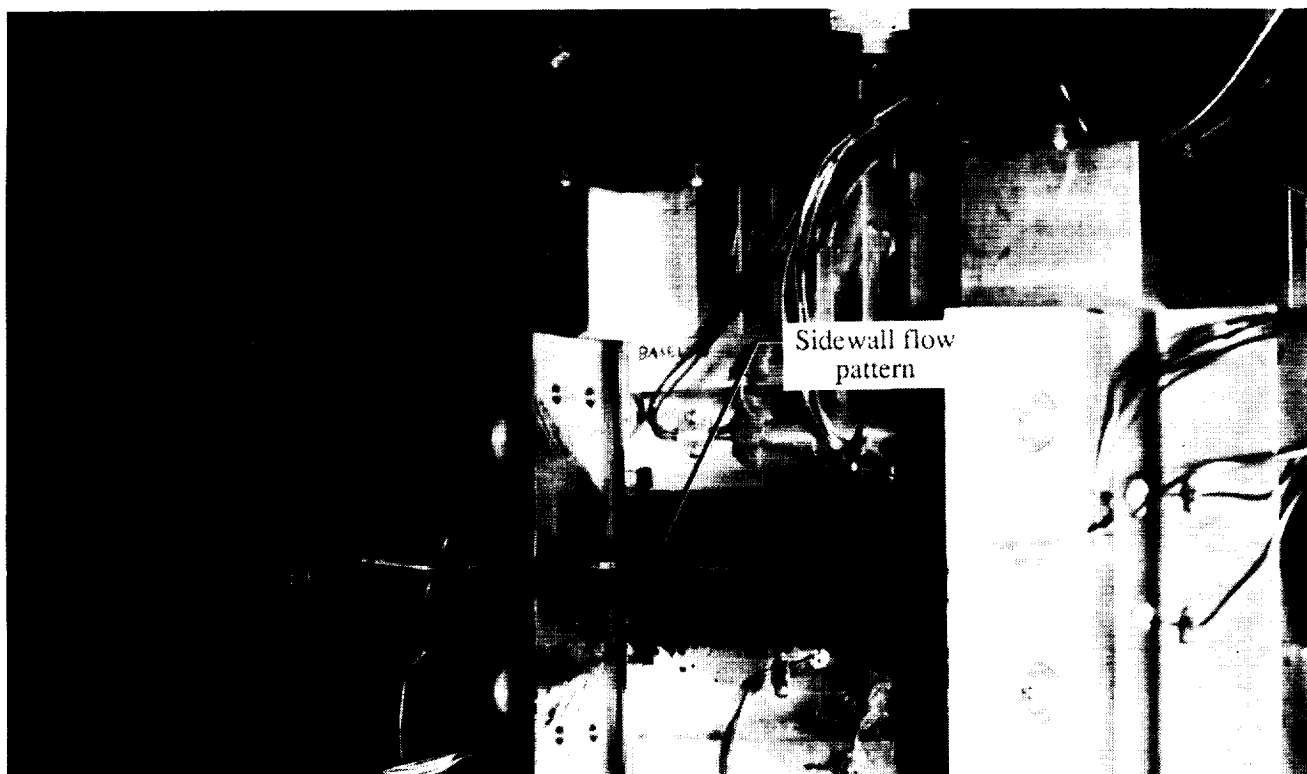
(c) $\varepsilon = 2.405$; $\omega_{si} = 0$.

Figure 24. Continued.

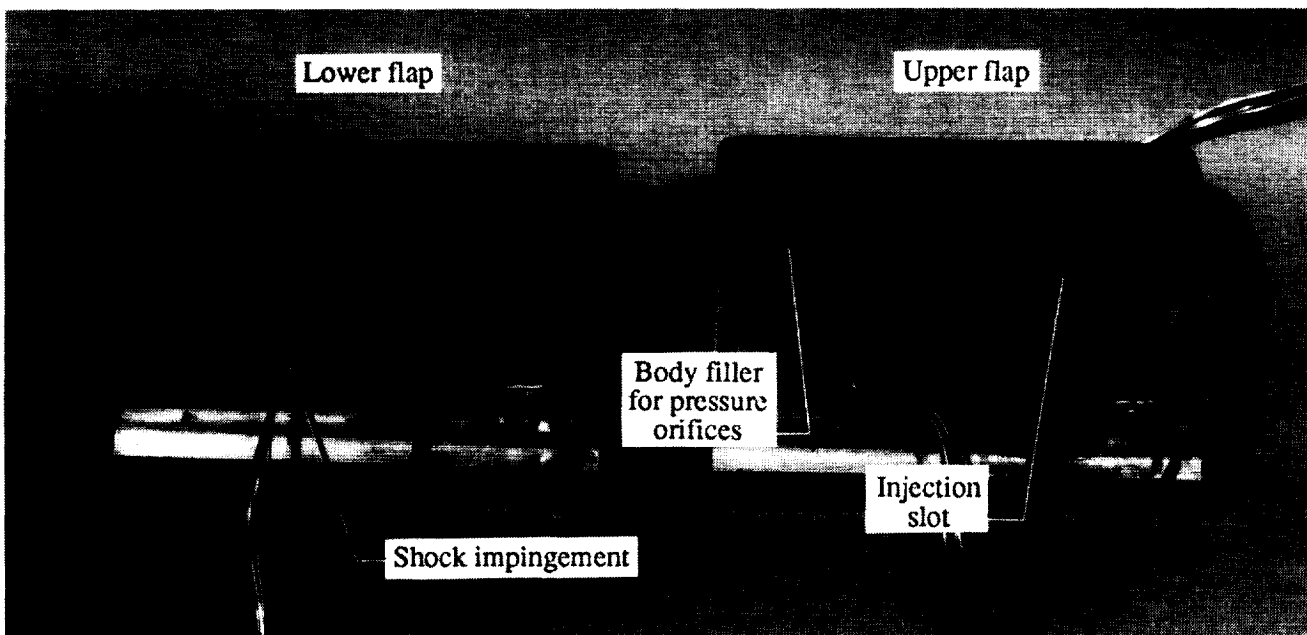


(d) $\varepsilon = 2.405$; $\omega_{si} = 0.10$.

Figure 24. Concluded.



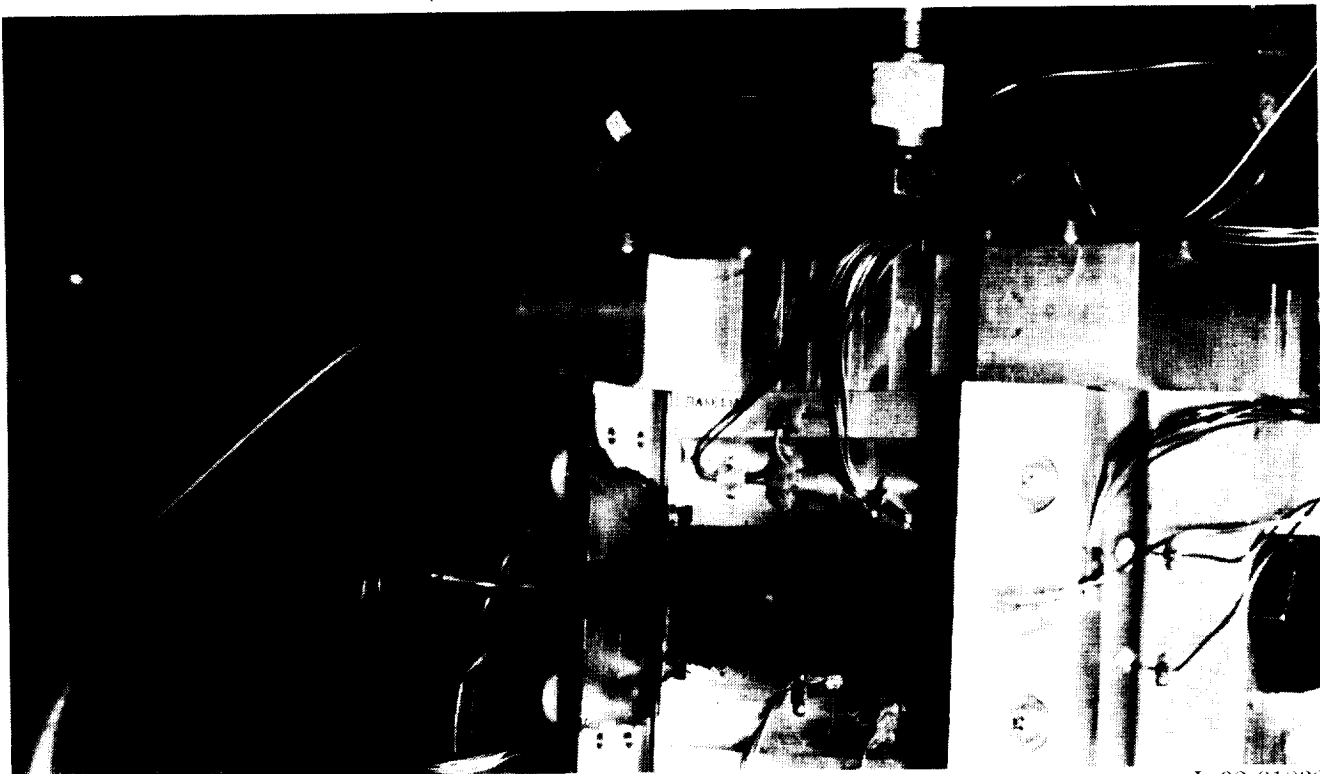
L-92-01836



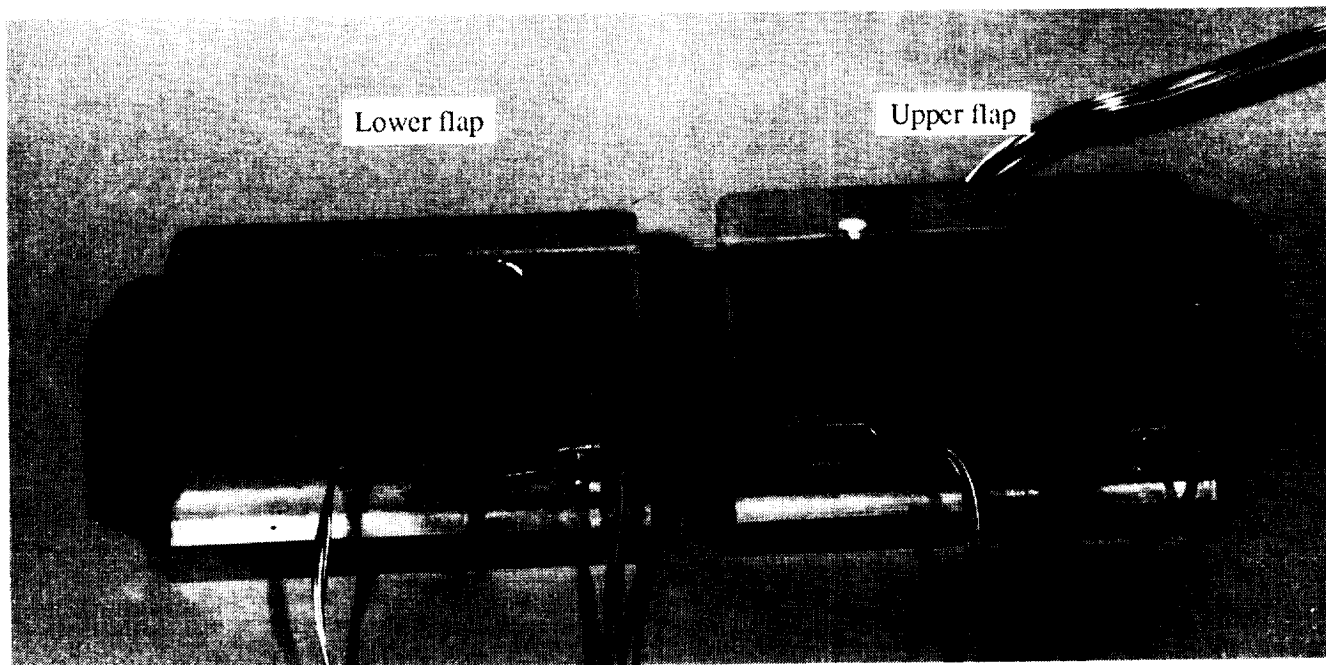
L-92-01833

(a) Forward injection; $\omega_{si} = 0.05$.

Figure 25. Photographs of internal surface flow patterns of nozzle with slot injection. $\epsilon = 1.502$; NPR = 6.4.



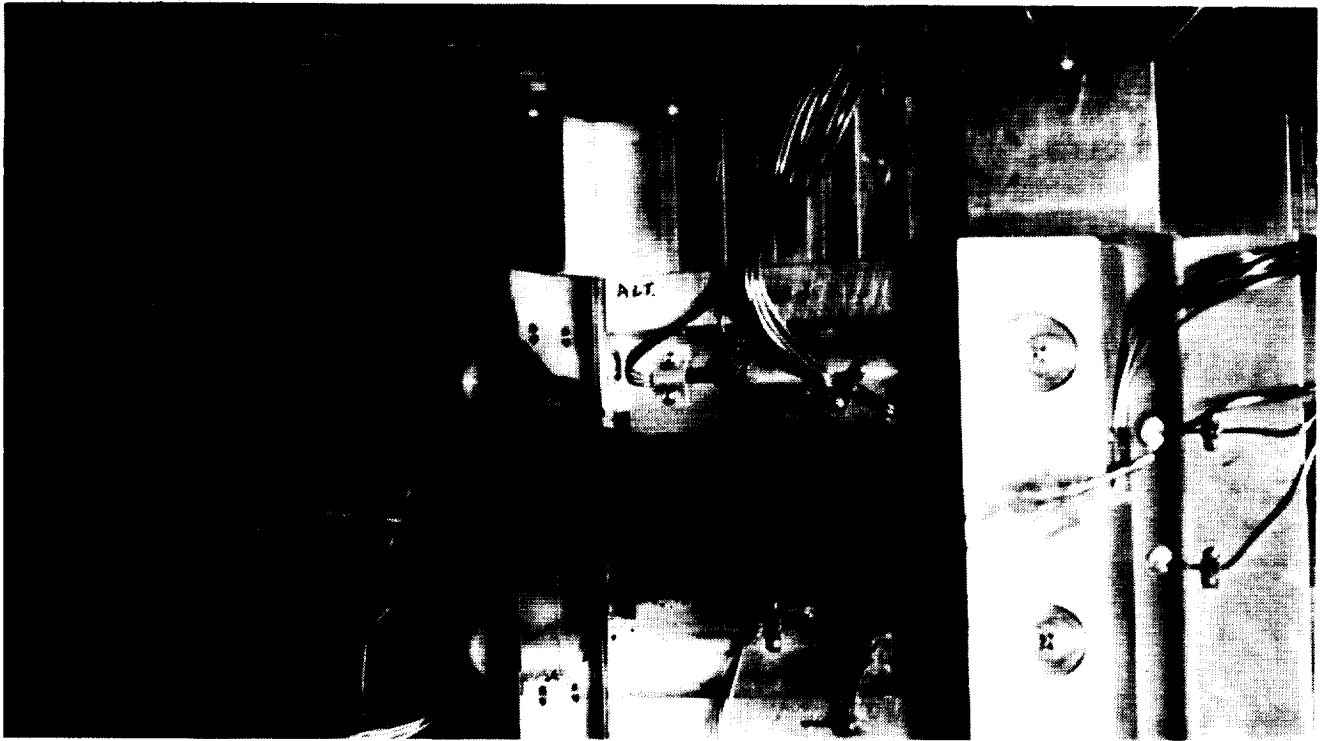
L-92-01832



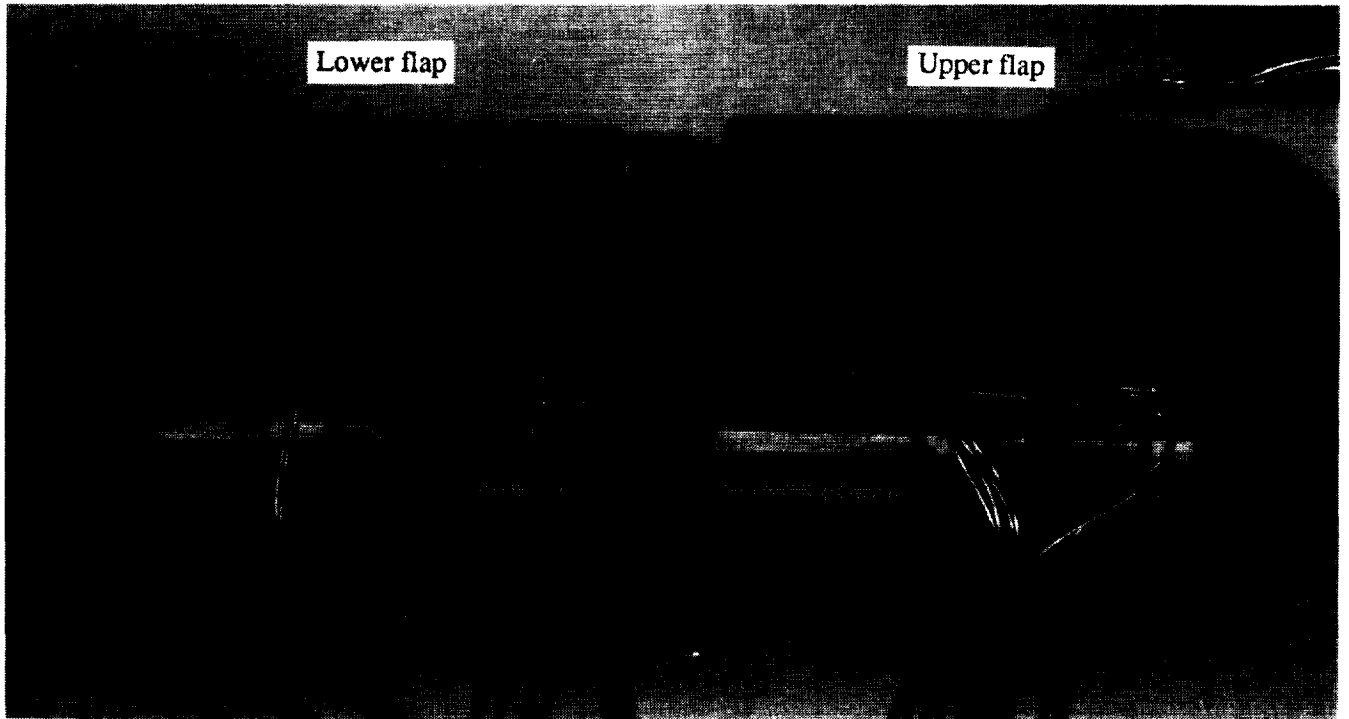
L-92-01846

(b) Forward injection; $\omega_{si} = 0.10$.

Figure 25. Continued.



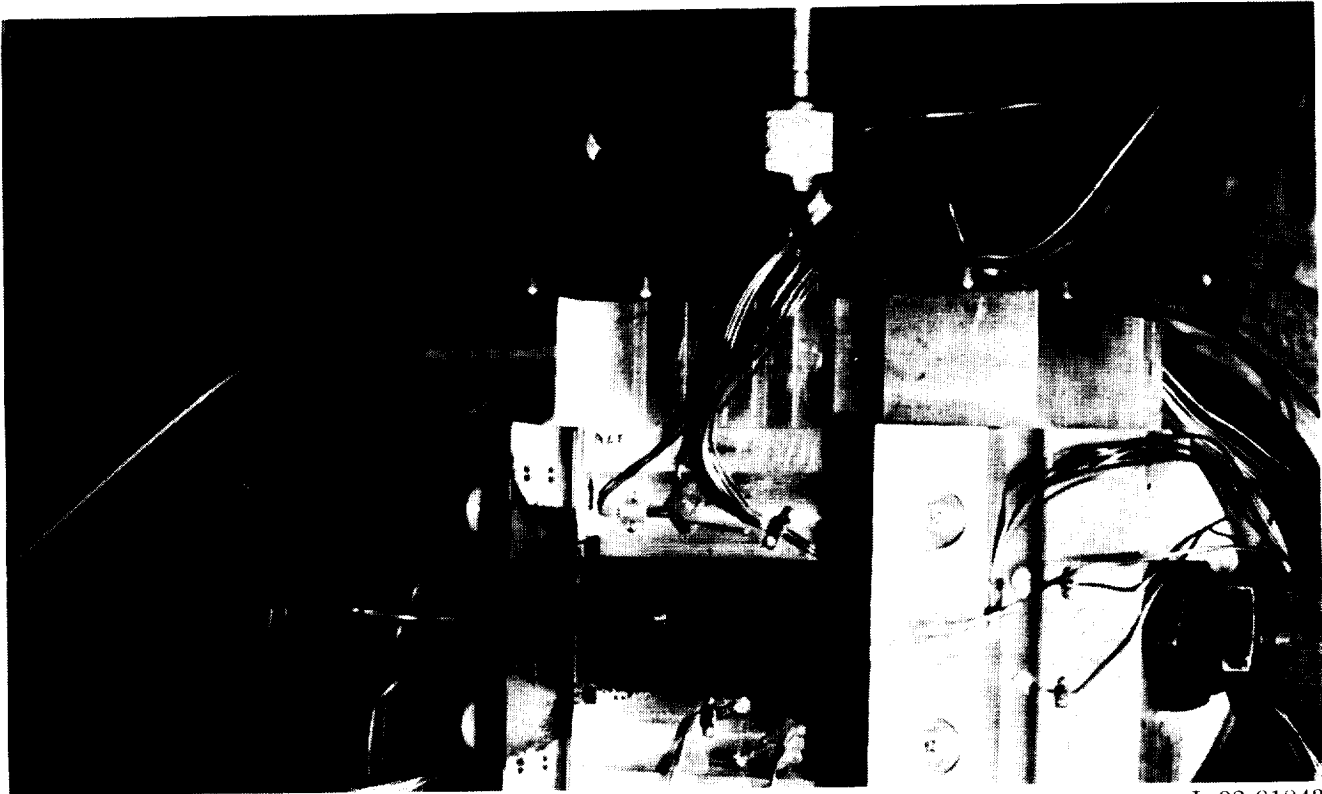
L-92-01845



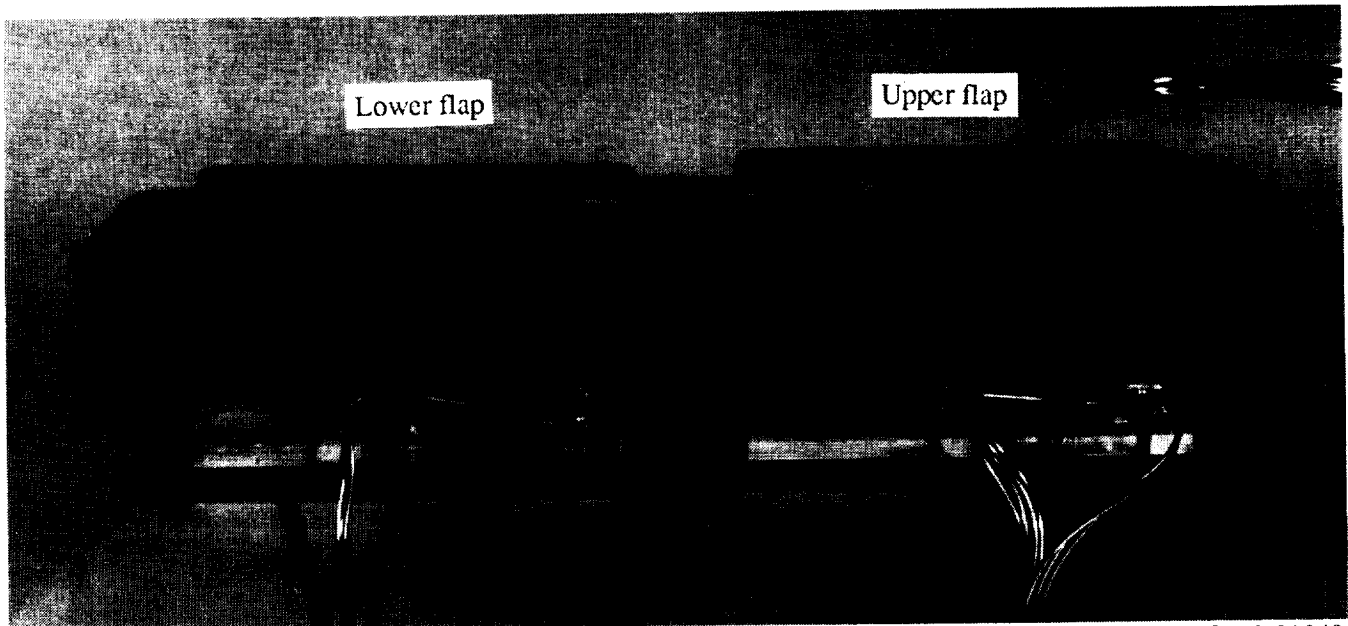
L-92-01844

(c) Aft injection; $\omega_{si} = 0.05$.

Figure 25. Continued.



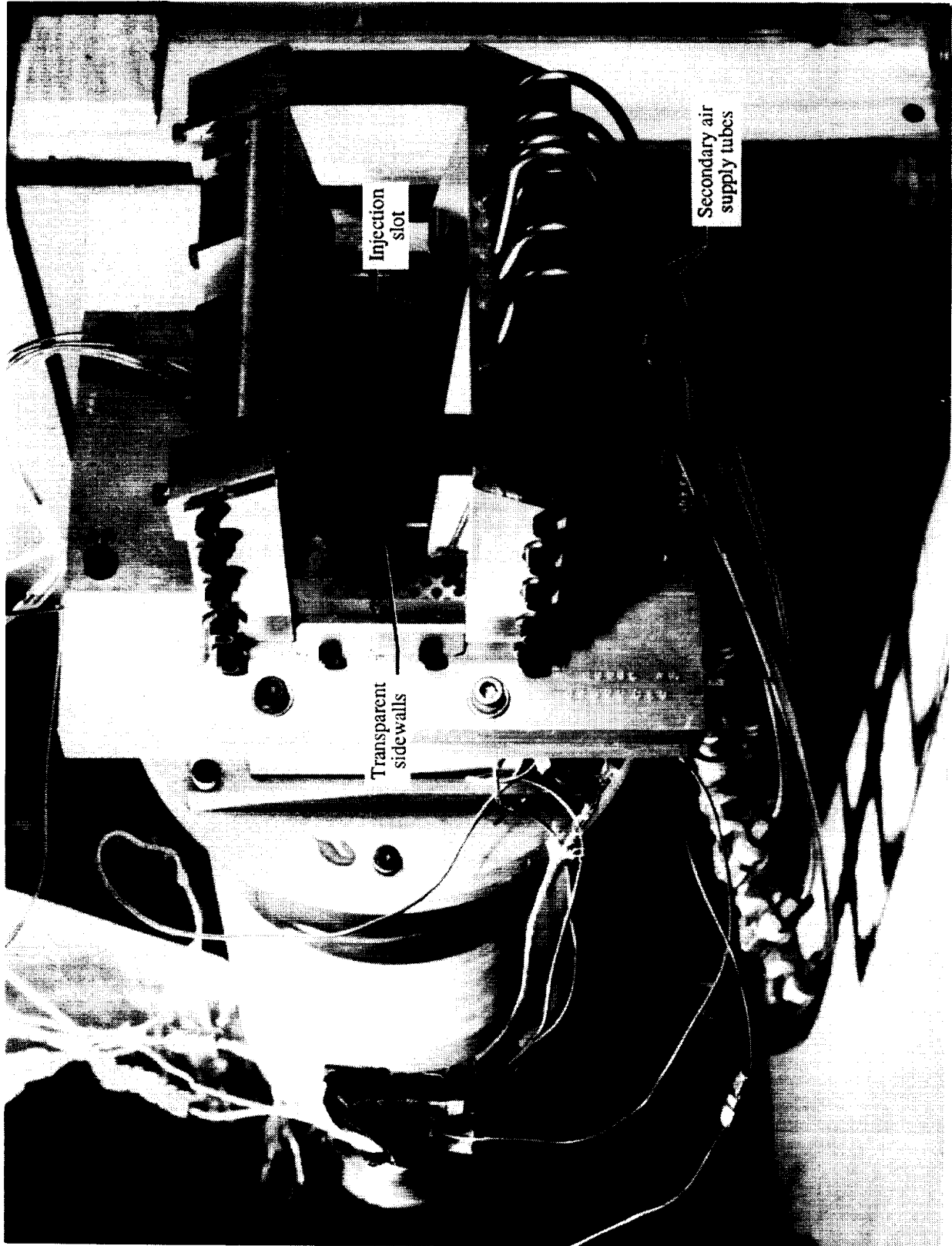
L-92-01843



L-92-01842

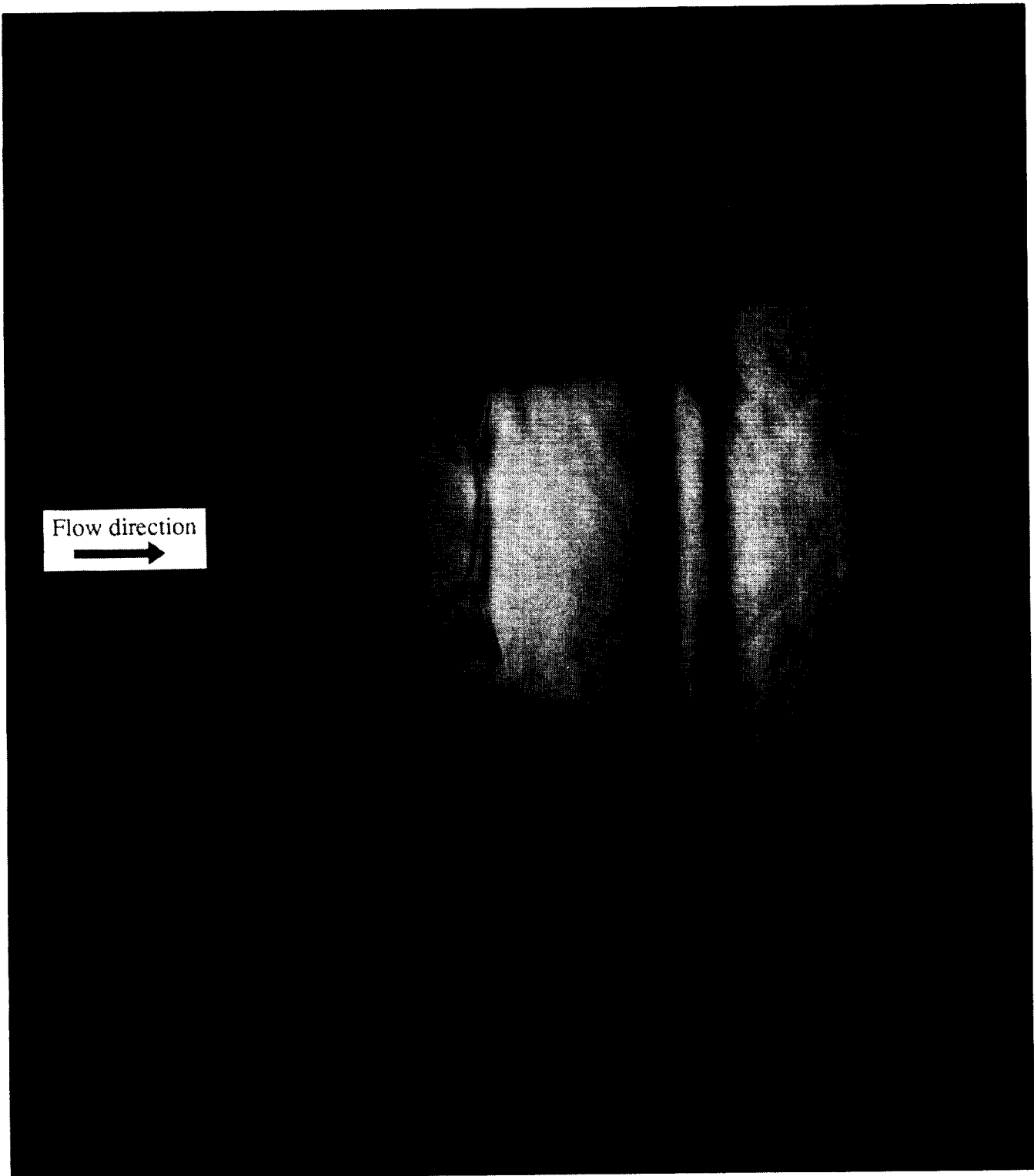
(d) Aft injection; $\omega_{si} = 0.10$.

Figure 25. Concluded.



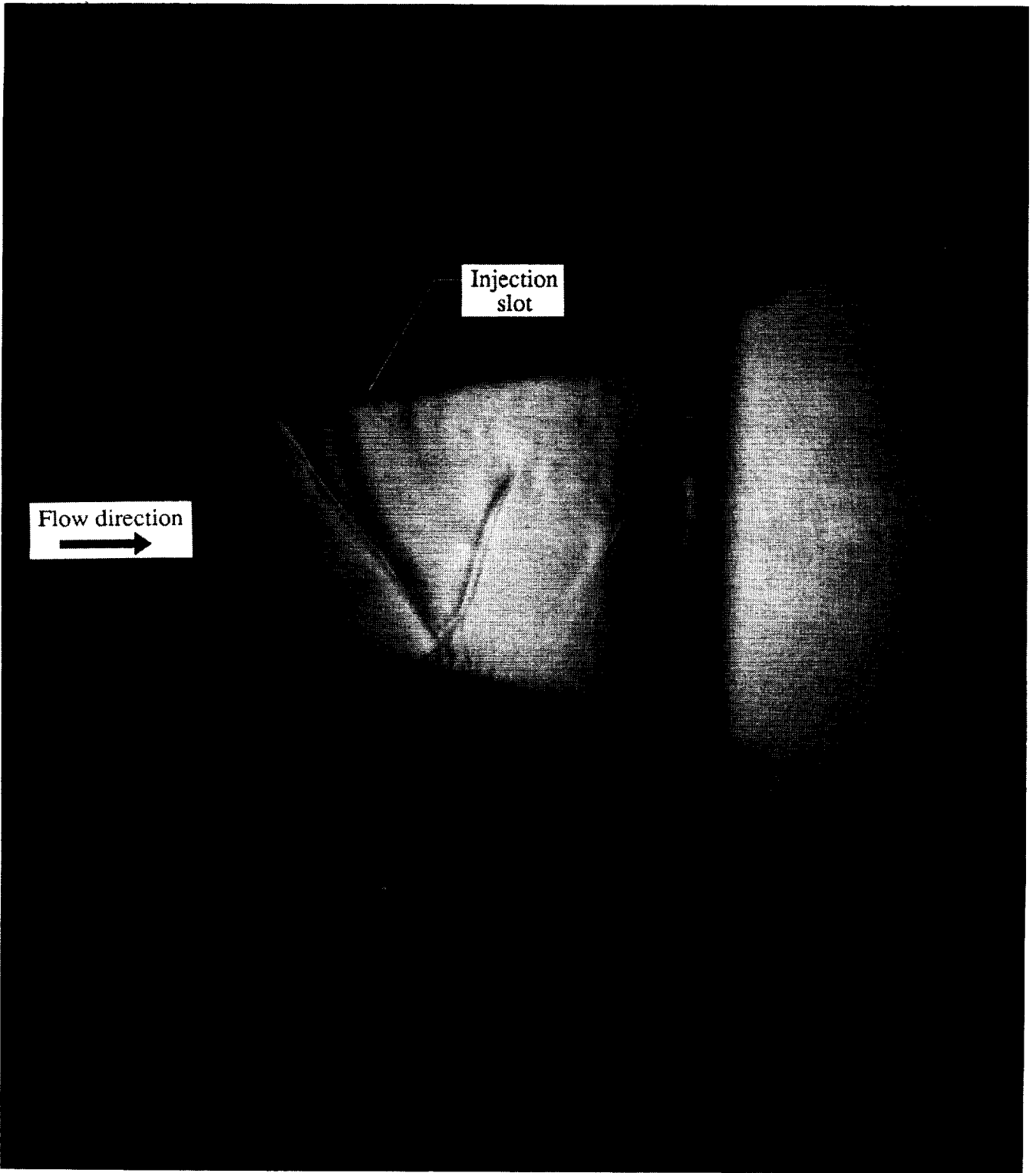
L-92-9528

Figure 26. Photograph of nozzle used for internal schlieren flow visualization.



(a) No slot injection.

Figure 27. Focusing schlieren photographs of internal flow field of 2-D C-D nozzle at $NPR = 2$.



(b) Slot injection through upper flap.

Figure 27. Concluded.



REPORT DOCUMENTATION PAGE

Form Approved
OMB No. 0704-0188

Public reporting burden for this collection of information is estimated to average 1 hour per response, including the time for reviewing instructions, searching existing data sources, gathering and maintaining the data needed, and completing and reviewing the collection of information. Send comments regarding this burden estimate or any other aspect of this collection of information, including suggestions for reducing this burden, to Washington Headquarters Services, Directorate for Information Operations and Reports, 1215 Jefferson Davis Highway, Suite 1204, Arlington, VA 22202-4302, and to the Office of Management and Budget, Paperwork Reduction Project (0704-0188), Washington, DC 20503

1. AGENCY USE ONLY (Leave blank)	2. REPORT DATE December 1994	3. REPORT TYPE AND DATES COVERED Technical Memorandum	
4. TITLE AND SUBTITLE Static Investigation of Two Fluidic Thrust-Vectoring Concepts on a Two-Dimensional Convergent-Divergent Nozzle		5. FUNDING NUMBERS WU 505-62-30-01	
6. AUTHOR(S) David J. Wing		8. PERFORMING ORGANIZATION REPORT NUMBER L-17350	
7. PERFORMING ORGANIZATION NAME(S) AND ADDRESS(ES) NASA Langley Research Center Hampton, VA 23681-0001		10. SPONSORING/MONITORING AGENCY REPORT NUMBER NASA TM-4574	
9. SPONSORING/MONITORING AGENCY NAME(S) AND ADDRESS(ES) National Aeronautics and Space Administration Washington, DC 20546-0001		11. SUPPLEMENTARY NOTES	
12a. DISTRIBUTION/AVAILABILITY STATEMENT Unclassified-Unlimited Subject Category 02 Availability: NASA CASI (301) 621-0390		12b. DISTRIBUTION CODE	
13. ABSTRACT (Maximum 200 words) A static investigation was conducted in the static test facility of the Langley 16-Foot Transonic Tunnel of two thrust-vectoring concepts which utilize fluidic mechanisms for deflecting the jet of a two-dimensional convergent-divergent nozzle. One concept involved using the Coanda effect to turn a sheet of injected secondary air along a curved sidewall flap and, through entrainment, draw the primary jet in the same direction to produce yaw thrust vectoring. The other concept involved deflecting the primary jet to produce pitch thrust vectoring by injecting secondary air through a transverse slot in the divergent flap, creating an oblique shock in the divergent channel. Utilizing the Coanda effect to produce yaw thrust vectoring was largely unsuccessful. Small vector angles were produced at low primary nozzle pressure ratios, probably because the momentum of the primary jet was low. Significant pitch thrust vector angles were produced by injecting secondary flow through a slot in the divergent flap. Thrust vector angle decreased with increasing nozzle pressure ratio but moderate levels were maintained at the highest nozzle pressure ratio tested. Thrust performance generally increased at low nozzle pressure ratios and decreased near the design pressure ratio with the addition of secondary flow.			
14. SUBJECT TERMS Thrust-vectoring nozzles; Fluidics; Fluidic thrust vectoring; Coanda effect; Shock vector control		15. NUMBER OF PAGES 203	
		16. PRICE CODE A10	
17. SECURITY CLASSIFICATION OF REPORT Unclassified	18. SECURITY CLASSIFICATION OF THIS PAGE Unclassified	19. SECURITY CLASSIFICATION OF ABSTRACT Unclassified	20. LIMITATION OF ABSTRACT